NASA CONTRACTOR REPORT

NASA CR-193862

RESEARCH REPORTS - 1993 NASA/ASEE SUMMER FACULTY
FELLOWSHIP PROGRAM

The University of Alabama in Huntsville
Huntsville, Alabama
and
The University of Alabama
Tuscaloosa, Alabama

Final Report

Prepared for NASA, George C. Marshall Space Flight Center
Marshall Space Flight Center, Alabama 35812

RESEARCH REPORTS

1993 NASA/ASEE SUMMER FACULTY FELLOWSHIP PROGRAM

George C. Marshall Space Flight Center

The University of Alabama in Huntsville

and

The University of Alabama

EDITORS:

Dr. Gerald R. Karr
Chairman of Mechanical & Aerospace Engineering
The University of Alabama in Huntsville

Dr. Charles R. Chappell
Associate Director for Science
Marshall Space Flight Center

Dr. Frank Six
University Affairs Officer
Marshall Space Flight Center

Dr. L. Michael Freeman
Associate Professor of Aerospace Engineering
The University of Alabama

REPORT DOCUMENTATION PAGE

Form Approved
OMB No. 0704-0188

1. AGENCY USE ONLY *(Leave blank)*	2. REPORT DATE November 1993	3. REPORT TYPE AND DATES COVERED Contractor Report

4. TITLE AND SUBTITLE

Research Reports - 1993 NASA/ASEE Summer Faculty Fellowship Program

5. FUNDING NUMBERS

NGT-01-008-021

6. AUTHOR(S)

G. Karr, R. Chappell, F. Six, M. Freeman, Editors

7. PERFORMING ORGANIZATION NAME(S) AND ADDRESS(ES)

The University of Alabama in Huntsville and
The University of Alabama, Tuscaloosa, Alabama

8. PERFORMING ORGANIZATION REPORT NUMBER

9. SPONSORING / MONITORING AGENCY NAME(S) AND ADDRESS(ES)

National Aeronautics and Space Administration
Washington, DC 20546

10. SPONSORING / MONITORING AGENCY REPORT NUMBER

NASA CR-193862

11. SUPPLEMENTARY NOTES

12a. DISTRIBUTION / AVAILABILITY STATEMENT

Unclassified/Unlimited

Date: *11-1-93*

Dr. Frank Six, University Affairs Officer

12b. DISTRIBUTION CODE

13. ABSTRACT *(Maximum 200 words)*

For the 29th consecutive year, a NASA/ASEE Summer Faculty Fellowship Program was conducted at the Marshall Space Flight Center (MSFC). The program was conducted by the University of Alabama in Huntsville and MSFC during the period June 1, 1993 through August 6, 1993. Operated under the auspices of the American Society for Engineering Education, the MSFC program, as well as those at other NASA centers, was sponsored by the Office of Educational Affairs, NASA Headquarters, Washington, DC. The basic objectives of the programs, which are in the 30th year of operation nationally, are (1) to further the professional knowledge of qualified engineering and science faculty members; (2) to stimulate an exchange of ideas between participants and NASA; (3) to enrich and refresh the research and teaching activities of the participants' institutions; and (4) to contribute to the research objectives of the NASA centers.

The Faculty Fellows spent 10 weeks at MSFC engaged in a research project compatible with their interests and background and worked in collaboration with a NASA/MSFC colleague. This document is a compilation of Fellows' reports on their research during the summer of 1993. The University of Alabama in Huntsville presents the Co-Directors' report on the administrative operations of the program. Further information can be obtained by contacting any of the editors.

14. SUBJECT TERMS Advanced projects; astrionics; payload and orbital systems; preliminary design; materials and processes; propulsion; space science; structures and dynamics; mission operations; systems analysis and integration information systems; space transportation and exploration.

15. NUMBER OF PAGES
253

16. PRICE CODE
NTIS

17. SECURITY CLASSIFICATION OF REPORT Unclassified	18. SECURITY CLASSIFICATION OF THIS PAGE Unclassified	19. SECURITY CLASSIFICATION OF ABSTRACT Unclassified	20. LIMITATION OF ABSTRACT Unlimited

TABLE OF CONTENTS

NASA/ASEE SUMMER FACULTY FELLOWSHIP PROGRAM

MARSHALL SPACE FLIGHT CENTER
THE UNIVERSITY OF ALABAMA IN HUNTSVILLE

INTEROPERABILITY THROUGH STANDARDIZATION:
ELECTRONIC MAIL, AND X WINDOW SYSTEMS

Prepared By: Ashok T. Amin

Academic Rank: Associate Professor

Institution and
Department: University of Alabama in Huntsville
                             Computer Science Department

MSFC Colleague: Alan Forney

NASA/MSFC:

        Office: Information Systems Office
        Division: Systems Engineering and Integration Division

I

1.0 Introduction

Since the introduction of computing machines, there has been continual advances in computer and communication technologies and approaching limits. The user interface has evolved from a row of switches, character based interface using teletype terminals and then video terminals, to present day graphical user interface. It is expected that next significant advances will come in the availability of services, such as electronic mail and directory services, as the standards for applications are developed and in the 'easy to use' interfaces, such as Graphical User Interface for example Window and X Window, which are being standardized.

Various proprietary electronic mail (email) systems are in use within organizations at each center of NASA . Each systems provides email services to users within an organization, however the support for email services across organizations and across centers exists at centers to a varying degree and is often not easy to use. A recent NASA email initiative is intended "to provide a simple way to send email across organizational boundaries without disruption of installed base" [4]. The initiative calls for integration of existing organizational email systems through gateways connected by a message switch, supporting X.400 and SMTP protocols, to create a NASA wide email system and for implementation of NASA wide email directory services based on OSI standard X.500. A brief overview of MSFC efforts as a part of this initiative are described.

Window based graphical user interfaces make computers easy to use. X window protocol has been developed at Massachusetts Institute of Technology in 1984/1985 to provide uniform window based interface in a distributed computing environment with heterogeneous computers. It has since become a standard supported by a number of major manufacturers. X Window systems, terminals and workstations, and X Window applications are becoming available. However impact of its use in the Local Area Network environment on the network traffic are not well understood. It is expected that the use of X Window systems will increase at MSFC especially for Unix based systems. An overview of X window protocol is presented and its impact on the network traffic is examined. It is proposed that an analytical model of X window systems in the network environment be developed and validated through the use of measurements to generate application and user profiles.

2.0 NASA Email Initiative

NASA centers typically have one or more types of proprietary email systems such as ccMail, Quick Mail, All-In-One, etc.. Providing email service to users on different email systems within and across centers can be problematic. NASA email initiative is intended to provide easy-to-use email services for exchange of messages between users within and across centers and to facilitate use of email services by providing directory services for email addresses. The implementation of the initiative is based on use of standards- X.400 for Message Handling and X.500 for Directory services [5].

Standards for Message Handling and Directory Services

The model of the Message Handling System (MHS), shown in Figure 1, is based on the familiar postal mail system. A MHS consists of User Agents (UA) which interface with Message Transfer Agents (MTA) of the Message Transfer Subsystems (MTS), and a Message Store (MS) for storage of messages in transit. The X.400 standard defines protocols for communication between MTAs, for access to MTA by MS and UA, and for access to MS by UA. It supports text, voice, facsimile, teletext, videotex etc., and provides for non-repudiation of submission and delivery. A justifiable criticism of the X.400 is lack of standards for the user interface to the UA since it is envisioned that email will be universal service in the sense that a telephone service is universal. Further utility of email system depends mainly on the functionality its UA provides to the user.
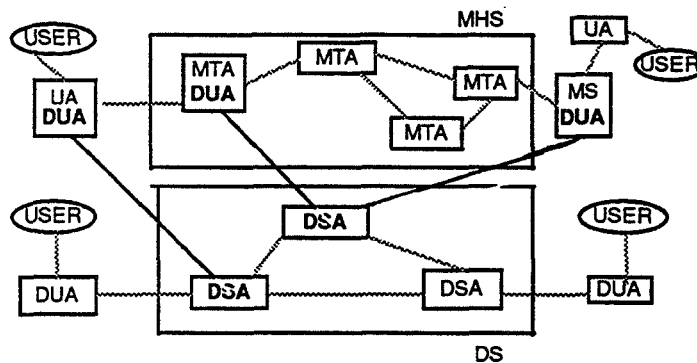
Message Handling System and Directory System.
Figure 1.

The model of the directory service, shown in Figure 1, is based on the familiar telephone directory services. The directory system consists of Directory Services Agents (DSA) and Directory User Agents (DUA). The directory is distributed and each part of the directory is expected to be assigned to a DSA, however a DSA may be assigned more than one part. The X.500 defines protocols for DSA access by DUA and for communication between DSAs. It supports authentication of user and of the information. Here again the user interface to DUA has not been defined. Though the directory is intended to contain information about objects such as persons, organizations, processes, in the communication system, it is expected that MHS will be a major user of the directory services for interpersonal message service. An integrated view of the two system is depicted in Figure 1 where DUA may be integrated with MHS components.

MSFC Implementation of the Email Initiative

Email systems at MSFC may be classified based whether they are managed by Information System Office (ISO) or not. The ISO managed email systems are interconnected through a hierarchy of gateways leading to a central switch (also serves as DEC X.400 gateway) which routes email to destination email system gateway within MSFC or outside typically to other centers. The user agents of these systems provide a

highly functional user interface. However the addressing schemes used by these systems are different. Of the email systems not managed by ISO, Unix based email systems using Simple Message Transfer Protocol (SMTP) have universal connectivity to other email systems using SMTP over the Internet.

A message switch is central to the implementation at MSFC. The switch, a CDC EP/IX Mail*Hub, supports X.400 and SMTP, fax gateways, has integrated X.500 directory, and provides for address translation between X.400 and SMTP. It will provide for interoperability across all email systems at MSFC and facilitate simple addressing based on first-name and last-name through the X.500 directory services. The Electronic Mail Implementation Group has defined requirements on the content of the directory entry, and directory access servers. However except for query-by-mail, no requirements for DUA for on-line directory access by users have been specified.

3.0 X Window Systems in Local Area Network Environment

Graphical user interfaces (GUI) have revolutionized the user interaction with computer. In comparison with the character based interface, GUI is easy to use and learning to use a new application is even easier. The X window system, which implements X window protocol, provides a device independent pixel based graphics for management of hierarchical , resizable windows. The protocol can be used over any reliable byte stream. X window system permits multiple applications running simultaneously on local and remote hosts to manipulate its window on the display. It was originally developed for use with distributed applications.

Client/Server Computing

Information systems are moving from centralized mainframe computing to file server based computing in which specialized processors manage a file store and provide file services to PCs and work stations interconnected over a Local Area Network (LAN). X window systems are available in the form of X terminals and X work stations and PCs. X terminals are employed in a client/server architecture for Army's RCAS in which X terminals, file servers and application servers are interconnected over a LAN, and various sites are interconnected over a dedicated lines. Little is known about the traffic implications of X window systems in the network environment.

X Window Protocol and Networking

X window protocol is used for communication between a client application running on local host or a remote host and the X server of the X window system. It was intended to support distributed applications. Therefore, it has been designed to be efficient in the network environment. Figure 2 shows a view of X window system operation from a network traffic perspective.

A client sends draw requests and information requests to the server, and the X server sends user inputs (events), replies, and error reports to the appropriate client. The events and error reports are of 32 byte size, while requests and replies are multiples of 4 byte size with a reply being at least 32 byte in size. The server manages windows, does all drawing, and interfaces with the device drivers to get keyboard and the mouse inputs.

It also manages of-screen memory, window, fonts, cursors, and the colormaps. The graphic context , the information about how graphic requests are to be interpreted is
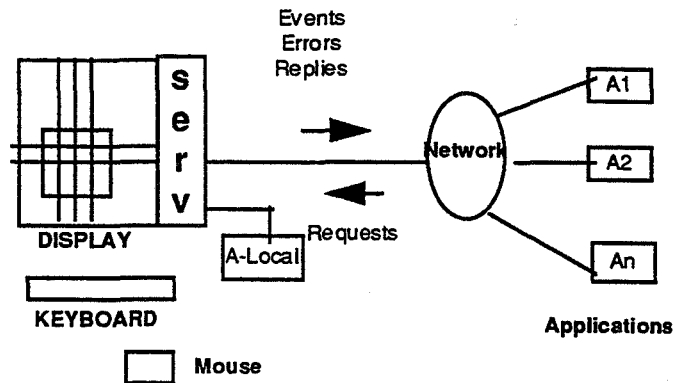
X Window System in a Network
Figure 2.

cached by the server, so that this information need not be sent over the network for each graphic request to be interpreted. Other similar abstractions stored in the server include window- allows server to manage which parts of the screen are displaying which parts of which window, Pixmap- an off screen virtual drawing surface that must be copied into a window to become visible, color map- which allows user to easily specify color for graphic requests.

Previous studies on the traffic impact of the X window protocol in the academic environment showed that the protocol is very efficient and impact on the network traffic is not significant. However, measurements are needed in non-academic environments to better understand the traffic impact. Little is known about the traffic impact in an when X window systems coexist with PCs in a file server environment. Development of analytical models and measurements to validate models are suggested for further work in this area.

References

[1] Standard object attribute formats for NASA X.500 directory implementations, version 1, Electronic Messaging Group, June 25, 1993.
[2] Dunwoody J. C. and Linton M. A., "A Dynamic Profile of Window System Usage", IEEE Symposium on Local Area Networks, pp.90-99, 1988.
[3] Nye A., "Networking and the X Window System", in Unix Networking (Eds. S. G. Kochan and P. H. Wood), Hayden Books, 1989.
[4] Lynn J. C., "NASA-Wide Electronic Mail (E-Mail) Initiative", Memorandum to Information Resource Oversight Council (IORC) Members, June 11, 1993.
[5] Plattner B., Lanz C., Muller M., and Walter T., X400 Message Handling, Addison-Wesley, 1991.
[6] Scheifler R. W. and Gettys J., "The X Window System", ACM transactions on Graphics, vol.5, no.2 , pp.79-109, 1986.

1993

NASA/ASEE SUMMER FACULTY FELLOWSHIP PROGRAM

MARSHALL SPACE FLIGHT CENTER
THE UNIVERSITY OF ALABAMA IN HUNTSVILLE

RISK IDENTIFICATION AND REDUCTION IN INTEGRATED PRODUCT TEAMS

Prepared by: Robert G. Batson, Ph.D.

Academic Rank: Professor

Institution and
Department: The University of Alabama
                           Department of Industrial Engineering

MSFC Colleague(s):   Glen D. Ritter
                           L. Don Woodruff

NASA/MSFC:

    Office: Systems Analysis and Integration
    Division: Systems Definition
    Branch: Aerospace Systems Branch

Introduction

This brief report summarizes research and planning conducted during Summer 1993 for MSFC on the subjects of risk identification, assessment, and management. Research findings are presented, citing useful references. The major output of this work, the AXAF-S Project Risk Management Plan is outlined.

Body

Risk Identification, the first step in the three-step risk analysis process (1), consists of definition and characterization of all potential problems including analysis of cause-and-effect, primary/secondary impacts on the project, and a qualitative assessment of whether each potential problem is high, medium, or low risk. Risk identification is best done via team meetings, individual interviews, or questionnaires--using the experience and technical details available in the project. There are other sources of risk identification information (Garland Bauch, NASA/JSC GM3/SSP Configuration Management, identified over fifty possibilities in collaboration with the author during July 1993) which may fit neatly into the following six categories: 1) Checklists, lessons learned, and so-called risk "templates"; 2) One-on-one interviews, questionnaires; 3) Formal project or engineering reviews; 4) Cause-and-effect diagrams, brainstorming; 5) Tiger Teams, external reviews; 6) Extracts from project documents such as planning documents in the "illities", and requirements documents.

Risk assessment, the second step in risk analysis, uses information from risk identification, probability encoding techniques, and various quantitative methods to synthesize the input uncertainties into an overall assessment of program risk. Risk assessment techniques and the necessary math models they use are fully detailed in (1, 2).

Risk management (4) uses information from risk identification and risk assessment in decision-making in order to reduce risk. Risk management occurs when the appropriate manager or team takes action to avoid a risk, or to handle it in some way. Risk management strategies are numerous, and must fit the given project or situation. General categories of risk management strategies are: 1) Risk avoidance--select a lower risk alternative, or eliminate a requirement or system element; 2) Risk control--actions taken to either reduce the probability of a problem occurring, or to mitigate the consequences if it should occur; 3) Risk transfer--either transfer or share risk through mechanisms such as contract-types and warranties, or change the risk from one form (e.g., schedule) to another (cost); 4) Risk assumption--based on an informed understanding of the potential problem (i.e., its probability and consequences), agree to do nothing and accept the consequences should the problem occur; 5) Knowledge and research--when a team cannot select strategies 1-4 based on inadequate information, they may appoint a Tiger Team or even set-up a small R&D project to increase their knowledge of the risk.

Finally, a sixty-page "AXAF-S Project Risk Management Plan" was written. This comprehensive plan for a project risk analysis activity, focused on the AXAF-S top-level team (the Core Product Development Team) as the decision authority for risk management and tracking, includes the results of the preliminary AXAF-S risk area identification activities as a series of tables in Section 4.0. An outline of this plan is provided in Table 1 below. The Risk Reduction Plans and concept for the Risk Tracking System are based on ideas in (4, Chapter 12 and 13) .

Table 1. AXAF-S Project Risk Management Plan Table of Contents

References

1.   Batson, R.G., Program Risk Analysis Handbook, NASA Technical Memorandum TM-100311, NASA George C. Marshall Space Flight Center, August 1987.

2.   Information Spectrum, Inc., Risk Assessment Techniques: A Handbook for Program Management Personnel, Defense Systems Management College Textbook, July 1993.

3.   Lockheed Missiles & Space Company, Systems Engineering Management Guide, Defense Systems Management College Textbook, 1983.

4.   The Analytic Sciences Corporation, Risk Management: Concepts and Guidance, Defense Systems Management College Textbook, March 1989.

1993

NASA/ASEE SUMMER FACULTY FELLOWSHIP PROGRAM

MARSHALL SPACE FLIGHT CENTER
THE UNIVERSITY OF ALABAMA IN HUNTSVILLE

VISCOELASTIC ANALYSIS OF SEALS FOR EXTENDED SERVICE LIFE

Prepared By:	Mark V. Bower, Ph. D., P. E.
Academic Rank:	Assistant Professor
Institution and Department:	The University of Alabama in Huntsville, Department of Mechanical and Aerospace Engineering
MSFC Colleague(s):	Thomas D. Bechtel Brian K. Mitchell

NASA/MSFC:

Laboratory:	Propulsion Laboratory
Division:	Mechanical Systems Division
Branch:	Fluid Systems Design Branch

Introduction

The space station is being developed for a service live of up to thirty years. As a consequence, the design requirements for the seals to be used are unprecedented. Full scale testing to assure the selected seals can satisfy the design requirements are not feasible. As an alternative, a sub-scale test program (2) has been developed by MSFC to calibrate the analysis tools to be used to certify the proposed design. This research has been conducted in support of the MSFC Integrated Seal Test Program. The ultimate objective of this research is to correlate analysis and test results to qualify the analytical tools which in turn, are to be used to qualify the flight hardware.

Seals are simple devices, in wide spread use. The most common type of seal is the O-ring. O-ring seals are typically rings of rubber with a circular cross section. The rings are placed between the surfaces to be sealed, usually in a groove of some design. The particular design may differ based on a number of different factors. This research is focused on O-rings that are staticly compressed by perpendicular clamping forces, commonly referred to as face seals. In this type of seal the O-ring is clamped between the sealing surfaces by loads perpendicular to the circular cross section.

Specific Problem Addressed

The Integrated Seal Test Program is currently performing load decay tests to be used in the qualification of the analysis tools. For these tests to provide an accurate benchmark for analyses the tests must produce accurate repeatable results. This study was undertaken to assure the quality of test results produced. To that end, test results from three different tests are evaluated for repeatability, in both load magnitudes and time dependent behavior. Further, in an initial attempt to qualify the analysis tool, the results are compared to finite element analysis results.

Method of Approach

The load decay tests being conducted under the Integrated Seal Test Program use a sub-scale test article to load an O-ring to a specified level of squeeze. The test article is closed with a single bolt at the center of the fixture. A load cell is attached to the bolt to measure the clamping force on the O-ring. The load cell output is converted to digital information by an analog to digital converter and stored with the time of measurement in data files using a dedicated 286 computer. Data files generated by the load test are transferred to other computers by floppy disc. After initial testing, the computer has been setup to automatically resume load measurements in the event of power loss. The test article is sub-scale in major diameter only. The cross section diameter of the O-ring (6.86 mm, 0.270 inches) and the squeezes (15%, 25%, and 40%) are of the same order as the full-scale design. The desired level of squeeze is obtained by clamping the test fixture down to a fixed shim height and the shims removed.

Due to the nature of the load decay tests, a single test will generate multiple data files with a very large number of data records. These files are combined into a single file and

reduced in size using Microsoft Excel (version 4.0) command and function macros developed for the research. These programs are documented in an associated report (1).

Two issues associated with repeatability of the load decay tests must be addressed to ensure test quality. They are: load magnitudes and time dependent behavior. Load magnitudes are be compared by plotting the loads from different tests on a single graph. The time dependent behaviors are compared by plotting the normalized loads from different tests on a single graph.

The effects of aging are studied in the same manner as the repeatability issues. In addition, results from testing of an aged specimen are compared with a virgin specimen by plotting the two sets of data on the same graph with the time axis for the aged specimen shifted horizontally. Time shifting of relaxation curves is a commonly accepted procedure in the analysis of viscoelastic materials. These results are not shown here due to space limitations.

Results

Results from three preliminary load decay tests performed on O-rings with no side wall contact are shown in Figure 1. The results are plotted on linear scales. Preliminary tests 1 and 2 were performed on virgin O-rings. Results from preliminary test 1 are indicated with filled squares, results from test 2 are indicated with filled circles, and results from tests on an aged O-ring are indicated with unfilled triangles. Note from the figure that the initial, i.e., maximum, load for test 1 is 3.76 kN (846 lbs.) while the initial load for test 2 is 4.92 kN (1105 lbs.). This is a percentage difference of 23.4% relative to the test 2 initial load. This difference may be explained by several factors: variation in O-ring cross section diameter from one specimen to another; lack of a reference point on the test article, resulting in angular displacement of the top relative to the bottom; and different shimming procedures. Each of these causes could result in a different squeeze level between tests, and hence different load magnitudes. However, shim height is the most significant factor. Review indicated that a shim height of 1.78 mm (0.070 inches) was used for test 1 and 1.75 mm (0.069 inches) for test 2 and the aged O-ring test. The gaps in the data plotted are due to suspension of data acquisition due to power losses.

Note in Figure 1 for test 1 minor fluctuations in the load value, approximately ± 44 N (± 10 lbs.), for times between approximately 1.5 million seconds and 2 million seconds. Preliminary analysis indicates that these fluctuations are due to thermal cycling. These fluctuations have a basic period of one day, with a secondary period found on seven days. The test article is located in a temperature controlled space. However, due to a number of factors, the temperature control system can not maintain a close control on the temperature.

The aged O-ring was thermally aged to accelerate the aging process. The load decay curve shown in Figure 1 was obtained for a specimen that was not loaded during the aging process. Note from the plot that the load values are significantly below those observed in either for tests of either virgin O-ring. A theoretical explanation for this result is not available at this time.
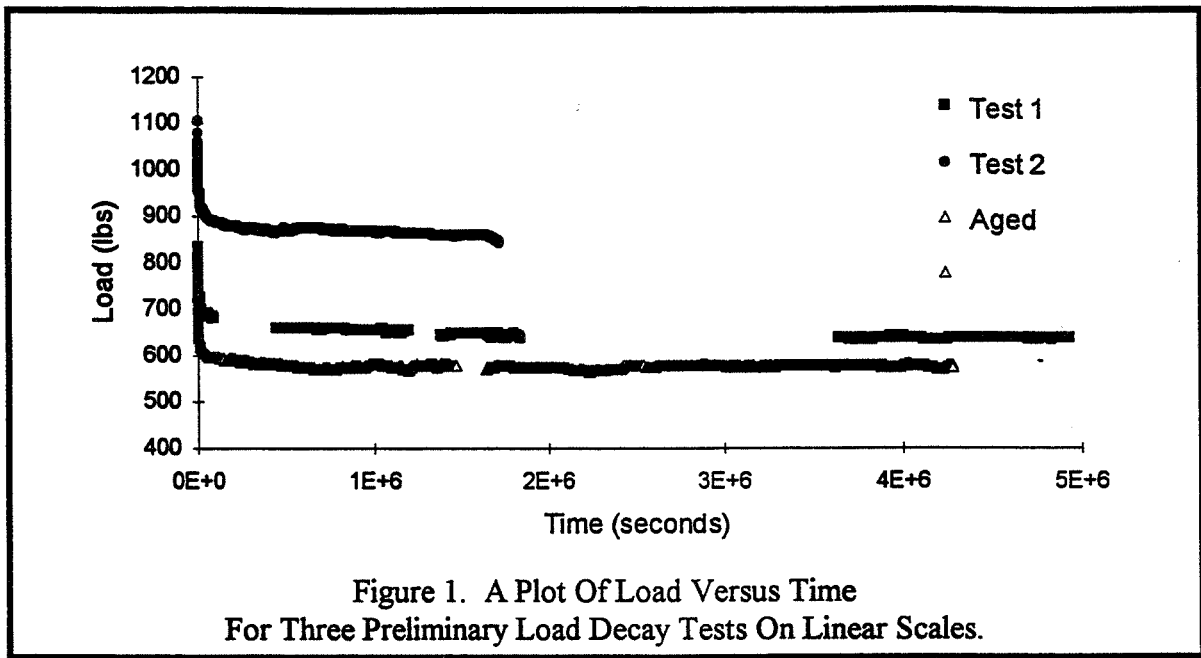
**Figure 1. A Plot Of Load Versus Time
For Three Preliminary Load Decay Tests On Linear Scales.**

Figure 2 shows a plot of the normalized load versus time for the preliminary tests performed on virgin O-rings shown in Figure 1, normalized stress relaxation data (2), and finite element analysis using the stress relaxation data (5). For these plots, the loads measured at each time are normalized with respect to the maximum load. Both the ordinate and abscissa for the plot are logarithmic scales. This figure shows that the results from the two preliminary tests are virtually indistinguishable from one another. Review of the numerical values shows less than one percent difference in the normalized values. These results show that the two load decay tests display the same time dependent behavior in spite of the 23.4% difference in initial load values. Further, one can conclude that what ever the cause of the differences in initial load, it does not affect the time dependent behavior of the seal in this load decay test (at least for the time observed by the test).

Note in Figure 2 that the normalized stress relaxation data curve is consistently below the load decay curves. The stress relaxation data was obtained from uniaxial testing O-ring material (V747) at a strain level roughly comparable to that used in the load decay tests. From other testing of O-ring material it is known qualitatively that the stress relaxation behavior changes with strain level; the rate of decay is faster at lower strain levels and slower at higher strain levels. On the basis of this and load decay test results shown, the operative strain level in the O-ring tested is expected to be above that used to obtain the stress relaxation data. Further, observe in the figure that the curve for the finite element analysis passes through the stress relaxation data. This is as expected from theory as implemented by the ABAQUS finite element code for a constant load analysis (3). On the basis of this conclusion and the foregoing discussion, the finite element analysis does not accurately describe the seal behavior because a proper stress relaxation curve was not available.

Figure 2. A Plot Of Normalized Load Versus Time
For Two Preliminary Load Decay Tests Of Virgin O-rings, Normalized Stress Relaxation
Data (2), and Finite Element Analysis Results (5) On Logarithmic Scales.
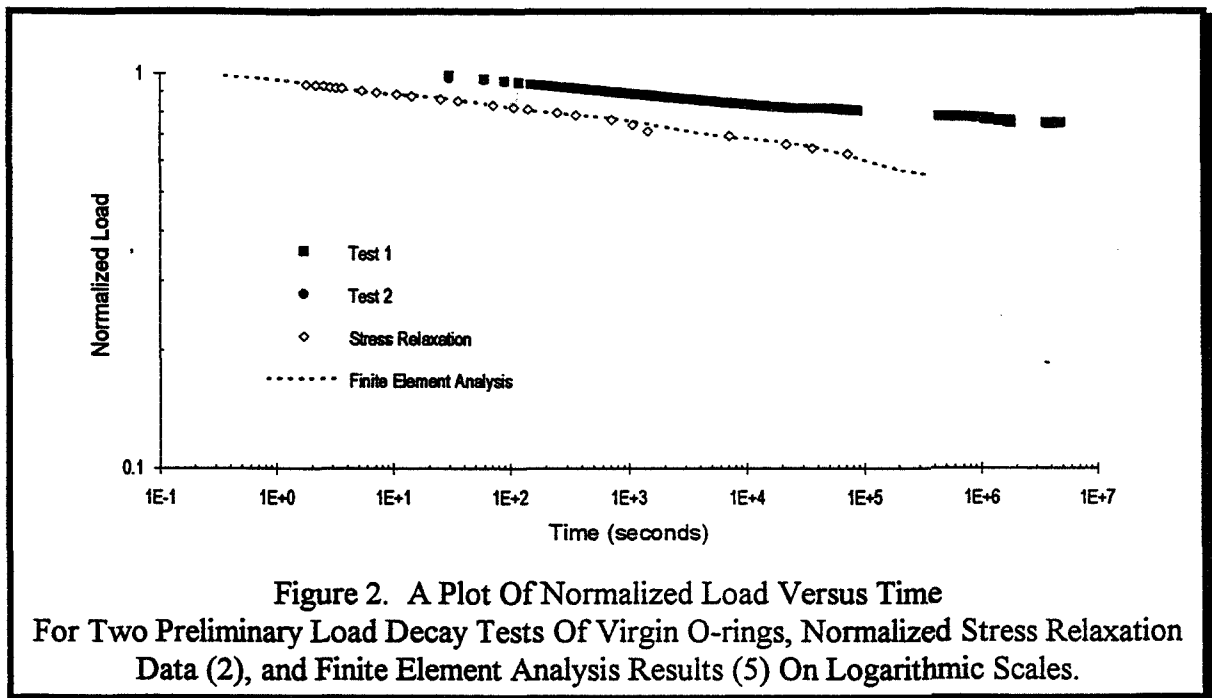
Conclusions

The conclusions from this review of the load decay tests and comparison of experimental results with finite element analysis results are:

1. The load decay tests are repeatable.
2. Minor changes in the test procedure are recommended, i.e., create a reference datum on the test article to ensure alignment is the same from test to test; use a consistent shimming method; and re-evaluate time intervals used between measurements to reduce data file size.
3. Temperature fluctuations should be controlled as much as possible to minimize impact on load decay testing.
4. Another mechanism other than simple stress relaxation is present, causing the load decay response to deviate from results predicted by finite element analysis.
5. Additional data processing capability is needed within EP43 to analyze the test results.

References

1. Bower, M. V., **Seal Life Testing**, NASA/MSFC, 1993.
5. Bowman, D., Internal communication, Parker Seals and NASA/MSFC, 1993.
2. Hibbitt, Karlsson & Sorensen, Inc., **ABAQUS Theory Manual**, Version 5.2, Pawtucket, RI, 1992.
3. Mitchell, B. K. and Flatt, L. W., **Design Parameter Test Plan for MSFC Integrated Seal Test Program**, NASA/MSFC, 1992.
4. Rogers, P., Internal communication, NASA/MSFC, ED24, 1993.

1993

NASA/ASEE SUMMER FACULTY FELLOWSHIP PROGRAM

MARSHALL SPACE FLIGHT CENTER
THE UNIVERSITY OF ALABAMA IN HUNTSVILLE

CAPE for CaPE

Prepared by: Joni Brooks

Academic Rank: Assistant Professor

Institution: Columbia State Community College
Department: Computer Information Systems

MSFC Colleague(s):   Steve Goodman, Ph.D. - NASA
                             Bill Crosson, Ph.D. - USRA

NASA/MSFC:

        Laboratory: Space Science
        Division: Earth Science & Applications
        Branch: Earth System Processes and Modeling

In an effort to improve short-term forecasting for the Kennedy Space Center region, Holle et al. (1992) investigated the effects of low level wind regimes on the distribution of cloud-to-ground lightning in central Florida. With a study period of 455 days, Holle et al. (1992) found "southwest flow contributed 66% of the total network flashes while also occurring on the most days (142)." Relationships among mesoscale thermodynamic variables and precipitation and/or lightning have been addressed in previous studies in Canada (Zawadzki, et al. 1981) and the Tennessee valley (Buechler, et al. 1990). Zawadzki et al. (1981) found "soundings, surface pressure, temperature and humidity obtained from a standard observation network were correlated with rain rates given by raingages and radar." Buechler et al. (1990) found "a fair relationship between CAPE (convective available potential energy) and daily cloud-to-ground activity" with a correlation coefficient of r =0.68. The present research will investigate the relationships among rainfall, cloud-to-ground (CG) lightning, CAPE, and low level wind flow using data collected during the CaPE (Convection and Precipitation/ Electrification Experiment) field program. The CaPE field program was conducted in east central Florida from July 8, 1991 to August 18, 1991.

To investigate low-level wind flow the present research uses the same wind regime classifications defined by Holle et al.(1992). For each day of the study period the mean wind vector was calculated, as described by Watson et al. (1987), from rawinsonde measurements from .3 km to 3 km (1000 ft. - 10,000 ft.). These data were obtained from the Cape Canaveral sounding nearest to 1000(GMT). When Cape Canaveral soundings were unavailable, CLASS soundings from Ti-Co Airport were used. Seven classes were defined as follows; Calm (wind speed <= 2.0 m/s); NE(23° - 113°); SE(113° - 158°); SO(158° - 203°); SW(203° - 293°); NW(293° - 338°); NO(338° - 023°). The phrase 'disturbed sea breeze' will be used to refer to days classified as SW and 'undisturbed' will be used to refer to days classified in the remaining six categories.
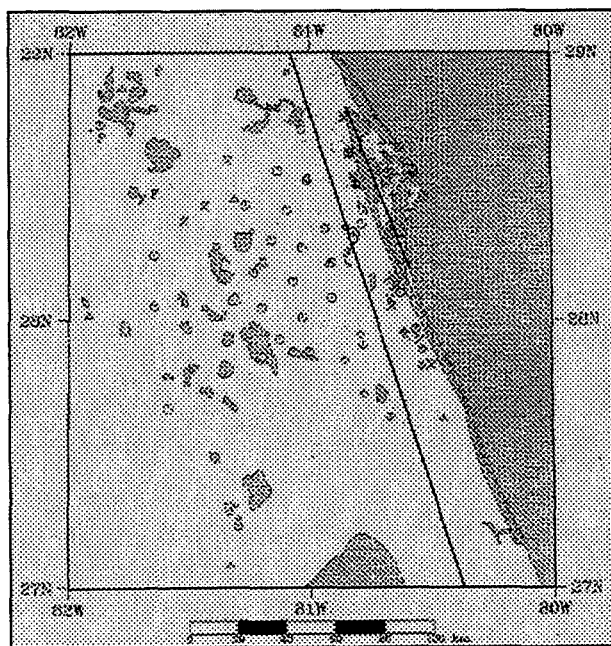
Figure 1

Daily area mean rainfall and rainrate maxima over one hour intervals were obtained from 83 raingages operated during the CaPE field program. The locations of the raingages sites are shown in Fig. 1. In an attempt to assess whether large-scale or local forcing dominates in determining the distribution and amount of precipitation, three subdivisions of the CaPE domain were defined and the number of raingages in each cluster were as follows: Merritt Island cluster - 20 gages; Coastal cluster - 25 gages; and Inland cluster - 38 gages.

Daily lightning frequency was obtained from archive data from the National Lightning Detection Network. Daily lighting frequency was calculated for the entire domain and for each of the three clusters described above. The interval 12Z-12Z was used to define a day for daily lightning frequency and daily area mean rainfall.

The sounding data used to define the day according to wind regime were also used to calculate CAPE and Bulk Richardson Number (R_ib). CAPE is a measurement of instability and is also referred to as available buoyant energy. The Richardson number represents the ratio of buoyant energy input into turbulence to the energy input from the shear of the mean wind flow (Fleagle and Businger, 1980). Calculations of CAPE and R_ib were made using SUDS (System for User-editing and Display of Soundings) software from the Atmospheric Technology Division of the National Center for Atmospheric Research.

In an attempt to determine if CAPE will be a better nowcasting tool than low level wind flow, this study examined the dependence of CAPE on wind direction in the lower troposhere. Fig. 2 is a plot showing this relationship for each Cape Canaveral sounding. A similar plot was created for each sounding at five locations from the CaPE data sets. For each location soundings were plotted according to time of day intervals defined as follows: Morning [0400-1300) GMT; Midday [1300-2100)GMT; and Evening [2100-0400) GMT. In all cases, there does not appear to be a correlation between CAPE and low-level wind flow.
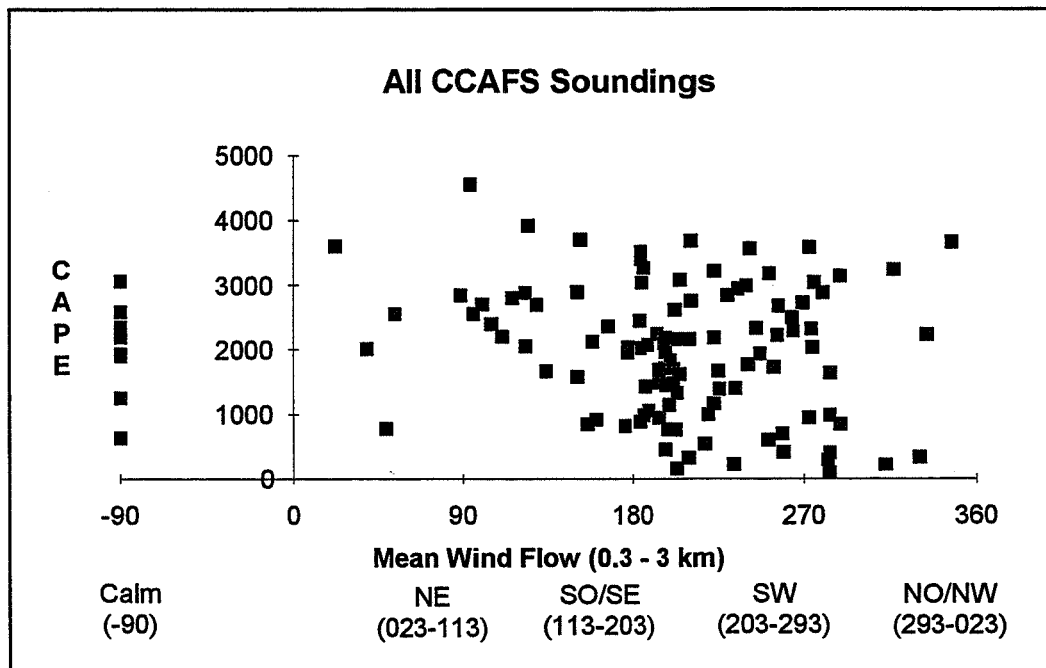
Figure 2

The next analysis attempts to answer the question "What is the correlation among rainfall, lightning, CAPE and R_ib for this study period?" Cape and R_ib were calculated for each day based on the sounding nearest to 1000 GMT from Cape Canaveral or Ti-Co. As shown in Table 1, poor correlations were found between CAPE and both rainfall and

lightning. Similar poor correlations were found when comparing R_ib to both rainfall and lightning.

	CAPE vs. Max. RF	CAPE vs. Mean RF	CAPE vs. Lightning	Mean RF vs. Lightning
Entire Area	-0.22	-0.39	0.05	0.44
Merritt Island	-0.33	-0.34	-0.01	0.44
Coastal Cluster	-0.27	-0.31	0.03	0.62
Inland Cluster	-0.15	-0.36	0.05	0.50

Table 1

The final analysis investigates the relationship among rainfall, lightning and low-level wind flow. Table 2 shows the distribution of CG lightning and rainfall based on low-level wind flow for the entire study area and each of the three cluster areas.

Area	Wind Flow	# of Days	% of Days	Tot. Lgt. Flashes	% of Tot Flashes	Tot. Mean RF(mm)	% of Tot RF
Entire	Disturbed	18	43.90	46132	61.67	124.87	55.52
	Undisturbed	23	56.10	28677	38.33	100.03	44.48
Merritt	Disturbed	18	43.90	679	87.39	107.80	53.33
	Undisturbed	23	56.10	98	12.61	94.34	46.67
Coastal	Disturbed	18	43.90	3833	69.20	141.54	64.86
	Undisturbed	23	56.10	1706	30.80	76.68	35.14
Inland	Disturbed	18	43.90	41620	60.77	122.83	50.38
	Undisturbed	23	56.10	26873	39.23	120.97	49.62

Table 2

For the entire study area 62% of lightning and 55% of rainfall occurred on SW-flow days which made up 43.9% of the study period. For the Merritt Island cluster 87% of the total lightning frequency occured on SW-flow days. These results support the earlier of findings of Holle et al. (1992).

In conclusion, for this study area it appears that the sea breeze propagates instability therefore larger values of CAPE are common. The low-level wind flow seems to be the better tool for nowcasting. Further study of daily rainfall and daily convection zones may increase the understanding of the role of the sea breeze in this study area.

REFERENCES

1. Buechler, D.E., Wright, P.D., and Goodman, S.J., 1990:Lightning/Rainfall Relationships During COHMEX. *Preprints Conf. on Atmos. Electricity.* Kananaskis Provincial Park, Alta, Canada.

2. Fleagle, Robert G. and Businger, Jvost A., An Introduction to Atmospheric Physics, Academin Press, NewYork, 1980.

3. Holle, R.L., Watson, A.I., Lopez, R.E., Howard, K.W., Ortiz ,R., and Li.,L., 1992: Meteorological Studies to Improve Short-range Forecasting of Lightning/Thunderstorms within the Kennedy Space Area; *Final Report for Memorandum of Agreement between the Office of Space Flight, NASA and The National Severe Storms Laboratory*, NOAA, Boulder, Colorado, 4-5.

4. Watson, A.I., Lopez, R.E., Ortiz, R., and Holle, R.L., 1987: Short-term forecasting of lightning at Kennedy Space Center based on the surface wind field. Proceedings, Symposium on Mesoscale Analysis and Forecasting Incorporating "Nowcasting," Vancouver, British Columbia, Canada, European Space Agency, Paris, Frace, 401-406.

5. Zawadzki, I., Torlaschi, E., and Sauvageau, R., 1981: The relationship between mesoscale thermodynamic variables and convective precipitation, J. Atmos. Sci., Vol. 38, 1535-1540.

6. Scientific Overview and Operations Plan for the Convection and Precipitation/ Electrification Experiment, National Center of Atmospheric Research, June 1991.

1993
NASA/ASEE SUMMER FACULTY FELLOWSHIP PROGRAM

MARSHALL SPACE FLIGHT CENTER
THE UNIVERSITY OF ALABAMA IN HUNTSVILLE

A REVIEW OF ISEAS DESIGN

Prepared by: Alex Bykat, Ph.D.

Academic Rank: Professor of Computer Science

Institution: Department of Mathematics and Computer Science
                         Armstrong State College
                         Savannah, GA 31419

MSFC Colleague: Dawn Trout

NASA/MSFC:

        Office: Systems Analysis & Integration Lab
        Division: Systems Definition Division
        Branch: Electromagnetics and Environments Branch

1. Introduction.

The Space Station Freedom will offer facilities for experimentation and testing not available and not feasible or possible on earth. Due to a restricted space availability on board, the experimentation equipment and its organization will be frequently changing. This requires careful attention to electromagnetic compatibility between experimentation and other SSF equipment. To analyze the interactions between different equipment modules, a software system ISEAS [6] is under development.

Development of ISEAS was approached in two phases. In the 1st phase a PC version prototype of ISEAS was developed. In the 2nd phase, the PC prototype will be adapted to a VAX range of computers. The purpose of this paper is to review the design of the VAX version of ISEAS, and to recommend any suitable changes.

2. Architecture of ISEAS.

ISEAS consists of the following components: interactive interface, analysis module, output module, and data base containing data used by analysis routines. ISEAS user communicates via the interface his requests for analysis instances, types of analysis result displays, and supplies appropriate data. The interface will be implemented using ORACLE/SQL relational database environment running on a VAX platform. User's requests are passed to the control module which performs the analysis. The analysis routines will be implemented in C. The output module offering different ways of result's presentation will be implemented in Fortran. The data base will be created using the services of the ORACLE/SQL running on a VAX platform.

3. Design methodology

ISEAS is to be developed using a structured software approach [3, p.4]. Structured methodology offers a methodical approach to development, yielding good system design, correct and efficient data model, smooth implementation, and a basis for ease of maintenance. The methodology spans a whole software life cycle which consists of essentially sequential phases: Project initiation, Requirements elucidation, Feasibility study, System Analysis, System Design, Implementation, Testing, Installation, and finally System Review. Once fielded, the System Maintenance follows.

The review is limited to Analysis and Design Stages. The purpose of the Analysis stage is to consider what is to be done and what are the system's data requirements, while the purpose of the Design stage is to consider how it is to be done.

3.1   Deliverables

At each of the Software Life Cycle stages, structured software methodology

predicates a number of deliverables. The System Analysis stage requires the following deliverables: 1) Context Diagram which presents a top level design of the system addressing its purpose and main functions, 2) Data Flow Diagrams which present processes within the system, functions that system will perform, and flow of data as these processes and functions are invoked, 3) Data models expressed via Entity Relationship Diagrams (ERD) which present the various data entities and relationships that are recognized by the system, 4) Decomposition Diagrams which present the logic of the system through hierarchical structure of the modules of the system. The System Design stage requires: 1) Transition Diagrams which present a reorganized Decomposition Diagrams after taking into account the module types in addition to their functionality, 2) Structure Charts which present the structure of system modules and their data interfaces, 3) Pseudocode or Action Diagrams which present the actions defining the modules.

3.2   Data Normalization

A Relational Database consists of data items, relations among them and operations that can be applied. Whereas "primitive" operations are defined by a chosen relational database -- in ISEAS case it is ORACLE -- definitions of relations are left to the system designers. To assure efficiency, to avoid data redundancy and inaccessibility, to protect against data loss, etc., the data must be normalized. It is a common practice to expect the relation tables to satisfy at least the first three (Codd) Normal Forms which present essentially steps for relationship transformation with the aim of assuring elimination of various anomalies (in particular data modification anomalies).

4. Review findings

The following summarizes review findings. A more detailed exposition can be found in [Bykat, 1993].

[3] presents ERD, Structured Charts, and Pseudocode. Omission of the other four items results in missing documentation of modules, inconsistencies, and possibilities for module design improvement. There are violations of the Structured Charts presentation semantics. Pseudo-code for a number of modules is missing.

Database table are presented but show violations of the first three normal forms.

Backup requirements as well as requirements concerning support of local and remote users [2, p.53] have not been addressed.

5   Conclusions.

ISEAS is a needed and timely project. The proposed version offers fundamental

capabilities but requires further technical (EMC) development and evaluation of the offered capabilities and their functionality. In particular, current calculations view the equipment and their components as "point sources". The size of the equipment, the location of a component within the equipment are not taken into consideration.

EMC analysis recommendations are essentially diadic: pass or fail. This could be addressed by calculations for repositioning the equipment to find a location in which initially failing equipment would pass the EMC criteria. A further extension would be finding optimal configuration of a given equipment for EMC purposes.

6   Recommendations.

The recommendations fall into three categories. The first category relates to the strategy of ISEAS development, the second category relates to technical issues, while the third category presents a path for further development of ISEAS.

6.1   Strategy.

The main goal of the ISEAS project is to provide a tool for evaluation and analysis of EMC for the Space Station Freedom. This goal should be enlarged to "provide a tool for evaluation and analysis of EMC for the EMC community at large and for the Space Station Freedom in particular".

There are a variety of applications where ISEAS (or its descendant) delivered on a workstation platform would be of considerable benefit. Many of these applications are in commercial areas (aircraft manufacturers, land/water-based vehicle manufacturers, etc.), while other are in government agencies (Navy, Air Force, etc). In such applications EMC considerations are important, if not critical (eg. interference with navigational equipment, etc.).

NASA is now at crossroads, searching for ways serve broader national needs". This will lead the agency towards much greater involvement in private sector through attempts to "push technology through the federal door and into commercial market-place"[1]. Such involvement has to be contemplated and planned a priori rather than as an afterthought. ISEAS offers an opportunity for such involvement.

I recommend therefore development of a VAX version in parallel with development of a workstation version of ISEAS operating in a multitasking Unix environment supporting X11 windowing environment, and with a suitable relational database.

---

[1] speech by Rep. Alan Mollohan (D-W.V.) delivered at the 31st Goddard Memorial Symposium, 3/9/93 (Space News, 6/14/1993, p.19)

6.2 Technical.

R1. Develop Data Flow Diagrams and Decomposition Diagrams. Revise and complete Design Phase documentation. Gain: Lead to correct structure of the system.

R2. Complete the normalization of data. Gain: Avoid data modification anomalies.

R3. A user interacts with ISEAS in two distinct modes: define and select. ISEAS code should adopt the same philosophy in presentation of forms and screens for data/request entry. Gain: ISEAS code will be much shorter and much more efficient.

R4. Partial description of entities during data input should not be accepted by ISEAS. Gain: ISEAS code will be much shorter and much more efficient.

R5. Before the input of new data affected files should be preserved as prior versions. Gain: efficient restoration of prior version.

R6. Extend analysis selection capability to allow any combination of analyses to be performed. Gain: Batch mode execution of analyses.

6.3 Future development.

An intelligent object oriented interface for ISEAS should be developed to offer ease of use and functionalities which current version lacks. It should offer a graphical mouse-relocatable component and connectivity icons to aid graphical environment data input, visual validation, and reconfiguration of analyzed environments. It would allow improved presentation of results through a 2-dimensional "interference regions", easing subsequent graphical modification of equipment configurations.

Electro-magnetic compatibility analysis is a ripe candidate for further automation through knowledge based methodology [4, 5]. Development of EASE-MagIC, an Expert Analysis System of Electro-Magnetic Interference and Compatibility, would serve this purpose. Such a knowledge based system can offer evaluations controlled through heuristic rules, on demand instructive explanations of the analysis and its conclusions, and through such explanations -- coupled with the proposed graphical interface -- it would offer a sophisticated tool for EMC training.

7. References.

1. Bykat A., "A detailed look at ISEAS design", NASA TR, 1993

2. BCSS, "Integrated Space Station Freedom Electromagnetic Compatibility Analysis System (ISEAS) VAX Requirements Specification Document (DS04)", NASA ISEASVAX-DS-04-1.0, April 1993

3. BCSS, "Integrated Space Station Freedom Electromagnetic Compatibility Analysis System (ISEAS) VAX Version Design Specification (DS08)", NASA ISEASVAX-DS-08-1.0, June 1993

4. Drozd A.L., "Overview of Present EMC Analysis/Prediction Tools and Future Thrusts Directed at Developing AI/Expert Systems", in IEEE EMC Symposium, Annaheim 1992, pp. 528-529

5. LoVetri J., Henneker W.H., "Fuzzy Logic Implementation of Electromagnetic Interactions Modelling Tool", in IEEE EMC Symposium, Annaheim 1992, pp. 127-130

6. Pearson S.D., Smith D.H., "A System Engineering Approach to Electromagnetic Compatibility Analysis for the Space Station Freedom Program", in EMC Symposium 1991, pp.

1993

NASA/ASEE SUMMER FACULTY FELLOWSHIP PROGRAM

MARSHALL SPACE FLIGHT CENTER
THE UNIVERSITY OF ALABAMA IN HUNTSVILLE

FINITE ELEMENT BASED ELECTRIC MOTOR DESIGN OPTIMIZATION

Prepared by: C. Warren Campbell, Ph.D., P. E.

Academic Rank: Associate Professor

Institution and
Department: The University of Alabama in Huntsville
                            Department of Civil and Environmental Engineering

MSFC Colleague(s):   Charles S. Cornelius
                            Rae Ann Weir

NASA/MSFC:
        Laboratory: Propulsion Lab
        Division: Component Development Division
        Branch: Control Mechanisms and Propellant
                                Delivery Branch

I.   INTRODUCTION

The purpose of this effort was to develop a finite element code for the analysis and design of permanent magnet electric motors. These motors would drive electromechanical actuators in advanced rocket engines. The actuators would control fuel valves and thrust vector control systems. Refurbishing the hydraulic systems of the Space Shuttle after each flight is costly and time consuming. Electromechanical actuators could replace hydraulics, improve system reliability, and reduce down time.

The organization of the code is shown in Figure 1. The motor preprocessor is a routine that does the following:

1) Receives data on the motor geometry, materials, windings, and currents
2) Generates the meshes and elements for the motor for different rotor positions
3) Renumbers the nodes for minimal storage using the minimum degree ordering algorithm
4) Dynamically allocates storage for coefficient arrays for the finite element analysis

The finite element model calculates the magnetic vector potential and stores the results in a file that can be accessed by the postprocessor.

The postprocessor will do the following:

1) Calculate flux densities and field intensities
2) Calculate torques and back emfs for the motor
3) Plot the results

The optimizer will take torques and information from the postprocessor and calculate a general objective function with internal penalty function constraints. Constraints could include magnitude of current densities, motor weight and volume, and cogging torque. Based on previous values of the objective function, the optimizer will select motor geometry for the next iteration. Optimization will continue until the motor design is optimized.

The optimization will begin with an initial motor design and will proceed toward an improved design. Care must be taken in the design of the mesh. Sometimes in finite element structural optimization, a mesh is generated which gives an accurate solution to the initial design, but as optimization proceeds, the mesh becomes too coarse for an accurate solution. Then the "optimized" design is invalid.

Clearly, the code will be very long running. Consider using

FEMOPT CODE ORGANIZATION
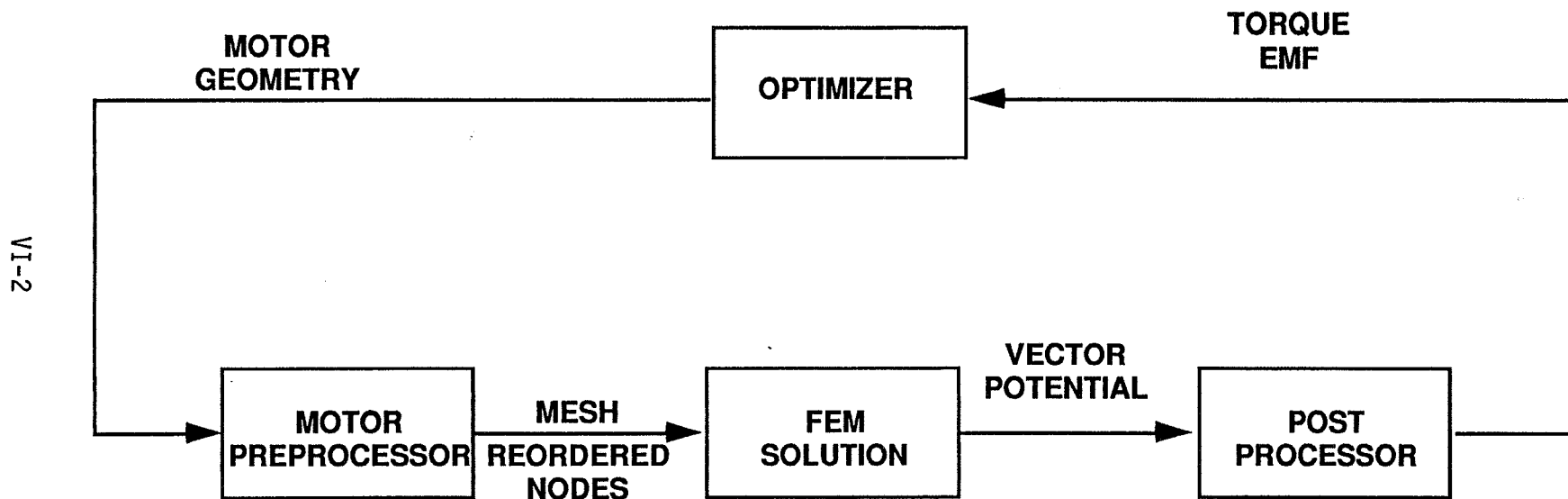
Figure 1. FEMOPT Code Structure

cogging as a constraint. For each value of the objective function the finite element code must find several solutions for different positions of the rotor.

The finite element code developed in this effort was based on the models in Silvester and Ferrari (3). The sparse matrix algorithms were taken from George and Liu (1). The optimizer will be an adaptation of code available from <u>Numerical Recipes in C</u> by Press, et al.(2).

II. APPROACH

The objective of this effort was to develop a finite element code with optimization that could run on a 386- or 486- class machine with up to 15,000 nodes in a two-dimensional problem. Since motors are very long compared to airgap widths and since we will not use rotor or stator skewing of magnets or teeth, the problem can be assumed to be two-dimensional. Also, these goals should be achievable without making users buy thousands of dollars of software.

Because of the ambitious goals for this project, as many of the routines as possible were based on existing code. At the beginning, I did not realize that the code in Silvester and Ferrari (3) was learning code in which coefficient arrays were dimensioned to the maximum number of nodes, that is A(maxnod, maxnod). For a 15,000 node problem (the goal for this effort), the coefficient array alone would require 15,000 by 15,000 = 225 Megawords of storage! For 4-byte words, this is a gigabyte of storage. Clearly, sparse matrix methods are required.

The need for sparse matrix methods significantly slowed the progress of the effort. Even though George and Liu is an excellent reference for solutions of finite element problems and though it has Fortran subroutines in the text, progress was extremely slow. This is because the routines in the text are spaghetti code that are extremely hard to debug and understand. The code uses variables that perform several functions and have values that change in mysterious ways at different places in the program. For these reasons, direct application of the routines would make the code difficult to understand, debug, and maintain. For these reasons, algorithms presented in George and Liu were used to write new code that was understandable, structured, and maintainable.

Borland C and C++ was chosen as the development language for many good reasons. The Borland package is inexpensive(~$300), well documented, and well written. It permits tracing line by line through the code viewing values of any variable at any point. It also allows the setting of breakpoints. The code can be executed to the breakpoints where

each variable of interest can be examined. This capability minimizes debugging effort. C was chosen because of its power. Desirable features include dynamic memory allocation, ability to implement data structures easily while writing readable code, and accessibility of computer graphics capabilities. Dynamic memory allocation means that large arrays can be created as needed, used, and then the memory deallocated for other uses. In C this is done cleanly without impact to any of the desirable features of the code. The same thing can be done in Fortran using equivalence statements, but the process can cause unexpected and untraceable errors in the code.

A strategy was found to be very useful for code development. The first step was to take simple test problems and use Mathcad (a mathematical spreadsheet easy to use and understand) to calculate values of the variables at every point in the execution of a program. With the line-by-line tracing ability of Borland C, values of the variables in the code and those calculated with Mathcad could be compared.

I also adapted an array dynamic allocation strategy from Press, et al. (3). C normally dimensions arrays from 0 to n - 1, where n is the array dimension. By the Numerical Recipes approach, arrays can be allocated from nlow to nhigh where nlow and nhigh are any values with nhigh > nlow. This is very useful in translating Fortran code with arrays dimensioned from 1 to n.

III. SUMMARY

In the first year of this task, work was done on the preprocessor and on the finite element solver. Next year the goal will be to add a nonlinear equation solver, a motor preprocessor, post processor, and optimizer.

IV. ACKNOWLEDGEMENT

Thanks are due to Charlie Cornelius and Rae Ann Weir whose support and encouragement were invaluable.

V.   REFERENCES

1.   George, Alan, and Liu, Joseph W., Computer Solution of Large Sparse Positive Definite Systems, Prentice-Hall, Englewood Cliffs, NJ, 1981.

2.   Press, William H., et al., Numerical Recipes in C, Cambridge University Press, New York, 1990.

3.   Silvester, P. P., and Ferrari, R. L., Finite Elements for Electrical Engineers, 2nd Edition, Cambridge University Press, New York, 1990.

1993

NASA/ASEE SUMMER FACULTY FELLOWSHIP PROGRAM

MARSHALL SPACE FLIGHT CENTER
THE UNIVERSITY OF ALABAMA IN HUNTSVILE

CHARACTERISTICS OF PRODUCTS GENERATED BY SELECTIVE SINTERING AND STEREOLITHOGRAPHY RAPID PROTOTYPING PROCESSES

Prepared By: Vikram Cariapa, Ph.D,P.E.

Academic Rank: Associate Professor

Institution and
Department: Marquette University,Department of
Mechanical and Industrial Engineering.

MSFC Colleague: Floyd E. Roberts III.

NASA/MSFC:

Office: Materials and Processes Laboratory
Division: Non-Metallic Materials and
Processes (EH31)
Branch: Ceramics and Coatings(EH34)

I. INTRODUCTION

The trend in the modern global economy towards free market policies has motivated companies to use rapid prototyping technologies to not only reduce product development cycle time but also to maintain their competitive edge.(1). A rapid prototyping technology is one which combines computer aided design with computer controlled tracking of a focussed high energy source(eg.lasers,heat) on modern ceramic powders, metallic powders,plastics or photosensitive liquid resins in order to produce prototypes or models. At present, except for the process of shape melting (2), most rapid prototyping processes generate products that are only dimensionally similar to those of the desired end product.

There is an urgent need, therefore,to enhance the understanding of the characteristics of these processes in order to realize their potential for production. Currently, the commercial market is dominated by four rapid prototyping processes, namely selective laser sintering,stereolithography, fused deposition modelling and laminated object manufacturing. This phase of the research has focussed on the selective laser sintering and stereolithography rapid prototyping processes. A theoretical model for these processes is under development. Different rapid prototyping sites supplied test specimens (based on ASTM 638-84,Type I) that have been measured and tested to provide a data base on surface finish, dimensional variation and ultimate tensile strength.

Further plans call for developing and verifying the theoretical models by carefully designed experiments. This will be a joint effort between NASA and other prototyping centers to generate a larger database, thus encouraging more widespread usage by product designers.

II. PROCESS CHARACTERISTICS

All rapid prototyping processes start with the development of a CAD model (usually a three dimensional solid model) of the finished part. This model is then "sliced" into different layers starting from the bottom of the part upwards. Each slice is then downloaded to the control computer for the actual creation of the part in the selected rapid prototyping machine.

A schematic view of a selective laser sintering machine is shown in Fig 1. The process is initiated by depositing a thin uniform layer of powder under carefully controlled temperature and atmosphere conditions (3). The levelling drum maintains the thickness of the layer between .003" and .010". The computer controlled laser beam rasters the top surface of
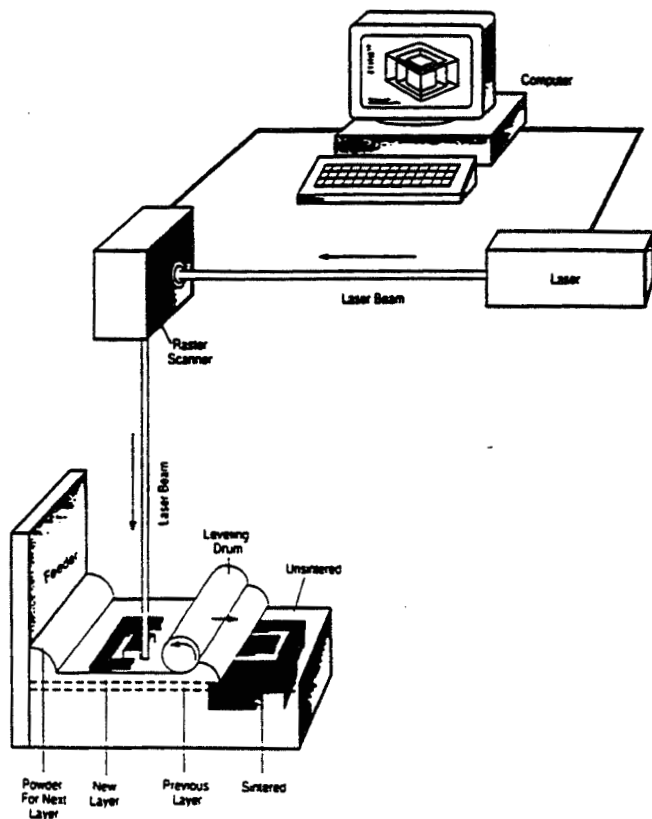
Figure 1. Schematic of Selective Laser Sintering Process.
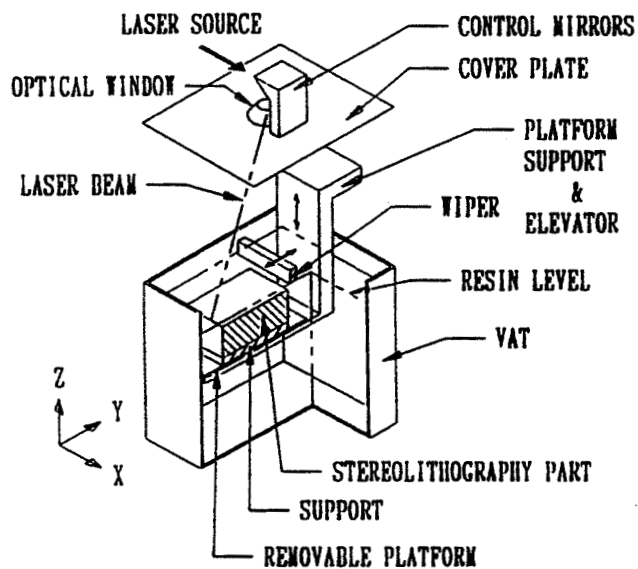
Figure 2   Setup of a Stereolithography Machine.

the powder bed according to the geometry of the "slice that is being processed. A typical diameter for the laser beam is 0.02" and its working output power ranges from 5 W to 50 W. This fuses the powder together at the interface of the beam. The scanning velocity of the laser beam on the surface of the powder ranges from 0.8-2.4 inches/s for metal and ceramic powders to 40 inches/s for polymers and waxes. At the end of the first layer, a second layer of loose powder is deposited and the process continues with the sintering material in the second layer binding to the previous layer. The process continues until the part is completed. Since the laser fuses only powder that it contacts, the finished part may be removed quite easily from the chamber.

A cross section of the stereolithography machine is shown in Fig 2. The process is initiated by raising the platform above the level of the resin by a predetermined amount. After a suitable waiting period, the laser traverses across this thin film to create what is known as a "supports" structure. This structure is created between the desired part and the platform to facilitate part removal without damaging it. The laser contacts the resin and polymerizes it thus creating a semi-rigid form of the desired geometry. The platform lowers below the resin layer for a recoating process and then raises again to a level that is one layer thickness below that of the

again to a level that is one layer thickness below that of the
previous layer, and the laser is activated again to scan the
new layer. This process continues until the support is
completed. The product is created on this support structure in
a similar fashion with the additional step in the process
sequence of moving the wiper across the surface of the resin
to maintain a uniform layer thickness of 0.005" to 0.010"
after each recoating step. In addition, the scanning pattern
may be changed to suit product geometry. After the product is
completed, it is then gently removed from the platform ,the
supports are carefully scraped away and the product is placed
in a post cure chamber for the final curing stage where it
attains its final properties.

III THEORETICAL BACKGROUND
       The principles behind the SLS process (3) indicate that
the lasing action melts the powder and a resulting binding
mechanism is a combination of melting of the powder and
viscous flow of the molten phase. Other contributing factors
include powder particle size and shape,powder properties at
different temperatures,laser power density, and chamber
atmosphere control.

       The SLA process is based on the principle that laser
scanning initiates the release of free radicals in the
photopolymeric resin. A chain reaction that results causes
polymerization of the resin (4,5). Important parameters that
also contribute to this process include hatch spacing, cure
depths, wait time and post cure strategies.

IV EXPERIMENTAL SETUPS
       Tensile test specimens (ASTM D638-84,Type 1) for the SLS
machine were created by Rocketdyne Inc.(CA),using
polycarbonate powder as the raw material. Parameters that were
varied were laser power (low and high), build direction (face
and edge) and use of sealant(no sealant and sealant). Surface
finish, gage length dimensions and ultimate tensile strength
were the obtained for each specimen.

       Similar test specimens made by the SLA process were
obtained from Pratt and Whitney (FL) and DEI (VA). Parameters
that were varied were the build direction (edge, face and
vertical) and layer thickness (0.005" and 0.010").Other
parameters were maintained at their default values.

V. SUMMARY OF THE RESEARCH.
       Since critical information on these two processes is
proprietary the theoretical models require further
development. Testing of the samples has allowed certain
deductions to be made. For example, surfaces of the SLS
process,parallel to the powder bed surface had a superior
surface finish (65 - 520 microinches) than those produced

perpendicular to the powder bed surface (144 - 840 microinches). In addition sealed products had better finishes than unsealed products. Dimensional deviations were in the range of).003" to 0.007". Ultimate tensile strength ranged from 1904 to 5616 psi. A statistical model predicted that the product with the highest strength (5378 psi) could be built with low laser power, flat orientation and be sealed with an epoxy. This was comparable to ASTM D3935-87 for polycarbonate material (5800 psi).

Only the Pratt and Whitney stereolithography samples were statistically satisfactory and generated products with a surface finish range of 42 - 240 microinches. The ultimate tensile strength values ranged from 2263 to 3162 psi (std. dev. range was 94 to 330 psi). Since the standard deviations of tensile strength was large ,no deductions can be made about the contribution of the individual process parameters. Also, since the post processing involved clamping of the parts, surface finish measurements must be treated with caution.

VI. CONCLUSIONS.

Some quantitative measures have been established about the SLS and SLA rapid prototyping processes. Further development on the theoretical models is required in order to enhance the quality of predictions about these processes. The range of parameters in rapid prototyping processes and corresponding variety in materials add complexity to this endeavor. Despite these issues rapid prototyping offers a tangible trend towards reduction in product development times.

VII ACKNOWLEDGEMENTS

VIII REFERENCES

1. Kutay,A.,"Strategic Benefits of Rapid Prototyping Technology", Proceedings of the National Conference on Prototyping, Dayton, OH, June 4-5,1990, pp 101-110.
2. Proceedings of the National Conference on Rapid Prototyping, Dayton, OH, June 4-5, 1990.
3. Bourell,D.L.,Marcus,H.L.,Barlow,J.W.,Beaman,J.J., "Selective Sintering of Metals and Ceramics", International Journal of Powder Metallurgy, v 28, n 4, 1992, pp369-381.
4. Jacobs.P.F. "Rapid Prototyping and Manufacturing", SME Press, Dearborn, MI, 1993.
5. Gatechair,L.R., Tiefenthaler,A.M.,"Depth of Cure Profiling of UV Cured Coatings", Radiation Curing of Polymeric Materials, C.E.Hoyle and J.F.Kinstle, Eds, American Chemical Society, Washington, D.C., 1990.

1993 NASA/ASEE SUMMER FACULTY FELLOWSHIP PROGRAM

MARSHALL SPACE FLIGHT CENTER

THE UNIVERSITY OF ALABAMA IN HUNTSVILLE

PERFORMANCE OF THE ENGINEERING ANALYSIS AND DATA SYSTEM II COMMON FILE SYSTEM

Prepared By: Linda S. DeBrunner, Ph.D.

Academic Rank: Assistant Professor

Institution and Department: University of Oklahoma
                                    School of Electrical Engineering

MSFC Colleagues: Marcellus Graham
                                    Sheila Fogle

NASA/MSFC:

    Office: Information Systems Office
    Division: Systems Development and Implementation
    Branch: Data Systems Branch

Introduction

The Engineering Analysis and Data System (EADS) was used from April, 1986 to July, 1993 to support large scale scientific and engineering computation (e.g. computational fluid dynamics) at Marshall Space Flight Center. The need for an updated system resulted in a RFP (2) in June 1991, after which a contract was awarded to Cray Grumman. EADS II was installed in February 1993, and by July 1993 most users were migrated.

EADS II (3) is a network of heterogeneous computer systems supporting scientific and engineering applications. The Common File System (CFS) is a key component of this system. The CFS provides a seamless, integrated environment to the users of EADS II including both disk and tape storage. UniTree software is used to implement this hierarchical storage management system. The performance of the CFS suffered during the early months of the production system. Several of the performance problems were traced to software bugs which have been corrected. Other problems were associated with hardware. However, the use of NFS in UniTree UCFM software limits the performance of the system.

The performance issues related to the CFS have led to a need to develop a greater understanding of the CFS organization. This paper will first describe the EADS II with emphasis on the CFS. Then, a discussion of mass storage systems will be presented, and methods of measuring the performance of the Common File System will be outlined. Finally, areas for further study will be identified and conclusions will be drawn.

EADS II

EADS II is a high performance computing network supporting scientific and engineering computing. The functions and implementation of EADS II are described in (2) and (3). The two key computing components of EADS II are the Vector Processor Compute System (VPCS) and the Virtual Memory Compute System (VMCS). The VPCS, a Cray Y-MP 8I/6128, is used for applications suitable for vector processing, while the VMCS, an SGI 4D/480, is used for applications with large memory requirements. In EADS I, the predecessor to EADS II, the VPCS needs were met by a Cray X-MP and the VMCS needs were met by an IBM 3084. Image processing applications are supported by the Image Processing System (IPS). The IPS consists of an SGI 4D/480 RE hub with 3 attached workstations. Mini-Supercomputers (MSCs) may be included at a future time to reduce the loading of the VPCS. Although there are no MSCs installed at this time, long term plans include the possibility of including small Cray Y-MP machines (Cray Y-MP 2E) to meet specific laboratory needs. These MSCs would be used for VPCS program development and for smaller applications.

A unique feature of EADS II is the integration of shared resources through the Common Output System (COS) and the Common File System (CFS). The COS provides printing capabilities for the users. Most printing facilities are located in the laboratories, while print queues are maintained on the VMCS. The Common File System (CFS), which provides hierarchical storage to all the EADS II machines, is the most interesting aspect of the EADS II architecture. Restoration of files to disk from tape is automatic. The CFS hardware consists of 2

IBM RS/6000-970 servers, 4 Maximum Strategy Disk Arrays (172 GB total), and 2 STK 4400 automatic cartridge libraries or silos (2.4 TB total). NSL UniTree software is used.

The CFS has 4 principal functions: Private Processor Storage (PPS), User File Storage (UFS), backup storage, and Archival Information Storage (AIS). The PPS consists of rotating magnetic disk storage (RMDS) and is used to store active user programs, operating system software, command procedures, and data. The UFS is RMDS which is allocated to users. The backup storage is used for routine backup of the PPS and UFS to tape. The AIS is used for long-term storage of information. Backup and archive management tools are also provided.

The EADS II computing components and shared resources are connected by a 3-level network. At the lowest level, Ethernet LANs connect systems within a building. Better performance is provided by the High Speed Network Backbone (HSNB), which uses the Fiber Distributed Data Interface (FDDI) technology. The HSNB provides access between central site and remote facilities. There are 2 FDDI rings which are interconnected by routers to each other and the building LANs. The highest level of performance is provided by the Back End High Performance Interconnect (BEHPI) network which is based on UltraNet. The BEHPI is used almost exclusively for moving data between central site computers and the CFS.

Mass Storage Systems

The IEEE-CS Technical Committee on Mass Storage Systems and Technology developed a "reference model" in the eighties which is used by manufacturers of mass storage products to describe the functions of their systems (1, 6). Although the reference model is not an IEEE standard, it is an important consideration in the development of mass storage systems.

The UniTree software is sold to companies by OpenVision (previously by DISCOS). The companies then port the code to their chosen platform. The product chosen to implement the EADS II CFS is NSL UniTree supplied by IBM. Most companies marketing UniTree products make modifications to improve performance or to add features. For example, Control Data Systems focuses on supporting a wide range of peripherals and has tuned their system to improve performance for various peripherals. On the other hand, Convex rewrote portions of the code that control the way the processes communicate. IBM has implemented Multiple Dynamic Hierarchies which allow multiple hierarchies on a single machine. They also have implemented a 3rd party transfer capability, called Network Attached Storage, which allows hosts to send data directly to the disk array without going through UniTree. Several other companies have developed mass storage systems including Epoch storage management tools, NetArchive, and Cray's Data Migration Facility.

Research facilities and universities have pioneered much of the work in the mass storage arena. For example, UniTree was developed at Lawrence Livermore National Laboratory (5). There are currently two mass storage systems developed by research facilities that are of particular interest--NAStore and AFS. NAStore, developed by NASA Ames Research Center, only blocks read operations until the first part of the data is available. So, for large files, access to the first byte of data is significantly faster. The Andrew File System (AFS) was developed by Carnegie-Mellon University to support distributed file access. It has been adapted by the Pittsburgh Supercomputing Center to include mass storage capabilities (4). AFS was chosen

since it is more scalable than NFS. NFS requires clients to communicate with the server to complete each transaction, but AFS maintains state information. Clients assume that they are using the most current version of a file's date until they are notified by a server. However, AFS was developed without consideration for the mass storage reference model.

Measuring the Performance of the Common File System

Three measurements of the CFS performance are currently being collected. All of these measurements are similar. Each measures the time required to perform several operations. None of these metrics generates statistics which can be readily compared to the expected performance or the performance of other systems. The principal function of these measurements is to identify degraded system performance relative to past system performance.

Every 10 minutes, Boeing Computer Support Services (BCSS) runs a script which checks for degraded system performance. This "10-Minute Metric" script measures the time required to change to a UniTree subdirectory ("cd") and list the directory contents ("ls"). In addition, Cray Grumman runs the "UNITREE Metric" hourly. Like the 10-Minute Metric, this metric measures the time required to perform simple file manipulations. It measures the time required to perform "ls", "ls -l", and to "tail" a file. Cray Grumman also runs a program every 3 minutes to check for degraded performance of the CFS. At this time, different programs are run on the VMCS and the VPCS. On the VPCS, the "3-Minute Metric" program measures the time required to open a file in a UniTree subdirectory and write a line to it. The corresponding program on the VMCS provides more complete information. It measures the number of NFS users, performs simple operations using NFS, and performs simple operations using FTP. Using NFS, the program performs a directory listing and copies a small file to a UniTree subdirectory. Using ftp, it "puts" a file in a UniTree subdirectory, performs a directory listing, and deletes the file. These measurements are inadequate for evaluating the overall performance of the CFS. A performance measurement tool is needed to allow EADS II to be compared to other systems.

Areas for Further Study

Several areas have been identified for future work. The most important is the development of a performance measurement tool. After measurement capabilities are developed, UniTree can be tuned to improve its performance in the EADS II environment.

The lack of knowledge about parallel processing on the SGI should also be remedied. By understanding the differences between parallel processing on the Cray and the SGI, users could be advised about the execution of their applications which are suited to parallel implementation. This should allow more users to use the SGI effectively.

Finally, a method of modeling networked computer systems should be investigated. This modeling would allow performance to be predicted before changes are made. Consequently, the effects of hardware changes and software load changes could be evaluated in a "what if" format.

Conclusions

The EADS II mass storage requirements are aggressive. Existing products have shortcomings with respect to these requirements. Since the EADS II CFS requires the most current technology, the efforts of the Storage System Standards Working Group will effect the future of mass storage technology. Awareness of standards will give system architects a better understanding of mass storage systems.

Current methods of measuring the performance of EADS II are inadequate. In the future, more meaningful measurements will be needed. As a beginning, EADS II should be evaluated using the tests run at Ames Research Center. In addition, a performance measurement tool tailored to the needs of EADS II should be developed. This tool will allow system administrators to evaluate the effects of hardware and software modifications, as well as changes in loading. It will also support comparisons with other mass storage systems.

Methods for modeling the system are needed to predict the effects of system modifications before implementation. Such a model will also support the analysis of predicted changes in loading. The model would allow various scenarios to be considered to choose the best solution.

Acknowledgment

References

(1) Coyne, R. A., "An Introduction to the Mass Storage System Reference Model, Version 5," *Proceedings of the Twelfth IEEE Symposium on Mass Storage Systems,* Monterey, California, April 26-29, 1993, pp. 47-53.

(2) *Engineering Analysis and Data System II (Class VII Computer System), Request for Proposal,* MSFC, NASA, RFP #8-1-9-AI-00120.

(3) *Engineering Analysis and Data System II Users Guide,* MSFC, NASA.

(4) Goldick, J. S., Benninger, K., Brown, W., Kirby, C., Maher, C., Nydick, D. S., Zumach, B., "An AFS-Based Supercomputing Environment," *Proceedings of the Twelfth IEEE Symposium on Mass Storage Systems,* Monterey, California, April 26-29, 1993, pp. 127-132.

(5) McClain, F., "DataTree and UniTree: Software for File and Storage Management," *Proceedings of the Tenth IEEE Symposium on Mass Storage Systems,* Monterey, California, May 7-10, 1990, pp. 126-128.

(6) Miller, S. W., "A Reference Model for Mass Storage Systems," *Advances in Computers,* Vol. 27, Yovits, M. C., editor, pp. 157-210.

1993

NASA/ASEE SUMMER FACULTY FELLOWSHIP PROGRAM

MARSHALL SPACE FLIGHT CENTER
THE UNIVERSITY OF ALABAMA IN HUNTSVILLE

WATER CYCLE RESEARCH ASSOCIATED
WITH THE
CaPE HYDROMETEOROLOGY PROJECT (CHymP)

Prepared by: Claude E. Duchon, Ph.D.

Academic Rank: Professor

Institution: University of Oklahoma
Department: School of Meteorology

MSFC Colleague: Steven J. Goodman, Ph.D. - NASA

NASA/MSFE:
    Laboratory: Space Science
    Division: Earth Science and Applications
    Branch: Earth System Processes and Modeling

I. Introduction

One outgrowth of the Convection and Precipitation/Electrification (CaPE) experiment that took place in central Florida during July and August 1991 was the creation of the CaPE Hydrometeorology Project (CHymP). The principal goal of this project is to investigate the daily water cycle of the CaPE experimental area by analyzing the numerous land and atmosphere in situ and remotely sensed data sets that were generated during the 40-days of observations.

The water cycle comprises the atmospheric branch and the land branch. In turn, the atmospheric branch comprises precipitation leaving the base of the atmospheric volume under study, evaporation and transpiration entering the base, the net horizontal fluxes of water vapor and cloud water through the volume and the conversion of water vapor to cloud water and vice-versa. The sum of these components results in a time rate of change in the water vapor or liquid water (or ice) content of the atmospheric volume. The components of the land branch are precipitation input to and evaporation and transpiration output from the surface, net horizontal fluxes of surface and subsurface water, the sum of which results in a time rate of change in surface and subsurface water mass. The objective of CHymP is to estimate these components in order to determine the daily water budget for a selected area within the CaPE domain.

This work began in earnest in the summer of 1992 and continues. Even estimating all the budget components for one day is a complex and time consuming task. The discussion below provides a short summary of the rainfall quality assessment procedures followed by a plan for estimating the horizontal moisture flux.

II. Daily Rainfall

The first step in any data analysis is to assess the quality of the data. With respect to the precipitation data, a quality assessment program began in June, 1992 and has taken one year to complete. Through this program reliable measurements of daily rainfall are now available for 212 raingages, most of which are in the area bounded by 27° and 29°N and 80° and 82°W. Fig. 1 shows the gage locations that resulted and the associated sponsors. Some of the raingages were operated specifically for the duration of the CaPE experiment and others were (and still are) continuously maintained by federal and state agencies and individual cooperators.

III. Water Vapor Flux

The estimation of atmospheric horizontal water vapor flux requires analyzing both rawinsonde and satellite data. The sounding sites, identified by hexagons in Fig. 1, are located within and around the water budget area (outlined by heavy line). The satellite data come from two sources, AVHRR on the NOAA polar orbiting satellites and VAS (VISSR Atmospheric Sounder) on GOES-7. The objective is to produce estimates of the divergence of water vapor flux every three hours for selected sequences of days. The plan for estimating the water vapor flux is outlined below.

In the early part of the CaPE experiment numerous problems arose with CLASS (Cross-Loran Atmospheric Sounding System) soundings so that only from 20 July to 12 August are

All Raingages - 212
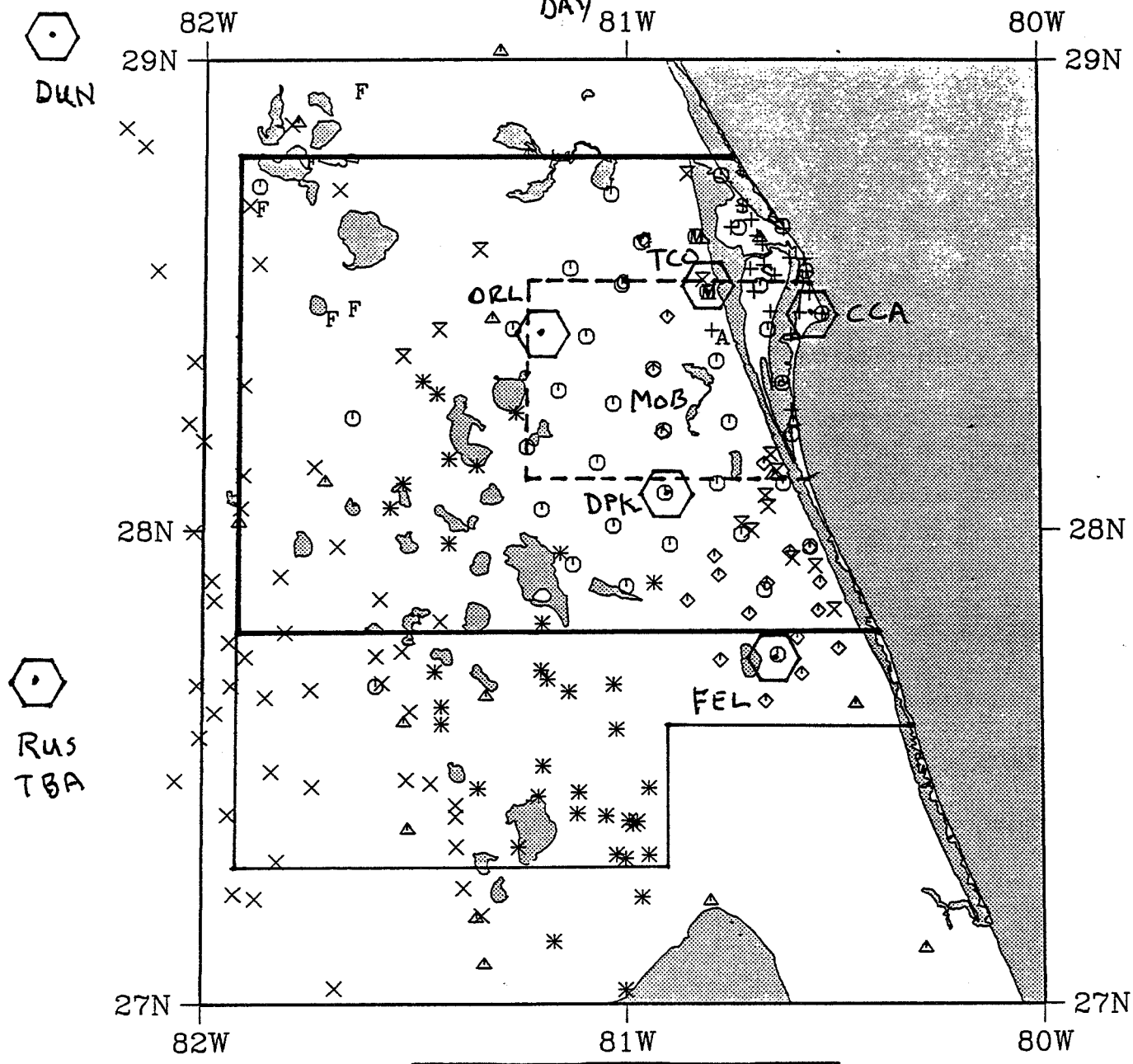
+	KSC/TRMM - 20	×	SWFWMD - 50
⋈	USGS - 14	A	USDA - 1
◇	USJRB - 19	M	MSFC - 2
△	NWS USAF - 20	G	U GA - 2
*	SFWMD - 3	S	FSU - 2
☉	PAMII - 40	F	U Fla - 5

there an adequate number of high quality soundings available for analysis. The time of soundings is linked to studies of large scale and small scale weather systems. The four outer CLASS sites (Dunnellon, Ruskin, Fellsmere and Daytona Beach) are connected to the large scale with 5 daily soundings taken every 3 hours beginning at 1100 UTC and ending at 2300 UTC. Soundings at Fellsmere and Dunnellon were taken also at 0800 UTC. The Deer Park and Tico Airport locations as well as the mobile CLASS unit were part of the small scale weather system study so that soundings were taken at variable times related to the current daytime storm activity. Cape Canaveral Air Force Station, Orlando and Tampa provided numerous additional soundings, mainly during daytime. During the 24 day period the number of soundings per day ranged from 28 to 48 with the vast majority of the soundings between 1000 and 2400 UTC. The maximum number of soundings between 0000 and 1200 UTC was 5 on one day; typically there were 2. Accordingly, there is a large gap in radiosonde coverage for this 12 hour period.

For many reasons, sondes are not always released at the scheduled time. Also, as noted, some stations have no set schedule. Thus, in order to develop a 3-hourly moisture and wind fields a scheme to incorporate data from surrounding times has to be developed.

Within the 24 day period noted above there are comparatively few days in which data are more or less continuously available from all observational systems--the optimal situation for calculating the daily water budget. Based on the following criteria each day was rated on a scale of 1 (poor) to 5 (good):

a. number of hours of WSI radar coverage given that it is raining (based on gages).

b. percent cloud cover around 1200 UTC derived from visual inspection of GOES visible imagery.

c. total number of atmospheric soundings and the number between 0000 and 1000 UTC.

d. number of times data from the 11μm and 12μm split-window channels on GOES-7 VAS (VISSR Atmospheric Sounder) are available.

e. number of hours of profiler winds.

The larger the value for each criterion, the higher the rating for that day. At this writing the split-window criterion has not been invoked because the selection of data to be ordered is in progress. Based on the remaining criteria the best periods are 26-30 July and 7-9 August.

A rawinsonde provides vertical profiles of wind and water vapor content which begin at a specific time and location at the surface. As the balloon rises its horizontal position changes in response to the wind field. If we consider 400 mb (about 7.5 km) to be the upper level of moisture calculation, which corresponds to about 98% of the integrated water content (IWC), and a balloon rise rate of 5 ms^{-1}, it will take 1400 seconds (23 minutes) to reach that altitude. With an average wind speed of 10 ms^{-1}, the drift will be 14 km. This is a significant fraction of the water budget analysis area so that, in general, balloon position must be taken into account. In addition, an accounting of time differences between soundings must be made.

The first step in rawinsonde data reduction is a vertical interpolation of each sounding to evenly spaced σ levels ($\sigma = P/P_{sfc}$). A resolution of $\Delta\sigma = 0.01$ (≈ 10 mb) will provide 40 levels of wind and water vapor content. Next, the data at each level are linearly interpolated in time and horizontal distance with data from the previous or following ascent to a common time. The result of the interpolations in space and time should be that all data for each level are valid at a single time.

The next step is to perform an objective analysis of the wind and water vapor content on each of the 40 σ-surfaces such that the gridded analysis extends beyond the water budget area. At this point information from VAS and AVHRR will be incorporated into the analysis. Gridded fields of IWC will be obtained using the physical split-window (PSW) technique developed by Dr. Gary Jedlovec at MSFC. The idea is to vertically distribute the VAS- and AVHRR- derived IWC at the same grid points as above according to the water content profile at those grid points derived through linear interpolation from the rawinsonde locations, as discussed above. The reason for incorporating satellite-derived IWC is to provide improved estimates of water content between rawinsonde stations. This may be especially important if there are significant spatial variations of IWC.

The final step is to integrate the moisture flux normal to the boundary around the exterior of the water budget at each level. The summation over all levels is equal to atmospheric water vapor divergence for that time. Assuming that 3-hourly estimates are available they are then summed to obtain the divergence for that day.

IV. Conclusion

After one year of quality assessment, a credible 42 day set of daily rainfall data for 212 stations has been produced. Thus the daily area-average precipitation component of the atmospheric branch has been essentially completed.

A strategy has been formulated to analyze the horizontal flux of water vapor employing rawinsonde and satellite data. Priority time periods have been selected so that satellite data can be now ordered. It is anticipated that the creation of a 3-dimensional grid of moisture and wind will be developed at OU and coordinated with Dr. Bill Crosson at MSFC. IWC data files will be produced by Drs. Jedlovec, Guillory and Crosson at MSFC.

V. Acknowledgments

Many thanks to Dr. Crosson and Joni Brooks for their major contributions to the raingage quality assessment and stimulating discussions on the water vapor analysis.

1993

NASA/ASEE SUMMER FACULTY FELLOWSHIP PROGRAM

MARSHALL SPACE FLIGHT CENTER
THE UNIVERSITY OF ALABAMA IN HUNTSVILLE

FOIL BEARINGS

Prepared By: David A. Elrod, Ph. D.

Academic Rank: Assistant Professor

Institution and Department: The University of Alabama in Huntsville
                            Mechanical and Aerospace Engineering Department

MSFC Colleague: Henry P. Stinson

NASA/MSFC:

    Laboratory: Propulsion
    Division: Component Development
    Branch: Turbomachinery

INTRODUCTION

The rolling element bearings (REB's) which support many turbomachinery rotors offer high load capacity, low power requirements, and durability. Two disadvantages of REB's are:

- rolling or sliding contact within the bearing has life-limiting consequences; and
- REB's provide essentially no damping.

The REB's in the Space Shuttle Main Engine (SSME) turbopumps must sustain high static and dynamic loads, at high speeds, with a cryogenic fluid as lubricant and coolant. The pump end ball bearings limit the life of the SSME high pressure oxygen turbopump (HPOTP). Compliant foil bearing (CFB) manufacturers have proposed replacing turbopump REB's with CFB's. CFB's work well in aircraft air cycle machines, auxiliary power units, and refrigeration compressors. In a CFB, the rotor only contacts the foil support structure during start up and shut down. CFB damping is higher than REB damping. However, the load capacity of the CFB is low, compared to a REB. Furthermore, little stiffness and damping data exist for the CFB. A rotordynamic analysis for turbomachinery critical speeds and stability requires the input of bearing stiffness and damping coefficients.

The two basic types of CFB are the tension-dominated bearing (Figure 1) and the bending-dominated bearing (Figure 2). Many investigators have analyzed and measured characteristics of tension-dominated foil bearings, which are applied principally in magnetic tape recording. The bending-dominated CFB is used more in rotating machinery.

This report describes the first phase of a structural analysis of a bending-dominated, multileaf CFB. A brief discussion of CFB literature is followed by a description and results of the present analysis.
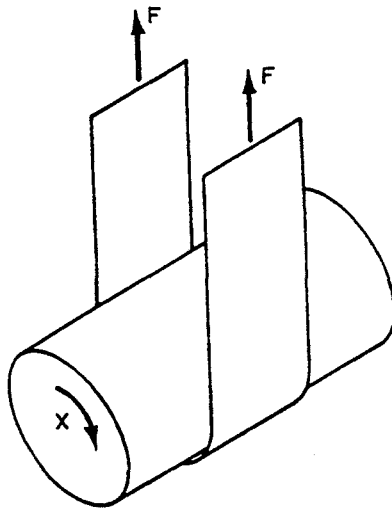
Figure 1. Tension-dominated foil bearing
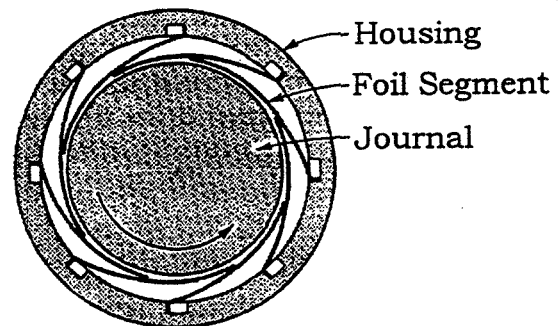
Figure 2. Bending-dominated foil bearing

ANALYSIS

Most of the analyses of bending-dominated CFB's have the following common characteristics:

- fluid inertia effects are considered negligible;
- the fluid film is compressible (as in most applications); and
- the equations for the compliant walls and fluid film are coupled in an iterative solution.

In addition, some investigators declare that the foil leaves in a multileaf CFB are more important than the fluid film in determining:

- bearing stiffness and damping;
- load capacity as a function of eccentricity;
- preload between the leaves and journal; and
- startup torque.

In a rocket engine turbopump application, the fluid film is incompressible, and inertia effects may be appreciable. However, the present model is an analysis of the multileaf structure only.

In a manner similar to the analyses of Oh and Rohde (1) and Trippett, Oh, and Rohde (2), the present model first solves for the assembly of overlapping leaves in the bearing housing. The solution is iterative, and is a function of the bearing housing radius r_b, the radius of curvature of the pre-formed leaves r_l, and the number of leaves n_l. Figure 3 shows the result for an input of $r_b = 0.8125$ inch, $r_l = 0.915$ inch, and $n_l = 8$. For a valid solution, the distance from the center of the bearing housing to the end of a leaf must equal the distance from the center to a point on the leaf $2\pi/n_l$ radians away.
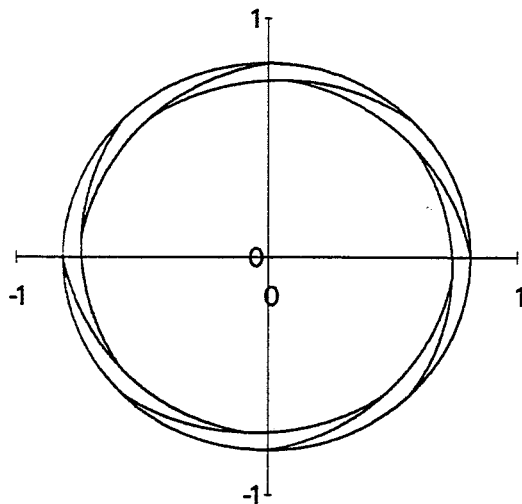
Input data:	
Leaf radius	0.9150 inch
Housing radius	0.8125 inch
Leaf length	1.102 inches
Number of leaves	8

Figure 3. Compliant foil bearing assembly, no rotor

After the foil leaves are assembled in the housing, rotor installation requires deformation of the leaves. The forces deforming the leaves are the rotor forces and leaf reaction forces. The constraints for rotor installation are:

- the minimum distance from the bearing housing center to the leaf is equal to the rotor radius;
- the distance from the housing center to a point on the overlapping part of one leaf must be less than the distance to the "overlapped" part of the next leaf; and
- the leaves can only push (not pull) on one another at contact points.

The application of Castigliano's theorem provides compliance functions which relate the deflection of each point on a leaf to rotor forces and leaf forces. The foil leaves are curved beams with one end fixed. The additional input data required for calculating the effect of rotor installation are the rotor radius r_r, the second moment of the area of the leaf cross section I, and Young's modulus for the leaf material E. The analysis calculates the rotor force required to satisfy the above list of constraints. Figure 4 is a plot of the housing center to leaf distance before and after installation of a 0.7885 inch rotor into the foil bearing of Figure 3. The leaves in the analysis are one inch wide, 0.006 inch thick, with a Young's modulus of 30 Mpsi. The arrows on the "after" leaf represent the locations of the forces required to install the leaf. Figure 5 shows the geometry of the bearing with the rotor installed.
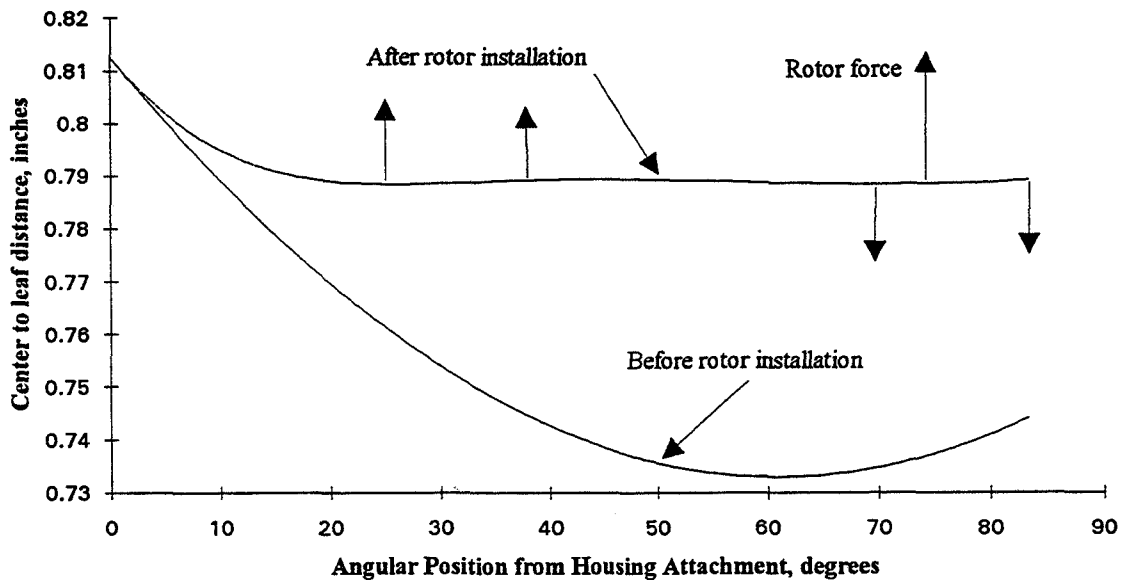
Figure 4. Compliant foil bearing - leaf distance from housing center

CONCLUSIONS

This report describes an analysis of the geometry of a multileaf, compliant foil bearing. The analysis solves for the assembly of preformed leaves in a bearing housing, and the installation of a rotor in the assembly. The analysis will be modified to include interleaf

friction forces, leaf backup support options, and an analysis of the deflection of the rotor due to an applied load. Predictions will be compared to MSFC test data. Future developments will include the interaction of the bearing fluid film.
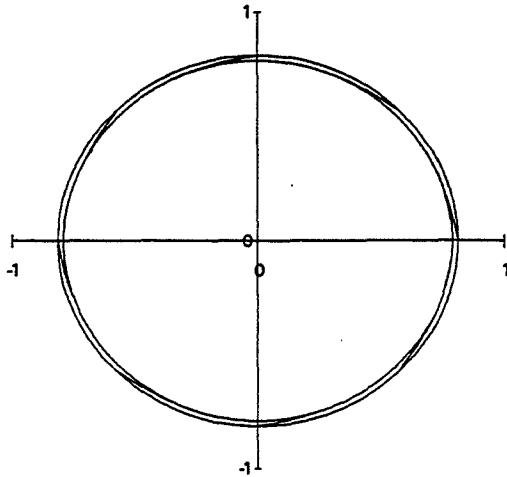
Input data:
Leaf radius	0.9150 inch
Housing radius	0.8125 inch
Leaf length	1.102 inches
Number of leaves	8
Rotor radius	0.7885 inch
I (area moment)	$1.8E-8$ in^4
E (Young's mod)	30E6 psi

Rotor force
0.72 lbf at 74 degrees
Leaf forces
0.39 lbf at 38 and 83 degrees
0.45 lbf at 25 and 70 degrees

Figure 5. Compliant foil bearing, rotor installed

REFERENCES

(1)   Oh, K. P., and Rohde, S. M., "A Theoretical Investigation of the Multileaf Journal Bearing," *ASME Journal of Applied Mechanics*, Vol. 98, No. 2, June 1976, pp. 237-242

(2)   Trippett, R. J., Oh, K. P., and Rohde, S. M., "Theoretical and Experimental Load-Deflection Studies of a Multileaf Journal Bearing," *Topics in Fluid Film Bearing and Rotor Bearing System Design and Optimization*, 1978, pp. 130-156

N94-24416

NASA/ASEE SUMMER FACULTY FELLOWSHIP PROGRAM

MARSHALL SPACE FLIGHT CENTER
THE UNIVERSITY OF ALABAMA IN HUNTSVILLE

DESIGN AND SPECIFICATION OF A CENTRALIZED MANUFACTURING DATA MANAGEMENT AND SCHEDULING SYSTEM

Prepared By:	Phillip A. Farrington
Academic Rank:	Assistant Professor
Institution and Department:	The University of Alabama in Huntsville
	Department of Industrial and Systems Engineering
MSFC Colleagues:	Paul Gill and Eutiquio Martinez
Laboratory:	Materials and Processes
Division:	Fabrication Services
Branch:	Process Automation & Modeling

Introduction

As was revealed in a previous study [1] the Materials and Processes Laboratory's Productivity Enhancement Complex (PEC) has a number of automated production areas/cells that are not effectively integrated, limiting the ability of users to readily share data. The recent decision to utilize the PEC for the fabrication of flight hardware [2] has focused new attention on the problem and brought to light the need for an integrated data management and scheduling system. This report addresses this need by developing preliminary design specifications for a centralized manufacturing data management and scheduling system for managing flight hardware fabrication in the PEC.

This prototype system will be developed under the auspices of the Integrated Engineering Environment (IEE) Oversight team and the IEE Committee. At their recommendation the system specifications were based on the fabrication requirements of the AXAF-S Optical Bench.

AXAF-S Optical Bench - Production Requirements

AXAF-S has a number of parts and components of which the Optical Bench Assembly is a key structural element. As shown in Figure 1 the Optical Bench Assembly consists of four primary components: the telescope tube, the telescope cone, the mounting pads, and the star tracker mounts. All of these, except the titanium mounting plates, will be fabricated from graphite cyanate composite materials. It is anticipated that all components will be fabricated in the PEC.

Optical Bench Assembly

Telescope Tube | Telescope Cone | Mounting Pads [2] | Star Tracker Mounts (2)

Titanium Mounting Plates [2] | Composite Mounting Pads [2]
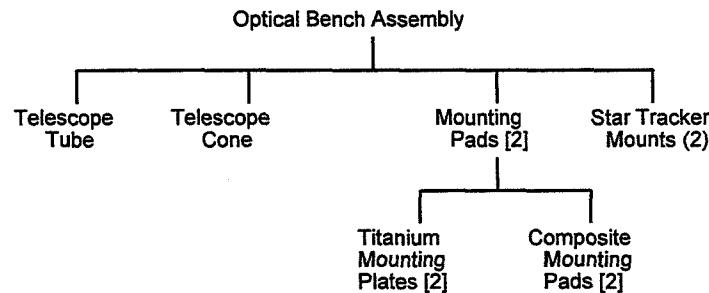
Figure 1: Bill of Material for Optical Bench Assembly

Analysis of preliminary process plans indicates that five work areas will be required to fabricate and assemble the optical bench. The work areas utilized in 4707, as illustrated in Figure 2, include the fiber placement machine, the hand lay-up area, the autoclave(s), the automated ultrasonic test system and an as yet undefined assembly area. The machine shop in 4705 will also be required, however, it will not be directly linked to the system. Instead the scheduling system, described in this document, should have the capability to pass data to and receive data from the Integrated Manufacturing Planning and Control System (IMPACS) used by NASA planning personnel (EH52).
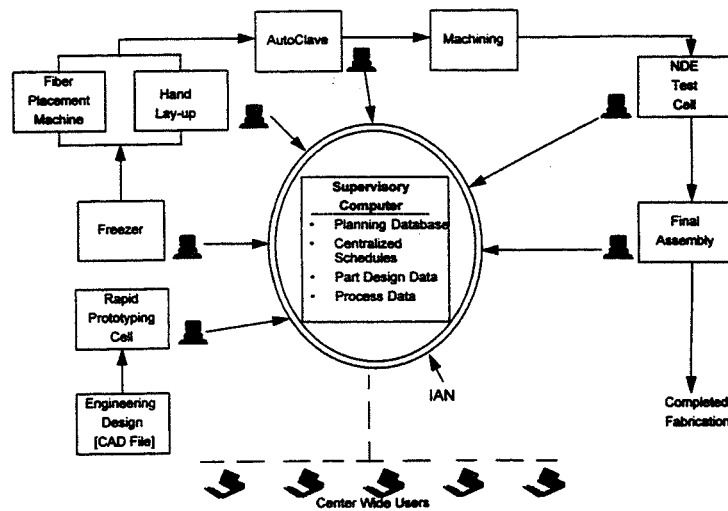
Figure 2: Centralized Data Management and Scheduling System for
Productivity Enhancement Complex

Note that in addition to the five fabrication cells two additional workstations
will also be linked to the centralized server. The SLA 250 - Stereolithography
machine and a composite material freezer in 4707 used for storage of the
graphite cyanate material for the optical bench. The SLA 250 was included
because it may be used extensively in the early stages of design and prototype
development. The link for the freezer was included in order to implement a
inventory management system for monitoring composite material usage.

The choice of hardware and software platforms were driven primarily by the
current systems in use at MSFC and the prevailing move away from mainframe
computing systems. MS-DOS based PC's were chosen as the hardware platform
because of their capability and cost effectiveness. In order to minimize overall
system costs it is recommended that existing hardware be used where possible.
The basic configuration should be an upgradeable 386 or 486 based PC with 8
megabytes of RAM, a 100-200 Mb hard disk drive, 2 floppy disk drives, MS-DOS
5.0 and Windows 3.1. Given the choice of PC's as the hardware platform it is
recommended that Novell Netware be chosen as the networking platform. Novell
was selected because of its extensive use throughout MSFC and its proven
performance capabilities.

This system will require the integration of a scheduling system and a relational
database management system. It is recommended that the scheduling system be
developed using Microsoft Project, a Microsoft Windows based scheduling
package and that Oracle be the choice for the relational database management
system. Both packages were pragmatic choices because of there widespread use
throughout MSFC. MS-Project is available on WPS and is the scheduling
package of choice for the AXAF-S program office. Likewise Oracle was chosen
because it is currently used for other applications, such as the IMPACS system
used by EH52 (Planning and Control Branch) and the 4707 Tool Crib Inventory

system, which could be integrated with the PEC system in the future. Overall, MS-Project and Oracle satisfy the performance requirements of the PEC system and should increase its compatibility with other systems at in place at MSFC.

System Functionality

The PEC data management and scheduling system will have three functional aspects: scheduling, file management and inventory management. This section will review the functional and data requirements for each.

Scheduling

The PEC scheduling system will integrate MS Project and Oracle into an application that allows NASA personnel to plan, monitor, and control the fabrication activities taking place within the PEC. This application will have three levels of functionality: planner level functionality, operator level functionality, and management/engineering level functionality.

The planner level is where detailed schedules will be developed, work order data input, and scheduling and planning reports developed. The primary task at this level is development and maintenance of the planning database. The type of data that will be input at this level includes: the project or work order number, the date the work order was received, the originator, the originator's organization, a description of the project, the desired start and completion dates, the resources/work stations required to complete the task(s), the work breakdown structure (WBS) code, the UPN number, and the CCBD number. Based on this information the planner will develop a base line schedule for the project being initiated. In order to reduce data redundancy and minimize data re-entry the schedules and data maintained in the PEC system should be transferable to other scheduling/planning systems currently used by NASA and/or NASA contractors, including: Open Plan, Time Line, Artemis, Primavera, and IMPACS. Initially, a full time planner will not be required for this system, however, as more fabrication projects come on-line a dedicated planner will become imperative. Given that the fabrication of flight hardware is a relatively new activity within the PEC the processes and procedures for the creating and management of planning and processing data have not been completely defined. Follow-on activities related to this project are being initiated that will address the requirements of the planning level of the system in greater detail.

At the operator level the primary concerns are with documenting the execution of scheduled tasks and providing the operator with the information required to complete the task at hand. At this level, initial entry into the system would involve presenting the operator with a prioritized list of tasks to be worked at their respective work area. Selecting a particular item, via a menu or mouse operation, should bring up the work order log-on window. At this point the operator would enter their name, organization, and identification number, with the system automatically capturing the log-on date and time from the system clock. Logging-off would entail a similar procedure with the system

querying the operator for their name, identification, number, organization, the level of completion of the task (i.e., 25%, 50%, 100%, etc.), then automatically recording the log-off date and time and updating the project schedule. After logging-on a task the operator would be presented with a screen showing processing information for the task. Information provided should include the current drawing number and revision, processing sheets/recipes, and the listing of NC files required for any fabrication equipment in their work area. In addition to providing the operator with access to the basic fabrication information the system should also provide the capability for capturing engineering and quality sign-off on fabrication setups and inspections. At present these are captured on paper, however, it is technologically feasible to do this electronically and it makes sense to build the basic functionality into the proposed PEC scheduling and data management system.

Finally at the management/engineering level the primary concern is project management. Users at this level are interested in the current status of component fabrication as well as material and resource usage. They will need access to Gantt charts and Pert networks showing the status of specific programs and projects. Three primary reports will need to be developed, a project status report, and resource and material usage reports. The project status report should indicate where a particular component is in its processing sequence, when fabrication was initiated, and the expected completion date/time. The resource usage report should provide information on work area usage (i.e., manpower and equipment) by project, while the material usage report should indicate the type and quantity of material used by project. In addition to reporting the system should also allow managers to perform what-if analysis on schedules to assess the impact of processing delays on the schedule.

File Management

In addition to the planning and scheduling capability outlined above, the PEC data management and scheduling system should also provide users with the capability to quickly and easily access input and output files from each process. Each workstation associated with an automated piece of equipment (i.e., the fiber placement machine, autoclave, and NDE automatic ultrasonic test system) should have the capability to access and down load control programs (e.g., NC programs in the case of the fiber placement machine) and to upload processing data from the controller.

Inventory Management

The inventory management aspect of the system will provide a computer based system for more effectively monitoring and tracking data on material information and usage history for all composite materials stored in the PEC. It is anticipated that the freezer inventory management system will be written in Oracle but will be accessed through the MS Project based scheduling system. The information stored in the system should include a NASA designated

material control number, the material description, the material type, the supplier name, the manufacture date, certification/recertification date, the lot number, the roll or spool number, the storage location (i.e., freezer number), the date initially stored in the freezer, current quantity in storage, cumulative time in the freezer, cumulative time out of the freezer, maximum allowable time out of the freezer and/or the maximum allowable age of the material, the identification number for the person withdrawing material, program number being charged, project/work order number being charged, the removal date and time, the identification number of the person returning the material, the quantity being returned, and the date and time the material was returned.

The freezer inventory management system should flag the user if the material has exceeded its maximum allowable age and/or the maximum cumulative time allowed outside the freezer. The system should also maintain a usage history on the material (i.e., quantity of material used for each program by project). Two basic reports, the material usage history report, and the freezer inventory report, will also be required to effectively manage the materials inventory. The material usage report should provide information on the quantity of each material type used by program and project/work order number. The freezer inventory report will provide information on the material currently stored in the freezer. The primary information presented should include the material control number, material description, material type, quantity in storage, and the cumulative time in and out of each freezer. This report should also flag items close to their expiration date (i.e., within two weeks, etc.).

Conclusion

This study is a first step in the transition of the PEC from a research and development facility to a production facility. As with all changes it will have its moments of pain and confusion, however, these can be minimized through effective planning. The centralized data management and scheduling system described herein is the beginning of this planning process. While this study has addressed many of the technical aspects of the system there are still several administrative issues that must be addressed. The most prominent issues to be addressed include the identification of the lead planning organization, and the delineation of processes and procedures for: development and maintenance of the planning database, the electronic capture of engineering and quality sign-off, the transfer of scheduling data to and from the AXAF-S program office, and the transfer of work order data to and from IMPACS. Follow-on activities are being initiated that will address these issues in greater detail.

References

(1)   Farrington, P.A. "Evaluation and recommendations for work group integration within the Materials and Processes Lab," Research Reports - 1992 NASA/ASEE Summer Faculty Fellowship Program, pp. XIV1-4.

(2)   Turner, J, "AXAF-S SRR Kick-Off Meeting", March 29, 1993.

1993

NASA/ASEE SUMMER FACULTY FELLOWSHIP PROGRAM

MARSHALL SPACE FLIGHT CENTER
THE UNIVERSITY OF ALABAMA IN HUNTSVILLE

TECHNOLOGY UTILIZATION OFFICE
DATA BASE ANALYSIS AND DESIGN

Prepared By: Stephen A. Floyd, Ph.D.

Academic Rank: Assistant Professor

Institution and
Department: University of Alabama in
                                Huntsville
                                Department of MIS

MSFC Colleague(s):   Ken Fernandez, Ph.D.
                                Martha Nell Massey

NASA/MSFC:

    Office: Technology Utilization
    Directorate: Institutional and Program Support

INTRODUCTION

NASA Headquarters is placing a high priority on the transfer of NASA and NASA contractor developed technologies and expertise to the private sector and to other federal, state and local government organizations. The ultimate objective of these efforts is positive economic impact, an improved quality of life and a more competitive U.S. posture in international markets. The Technology Utilization Office (TUO) currently serves seven states with its technology transfer efforts. Since 1989 the TUO has handled over one-thousand formal requests for NASA related technological assistance. The technology transfer process requires promoting public awareness of NASA technologies, soliciting requests for assistance, matching technologies to specific needs, assuring appropriate technology transfer and monitoring and evaluating the process. Each of these activities have one very important aspect in common: the success of each is highly dependent on the effective and efficient access, use and dissemination of appropriate high quality information. The purpose of the research reported here was to establish the requirements and develop a preliminary design for a database system to increase the effectiveness and efficiency of the TUO's technology transfer function. The research was conducted following the traditional systems development life cycle methodology and was supported through the use of modern structured analysis techniques. The next section will describe the research and findings as conducted under the life cycle approach.

ANALYSIS AND DESIGN

The purpose of the detailed analysis phase was three-fold: 1. the complete and thorough understanding of the TUO's technology transfer process, 2. the analysis of the feasibility of computer system support for the process and 3. the definition of scope for the system to be addressed by the research. The necessary understanding of the technology transfer process was gained using both traditional and structured methodologies. Information concerning the process was compiled from TUO documentation and report examination, personal interviews with all TUO and relevant contractor personnel (including Boeing Computer Support Services personnel), attendance at meetings and presentations, observation of day to day activities and through structured analysis modeling techniques. The process was modeled using the process and data modeling techniques of data flow diagramming and entity-relationship diagramming, respectively. The key processes and the necessary data/information flows and data stores necessary to support them were identified. The high level processes were then hierarchically decomposed down to the primitive process level. Concurrent with this effort the key business entities were identified and the required data were mapped to them.

The results of the analysis described above defined the business processes and entities falling within the established project scope. The scope of the project was defined by the TUO's Technology Assistance Board (TAB) process and more specifically by the problem request (PR) tracking and reporting requirements. The PR's are submitted by the client and can be likened to a customer order in a traditional business system. Receipt of a PR triggers the transaction process. At a high level the process consists of the following subprocesses: log-in (assignment of log-in number and entry into spreadsheet), evaluation (for scope and completeness), TAB review (consisting of further evaluation, assignment of a technology category, assignment of a responsible principal engineer (PE) and identification of appropriate MSFC lab and personnel possessing technology and or expertise to be applied), PE coordination and status reporting for active PR's and PR closure process. Each of the processes comprising a PR transaction were analyzed as to their input, process, output and data storage requirements.

The data modeling aspect of the analysis served to identify and define the key business entities and their relationships. The primary entities are the client - the individual or organization submitting a PR, the problem request, the technology source - the MSFC lab or individual that will address the problem request, and the principal engineer - the TUO individual with assigned responsibility for a given PR. The nature of the relationships among the entities were defined and the entity attribute specifications were developed. The data models were then used to develop the structure of the TUO database.

The analysis of the current TUO system led to the identification of several process related problems and issues. Key among these issues were:

- inability to effectively track PR's
- incomplete PR files
- lack of "strategic marketing" information
- processes heavily dependent on human information resources
- excessive time spent generating correspondence and management reports
- lack of information on technology resources and
- difficulty in coordinating TUO activities.

Based on these problems and issues and other information compiled during the analysis several opportunities for process improvement via computer support were identified. Major among these were the following:

- more effective PR tracking
- more precise and complete PR files

- existence of a non-volatile "corporate" database
- more comprehensive and readily available supporting information resources
- flexible and facilitated correspondence and report generation
- exception reporting
- more formalized procedures for transaction processing and
- facilitated information sharing.

Evaluation of currently available and "to be delivered" hardware and software coupled with an analysis of the operational capabilities of the TUO established the feasibility of developing and implementing a local area network based relational database system to address the problems and opportunities cited above. Such a system will allow implementation of a formal transaction processing system with the degree of information sharing, information archiving, application flexibility, data integrity, and ease of use defined by the end-users during the analysis process.

The recommended system would be developed using Microsoft's FoxPro for Windows relational database management system. This would provide multi-platform use across the PC's and Mac's currently used in the TUO. The Window's network environment would be provided by the Workstation Presentation System (WPS) currently being made available through Boeing Computer Services. The TUO has three such stations currently in operation with several more scheduled for the near future. This system will not only provide information and data sharing among TUO personnel but will serve as a window to the current and proposed E-mail systems which will link personnel to other MSFC organizational units, other NASA centers and to other outside government and private sector organizations. This linkage is of paramount importance in assuring the future effectiveness of the technology transfer process. Additionally, the WPS environment will provide TUO personnel with standard applications packages such as word processing, graphics, project management, presentation software and spreadsheet which afford opportunities for additional support, coordination and information sharing with respect to other aspects of the TUO function than those addressed by this research.

The recommended relational database environment will provide a Windows based, menu driven user interface which should allow easy transition for those TUO personnel currently using the Data General environment for word processing, data table (a limited spread-sheet type application) and e-mail applications. The relational architecture has been designed to offer the highest degrees of application flexibility, data integrity, maintainability, and future expandability. The data tables are designed to consolidate comprehensive information on an entity basis and to provide flexibility in establishing current and

potential future relationships among entities. The designed applications such as standard queries, correspondence generation, report generation and status monitoring were developed to meet the current end-user specified needs. The FoxPro Windows environment provides an applications generator which should allow TUO personnel to develop future applications with only a minimal amount of training. This will allow the TUO to more rapidly and effectively respond to the increasing demand for the transfer of technological expertise from NASA's laboratories.

CONCLUSIONS

This research has involved the analysis of the current process for transferring technologies from MSFC and contractor laboratories to the private and public sectors. The analysis has shown that the technology transfer process is heavily dependent on the timely and effective utilization of distributed information and has provided models to document the process. Most importantly it has established the feasibility and necessity for providing process support through the implementation of a networked database system. A recommended relational database system design has been developed which satisfies the defined end-user requirements and provides capability to handle future projected needs. The eventual implementation of such a system will hopefully serve as a model from which a comprehensive inter-agency system can be developed. Such a system is essential if we hope to render the technology transfer process as effective as it need be to help the country regain our preeminence in technologically driven markets.

ACKNOWLEDGMENTS

I wish to thank all the MSFC and contractor personnel associated with the Technology Utilization Office for their hospitality, time and honesty. Systems analysis methodologies are highly dependent on the willingness of end-users to share information and opinions with the analyst. The TUO personnel are to be commended for their participation in this process. Their hospitality allowed me to feel as "one of the family" during my ten week project. I also wish to extend individual thanks to my NASA colleagues Dr. Ken Fernandez and Ms. Nell Massey for initiating this effort and serving as points-of-contact for my information gathering efforts. Finally, to Mr. Ismail Akbay, the Director of the Technology Utilization Office, I extend my gratitude and appreciation, first as an educator, for providing me a meaningful fellowship opportunity, and second, as a citizen, for his dedication and devotion to the important mission of transferring federally funded technologies to help improve quality of life and provide a return on investment to taxpaying citizens.

1993

NASA/ASEE SUMMER FACULTY FELLOWSHIP PROGRAM

MARSHALL SPACE FLIGHT CENTER
THE UNIVERSITY OF ALABAMA IN HUNTSVILLE

A STUDY OF THE CORE MODULE SIMULATOR FLOOR
CAPABILITY

Prepared By: James W. Foreman

Academic Rank: Assistant Professor

Institution and
Department: Alabama A & M University,
                      Department of Civil Engineering

MFSC Colleagues: Charles R. Cooper
                      David Long

NASA/MSFC:

    Office: Systems Analysis and Integration Laboratory
    Division: Systems Test Division
    Branch: Development Test Branch

ABSTRACT

The floor of the Core Module Simulator(CMS) is required to support various combinations of dead load and live load during the testing process. Even though there is published data on the structural capability of the grating it is not always evident if the combined loadings with point loads will cause structural failure.

TECHNICAL APPROACH

A mathematical model of the 36 inch by 40 inch floor section was developed. The analysis was performed using finite element techniques. Unit loads were separately placed at the 15 locations shown in Figure 1. The internal moments at all 15 locations locations were determined for each load location yielding a 15 by 15 influence matrix. The total response at any location is determined from the following relationship:

$$\{M\} = [m]\{P\}$$

where $\{M\}$ is a 15 by 1 matrix of the resultant moments at the 15 locations as shown in Figure 1. The 15 by 15 influence moment matrix $[m]$ is developed by placing unit loads at the 15 locations shown in Figure 1, and $\{P\}$ is a 15 by 1 matrix of the applied loads.at these locations.

Once the influence matrix for the internal moments were determined, a BASIC computer program was developed to perform the matrix multiplication and select the maximum internal bending moments of the members.

The program is adaptable to the IBM PC or McIntosh computers The required input is the magnitude and location of the loads. The program also allows for the superposition of a uniform load over the entire floor area. This program written for this unique configuration provides a simplified method for determining the floor capability.

CONCLUSIONS

The solution of the CMS floor capability illustrates how the PC may be used to simplify problem solutions which require a higher level of expertise in a particular area such as structural analysis. this technique can be used in other fields such as electrical or fluid mechanics.
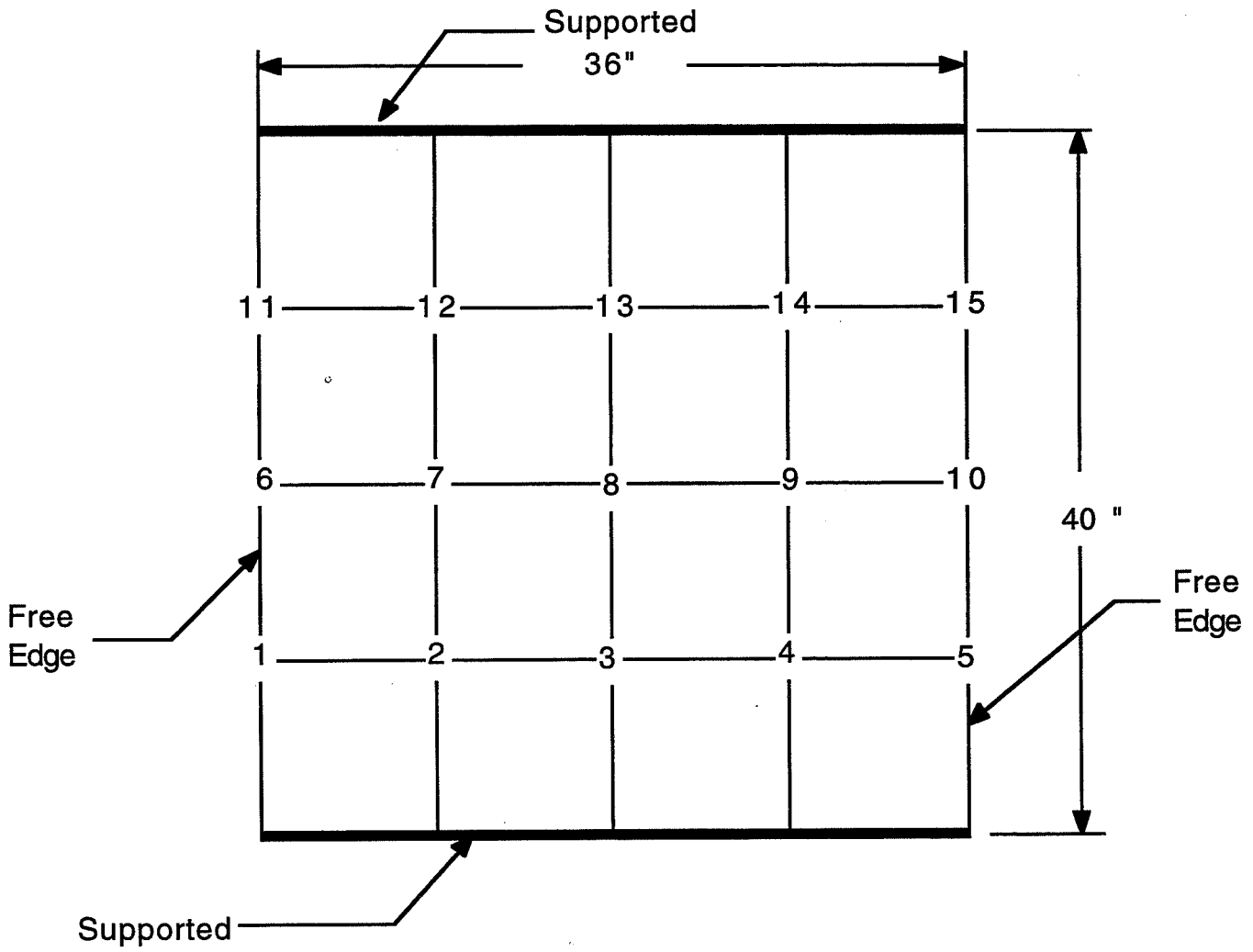
Figure 1 CMS Floor Layout

1993

NASA/ASEE SUMMER FACULTY FELLOWSHIP PROGRAM

MARSHALL SPACE FLIGHT CENTER
THE OHIO UNIVERSITY

A MINIMUM COST TOLERANCE ALLOCATION METHOD FOR ROCKET ENGINES

and

Robust Rocket Engine Design

Prepared By: Richard J. Gerth, Ph.D.

Academic Rank: Assistant Professor

Institution and Department: The Ohio University
                                   Department of Industrial and Systems Engineering

MSFC Colleague: David Seymour

NASA/MSFC:
Laboratory: Propulsion Laboratory
Division: Motor System
Branch: Performance Analysis

MINIMUM COST TOLERANCE ALLOCATION

Rocket engine design follows three phases: systems design, parameter design, and tolerance design. Systems design and parameter design are most effectively conducted in a concurrent engineering (CE) environment that utilize methods, such as Quality Function Deployment and Taguchi methods. However, tolerance allocation remains an art driven by experience, handbooks, and rules of thumb.

It was desirable to develop an optimization approach to tolerancing. The case study engine was the STME gas generator cycle. The design of the major components had been completed and the functional relationship between the component tolerances and system performance had been computed using the Generic Power Balance model. The system performance nominals (thrust, MR, and Isp) and tolerances were already specified, as were an initial set of component tolerances. However, the question was whether there existed an optimal combination of tolerances that would result in the minimum cost without any degradation in system performance.

The optimization model seeks to minimize the total system cost as determined by component tolerances subject to constraints on the tolerances:

$$MIN[total\,cost] = MIN\left[\sum_{i}^{n} C(tol_i)\right] \qquad [1]$$

subject to

$$T_k^2 \ge \sum_{i=1}^{n} G_{ik}^2 \cdot tol_i^2 \qquad (i = 1, \mathrm{K}, n)$$

$$toll_i \le tol_i \le tolu_i \qquad\qquad [2]$$

where:

$C(tol_i)$	Cost of producing tol_i;
tol_i	Tolerance of the ith component performance variable;
$toll_i, tolu_i$	Lower and upper limit of tol_i;
T_k	The kth system performance tolerance;
G_{ik}	Is the gain of the ith component performance variable to the kth system performance variable.

Equation [2] is a statistical tolerancing equation that models non-linear systems through a first order Taylor expansion where the gains G_{ik} are the first order partial derivatives. The linear Taylor approximation is generally valid for tolerance allocation problems since tolerances typically vary only by a small amount. The gains matrix was obtained from the generic power balance model mentioned above.

The greatest problem was determining the cost tolerance relationships, $C(tol_i)$. There are numerous models for cost tolerance equations, the most common of which are the reciprocal or inverse, reciprocal squared, and the negative exponential. However, these models have always been applied to specific manufacturing processes where the cause effect relationships between the process and tolerance were conceptually well understood. The conceptual difficulty at the high level of design in the STME study involved imagining how to tighten or loosen a component's performance, e.g., efficiency and how much such a change would cost. It is much easier to conceptualize changing the tolerance on a specific component element, such as the turbine blades, or the nozzlette diameter. The difficulty in part reflects the

relationship between systems designers who think of components as inputs and characterized by component performance variables, and component designers who think of component performance variables as outputs.

Two approaches were taken to relating cost and tolerances, and for lack of imagination termed the top-down and the bottom-up method. Both methods were implemented in Excel 4.0 for Windows and the optimization problem was solved using Excel's solver function.

In the top down method, the optimization model changes the component performance tolerances directly to minimize cost and satisfy the system constraints. The method is called top down because the changes in the component performance tolerances represent top level changes that are conceptually propagated down to the element level. The cost is, however, computed at the element level and proportioned out to the performance variables through a cost-contribution matrix.

The Top-Down method has several problems. First it assumes that tightening a particular component performance tolerance is achieved by tightening all the elements that affect it by the same amount. This clearly leads to contradictions when the same component affects two performance variables, one which tolerance is being tightened, and the other loosened. Thus, the top down method fails to model physical reality, namely that cost gains are achieved because tolerances are loosened on component elements which result in different component performance variations.

Second, the element-performance cost contribution matrix is likely to be difficult if not impossible to obtain. This is in part because the method does not model reality well, and in part because companies typically do not track costs in this manner. To rectify some of these problems, the Bottom-Up approach was developed.

In the bottom-up approach the solver here varies the low level component element tolerances and computes their impact on system performance through a two phase statistical stackup analysis (see eq. [2]). This requires two gains matrices: from system to component performance, and from component performance to component element tolerance.

The cost for each tolerance is determined from a family of cost-component-element-tolerance curves. The curves are computed for each element from a set of five standard cost-tolerance curves that were then scaled to match the initial design conditions. The five curves were created in conjunction with the component designers and range from a 1/4 reciprocal to a cubed reciprocal function with differing parameters. The scaling to the initial conditions involved knowing how much a particular element cost, how much of its total cost was due to creating a component of that functionality (nominal design) versus creating the same component with tighter tolerances, and the initial design tolerance. There were instances where going to tighter tolerances would require changing manufacturing processes with drastically different cost-tolerance behavior. In these cases the resulting cost tolerance curve had both a "jump" (discontinuous) as well as a change in slope.

The Bottom-Up approach appears to be the preferred method because it models reality more accurately, the data is more readily obtainable, and it is conceptually more appealing. The major difficulties are 3 fold. First, one must be able to obtain good gains matrices; second, it is imperative to have good cost estimates; and third, which is related to 2, it is necessary to better understand and estimate the standard cost tolerance curves for each element.

However, it is believed that in the tolerance design phase these estimates are typically not well known. Thus, the answer from the optimization problem will, in all likelihood, not be

the best possible answer. However, it is believed that by encouraging engineers to run the program they will have the necessary data to make informed decisions based on cost, and gain insight into the relationships between the variables at a systems level. Thus, the minimum cost tolerancing algorithm, when used by a cross functional team with other concurrent engineering tools, could have a significant impact on the cost of a design.

ROBUST ENGINE DESIGN

The purpose of the research was to develop a method for determining the set of optimal nominal design parameters that results in a system response that is least sensitive to variations in inlet conditions and between-component variations (manufacturing variations). Should the method prove to be successful, it could be expanded to include different cycle configurations, or become a means of evaluating the relative merits of different cycles.

Data were generated from a computer simulation program called The Generic Power Balance Model developed by RocketDyne Corporation. The program was specifically designed to aid rocket engine designers determine design configurations that would optimize system performance while ensuring conservation of mass and energy.

The particular cycle chosen for this project was a gas generator (GG) cycle to be used as an upper stage space engine. The primary system response variables of interest were thrust, mixture ratio (MR), and specific impulse (Isp). The various component environments were also considered to be important to design decisions since the environments often determine the maximum design conditions (MDCs) for the components. However, they were considered secondary to the system performance variables.

The method involved generating a series of on-design hardware configurations by altering control variables according to an L8 orthogonal array. The control variables used in the study are shown in Table 1. They were selected based on engineering knowledge and do not necessarily represent the most important design variables.

	Variable	level 1	level 2
A	Chamber Pressure	800 psia	1000 psia
B	Fuel Pump Head Coef	0.55	0.60
C	LOX Pump Head Coef	0.50	0.55
D	Fuel Turbine % Admission	50%	100%
E	LOX Turbine % Admission	50%	100%
F	Fuel Turbine Blade Angle	15°	30°
G	GG Temperature	1400°R	1600°R

Table 1. Control Variables for GG Cycle Engine.

A total of 14 noise factors representing the inlet conditions and random fluctuations in component efficiencies and resistances were considered. Creating an L16 noise array, however, would require an excessive number of simulation runs (8x16=128). Since an analysis on noise effects is meaningless, they were combined in a "worst case" fashion to ensure that the expected variability in system response is captured, thereby, reducing the number of required simulation runs. However, some factors affected the response variables in a different manner. For example, a decrease in the LOX inlet pressure would result in a decrease in thrust and MR and an increase in Isp. A decrease in the fuel inlet pressure would

also decrease thrust, but increase MR and decrease Isp. The following method was devised to determine which factors could be combined to ensure that the system would be exposed to the full range of potential noise conditions.

A gains matrix obtained from the STME study (a GG cycle low cost engine) indicated the direction of system response change with an increase in each of the noise factors. The signs of the gain factors were tabulated and all noise factors which induced a similar system response were grouped into the same class. This resulted in four classes, of which one was omitted because it contained only a single variable which gain value was very small. Thus, the outer array (noise array) was an L4 matrix with 3 noise variables.

The eight on-design configurations were run under each of the noise conditions as an open-loop off-design condition resulting in 8x4=32 off-design simulation runs. For each of the dependent variables the following statistics were computed and analyzed: average, variance, and signal to noise ratios. The ANOVAs showed that none of the control factors were significant (F=0) and the error term contributes over 90% of the variation in the data. This means that the noise factors had a greater effect on system performance than any of the control factors. This was true for all of the system performance variables as well as the component environment variables: GG temperature, the fuel pump discharge pressure, LOX pump discharge pressure, and MCC pressure. The analysis of the variation also showed that it could not be substantially reduced by any of the control factors.

The conclusion drawn from the results is that calibration of the engines is necessary to reduce the impact of component variations. The impact due to inlet conditions, however, will remain. Calibration of the engine is performed by running the off-design simulation under closed loop control by specifying two control parameters, typically the GG LOX injector resistance and the LOX turbine bypass orifice resistance. The control authority for each of these two resistances is defined here to be the full range of resistance required to balance the engine at nominal thrust and MR under worst and best case conditions.

There has been some difficulty in developing a calibration method, however, because under some on-design conditions there is insufficient flow to accommodate the necessary control authority, i.e., where the resistances are already so low under the on-design case that opening of the valves completely is not sufficient to balance the engine. Since the original on-design cases did not have a pressure drop across the control points, it may be necessary to compute a nominal pressure drop and include it in the on-design runs. This could possibly be done from the off-design data and knowing the thrust and MR gain as a function of the resistances. Since the system response ranges are known from the open-loop off-design runs, it would be straightforward to compute the required control authority and nominal resistance assuming a linear relationship between resistance and system response.

In summary, it appears that it is possible to use the generic power balance model to generate a robust design. It also appears that a certain amount of iteration may be necessary to simulate engine calibration. It is believed that it may be possible to predict the required control authority from the open-loop off-design runs alone, without further iteration. If this is true, then the optimal design can be determined and the calibration simulations need only be performed on that single design, thus eliminating the need for repeated iterations.

1993

NASA/ASEE SUMMER FACULTY FELLOWSHIP PROGRAM

MARSHAL SPACE FLIGHT CENTER
THE UNIVERSITY OF ALABAMA IN HUNTSVILLE

VALIDATION OF A NONINTRUSIVE OPTICAL TECHNIQUE FOR THE MEASUREMENT OF LIQUID MASS DISTRIBUTION IN A TWO-PHASE SPRAY

Prepared By: Roy Hartfield, Jr.

Academic Rank: Assistant Professor

Institution and
Department: Auburn University
                        Aerospace Engineering

MSFC Colleagues: Charles Schafer, Ph.D.
                        Richard Eskridge

NASA/MSFC:

        Office: Propulsion Laboratory
        Division: Motor Systems Division
        Branch: Combustion Physics Branch

VALIDATION OF A NONINTRUSIVE OPTICAL TECHNIQUE FOR THE MEASUREMENT OF LIQUID MASS DISTRIBUTION IN A TWO-PHASE SPRAY

Roy J. Hartfield, Jr.
Aerospace Engineering, Auburn University

Introduction

The work presented herein is the continuation of an optical technique development program initiated as part of the 1992 Summer Faculty Fellowship Program. The 1992 work consisted of the formulation and implementation of a technique involving the spatial deconvolution of fluorescence data from a uniformly illuminated, seeded dense spray to obtain quantitative measurements of the liquid density profiles. This measurement approach largely overcomes substantial scattering problems associated with other optical approaches for two-phase flows.[1] However, to apply this measurement approach with confidence to unknown flows, the technique must be validated. Consequently, technique validation using classical grid patternator techniques has been the focus of the current work. This work has included the design and construction of a patternator rig and the implementation of a test program designed for the comparison of patternator data with the deconvolved optical data. The flow field used for the validation is the plume of an axisymetric swirl coaxial LOX injector being considered for use in the Space Transportation System Main Engine. The flow facility is an improved version of the test rig which was constructed in 1992 for the initial technique development. This report includes a brief description of the optical measurement technique and the patternator rig and a presentation of the data comparisons.

Optical Technique and Patternator Rig

Several optical techniques for quantitatively investigating specific liquid spray plumes have been developed.[2,3,4] A phase/Doppler interferometer has been used to determine drop-size and velocity components in a plume similar to the plume investigated herein.[5] However, these previously-developed techniques are primarily applicable to spray plumes in which the droplet distribution is sparse and the signal from one drop is not substantially interfered with by the presence of the remainder of the spray. The optical measurement approach employed herein involves the uniform illumination of the axisymetric plume and a subsequent inversion of the measured fluorescence from R6-G dye seeded into the water used for the LOX simulate. By illuminating the plume uniformly, scattering, which inherently limits the quantitative applicability of planar imaging and interferometric schemes, is made more uniform and nonuniform contributions associated with scattering are minimized. Uniform illumination, however, does not provide a direct measure of the mass distribution in a particular plane. The radial distribution of the signal collected using uniform illumination may be determined using any of a variety of deconvolution techniques provided the distribution is known to be axisymetric. For this work, the Abel inversion procedure was chosen. For the problem at hand, it may be shown that the Abel integral equation to be solved can be reduced to

$$\epsilon(r) = -\frac{1}{\pi} \int_r^R \frac{I'(y)}{\sqrt{y^2 - r^2}} \, dy$$

where $\epsilon(r)$ is the radial signal distribution, R is the maximum plume diameter at the deconvolution height, y is the distance from the center of the plume measured on the raw data and $I'(y)$ is the derivative of the measured signal at location y.[6] Deconvolution techniques such as this are inherently dependent on the derivative of the measured distribution. This makes the determination of the distribution sensitive to noise in the data. To minimize this effect, an even-ordered polynomial curve fit is applied to the data. Equation 1 is then applied numerically to the curve fit using FORTRAN. The data for the deconvolutions is collected using a RCA video camera and an EPIX frame grabber card installed in an IBM compatible 386 personal computer.

The mechanical patternator is composed of the head, which is a linear array of twenty-three square 1/8" brass tubes, and the collector, which is a bank of 1/2" glass tubes connected by a low pressure manifold. The head, shown in the photograph in Fig. 1, is fitted with a hinged flap which can cover or uncover all of the tubes in the array simultaneously. The collector, shown in Fig.2, is fitted with individual scales for each tube and flapper doors on the bottom of each tube allow the patternator to be quickly reset after each run. The patternator is operated by establishing the flow to be probed with the head covered, lowering the pressure in the collector manifold (to insure that droplets falling on the patternator head are captured), uncovering the head until at least one collector tube is nearly full, recovering the head and then stopping the flow.

Figure 1: Patternator head.
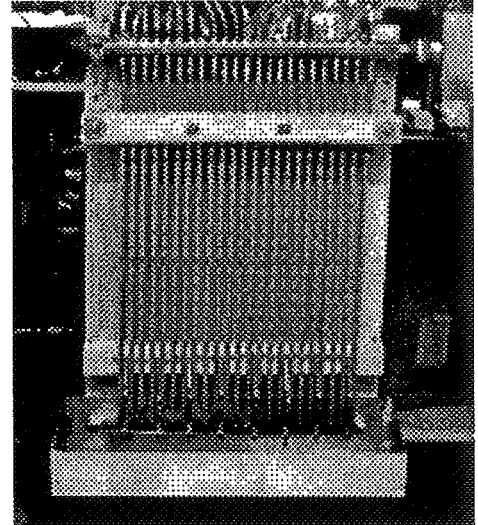
Figure 2: Patternator collector

Measurements

An image of the fluorescence signal in the swirl spray with a drive pressure of 50 psi resulting from uniform illumination is presented in Fig. 3. Note that, although the mass density is known to be nearly zero at the plume center, a substantial signal is present near the center of the image. This signal comes from the near and far edges of the plume. Several radial sections of this fluorescence data were inverted and a representative inversion compared with patternator data is shown in Fig. 4. The peaks of the data have been artificially forced to match and
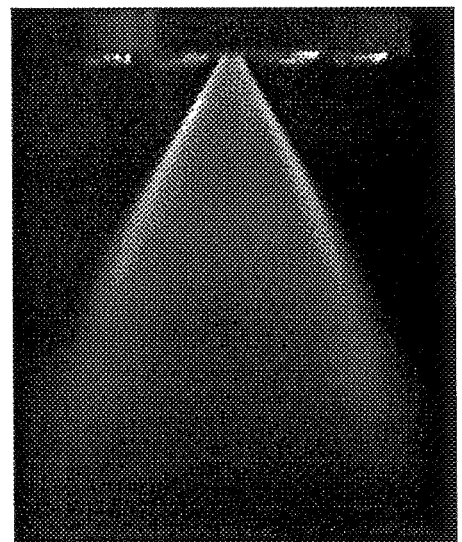
Figure 3: Fluorescence Signal.

C-2

the agreement in profiles is reasonably good; however, it was believed that a lack of atomization in the plume and problems with low signal and background correction were degrading the quality of the data. To address this issue, 1 µs shadowgraphs were taken at the 50 psi drive pressure and at 300 psi drive pressure (which is closer to projected operating conditions). These shadowgraphs are shown in Figs. 5 and 6 respectively. Clearly, at 50 psi, the injectant plume has atomized very little in the near field of the injector; however at 300 psi, atomization has progressed much closer to the injector exit. For this reason, additional

Figure 4: Comparison of Data at Z/D = 20.
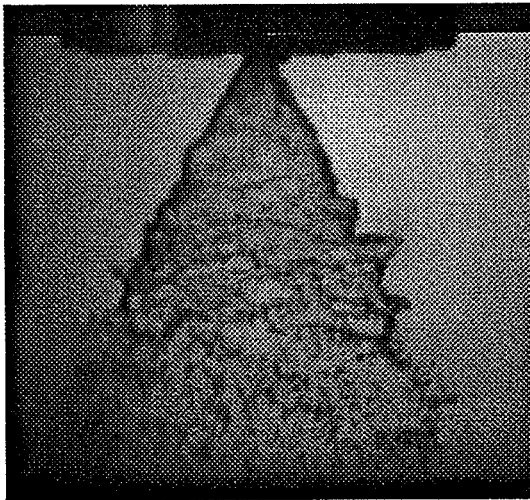
Figure 5: 1 µs shadowgraph at 50 psi.
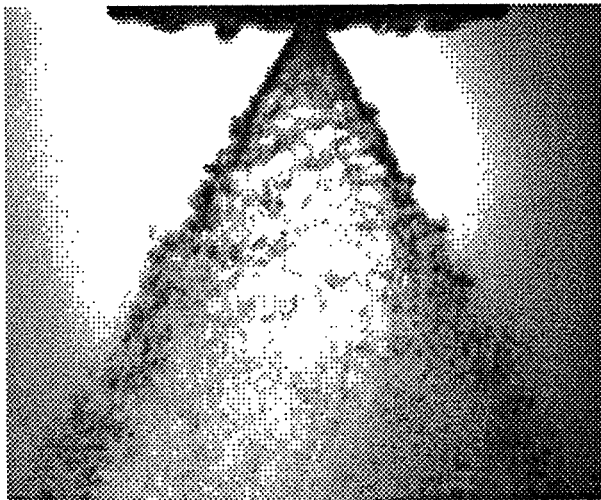
Figure 6: 1 µs shadowgraph at 300 psi.

fluorescence data and patternator data were obtained at the higher operating pressure. In addition to increasing the atomization, some adjustments were made in the optical arrangement. The laser power was increased to obtain better signal to noise ratios and the background was substantially reduced. The comparison between the data at 300 psi is shown in Fig. 7. With the improved signal levels, no need for background correction, and the improved atomization, the deconvolved signal, which is a measure of the mass density profile, agrees functionally quite well with the mass flux distribution measured using the patternator.
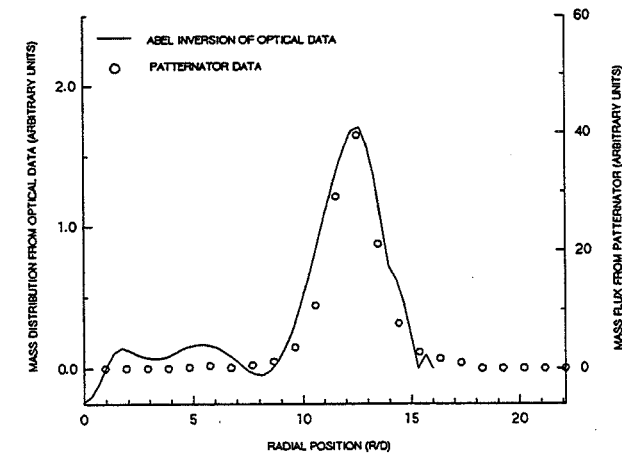
Figure 7: Comparison of data at Z/D = 20 for 300 psi drive pressure.

Summary and Future Work

Developmental work for a nonintrusive LIF measurement technique for mass distribution in dense sprays has been conducted. A grid patternator has been designed, constructed and operated as part of an effort to validate the optical measurement approach. Good agreement between the profiles of mass flux obtained using the patternator and the mass density distribution obtained using the optical measurements was obtained in a high pressure spray.

Planned future work includes additional optical technique development including the extension of the technique to multiangular imaging for use with non-symmetric flows. Additional improvements in the technique may include the use of a higher quality detector and improvements in the deconvolution algorithm. The investigation and potential development of additional nonintrusive techniques, including X-RAY absorption, nuclear magnetic resonance and neutron beam absorption is also planned.

Acknowledgements

References

1.   Hartfield, R. and Eskridge, R., " Experimental Investigation of a Simulated LOX Injector Flow Field," AIAA paper 93-2372, AIAA/SAE/ASME/ASEE Twenty-Ninth Joint Propulsion Conference and Exhibit, June 28-30, 1993, Monterey, CA.

2.   Melton, L. A., and Verdieck, J. F., "Vapor/Liquid Visualization in Fuel Sprays," Combustion Science and Technology, 1985, Vol 42, pp. 217-222.

3.   Chraplyvy, A. R., "Nonintrusive Measurements of Vapor Concentrations Inside Sprays," Applied Optics, Vol. 20, No. 15, August 1, 1991.

4.   Ingebo, R. D. and Buchele, D. R., "Small-Droplet Spray Measurements With a Scattered-Light Scanner," NASA Technical Memorandum 100973, prepared for ASTM Second Symposium on Liquid Particle Size Measurement Techniques, Atlanta, GA, November 1988.

5.   Zaller, M. and Klem, M. D., "Coaxial Injector Spray Characterization Using Water/Air as Simulants," The 28th JANNAF Combustion Subcommittee Meeting, Vol. 2. pp. 151-160.

6.   Shelby, R. T., "Abel Inversion Error Propagation Analysis," Master of Science Thesis, The University of Tennessee, June 1976.

1993

NASA/ASEE SUMMER FACULTY FELLOWSHIP PROGRAM

MARSHALL SPACE FLIGHT CENTER
THE UNIVERSITY OF ALABAMA

IMPACT DAMAGE IN FILAMENT
WOUND COMPOSITE BOTTLES

Prepared By: Alton L. Highsmith

Academic Rank: Assistant Professor

Institution and
Department: University of Alabama
                           Department of Aerospace Engineering

NASA/MSFC:

    Office: Materials and Processes Laboratory
    Division: Non-Metallic Materials Division
    Branch: Polymeric Materials Branch

MSFC Colleague(s):   Frank Ledbetter

Increasingly, composite materials are being used in advanced structural applications because of the significant weight savings they offer when compared to more traditional engineering materials. The higher cost of composites must be offset by the increased performance that results from reduced structural weight if these new materials are to be used effectively. At present, there is considerable interest in fabricating solid rocket motor cases out of composite materials, and capitalizing on the reduced structural weight to increase rocket performance. However, one of the difficulties that arises when composite materials are used is that composites can develop significant amounts of internal damage during low velocity impacts. Such low velocity impacts may be encountered in routine handling of a structural component like a rocket motor case. The ability to assess the reduction in structural integrity of composite motor cases that experience accidental impacts is essential if composite rocket motor cases are to be certified for manned flight. While experimental studies of the post-impact performance of filament wound composite motor cases have been performed (2,3), scaling impact data from small specimens to full scale structures has proven difficult. If such a scaling methodology is to be achieved, an increased understanding of the damage processes which influence residual strength is required.

The study described herein was part of an ongoing investigation of damage development and reduction of tensile strength in filament wound composites subjected to low velocity impacts. The present study, which focused on documenting the damage that develops in filament wound composites as a result of such impacts, included two distinct tasks. The first task was to experimentally assess impact damage in small, filament wound pressure bottles using x-ray radiography. The second task was to study the feasibility of using digital image processing techniques to assist in determining the 3-D distribution of damage from stereo x-ray pairs.

For the first task, the experimental determination of impact damage in filament wound bottles, 5.75 in. diameter bottles were used. The bottles were wound with a pattern XOOXOO, where X represents a layer of helical windings (in this case, a layer with strands oriented at $\pm 11.5°$ to the cylinder axis) and O represents a single layer with strands oriented in the hoop direction. Note that a helical layer has twice the thickness of a hoop layer, since a helical layer represents strands oriented in two directions. Three different material systems were studied, all of which were reinforced with IM7 carbon fibers. The three different matrix systems were a standard epoxy (3501-6ATL) and two toughened epoxies (X8553-45, 977-2).

A drop tower-type impact testing machine was used to impact the specimens, which were placed in a removable cradle which was attached to the bottom of the test frame for impact testing. Impact energy was controlled by adjusting the height from which the crosshead assembly was dropped. Based on some preliminary impact tests, three impact energies -- low (3.0 in.-lb.), intermediate (5.0 in.-lb.) and high (7.0 in.-lb.) were used. Each bottle used in the damage documentation study was subjected to three impacts (one at each of the three levels) at locations evenly spaced around the circumference of the bottle. Dynamic impact data was collected from the 0.5 in. diameter instrumented impact tup during impact.

After being impacted, the domes were cut off of the bottle and the cylindrical region was cut into 3 segments, with each segment containing a single impact site. Each segment was then inspected via dye-penetrant enhanced x-ray radiography (1). The dye penetrant used was a zinc iodide solution (60 g zinc iodide, 10 ml. water, 10 ml. isopropyl alcohol, 10 ml. Kodak "Photo-Flo 200"). A small dam encircling the impact site was made using plumbers putty. This dam was filled with the zinc iodide solution, which was allowed to seep into the specimen for at least four hours. The dye penetrant filled those damage events (matrix cracks, delaminations) which it could flow into. The zinc iodide thus rendered these areas more opaque to x-rays that the surrounding undamaged regions. Three radiographs were taken of each segment using different angles of incidence of the x-ray beam -- one with an angle of incidence of 82.5°, one with an angle of incidence of 90°, and one with an angle of incidence of 97.5°. The same cradle used for the impact tests was used to hold the x-ray film and segment during radiography, so that the x-ray film was wrapped around the curved segment. The 90°, or normal incidence x-ray provided a planform view of damage in the specimen. The other two x-rays formed a stereo pair and, when viewed using a stereo viewer, provided a three dimensional view of damage in the specimen (1). Using such a stereo imaging process, it was possible to resolve the location of damage through the thickness of the specimen.

A normal incidence x-ray radiograph taken from a specimen with the standard epoxy matrix subjected to a high energy impact is shown in Fig. 1. Note that the horizontal direction in the radiograph corresponds to the hoop direction. Also, in an undamaged specimen, the radiograph should have a darker tone at the left and right edges because of the curvature of the cylindrical segment. The sharp lines that appear in the radiograph correspond to matrix ply cracks that were decorated with dye penetrant. Such features are evident in all three of

Figure 1. X-ray radiograph of Specimen C 067-068, high energy impact.

the filament winding directions. The oval region that is centered on the actual impact site corresponds to the delaminated area of the specimen. A stereoscopic inspection of the damage reveals that delaminations occur at every interface, and that the overall oval geometry results from the "superposition" of the distinct delaminations.

The delamination seen in Fig. 1 is quite extensive, covering almost the full height of the cylindrical portion of the pressure bottle. This is typical of the specimens with the standard epoxy matrix. Similar damage states are seen in the specimens with toughened epoxy matrices, but the size of the damaged region is smaller in the toughened systems than in the standard epoxy system. In addition, lower impact energies generally (but not always) yield smaller delaminated areas.

Figure 1 also shows two heavily damaged (very dark) areas located away from the central impact site. A close stereoscopic inspection of these regions located to the left and right of the impact site reveals that there is fiber fracture at these locations. The fiber fracture developed in the helical layers, especially in the innermost helical layers. The location of this fiber fracture was apparently governed by the deflected shape assumed by the pressure bottle during impact. While this type of fiber fracture was most common, a second type of fiber fracture, as represented by the radiograph in Fig. 2, was also observed. This second fiber fracture mode has fiber fracture in the exterior hoop layers emanating from the impact site. The delaminated area is relatively small, even for a toughened epoxy, and closely follows the line of fiber fracture. At present, the factors influencing which fiber fracture mode will dominate are not well understood. It is believed that preexisting flaws can promote hoop direction fiber fracture.
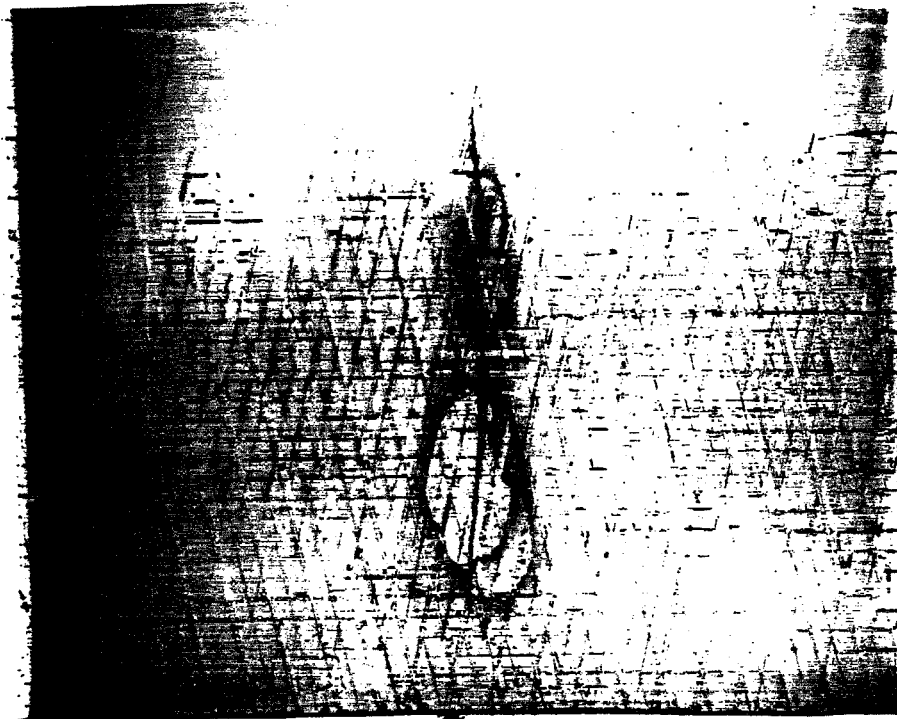
Figure 2. X-ray radiograph of Specimen C 113-114, medium energy impact.

The second task undertaken in the present study was to assess the feasibility of determining the 3-D distribution of damage using digital image processing of stereo radiographs. In this preliminary effort, attention was focused on extracting damage information from a single radiographic image, and representing that information in digital form. Reconstruction of the 3-D damage state would ultimately be accomplished by reconciling such digital information from two or more views of the composite.

To this point, efforts have focused on extracting ply crack information from radiographs. First, the radiograph is digitized using a scanner, and stored using the Tagged Image File Format, i.e., a the digital image is stored as a TIFF file. An 8 bit digitization was used, resulting in a 256 shade gray scale. A variety of image processing routines were written in the Turbo C++ programming language, for "enhancing" such digital images and for extracting features from the image. In this preliminary study, the best results were obtained by first sharpening the digitized image using an unsharp filter [4]. Then, a constant gray value (about 85% of the image average was found useful) was subtracted from the image. This eliminated extraneous features in the largely uniform gray area surrounding the damaged zone. Finally, a line detection routine was developed for extracting lines of a prescribed orientation from the image. Using this line extraction routine, it was possible to isolate hoop direction, or $+\theta$ direction, or $-\theta$ direction ply cracks. The extracted lines correlated quite well with features in the original image.

In summary, the experimental program has shown that toughened epoxy systems do reduce the amount of matrix damage, especially delamination, that develops during impact. Fiber fracture has been found to follow one of two modes -- one mode has fiber fracture in the interior helical layer at locations dictated by the deflected shape of the pressure bottles, and one mode has fiber fracture in the exterior hoop layers emanating from the impact site. In addition, a preliminary study has indicated that digital image processing techniques show promise for extracting the 3-D damage distribution from stereo radiographs.

REFERENCES

1. Jamison, R.D., "Advanced Fatigue Damage Development in Graphite Epoxy Laminates," Ph.D. dissertation, Virginia Polytechnic Institute and State University, Aug. 1982.

2. Madsen, C.B., Morgan, M.E., and Nusimer, R.J., "Scaling Impact Response and Damage in Composites. Damage Assessment for Composites - Phase I Final Report," AL-TR-90-037, Hercules Aerospace Co. for Astronautics Laboratory, AFSC, Edwards AFB, CA, August 1990.

3. Morgan, M.E., Madsen, C.B., and Watson, J.O., "Damage Screening Methodology for Design of Composite Rocket Motor Cases," JANNAF Propulsion Meeting, Indianapolis, Feb. 1992.

4. Pratt, William K. Digital Image Processing, 2nd Ed., John Wiley and Sons, New York, 1991.

1993

NASA/ASEE SUMMER FACULTY FELLOWSHIP PROGRAM

MARSHALL SPACE FLIGHT CENTER
THE UNIVERSITY OF ALABAMA IN HUNTSVILLE

OCTAVE: A MARSYAS POST-PROCESSOR FOR COMPUTER-AIDED CONTROL SYSTEM DESIGN

Prepared by:	A. Scottedward Hodel, Ph. D.
Academic Rank:	Assistant Professor
Institution and	Department of Electrical Engineering
Department	Auburn University
MSFC Colleague(s):	D. P. Vallely
NASA/MSFC:	
Office:	Structures and Dynamics Laboratory
Division:	Control System Division
Branch:	Mechanical Systems Control Branch

1 Introduction

MARSYAS is a computer-aided control system analysis package for the simulation and analysis of dynamic systems. In the summer of 1991 MARSYAS was updated to allow for the analysis of sampled-data systems in terms of frequency response, stability, etc. This update was continued during the summer of 1992 in order to extend further MARSYAS commands to the study of sampled-data systems. Further work was done to examine the computation of openat transfer functions, root-locii and w—plane frequency response plots. At the conclusion of the summer 1992 work it was proposed that control-system design capability be incorporated into the MARSYAS package. It was decided at that time to develop a separate "stand-alone" computer-aided control system design (CACSD) package. This report is a brief description of such a package.

A popular CACSD design environment is provided with commercial versions of Matlab, e.g., Simulink (tm) by the MathWorks. The Matlab design environment comprises (1) a compiled main program with a command parser and necessary intrinsic functions for matrix data manipulation, and (2) command scripts, called m-files, which may be used in a fashion similar to Unix shell scripts in order to create an increased function set for the user. The MathWorks has developed several "toolboxes," or sets of such m-files, for specific purposes such as signal processing, state-space control system design, robust control, etc. Since m-files are text-file scripts, their source code is available for viewing by the user. However, source code for any commercial Matlab is proprietary to the vendor and is not available.

In 1992, John Eaton, a post-doc at the University of Texas, began development of a free-ware Matlab look-alike program to be made available under the same licensing terms as that of the Free Software Foundation. That is, the program cannot be sold in whole or in part, and its source code must be freely made available. The numerical routines in Octave are taken from accepted FORTRAN routines in packages such as EISPACK, LINPACK, LAPACK, and the user interface and command execution routines are written in C++ and C. Under a follow-on grant from MSFC, work was begun at Auburn University on preliminary versions of Octave to incorporate new functions into Octave that would aid in the development of a control systems toolbox for this program. This work was continued during the Summer Faculty Fellowship Program during summer of 1993; all code developed was submitted and incorporated into the official Octave distribution. The code development is still ongoing; however, the design environment provided by the current version (0.74.5) is sufficiently functional that it can be used for a wide variety of applications. Version 1.0 of Octave is expected to be released shortly (prior to the end of 1993).

The remainder of this report is organized as follows. In Section 2 is presented a description of the planned MARSYAS design environment. Following this, in Section 3 a design example using current MARSYA/OCTAVE functions is presented. Finally, in Section 4 we discuss planned enhancements to the MARSYAS/OCTAVE system.
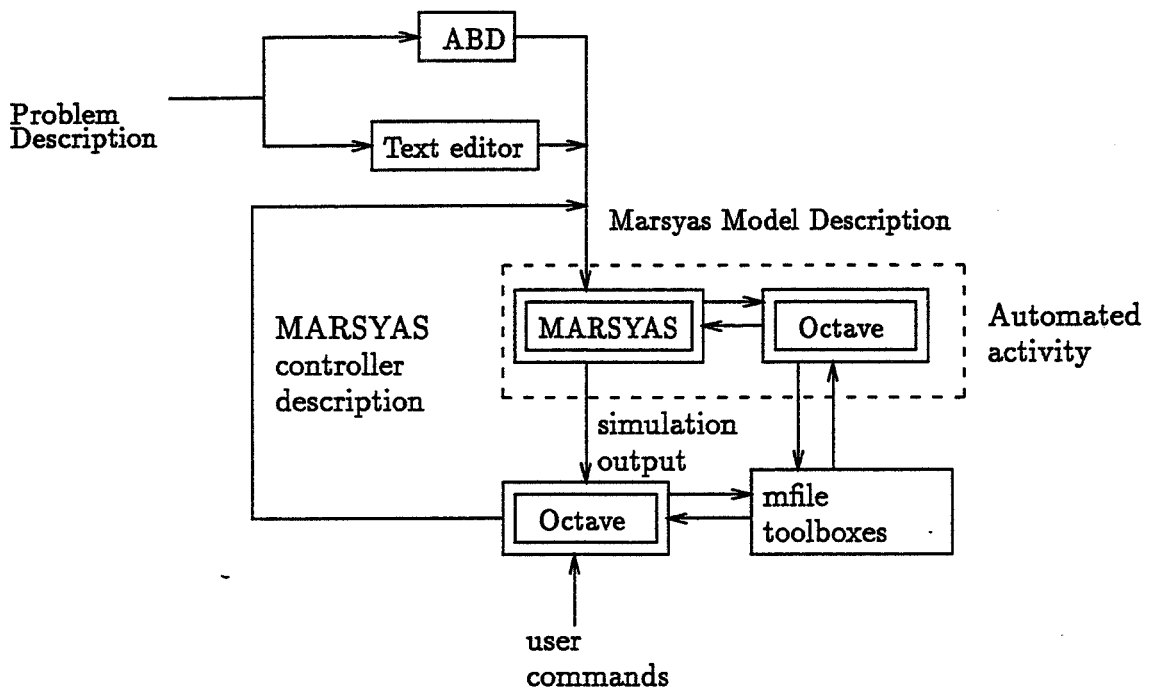
Figure 1: Desired MARSYAS design environment

2 Planned MARSYAS Design Environment

The desired MARSYAS design environment is shown in Figure 1. Those portions that are under development are shown in dashed-lines, those that are planned are shown in dotted lines. The user, once determining their problem description, writes a MARSYAS model description of the corresponding dynamic system. MARSYAS is run as a batch process; while not currently implemented, it is planned to modify MARSYAS in order to allow the Marsyas analysis phase to make use of Octave. The results of the analysis and simulation phase of MARSYAS are read into OCTAVE via m-file marsyas_in.m, which currently loads the system linearization (A, B, C, D) for either continuous or discrete-time systems. From within Octave, the user interactively uses m-file scripts in order to design a controller that meets desired design criteria, and then uses the m-file marsyas_out to store a MARSYAS model description of the designed controller. This controller may be then be verified with the nonlinear MARSYAS model description with a subsequent MARSYAS run, and further controller modifications may be made interactively from within OCTAVE.
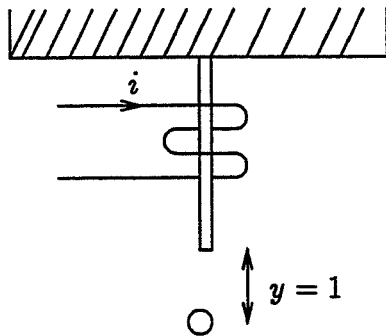
Figure 2: Magnetically suspended ball

3 Design example

The Octave design toolbox currently contains only one function: linear quadratic Gaussian (LQG) controller design. As an example of the MARSYAS/Octave design environment, consider the magnetically suspended ball system shown in Figure 2 The corresponding MARSYAS description module is

```
CONSTANT: G = 9.8$
MODEL: BALL\DYNAMICS,EQUATION$
INPUTS: IM $
OUTPUTS: X,XDOT$
EQUATION: X'' = G - (IM**2)/(X**2)$
       : XDOT = X' $
END$
```

A MARSYAS simulation was run to obtain a linearization of the above non-linear system, and the resulting data were employed by the following Octave m-file:

```
[a,b,c,d] = marsyas_in()
[n,m] = size(b);
[p,m] = size(d);
disp('open loop poles:')
poles= eig(a)'
% state feedback design
[k,x,e] = lqr(a,b,eye(n),10*eye(m));
disp('closed-loop state-feedback poles are')
poles = eig(a-b*k)'
% state estimator design
[l,x2,e] = lqe(a,eye(n),c,eye(n),0.01*eye(p))
```

```
bc = 1';
cc = k;
dc = zeros(m,p);
ac = a - 1'*c - b*cc;
marsyas_out(ac,bc,cc,dc)
```

The commands m,arsyas_in and marsyas_out are used to interact with the MARSYAS
program, and the Octave m-files lqr and lqe are Octave scripts that solve the appropriate al-
gebraic Riccati equations in order to obtain the desired controller. The MARSYAS controller
description thus obtained is

```
MODEL: OCTAVE, EQUATION $
INPUTS: U1, U2$
* 1: X $
* 2: XDOT $
OUTPUTS: Y1$
* 1: I\MAG $
EQUATION: X1' =  -2.700417E+01 * X1 -2.653148E+01 * X2
            +   6.831738E+00 * U1 +   1.792014E+01 * U2 $
        : X2' =  -5.831738E+00 * X1 -8.184793E+00 * X2
            +   8.184793E+00 * U1 +   6.831738E+00 * U2 $
        : Y1 =  -1.450893E+00 * X1 -6.276922E+00 * X2 $
END$
```

and is incorporated into the original simulation by adding a main model block:

```
MODEL: MAIN, EQUATION$
INPUTS: I\MAG $
OUTPUTS: X,XDOT$
EQUATION: IM = I\MAG - ID $
        : XERR = X-1 $
SUBMODEL: BALL\DYNAMICS; INPUTS: IM; OUTPUTS: X,XDOT $
SUBMODEL: OCTAVE; INPUTS: XERR,XDOT; OUTPUTS: ID $
END$
```

4 Planned Work

Planned enhancements to the MARSYAS Octave environment include

1. advanced design options,

2. improved user documentation (on-line and off-line), and

3. absorption of MARSYAS analysis phase into Octave

Ultimately, it is expected that Octave will prove itself as a good production code for use in
control system design at MSFC.

1993
NASA/ASEE SUMMER FACULTY FELLOWSHIP PROGRAM

MARSHALL SPACE FLIGHT CENTER
THE UNIVERSITY OF ALABAMA IN HUNTSVILLE

ON THE ANALYSIS OF CLEAR AIR RADAR ECHOES
SEVERELY CONTAMINATED BY CLUTTER

Prepared By:	H. Mario Ierkic V., Ph.D.
Academic Rank:	Associate Professor
Institution and Department:	University of Puerto Rico–Mayagüez Electrical and Computer Engineering Department
MSFC Colleague:	Steve Smith, Ph.D.
NASA/MSFC:	
Laboratory:	Space Science
Division:	Earth Science & Applications
Branch:	Earth System Processes and Modeling Branch

Introduction

Many radar systems work in environments where clutter returns overwhelm the atmospheric echoes. Sometimes by as much as 50 dB.

At the Arecibo Observatory (AO), for example, clutter levels are conspicuously high. This situation greatly reduces its usefulness for lower atmospheric studies. It is not possible in general, to observe height profiles of the vertical component of the wind velocity. This parameter is important to understand planetary scale circulation, mountain and lee waves, turbulence, tropospheric and stratospheric interactions and vertical transport of horizontal momentum. Moreover, and to show another aspect of the problem, it has been suggested (Gonzalez and Ierkic, 1993) that clutter returns may sometimes be confused for atmospheric echoes.

There is growing interest to find practical ways to counteract the deleterious effects of clutter, noise, interference, and of non-ideal radar equipment. Techniques that have been proposed include Adaptive Radar Signal Processors (Farina and Studer, 1987) and Least Squares Fitting Methods (Yamamoto et al., 1988). Of course, these techniques are non exclusive.

Few workers have recognized the importance of understanding the origin and propagation characteristics of the various contaminating signals,in particular of the clutter. This understanding can be used to formulate the Rules of a Knowledge- Based System that directs the Data Analysis Process (Gowrishankar and Bourbakis, 1992; Sigillito and Hutton, 1990). It is convenient that the resulting Expert System operates in the frequency domain and that the data analysis consists of the parameterization of spectra using non-linear fitting methods (Numerical Recipes, 1992). The analysis should yield yield echo intensities, average Doppler velocities and spectral widths. Visualization methods are required to guide the fitting process with user intervention.

Clutter propagation characteristics

Improved understanding of the various detected signals will help devise optimized radar processors capable of compensating for propagation effects.

Measurements of fading and phase variation of microwave and optical signals have been carried out for a period over three decades now. Janes et al. (1970), for example, compared simultaneous line of sight signals at 9.6 and 34.5 GHz propagated over distances close to 65 km long in Hawaii. They found that the power spectra of fading were similar in shape at the two radio frequencies but with higher spectral density content at 34.5 GHz than at 9.6 GHz particularly in the range from 0.1 to 5 Hz. On the other hand, the power spectra of the phase variation– expressed in terms of parts per million change in radio path length– show identical power spectra from 0.01 to 5Hz and follow a power law f^{-n} with $n \approx 2.6$.

It is convenient to write the detected signal c in terms of its amplitude and phase,

$$c = |c|\, exp(i\, \varphi)\,. \tag{1}$$

These results can be extrapolated to describe fading and phase variation characteristics at frequencies of interest to us. For example, at 50 and 430 MHz $|c|$ will vary appreciably

only for time scales longer than one minute. Phase changes, on the other hand, have the same functional form at all radio frequencies and they are linearly proportional to the probing frequency. Phase excursions will be 430/50 or 8.6 times bigger at 430 than at 50 MHz. Due to the exponential dependence in (1) –reminiscent of the FM communication mode– the bandwidth ratio at the two probing frequencies is bigger than 8.6.

Another source of clutter alteration that needs to be considered is the one produced by foliage disturbed by surface wind speeds.

At AO these effects can be studied simultaneously at the two frequencies mentioned previously. Moreover at 430 MHz it may be possible to detect two circular polarizations and use the one devoid of atmospheric echoes to neutralize the clutter. Of course, this procedure only works if both clutter polarizations are independent and proportional.

For completenes, albeit not related directly to clutter, let us mention that it is worth looking into the evaluation of the relative contribution of propagation vis-a-vis turbulence in the doppler widening of the signals in the GHz range.

Knowledge-based spectral analysis system

The knowledge-based system controls data processing. It is driven by data and it is responsive to a World Model. The model is defined in term of hypotheses and rules based in the the knowledge of specialists.

The expert system transforms the data as required using appropriate algorithms and verifies that the results comply with the rules of the world model. It is also capable of making inferences aimed toward conflict resolution.

Gradually, the expert system can grow in the learning curve and consequently demand less user assistance. Alternatively, it can grow to take on more complicated scattering environments for example, precipitation, lightning, foliage, ocean clutter etc..

It is is assumed here that the radar spectra can be described by Gaussian functions. Some of the rules that can guide the analysis process are mentioned next. Before, note that they are not as yet complete and that they will vary from station to station.

The following rules should help verify data integrity: a) adequate System Temperature values, b) S/N indicating system is in fact operating, c) real time quality flags to help document contingencies and to complement the observer's Log book.

Some further rules to assist in data processing are: a) reasonable upper bounds for the spectral widths of clutter, b) estipulation of plausible wind shears, c) acceptable time variability in the various parameters, and d) checks for frequency aliasing.

It is worth saying that sometimes fairly simple hints (e.g. Doppler shift is positive) can be valuable in the data reduction.

Signal Analysis System

To maximize the success of the signal processing algorithms the radar hardware has to work according to specifications and the experiments have to be well designed. At Arecibo for example, and as a matter of fact, it is not wise to use coded pulses to monitor the troposphere, or to carry on measurements while moving the antenna beam.

A brief description of the processing sequence is now in order.

The time series that results from coherently adding the returns needs to be examined first in order to subtract the clutter. Early subtraction of clutter has a double purpose: a) it reduces the distortion of the spectra of the atmospheric returns and of the noise, b) it presents the fitting algorithms with spectral data of comparable range of values. A sensitive issue here is the width of the notch filter to be used.

Proceed to obtain the spectra with the FFT algorithm, possibly weighting the data. And in the later case overlap data points to restore their information content. Optionally, run a median filter accross the spectra to account for outliers. Estimate and subtract the noise. Note that noise can be height dependent. Correct for coherent integrations (Farley, 1983). Display 2-D (frequency vs range) color or gray scale spectral profiles. To help focus on the true velocity profile this image can be examined with pattern recognition techniques to reject suspect features. At user request generate plots of spectral profiles. These plots should be flexible to allow diverse representations: Linear, log, normalized relative to a peak, normalized relative to the noise. Add a baseline value of a couple of dB to the 2-D periodograms to compensate for echo strength loss with range.

Interactively provide first guesses using the displays just described and proceed with the parameterization of the spectra. Fitting should be done locally around the frequency bins with spectral densities larger than the noise. Initially the fitting scheme should have at most 7 parameters: dc (1), Gaussians for clutter and atmospheric echoes (6). Overlay the results of the parameterization over the data plots. Assess quality of results using spatial– ranges above and below– and temporal– periods before and after– consensus criteria (Wilfong et al., 1992).

Accept or reject results of the analysis. In the former case save the parameters and the variables used in the analysis. Otherwise restart analysis procedure.

Gradually the expert system should control the analysis more exhaustively.

Conclusions

This work provides a framework to develop a robust data driven expert system to retrieve useful results from contaminated radar data. It summarizes some of the common wisdom dispersed in the literature (e.g. Wilfong et al., 1992) and intends to engage colleagues to contribute fresh approaches. It also constitutes the basis for a proposal for telescope time to the AO to study the effects of clutter and the means to ameliorate them.

In order to devise a knowledge-based system it is important to have adequate understanding of the various signals present at the receiving end. Similarly important is the formulation of rules whose compliance will guide the data reduction algorithms. Note that here there are three modules intervening in the analysis: data, inference system, and the algorithms.

It is worth stating that the verification of the rules of the expert system is a non trivial procedure and requires careful consideration. It is in general a difficult step to implement. It may use techniques borrowed from Pattern Recognition and rely on Interactive Visualization to permit effective user intervention.

Acknowledgement

References

[1] Farina A., F. A. Studer, (1987) " Adaptive implementation of the optimum radar signal processor" *IEE Radar, Sonar, Navigation and Avionics Series. Peter Peregrinus Ltd.*

[2] Farley D. T., (1983) " Coherent integration", *Handbook for MAP*, 507.

[3] González D. A. J., H. M. Ierkič V. (1993) " Tropospheric refraction and hard backscattering in 430 MHz observations of the middle atmosphere at Arecibo," *Poster presentation at the CEDAR workshop in Boulder, Colorado.*

[4] Gowrishankar T. R., N. G. Bourbakis (1992) " Specifications for the development of a knowledge based image understanding system," *Chapter 18 of: Artificial intelligence methods and applications; World Scientific Publishing Co.,* 571–589.

[5] Janes H. B., M. C. Thompson, D. Smith, A. W. Kirkpatrick (1970) " Comparison of simultaneous line of sight signals at 9.6 and 34.5 GHz," *IEEE Trans. Antennas and Propagation,* 18, 447–451.

[6] Press W. H., S. A. Teukolsky, W. T. Vetterling, B. P. Flannery (1992) " Numerical Recipes," *Cambridge University Press,* 994pp.

[7] Sigillito V. G., L. V. Hutton (1990) " Case study II: radar signal processing," *Chapter 11 of: Neural Networks PC tools; Academic Press,* 235–250.

[8] Wilfong T. L., R. L. Creasey, S. A. Smith, (1992) " High temporal resolution velocity estimates from the NASA 50 MHz winf profiler," *American Institute of Aeronautics and Astronautics, AIAA 92–0719.*

[9] Yamamoto M., T. Sato, P. T. May, T. Tsuda, S. Fukao, S. Kato, (1988) " Estimation error of spectral parameters of mesosphere stratosphere troposphere radars obtained by least squares fitting method and its lower bound," *Radio Sci.*, **23**, 1013–1021.

1993

NASA/ASEE SUMMER FACULTY FELLOWSHIP PROGRAM

MARSHALL SPACE FLIGHT CENTER

A COMPILATION OF TECHNOLOGY SPINOFFS FROM THE U.S. SPACE SHUTTLE PROGRAM

Prepared By: David Jeff Jackson, Ph.D.

Academic Rank: Assistant Professor

Institution and   The University of Alabama,
Department: Department of Electrical Engineering

MSFC Colleagues: Alex McCool
                         Jim Ellis

NASA/MSFC Office: Space Shuttle Projects Office

Introduction

As the successful transfer of NASA-developed technology is a stated mission of NASA, the documentation of such transfer is vital in support of the program. The purpose of this report is to document technology transfer, *i.e.* "spinoffs", from the U.S Space Shuttle Program to the commercial sector. These spinoffs have their origin in the many scientific and engineering fields associated with the shuttle program and, as such, span many diverse commercial applications. These applications include, but are not limited to, consumer products, medicine, industrial productivity, manufacturing technology, public safety, resources management, materials processing, transportation, energy, computer technology, construction, and environmental applications.

To aide to the generation of this technology spinoff list, significant effort was made to establish numerous and complementary sources of information. The primary sources of information used in compiling this list include: the NASA "Spinoff" publication, NASA Tech Briefs, the Marshall Space Flight Center (MSFC) Technology Utilization (TU) Office, the NASA Center for Aerospace Information (CASI), the NASA COSMIC Software Center, and MSFC laboratory and contractor personnel. A complete listing of resources may be found in the bibliography of this report. Additionally, effort was made to insure that the obtained information was placed in electronic database form to insure future access, and subsequent updating, would be feasible with minimal effort.

Technology Transfer Information Resources

As stated, the spinoff compilations were obtained from several sources. A listing of these sources including the number of items from each is given in Table 1.

Information Source	Items
MSFC TU Office	15
NASA "Spinoff"	74
NASA Tech Briefs	235
COSMIC Software Center	146
Laboratory and Contractor Personnel	6

Table 1. Information Sources for Compilation of Technology Spinoffs

Although these resources are broad in their coverage of technology spinoffs, the author believes that this listing represents only a small fragment of the actual successful technology transfers that have taken place throughout the life of the shuttle program. The true number of spinoffs may be impossible to document due to initially insufficient recording during early years of the program and the natural tendency of the technology transfer process to dilute itself.

Each information resource contributes to the overall documentation of the technology transfers, however, the information obtained from the MSFC TU office and the NASA "Spinoff" publication represent those spinoffs which are most likely to enthuse the typical

citizen about the wealth of products and services whose origins lay in the shuttle program. The other information resources represent potential spinoffs, emerging spinoffs, or those spinoffs of a sufficiently technical nature as to indifferentiate the reader as to their origin. Data specific to each information source is described below.

The spinoff items documented from the MSFC TU office are diverse and among the best documented in the form of the office's Technology Transfer Reports and the TU Office Annual Report. However, in the interest of spinoff traceability, several improvements may be made to the form of these reports. Specifically, the inclusion of specific laboratories and contact points within the laboratories and contractor personnel will make accountability and traceability of the technology transfer process more complete. Additionally, contract numbers and periods of performance, where applicable, will insure proper credit is given to original technology developers.

The NASA "Spinoff" publication represents the broadest documentation of technology spinoffs available. However, at this point in the transfer process, many good examples remain undocumented. It is therefore not sufficient to rely only upon the "Spinoff" publication to document technology transfers. Tables 2, 3, and 4 give additional details concerning spinoffs documented.

Focus Areas	Number of Items
Industrial Productivity	23
Public Safety	13
Health & Medicine	6
Computer Technology	2
Energy	4
Transportation	2
Consumer/Home/Recreation	15
Technology Demonstration	1
Manufacturing Technology	13
Environmental	3
Resources Management	2
Construction	1

Table 2. Distribution of Spinoff Areas

Clearly the information contained in Table 3 indicates that additional effort is necessary in documenting the technology transfer process. This documentation is critical to the continued growth and visibility of the technology spinoffs.

Information Source	Number of Items
UNKNOWN	30
Clipping Service	21
NASA Field Center	12
Other	11

Table 3. Sources of Spinoff Information

Transfer Mechanism	Number of Items
NASA Tech Brief	13
NASA Contract	4
Contractor Diversification	18
Personnel Transfer	4
Technology Demonstration	3
COSMIC	4
UNKNOWN	15

Table 4. Technology Transfer Mechanisms

The NASA Tech Briefs publication represents the largest number of potential spinoffs in all the resources documented. More than 200 items published have their origin in or were used and modified in the shuttle program. Additionally, the number of requests for information, in the form of Technical Support Packages (TSPs), is quite large. For those items which have a TSP available through CASI an average of approximately 200 requests per item have been processed. If only a small percentage of these requests have resulted in a successful technology transfer, then a large number of potential "success stories" remain undocumented. Additional research into these requests, through information available from CASI, is necessary to document this hypothesis.

The COSMIC Software Center has documented a large number of programs whose origin are in or related to the shuttle program. Additionally, many requests for this software or documentation have been processed through the COSMIC Center. Approximately 600 requests for shuttle software and 1500 requests for documentation have been processed to date. Additional research into these requests, through information available from COSMIC, is necessary to document properly the potential technology transfers.

Technology transfer information has also been provided through contractor and laboratory personnel at the Marshall Space Flight Center. Although not always mature, these cases represent emerging technologies available for technology transfer. Specific technologies which show promise for successful technology transfer include environmental applications, new materials testing procedures including nondestructive evaluation, new welding processes including weld seam tracking and defect minimization procedures, and others. The research efforts at Productivity Enhancement Complex at the Marshall Space Flight Center are representative of these advancements and should be appropriately noted.

Additional resources for documenting technology transfer, which have not been used but are available, include the NASA patent licensing process, additional electronic databases (NTB Online, Spacelink, etc.), and the Technology 2000 Conference series. Each of these resources hold promise for documenting additional technology transfer.

Conclusions and Recommendations

Although this report is viewed, by the author, as a success in initially documenting examples of technology transfer, a number of improvements may be made to insure

continued growth and successful documentation of the NASA spinoffs. These include: an incorporation, expansion, and updating of existing electronic databases for documenting technology transfer (NASA RECON, CASI databases, NTB Online, COSMIC, Spacelink, etc.) to a single point of documentation; an updating and standardization of the technology transfer reporting process across the NASA field center TU offices (the MSFC TU office could be used effectively as a model for this change); and, a procedure adopted to insure new technology development is properly documented with information necessary to document promote new technology transfers and subsequent database documentation.

Bibliography

1. Gurney, Gene *Space Technology Spinoffs* New York: Franklin Watts, Inc., 1979
2. *Directory of Federal Technology Transfer*, National Science Foundation, NSF 75-402, 153-164, June 1975.
3. TABES90, 6th Annual Technical and Business Exhibition and Symposium, May 15-16, 1990. Von Braun Civic Center, Huntsville, AL.
4. Grissom Jr., Fred, Chapman Richard, *Mining the Nation's Brain Trust: How to Put Federally-Funded Research to Work For You*, Reading, Massachusetts: 1992.
5. Chapman, Richard, *An Exploration of Benefits From NASA "Spinoff"*, June 1989
6. *Focus on the Future: Advancing Today's Technology*, NASA Marshall Space Flight Center
7. NASA Tech Briefs, (numerous issues)
8. NASA Spinoff, (numerous issues)
9. Technology 2000 Conference Proceedings, 1990
10. Technology 2001 Conference Proceedings, 1991
11. Technology 2002 Conference Proceedings, 1992

1993

NASA/ASEE SUMMER FACULTY FELLOWSHIP PROGRAM

MARSHALL SPACE FLIGHT CENTER
THE UNIVERSITY OF ALABAMA IN HUNTSVILLE

WELD FRACTURE CRITERIA FOR COMPUTER SIMULATION

Prepared By: Wartan A. Jemian, Ph. D.

Academic Rank: Professor

Institution and
Department: Auburn University,
                          Materials Engineering

MSFC Colleague: Arthur C. Nunes, Jr., Ph. D.

NASA/MSFC:

          Office: Materials & Processes Laboratory
          Division: Metallic Materials & Processes Division
          Branch: Metallurgical Research

Introduction

Due to the complexity of welding, not all of the important factors are always properly considered and controlled. An automatic system is required. This report outlines a simulation method and all the important considerations to do this. As in many situations where a defect or failure has occurred, it is frequently necessary to trouble shoot the system and eventually identify those factors that were neglected. This is expensive and time consuming. Very frequently the causes are materials-related that might have been anticipated. Computer simulation can automatically consider all important variables. The major goal of this presentation is to identify the proper relationship of design, processing and materials variables to welding.

Welding

An arc welded structure is usually described in terms of a fusion zone, a heat affected zone (HAZ) and the base metal. The properties of the fusion zone are dominated by details of the solidification process and the HAZ is a modification of the base metal by prolonged exposure to elevated temperatures. Welding also produces changes in geometry that are manifest in visible features.

There are three stages in the simulation. The first stage is to determine the geometry of the welded structure, which is based on the welder's input of part thickness, welding power and speed. Residual stress is also a significant factor in welding and must be computed. The simulationist, who must also understand welding, sets the parameters for arc efficiency, partitioning between point and line source and physical properties of the system. A grid is assigned to the weld in the first stage and is followed throughout the simulation. Figure 1 illustrates the shape of the weld bar and its regions of microstructure.

The goal of the second stage operations is to assign a flow curve to each element. This involves the simulation of microstructure and properties. The width and geometry of the fusion zone and the determination of temperature gradient in the liquid lead to a specification of property controlling features. The changes in the HAZ are computed from thermal exposures.

The final stage is the determination of fracture details. Each step is based on the concept that the response of each element in the structure is governed, solely, by its condition and loading. The program uses object oriented programming methods, see Booch (1). Thus, the simulation of weld structure is planned for a number of source code classes in a library organized into objects that define shape, regional structure, operational parameters and microstructural parameters. The simulation third stage uses these objects to reach the final result.

Weld Structure

Weld structure is established by simulating the geometry of the weld pool. The equilibrium phase diagram and other materials-specific reference tools provide information about melting point, freezing range, chemical partitioning and solubility. The principal operating parameter is the energy input which is the ratio of total input power to welding speed. Easterling (3) describes the thermal distribution in welding which is characterized by the flow of heat away from a moving source. The governing equation is equation 2. Equations (1) and (2) define the information that must be provided.

$$q = \eta \, E \, I \qquad\qquad [1]$$

Where q is the total input power
η is the arc efficiency
E is the arc voltage
and I the beam current.,

The boundary conditions for integrating equation (2) are based on the geometry of the base metal.

$$\frac{\partial^2 T}{\partial X^2} + \frac{\partial^2 T}{\partial y^2} + \frac{\partial^2 T}{\partial z^2} = -2\lambda v \frac{\partial T}{\partial X} \qquad\qquad [2]$$

Where X, y and z are a Cartesian coordinate
system fixed to the motion of the arc along X,
T is the absolute temperature
λ is the thermal conductivity
and v is the heat capacity.

The size of the reinforcement depends on the base metal preparation,
distortion during welding, width of the fusion zone and amount of filler
added.

Flow Curve

The key parameters of the flow curve are the elastic slope, the
strain hardening exponent, and coordinates of the UTS and breaking
point. Each of the latter parameters on processing. Cottrell (2) reviews
the governing principles. The results of a tensile test can be presented
as an engineering stress-strain curve.
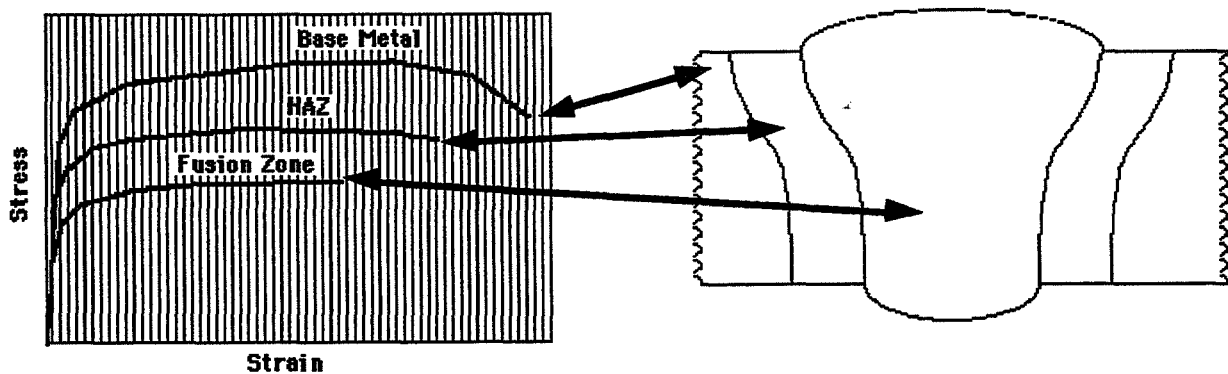
**Figure 1. Stress-strain curves of typical parts of the welded
structure.**

The flow curve is different at each point as shown in Figure 1.
The base metal has the optimum values of strength and ductility since it
has been heat treated to the optimum prior to welding. The alloy in the
fusion zone is completely changed with the development of a dendritic
structure. The HAZ is that part of the unmelted base metal that has
been subjected to elevated temperatures for enough time to allow
changes. Each process is represented by one or more governing
relations which are used to adjust the features of the flow curve.

The stress on an element varies inversely with section area. The initial deformation is elastic. As the loading increases, the stress is reached where significant plastic flow occurs, represented by the strain hardening exponent. At higher levels of deformation vacancy production becomes important. This counteracts and limits work hardening, resulting in the UTS that is a prominent part of engineering stress-strain curves. Each parameter of the flow curve is considered separately.

Properties

The mechanical test is simulated in incremental steps of sample extension as shown by the strain increments in figure 1. Every element is evaluated at each step. The calculated stress is compared with the failure stress of each element. Eventually there will be an element that is the first to reach its failure stress and this will be marked for the point of fracture initiation. The sequence and positions of the other elements that fail will also be recorded to describe the shape of the failure surface. The overall extent of sample elongation determines weld ductility.

Conclusions

The integrated weld simulation system is planned to provide information about welding with a specified alloy that is equivalent to actually making a weld in the shop. The proposed system includes all details of materials properties and behavior that are required in trouble shooting and are too complex to include in most specifications. The simulation is planned for speed and accuracy and produces reports with lists of results, parameters used in the simulation, and approximations that were invoked. This is more information than is usually available.

References

1. Booch, G. C., *Object Oriented Design with Applications*, The Benjamin/Cummings Publishing Co., (1991).
2. Cottrell, A. H., *The Mechanical Properties of Matter*, John Wiley & Sons., Inc., (1964).
3. Easterling, K. E., *Introduction to the Physical Metallurgy of Welding*, Butterworths & Co., (1983).

1993

NASA/ASEE   SUMMER FACULTY FELLOWSHIP PROGRAM

MARSHALL SPACE FLIGHT CENTER
THE UNIVERSITY OF ALABAMA IN HUNTSVILLE

MEASURING THE DYNAMICS OF STRUCTURAL CHANGES IN
BIOLOGICAL MACROMOLECULES FROM LIGHT SCATTERING DATA

Prepared By: Adriel D. Johnson, Ph.D.

Academic Rank: Assistant Professor

Institution and
Department: University of Alabama in Huntsville
                          Department of Biological Sciences

MSFC Colleague: David A. Noever, Ph.D.

NASA/MSFC:

    Office: Space Sciences Laboratory
    Division: Microgravity Sciences and Applications
    Branch: Biophysics

Examining techniques to study the dynamics of structural changes in various molecules has been an on going goal of the space program. How these phenomena occur in biological systems would be necessary for life to remain functional in the space environment. Hierarchy of biological organization is attained when cells join together small organic molecules to form larger and more complex molecules. Characterizing the architecture of a particular macromolecule helps determine how that molecule works in the living cell and is fundamental to the diversity of life. Understanding this arrangement involves the correlation of the structure of macromolecules with their functions.

A light scattering photometer was developed for detecting continuous measurement of the angular spectrum of light scattered by dynamically changing systems (2). The analysis of light scattered by biological macromolecules can be used to determine concentration, size, shape, molecular weight, and structural changes of cells, such as erythrocytes (2). Some light scattering photometers can collect and store 120 angular scattering spectra per minute, with an angular resolution of 0.2 degrees which can be displayed with computer graphics (2). The light scattering photometer functions to produce and detect scattered light, determines scatter angles, and collects, stores, analyzes data.

The summer project involved the theoretical development of a system which could be used to measure the dynamic changes of erythrocytes during ground based studies and under conditions of low-gravity on the KC-135 research plane. Previous ground laboratory studies and space shuttle studies have shown differences in the kinetics and morphological aggregation of erythrocytes from patients with specific pathophysiological conditions (1). The erythrocyte aggregates formed in space from these patients showed a rouleaux formation while the same samples showed severe clumping and sludging on the ground (1). Erythrocytes from normal individuals showed a rouleaux formation (3) on the ground while having a random swarm-like pattern in space (1).

Developing a system using the light scattering photometer may provide a technique to evaluate the dynamic changes observed in space from erythrocytes representative of various pathophysiological conditions and different animal species. A primary objective would be to determine the relationship of the functional organization and the spatial arrangement of the erythrocytes. Procedures for both ground based and space studies need to be developed for erythrocyte collection, preparation, and storage; incorparating the erythrocytes from storage into the light scattering photometer; measuring the erythrocyte angular changes and computer analyzing the data; and collecting, preparing, and storing the erythrocytes for histological evaluation. These developmental procedures will be

employed for both ground based studies and studies in the KC-135 research plane. The ultimate goal will be to prepare a system which could evaluate the dynamic changes for any macromolecule during future space shuttle missions and for the space station.

References

1. Dintenfass, L., Osman, P., Maguire, B. and Jedrzejczyk, H. Experiment on aggregation of red cells under microgravity on STS 51-D, Space Research, Vol. 6, No. 5, 1986, 81-84.

2. Morris, S.J., Shultens, H.A., Hellweg, M.A., Striker, G. and Jovin, T.M. Dynamics of structural changes in biological particles from rapid light scattering measurements, Applied Optics, Vol. 18, No. 3, February 1979, 303-311.

3. Tuszynski, J.A., and Kimberly Strong, E. Application of the Frohlich theory to the modelling of rouleau formation in human erythrocytes, Journal of Biological Physics, Vol. 17, 1989, 19-40.

1993

NASA/ASEE SUMMER FACULTY FELLOWSHIP PROGRAM

MARSHALL SPACE FLIGHT CENTER
THE UNIVERSITY OF ALABAMA

WELD JOINT CONCEPTS FOR ON-ORBIT REPAIR OF SPACE STATION
FREEDOM FLUID SYSTEM TUBE ASSEMBLIES

Prepared By: Steven D. Jolly, Ph.D.

Academic Rank: Research Associate

Institution and
 Department: University of Colorado at Boulder,
                                Department of Aerospace Engineering Sciences

MSFC Colleague(s):   Clyde S. Jones III
                                Carolyn K. Russell

NASA/MSFC:

        Office: Materials and Processes Laboratory
        Division: Metallic Materials and Processes
        Branch: Metals Processes

INTRODUCTION AND BACKGROUND

Because Space Station Freedom (SSF) is an independent satellite, not depending upon another spacecraft for power, attitude control, or thermal regulation, it has a variety of tubular, fluid-carrying assemblies on-board. The systems of interest in this analysis provide breathing air (oxygen and nitrogen), working fluid (two-phase anhydrous ammonia) for thermal control, and mono-propellant (hydrazine) for station reboost.

The tube assemblies run both internally and externally with respect to the habitats. They are found in up to 50 ft. continuous lengths constructed of mostly AISI 316L stainless steel tubing, but also including some Inconel 625 nickel-iron and Monel 400 nickel-copper alloy tubing. The outer diameters (OD) of the tubes range from 0.25-1.25 inches, and the wall thicknesses between 0.028-.095 inches. The system operational pressures range from 377 psi (for the thermal control system) to 3400 psi (for the high pressure oxygen and nitrogen supply lines in the ECLSS).

SSF is designed for a fifteen to thirty year mission. It is likely that the TA's will sustain damage or fail during this lifetime such that they require repair or replacement. The nature of the damage will be combinations of punctures, chips, scratches, and creases and may be cosmetic or actually leaking. The causes of these hypothetical problems are postulated to be:

1. Faulty or fatigued fluid joints— both QD's and butt-welds;
2. Micro-meteoroid impacts;
3. Collision with another man-made object; and
4. Over-pressure strain or burst (system origin).

While the current NASA baseline may be to temporarily patch the lines by clamping metal c-sections over the defect, and then perform high pressure injection of a sealing compound, it is clear that permanent repair of the line(s) is necessary [Anderson 1991]. This permanent repair could be to replace the entire TA in the segment, or perhaps the segment itself, both alternatives being extremely expensive and risky. The former would likely require extensive EVA to release TA clamps an pose great risk to other engineering subsystems, and the latter would require major de-servicing of the Station.

DESIGN CONSIDERATIONS

For joining TA's in thin-walled pressure vessel applications the butt-weld is the preferred method because the resulting tube can be considered to transmit stress in the same manner as the original TA. The truth is, however, that when a metal is welded both the weld and the heat affected zone (HAZ) have different material properties than the base metal. This is true whether the application is tube welding or plate welding, or any other welding [Davies 1984, Masubuchi 1980, ASM 1985].

Designing Weld Joints for On-Orbit Repair Requires Consideration of All Systems & Structures Issues

❑ **Vacuum/Micro-g Welding**
  ◆ process characteristics, weld pool behavior, thermal requirements, weld quality

❑ **Design Strength**
  ◆ dominant stresses, concentrations, post-weld properties, margins of safety

❑ **Preparation of Tube Assembly**
  ◆ removing: oils, dirt, oxidation, outgassing accretions, contaminants, residual fluid

❑ **Cutting**
  ◆ burrs, bevels, chips, squareness, accuracies

❑ **Cleanliness**
  ◆ purge schedules, weld contamination, system contamination, materials interactions

❑ **Inspection/Verification**
  ◆ weld in-process, weld post-process, leak tests, system testing

❑ **Special Issues**
  ◆ access, jigs, gap, thermal, lighting, safety, simplicity, reliability, time, sequencing, interruption, vibration

NASA/ASEE Summer Faculty Fellowship Program   SDJ8493 6

Figure 1. Issues for Design of Weld Joints for In-Space Repair

Figure 1 illustrates the drivers for the weld joint design. The conclusions of these considerations became then, the design criteria for the study.

The criteria are:
1. The weld joint design for in-space repair applications must provide much greater compliance (with respect to cutting the TA and the replacement) than the maximum allowable gaps of the standard butt-weld (.008 inches), perhaps on the order of .5 inches.
2. This compliance must be gained without surrendering weld quality and post-weld structural performance such that positive margin exists using the standard factor of safety for SSF.
3. The weld joint needs to be self-aligning and self-latching, as much as possible.
4. The hardware should be designed and fabricated with the astronaut's glove in mind, i.e. as large as is feasible, easy to handle.
5. The repair procedure and associated hardware design should minimize the required orbital support equipment.
6. If possible, the weld joint and weld procedure should minimize contact of the weld pool with the inside diameter of the tube assembly assuming that the fluid residuals are degrading to the weld process, or that subsequent cleaning of the TA interior is required to return to service.

DESIGN CONCEPTS

Considering the above design criteria, the most logical, generalized weld joint design to consider for in-space TA repair applications appears to be like that shown in Figure 2.
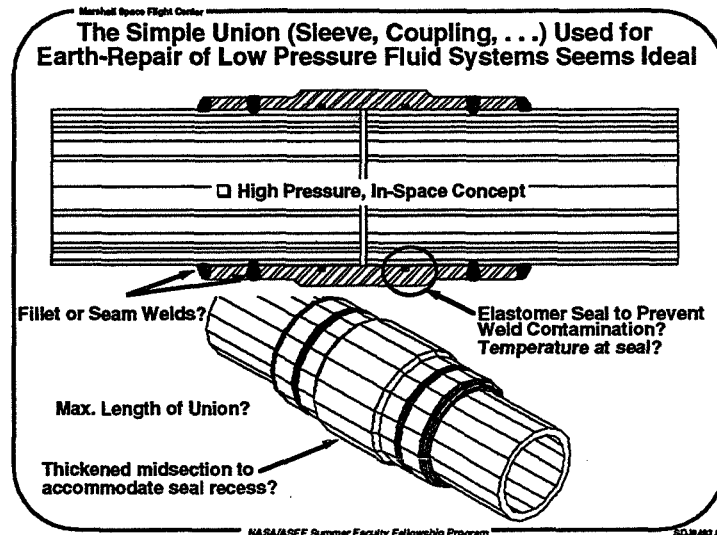
Figure 2. Family of Concepts Using Either Fillets and Seams (With or Without Seals)

The primary stresses in this concept are a result of internal pressure on a thin-walled vessel. Commonly called hoop and axial stress they can be predicted with thin shell theory of classical mechanics. For values below the elastic limit Figure 3 shows a simple model for computer evaluation and allows "quick look" design analysis..
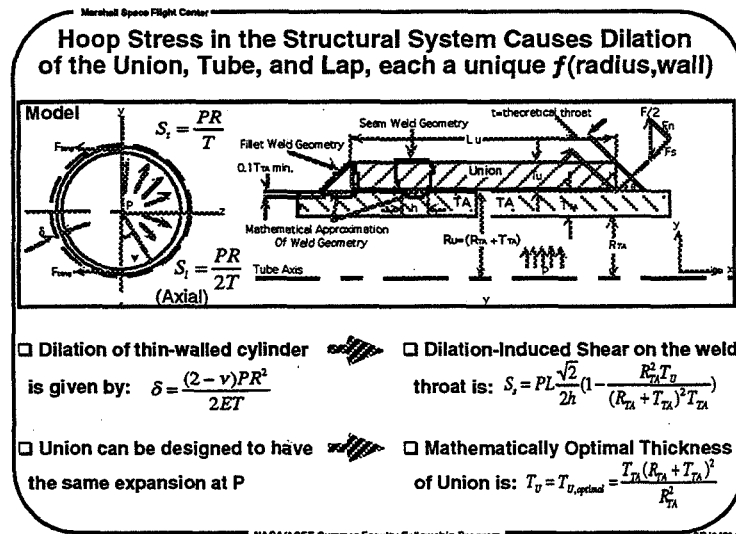
Figure 3. Stress Analysis Model of Weld-Union Concept

SUMMARY AND CONCLUSIONS

❑ Overall, it is clear that a large portion of the complexity of on-orbit, permanent repair of high pressure, thin-walled tubing is not really a function of the joint design being utilized in the repair.

❑ The fillet or seam welded union such as that introduced in this paper would appear to provide the best weld joint from an all-around process perspective. The

butt-weld used for terrestrial manufacturing of the SSF hard lines is definitely superior from a structural perspective compared to a union with $T_U < T_{U,optimal}$, but it is a difficult in-space repair technique for TA's.
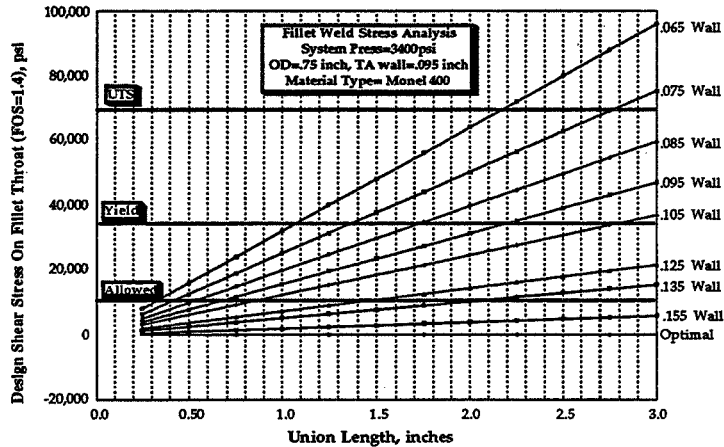
Figure 17. Analysis Yields Positive Margins for Near-Optimal Union Thicknesses

In summary, when:

1) $T_U < T_{U,Optimal}$ the weld throat is shear stressed radially outward;

2) $T_U = T_{U,optimal}$ the weld throat has no shear stress (just hoop and axial stress); and

3) $T_U > T_{U,Optimal}$ the weld throat is shear stressed radially inward.

ACKNOWLEDGMENT

The author would like to acknowledge the help of his NASA colleagues Chip Jones and Carolyn Russell, Dr. Arthur Nunes who was very helpful and finally, Mr. Ray Anderson of MDSSC who has been an invaluable resource of information, documents, and all around help.

REFERENCES
1. Anderson, R. H., "EVA/Telerobotic Fluid Line Repair Tool Development", Welding In Space and the Construction of Space Vehicles by Welding, proceedings, American Welding Society, 1991, Miami, FL
2. ASM, Metals Handbook, Desk Edition, American Society For Metals, 1985, OH
3. Davies, A.C., The Science and Practice of Welding, Vol. 2, Cambridge University Press, 1984, Bath, Great Britain, p.41
4. Masubuchi, K., Analysis of Welded Structures, International Series on Materials Science and Technology, Vol. 33, Pergamon Press, 1980, New York, N.Y.

1993

NASA/ASEE SUMMER FACULTY FELLOWSHIP PROGRAM
MARSHALL SPACE FLIGHT CENTER
THE UNIVERSITY OF ALABAMA

DIFFUSION ON Cu SURFACES

Prepared by: Majid Karimi, Ph. D.

Academic Rank: Assistant Professor

Instittution: Indiana University of
                                    Pennsylvania

Department: Physics

NASA/MSFC

       Office: EH22

       Division: Metallic Materials

       Branch: Metallurgical & Failure
                                    Analysis

MSFC Colleague: Ilmars Dalins, Ph. D.

Introduction

Understanding surface diffusion is essential in understanding surface phenomena, such as crystal growth, thin film growth, corrosion, physisorption, and chemisorption. Because of its importance various experimental and theoretical efforts have been directed to understand this phenomena. Field Ion Microscope (FIM) has been the major experimental tool for studying surface diffusion. FIM have been employed by various research groups to study surface diffusion of adatoms. Because of limitations of the FIM such studies are only limited to a few surfaces; nickel, platinum, aluminum, iridium, tungsten, and rhodium (4, 5). From the theoretical standpoint, various atomistic simulations are performed to study surface diffusion. In most of these calculations the Embedded Atom Method (EAM) of Daw and Baskes(2) along with the molecular static (MS) simulation are utilized. The EAM is a semi-empirical approach for modeling the interatomic interactions. The MS simulation is a technique for minimizing the total energy of a system of particles with respect to the positions of its particles.

One of the objectives of this work is to develop the EAM functions for Cu and use them in conjunction with the molecular static (MS) simulation to study diffusion of a Cu atom on a perfect as well as stepped Cu(100) surfaces. This provide a test of the validity of the EAM functions on Cu(100) surface and near the stepped enviroments. In particular, we construct a terrace-ledge-kink (TLK) model (figure 1) and calculate the migration energies of an atom on a terrace, near a ledge site, near a kink site, and going over a descending step. We have also calculated formation energies of an atom on the bare surface, a vacancy in the surface, a stepped surface, and a stepped-kink surface. Our results are compared with the available experimental and theoretical results.

Methodology

Pair potentials suffer at least from two major problems. Cauchy pressure $C_{11}-C_{12}=0$ and single vacancy formation energy is equal to the cohesive energy $E_{1v}=E_c$. For a metal $C_{11} \neq C_{12}$ and $E_{1v} \neq E_c$. To overcome these and other shortcomings, the EAM potential is developed for Cu. In the EAM, energy of each atom is approximated with sum of the embedding and two body contributions,

$$E_i = F_i(\rho_i) + .5\Sigma\ \phi(r_{ij}), \qquad\qquad (1)$$

where $F_i(\rho_i)$ is the embedding energy of atom i which can be interpreted as the energy that is required to embed an atom into the electronic charge created by the other atoms, ρ_i is the charge density at site i, $\phi(r_{ij})$ is the two body potential between atoms i and j, and r_{ij} is the separation distance between atoms i and j. ρ_i is approximated with the superposition of atomic charge densities(1, 2). Functional forms are considered for F and ϕ and their parameters are determined by fitting to the bulk properties of crystalline solid (1, 2).

In our calculations, we have employed two sets of EAM potentials one developed by us(2) and the other one developed by Adams et.al.(3). We have utilized the above EAM potentials along with the MS simulation to calculate formation energies of an atom on the surface, a vacancy on the surface, stepped surface, and stepped kink surface. We have also calculated migration energies of an atom on the bare surface, near a ledge, near a kink, and over a descending step.

Results

a) Adatom formation and migration energies

Our lattice is a slab of 12 parallel layers with 144 atoms per layer. An atom is placed on the surface layer and the formation and migration energies of the adatom are calculated from the following formulas(4, 5),

$$E^f_{1a}=E(N+1,1) - E(N,0)+E_S \quad , \qquad (2a)$$
$$E^m_{1a}=E_{sad} - E_{min} \qquad , \qquad (2b)$$

where E^f_{1a} is the formation energy of an adatom, $E(N+1,1)$ is the total minimized energy of the lattice of N atoms and one adatom, $E(N,0)$ is the minimized energy of the lattice of N atoms, E_S is the sublimation energy(negative of cohesive energy), E^m_{1a} is the migration energy of an adatom, E_{sad} is the minimum total energy of the system with adatom at the saddle point , and E_{min} is the minimum total energy of the system with adatom in a lowest energy binding site. Our results for E^f_{1a}, E^m_{1a}, and activation energy $Q_{1a}=E^f_{1a} + E^m_{1a}$ are .71ev, .48ev, and 1.19 ev, respectively.

b) Vacancy formation and migration energies

A vacancy is created in the surface of the slab in part (a) and formation E^f_{1v} and migration E^m_{1v} energies of the vacancy are calculated from the following formulas (4, 5),

$$E^f_{1v}=E(N-1,1) - E(N,0) - E_S \quad , \qquad (3a)$$
$$E^m_{1v}=E_{sad} - E_{min} \qquad , \qquad (3b)$$

where $E(N-1,1)$ is the minimized energy of the lattice of N atoms and one vacancy. Our results for E^f_{1v}, E^m_{1v}, and Q_{1v} are .59 ev, .35 ev , and $Q_{1v}=.95$ ev , respectively.

c) Formation energies of steps

A step similar to one in figure 1 is constructed and its formation energy is calculated using the following formula (4, 5),

$$E_{step} = E - N_1 E_u + N E_S \quad , \qquad (4)$$

where E is the total minimized energy of the system of N atoms with step, N1 is the total numbers of atoms of upper and lower terraces, and Eu is the surface energy. Our results for the formation energies of steps with and without kink are .11 ev/A and .05 ev/A , respectively.

d) Migration energies of an atom for various moves

Migration energies of an atom for various moves on a stepped surface(shown in figure 1) are calculated using formula 2b. Our results for migration energies of moves

a, b, c, d, e, f are .485 ev, .246 ev, .507 ev, .834 ev, .522 ev, .and 355 ev, respectively.

e) Migration energies of an atom on bare surfaces

Migration energies of an atom on Cu(100), Cu(110), Cu(111) are calculated using formula 2b. Our results are E^m_{1a}=.48 ev, $E^m_{1a}(110)\parallel$=.23 ev, $E^m_{1a}(110)\perp$=.30 ev, and $E^m_{1a}(111)$=.026 ev for (100), (110), and (111) surfaces.

Summary and conclusion

a) Vacancy diffusion is dominant diffusion on Cu(100) surface. This is in agreement with another simulation results.

b) Migration energies of an adatom follows the following trend, $E^m_{1a}(100) > E^m_{1a}(110 > E^m_{1a}(111)$. This is consistent with other simulations and experiments.

c) The formation energies of an adatom, a vacancy, a step without kink, a step with kink are calculated. The trend is consistent with other simulations.

d) Migration energy of an atom along the ledge on a Cu(100) stepped surface is smaller than its corresponding value on a bare Cu(100) surface. This is consistent with another simulation.

e) Migration energy of an adatom over a descending step is slightly larger than its corresponding value on a bare Cu(100) surface. This result is in qualitative agreement with another computer simulation.

References

1. M. S. Daw and M. I. Baskes, Phys. Rev. B29, 6443 (1984).
2. M. Karimi and M. Mostoller, Phys. Rev. B45, 6289 (1992).
3. J. B. Adams, S. M. Foiles, and W. G. Wolfer, J. Mater. Res. 4, 102 (1989).
4. C. L. Liu, J. M. Cohen, J. B. Adams, and A. F. Voter, Surf. Sci. 253,334 (1994).
5. C. L. Liu and J. B. Adams, Surf. Sci. 265, 262 (1992).
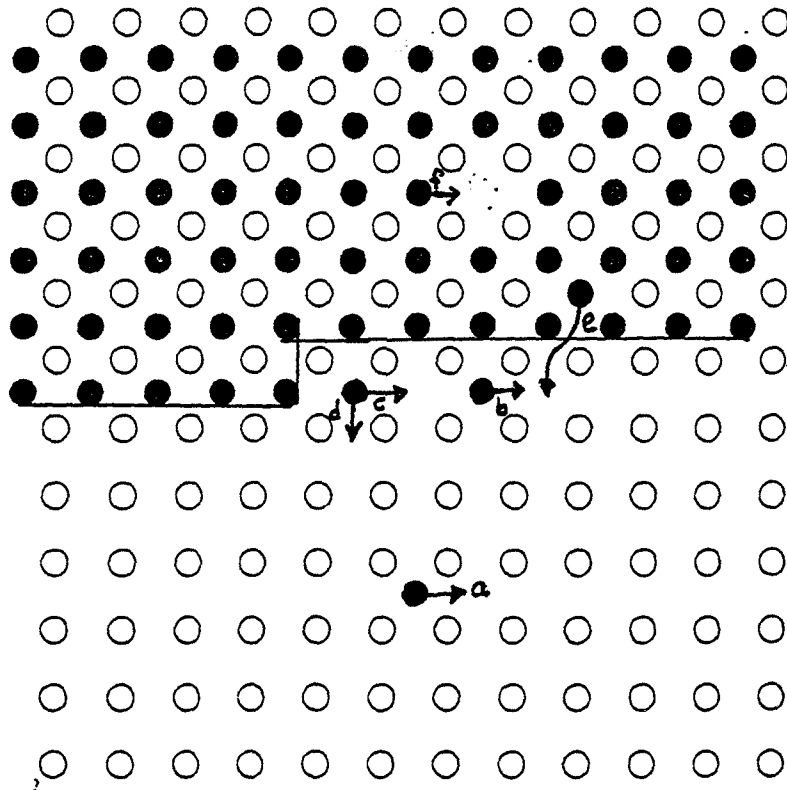
Fig. 1

1993

NASA/ASEE SUMMER FACULTY FELLOWSHIP PROGRAM

MARSHALL SPACE FLIGHT CENTER
THE UNIVERSITY OF ALABAMA IN HUNTSVILLE

J-INTEGRAL PATCH FOR FINITE ELEMENT ANALYSIS OF DYNAMIC FRACTURE DUE TO IMPACT OF PRESSURE VESSELS

Prepared By: Boris I. Kunin, Ph.D.

Academic Rank: Assistant Professor

Institution and
  Department: University of Alabama in Huntsville
                        Department of Mathematical Sciences

MSFC Colleague: Rene Ortega

NASA/MSFC:

        Laboratory: Structures and Dynamics
        Division: Structural Analysis
        Branch: Thermostructural Analysis

1. Introduction

Prediction of whether a pressurized cylinder will fail catastrophically when impacted by a projectile has important applications ranging from perforation of airplane's skin by a failed turbine blade to meteorite impact of a space station habitation module. This report summarizes the accomplishment of one task for a project, whose aim is to simulate numerically the outcome of a high velocity impact of pressure vessels. A finite element patch covering a vicinity of a growing crack has been constructed to estimate the J-integral (crack driving force) during the impact. Explicit expressions for the J-integral through the nodal values of displacement, strain, and stress have been written. The patch is to be used repeatedly to estimate the amount of crack growth during the the time of the impact. The resulting crack size is to be compared to an estimated critical crack size for the pressurized cylinder.

A literature search produced a number of papers dealing with evaluation of J-integral within finite element environment. Most of the research reports, however, present the shape of the finite element mesh only, with no detail on node locations. Such information was hard to utilize in the absence of an automated mesh generator. As a result, the simplest mesh was chosen for the patches, following (2). The same search turned up studies of the accuracy of finite element J-integral evaluations as well as the effect of the choice of the contour of integration. This provided a rational basis for the choices made in the present work.

A complementary literature search has been done to collect data on fracture toughness of 2219 aluminum alloys, since this material property enters the employed crack growth criterion.

The third literature search concerned reports on high- and hypervelocity impact studies (both experimental and theoretical) to form a basis for comparison with the numerical simulations produced by the entire project.

Complete computational details and the three literature reviews have been left with Rene Ortega.

2. Circumferential and Axial Patches

Both patches have the shape of a rectangle with an edge crack mapped onto a portion of the cylinder's surface as shown in Fig 1. The finite element mesh consists of 8-node isoparametric elements (1). Of these only the four which surround the crack tip are distorted, namely, the five nodes neighboring the crack tip are placed at the quarter distance from the tip instead of being half distance away (see Fig 2). Formulas shown in Fig 1 permit to find the 3D coordinates of any node.

3. J-integral expressions

J-integral is the following contour integral:

$$x = R\left(\cos\frac{hC}{R} - 1\right)$$
$$y = R \sin \frac{hC}{R}$$
$$z = -hB$$

$$x = R\left(\cos\frac{hB}{R} - 1\right)$$
$$y = R \sin \frac{hB}{R}$$
$$z = hC$$
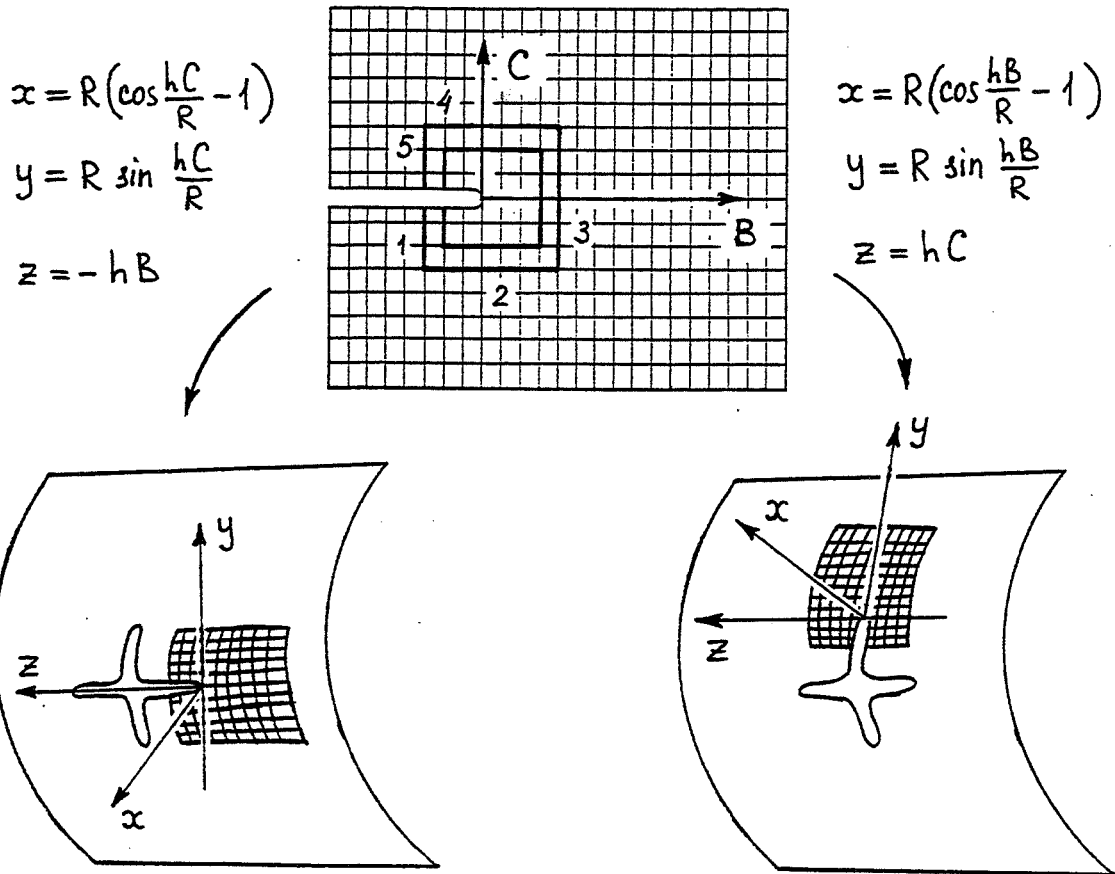
FIG. 1
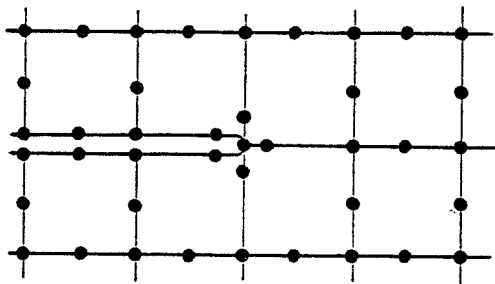
FIG. 2
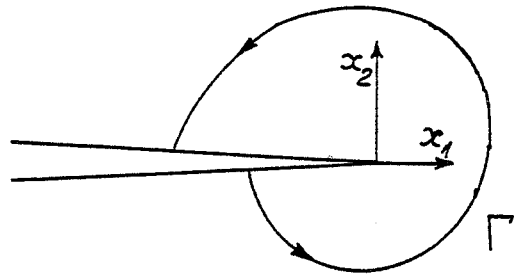
FIG. 3

$$J = \int_{\Gamma} (w\, n_1 - T_i\ \partial u_i/\partial x_1\ )ds \qquad\qquad [1]$$

where w is the strain energy density, T_i is the traction, x_1 is the coordinate in the direction of the crack, and Γ is any contour that begins on one face of the

crack and ends on the other (see Fig 3). The integral has the meaning of the potential energy release per unit crack advance (known as 'the energy release rate', or 'the crack driving force').

Explicit expressions for the J-integral through the nodal values of displacement, strain , and stress have been written for the two contours shown in Fig 1. The structure of those expressions is exemplified below for the inner contour.

Eq [1] is rewritten as

$$J = I_1 - I_2 \tag{2}$$

where

$$I_1 = \int_\Gamma w \, dx_2 \tag{3}$$

and

$$I_2 = \int_\Gamma \sigma_{ij} \, (\partial u_i / \partial x_1) \, n_j \, ds \tag{4}$$

The contour is split into five paths $\Gamma_1,...,\Gamma_5$ (see Fig 1), and the integrals [3,4] become the sums of the integrals over these paths:

$$I_k = I_{k1} + ... + I_{k5} , \quad k = 1,2. \tag{5}$$

As examples, the expressions for I_{11} and I_{21} through he nodal values of u_2, ε_{ij}, and σ_{ij} are shown here:

$$I_{11} = - (h/6) (w^{229} + 4w^{244} + 2w^{255} + 4w^{270} + w^{281}) \tag{6}$$

$$I_{21} = - (h/6) (f^{229} + 4f^{244} + 2f^{255} + 4f^{270} + f^{281}) \tag{7}$$

where h is the mesh size, the upper indecies refer to node numbers,

$$w = \sigma_{ij} \, \varepsilon_{ij} / 2 \tag{8}$$

$$f = \sigma_{11} \, \varepsilon_{11} + \sigma_{12} \, (\partial u_2 / \partial x_1) \tag{9}$$

and, as a matter of example, the expression for $\partial u_2 / \partial x_1$ through the nodal values of u_2 is shown:

$$(\partial u_2 / \partial x_1)^{244} = (1/2h)(u_2^{257} + u_2^{231} - u_2^{227} - u_2^{253})$$

$$+ (1/h)(u_2^{254} + u_2^{243} + u_2^{228} - u_2^{230} - u_2^{245} - u_2^{256}) \tag{10}$$

3. Testing of the patch

To verify the numerical procedures, comparison has been proposed with an existing solution for a rectangular plate with an edge crack parallel to the clamped edges (4).

4. Discussion

The energy release rate and its J-integral representation employed in this study corresponded to static (or slowly growing) crack, whereas the crack under consideration is a fast growing one. However, it is known that the energy release rate for a moving crack is related to the static one as $G^{dyn} = g(v)G^{stat}$, where $g(v)$ is a monotonically decreasing function of the crack velocity v which goes from 1 at v = 0 to 0 at v reaching the Rayleigh wave speed (3). Therefore employing G^{stat} overestimates the crack driving force and thus is conservative when a possibility of a catastrophic failure of the cylinder is considered.

If, nevertheless, the estimates will result in unrealistically large crack sizes at the end of the duration of the impact, expressions for dynamic J-integrals and their evaluation in finite element environment are available (see the literature review).

Finite element models of elastic-plastic crack growth in the presence of both small and large scale yielding are also available in the literature (see the literature review).

Acknowledgment

References

1. Barsoum, Roshdy, On the use of isoparametric finite elements in linear fracture mechanics, *Int. J. for Numerical Methods in Engineering*, 10 (1976), 25-37.

2. Hurlbut, Arthur, Finite Element Modeling of Crack Growth and Failure of Composite Laminates, Ph.D. Thesis, Clarkson University, 1985.

3. Kanninen, Melvin and Popelar, Carl, Advanced Fracture Mechanics, Oxford University Press, New York, 1985.

4. Torvik,P.J., On the determination of stresses, displacements, and stress-intensity factors in edge-cracked sheets with mixed boundary conditions, Trans. ASME, Ser E, J. Appl. Mech. 46 (1979), 611-617.

1993

NASA/ASEE SUMMER FACULTY FELLOWSHIP PROGRAM

MARSHALL SPACE FLIGHT CENTER
THE UNIVERSITY OF ALABAMA IN HUNTSVILLE

CFD SIMULATION OF COAXIAL INJECTORS

Prepared By: D. Brian Landrum, Ph.D.

Academic Rank: Assistant Professor

Institution and   University of Alabama in Huntsville
  Department: Department of Mechanical and Aerospace
                             Engineering

MSFC Colleagues: Ten See Wang
                             P. Kevin Tucker

NASA/MSFC:

      Offices: Structures and Dynamics Laboratory
      Division: Aerophysics
      Branch: Computational Fluid Dynamics

CFD SIMULATION OF COAXIAL INJECTORS

D. Brian Landrum, Ph.D.
Assistant Professor
Department of Mechanical and
Aerospace Engineering
University of Alabama in Huntsville

INTRODUCTION

The development of improved performance models for the Space Shuttle Main Engine (SSME) is an important, ongoing program at NASA MSFC. These models allow prediction of overall system performance, as well as analysis of run-time anomalies which might adversely affect engine performance or safety. Due to the complexity of the flow fields associated with the SSME, NASA has increasingly turned to Computational Fluid Dynamics (CFD) techniques as modeling tools.

An important component of the SSME system is the fuel preburner, which consists of a cylindrical chamber with a plate containing 264 coaxial injector elements at one end. A fuel rich mixture of gaseous hydrogen and liquid oxygen is injected and combusted in the chamber. This process preheats the hydrogen fuel before it enters the main combustion chamber, powers the hydrogen turbo-pump and provides a heat dump for nozzle cooling. Issues of interest include the temperature and pressure fields at the turbine inlet, and the thermal compatibility between the preburner chamber and injector plate. Performance anomalies can occur due to incomplete combustion, blocked injector ports, etc. The performance model should include the capability to simulate the effects of these anomalies.

The current approach to the numerical simulation of the SSME fuel preburner flow field is to use a global model based on the MSFC sponsored FDNS code (1). This code does not have the capabilities of modeling several aspects of the problem such as detailed modeling of the coaxial injectors. Therefore, an effort has been initiated to develop a detailed simulation of the preburner coaxial injectors and provide gas phase boundary conditions (species concentrations, pressures, temperatures, etc.) just downstream of the injector face as input to the FDNS code. This simulation should include three-dimensional geometric effects such as proximity of injectors to baffles and chamber walls and interaction between injectors.

This report describes an investigation into the numerical simulation of GH2/LOX coaxial injectors. The following sections will discuss the physical aspects of injectors, the CFD code employed, and present preliminary results of a simulation of a single coaxial injector for which experimental data is available. It is hoped that this work will lay the foundation for the development of a unique and useful tool to support the SSME program.

PHYSICAL ASPECTS OF COAXIAL INJECTORS

Liquid propellant rocket injection is a complex combination of physical process including liquid atomization and evaporation, and chemical reactions. The complexity is increased by the fact that at least one of the constituents exists in both the liquid and vapor phases. In order to make the injection simulation problem numerically tractable, these physical processes are described by sub-models. The following two sections describe the sub-models for atomization and evaporation. The current study did not include the effects of chemical reactions and therefore this sub-model will not be discussed.

Injection / Atomization

In a coaxial injector the core liquid propellant jet is broken into smaller droplets through shear forces imposed by the co-flowing, high velocity, annular gas jet surrounding it. A cursory review of current atomization modeling capabilities and the experimental validation data base was recently presented by Liang, et al. (2). Currently, there are two primary approaches to the modeling of an atomizing liquid jet. The first approach, known as the Jet Embedding Technique (3), resolves the intact jet shape exactly with an adaptive grid. Simplified equations of motion are solved within the core to model its growth and subsequent atomization.

The second approach to atomization modeling is known as the Blob Atomization Model. This approach is based on the Reitz's approximation of the surface wave dispersion equation for a round jet (4) in conjunction with a Taylor Analogy Breakup model (5). The model assumes that the liquid jet can be represented by injected drops which are the diameter of the injection port. Linear stability theory is then used to model secondary breakup into smaller drops. Atomization is a function of droplet aerodynamics, liquid surface tension, and liquid viscosity. This approach does not allow the shape of the jet to be resolved. Numerically, the technique can be coupled to a Volume Of Fluid (VOF) technique (6), in which the fractional volumes of liquid, droplets and gas are tracked within each computational cell. The Blob Atomization and VOF approaches were used in the simulation described in this report.

Evaporation

A sub-model is also required to simulate the effects of evaporation of the cold liquid into the warmer surrounding gas. A vapor-liquid film model is used on the droplet surface. Quasi-steady state diffusion and energy equations are solved for the droplet heating rate and evaporation rate. The resultant equations used are presented by Liang and Ungewitter (see Reference 4).

For many injector scenarios the evaporation occurs at subcritical conditions where the droplet surface temperature is assumed to be the liquid saturation temperature. For the case of SSME preburner LOX injection, the chamber pressure far exceeds the critical pressure. In this situation the surface of the LOX droplet can be in a critical state while the interior of the droplet remains below the critical temperature. A supercritical evaporation model must ultimately be used. Reference 4 describes such a model although only subcritical evaporation was considered in the preliminary study documented in this paper.

COMPUTATIONAL CODE AND MODIFICATIONS

The numerical simulation was based on the Multiphase All-Speed Transient (MAST) code of Chen (7). This code uses a time accurate, temporal marching technique. The method is pressure based and also uses a operator-splitting algorithm to allow for various speed regimes in the flow field. A stochastic particle tracking method is incorporated (8). MAST uses a VOF technique, but simulation results indicate that this may not be totally active. The MAST code also includes a limited capability to generate computational grids. Options to generate uniform, exponentially stretched and mixed grids are available.

The MAST code was modified for this study. Although the numerical structure of the code is generalized for arbitrary fluid constituents, many thermofluid properties in the current version were hardwired for air. These properties had to be replaced with values representative of hydrogen and LOX. First, various thermofluid properties for the gaseous hydrogen were inserted. The second major task consisted of assembling a LOX data base. Required parameters included vapor pressure, latent heat of vaporization, surface tension, and viscosity of LOX as a function of temperature. A representation of the binary diffusion of oxygen into hydrogen also had to be provided.

EXPERIMENTAL DATA

A large experimental data base exists for coaxial injection using a variety of test liquids and gases. This data base is summarized in Reference 2. A capability for simulation of coaxial injection is currently being demonstrated at the Pennsylvania State University Propulsion Engineering Research Center (PSU/PERC). The hardware consists of a cylindrical chamber with an injector assembly at one end and a nozzle section at the other. The dimensions of the injector are comparable to the fuel preburner elements used in the SSME. Details of the injector assembly hardware are described by Pal, et al. (9). Both cold flow GN2/H2O and hot -fire GH2/LOX injection has been performed in the laboratory to date. Because of the potential of this laboratory to produce validation data, a simulation of the PSU/PERC injector was chosen as the test case of this study.

INJECTOR SIMULATION RESULTS

The PSU/PERC chamber was modeled with an axisymmetric computational grid shown in Fig. 1. Only one-quarter of the length of the chamber was modeled. The upper half of the chamber was modeled so that the first grid line is the combustion chamber axis. For this preliminary investigation the numerically simulated injector did not include the LOX post recess. A fine uniform grid was used in the hydrogen annulus region. The grid was exponentially stretched from this region down to the chamber axis and upwards to the chamber wall. The total grid was 60 axial by 50 radial points. An injection boundary condition was applied at the hydrogen annulus and the downstream boundary condition was to fix the pressure at the quoted value for the hot-fire tests. The chamber axis was a symmetry boundary condition and all other surfaces were modeled with no-slip wall boundary conditions. Consistent with the blob injection used in the MAST code, LOX droplets were created at the i=2, j=2 grid point. These droplets could then convect or breakup in the chamber.

Several simulations were performed in order to investigate the capabilities of the MAST code. These consisted of hydrogen injection only, LOX droplet injection only and coaxial GH2/LOX injection. Representative results are illustrated in Figs. 2 and 3 where the location of LOX droplet parcels in the computational domain are plotted at a time of 0.5 msec. Figure 2 shows the parcel distribution for LOX injection into static hydrogen. The droplets have penetrated a short distance into the chamber with no significant lateral dispersion. In Fig. 3 the LOX droplets are injected with the surrounding hydrogen jet. The axial penetration is comparable to the LOX injection only. The significant difference is the dispersion of the droplets laterally into the chamber. An interesting result of the simulation was that no droplet evaporation was seen during the time simulated. This may be due to the small magnitude of the temperature gradient between the LOX droplets (injected at 117 K) and the injected and ambient hydrogen gases (both at 289 K). This behavior may also indicate that the code is not accurately modeling the evaporation.

CONCLUSIONS / FUTURE WORK

A preliminary study of numerical simulation of GH2/LOX coaxial injection has been performed. The MAST code was modified with thermofluid properties for hydrogen and oxygen. The modeled injector was based on hardware currently being used at Penn State University. Several aspects of the injection problem were simulated in order to evaluate the capabilities of the MAST code. Qualitative results indicate that the effects of the annular hydrogen jet are to disperse the LOX droplets laterally. No droplet evaporation was predicted. This may be due to the temperature gradients simulated or indicate a failure of the code evaporation model. Further analysis is required.

In general the MAST code was difficult to implement. Many of the thermofluid

parameters were hardwired for air and had to be changed. There is also some question as to whether the incorporated sub-models are correctly implemented. But, this criticism must be tempered by the fact that this is the first time that the code has been used to model a coaxial injection case. Further investigation into the code capabilities is therefore warranted.

Future work should include incorporation of H2-O2 gas chemistry into the simulation. The capability to model supercritical evaporation should also be included in the code. Detailed validation studies should then be performed using the Penn State GN2/H2O and GH2/LOX data.

ACKNOWLEDGEMENTS

REFERENCES

1. Chen, Y. S., "FDNS - A General Purpose CFD Code: User's Guide," *ESI-TR-93-01*, Engineering Sciences, Inc., May 1, 1993.

2. Liang, P. Y., Przekwas, A. J., and Santoro, R. J., "Propellant Injection and Atomization," Presented at the Combustion-Driven Flow Technology Team Meeting, NASA MSFC, July ??, 1993,.

3. Przekwas, A. J., Chuech, S., and Singhal, A. K., "Numerical Modeling of Primary Atomization of Liquid Jets," *AIAA 89-0163*, 1989.

4. Liang, P. Y. and Ungewitter, R., "Multi-Phase Simulations of Coaxial Injector Combustion," *AIAA 92-0345*, 1992.

5. Seung, S. P., Chen, C. P., and Chen, Y. S., "Development of an Atomization Methodology for Spray Combustion," presented at the 11th Workshop for CFD Applications in Rocket Propulsion, NASA MSFC, April 20-22, 1993.

6. Liang, P. Y. and Schuman, M. D., "Atomization Modeling in a Multiphase Flow Environment and Comparison with Experiments," *AIAA 90-1617*, 1990.

7. Chen, C. P., Jiang, Y., Kim, Y. M., and Shang, H. M., "A Computer Code for Multiphase All-Speed Transient Flows in Complex Geometries," NASA CR (unnumbered), October, 1991.

8. Kim, Y. M., Shang, H. M., Chen, C. P., and Ziebarth, J. P., "Numerical Modeling for Dilute and Dense Sprays," presented at the 10th Workshop for CFD Applications in Rocket Propulsion, NASA MSFC, April 28-30, 1992.

9. Pal, S., Moser, M. D., Ryan, H. M., Foust, M. J., and Santoro, R. J., "Flowfield Characteristics in a Liquid Propellant Rocket," *AIAA 93-1882*, 1993.
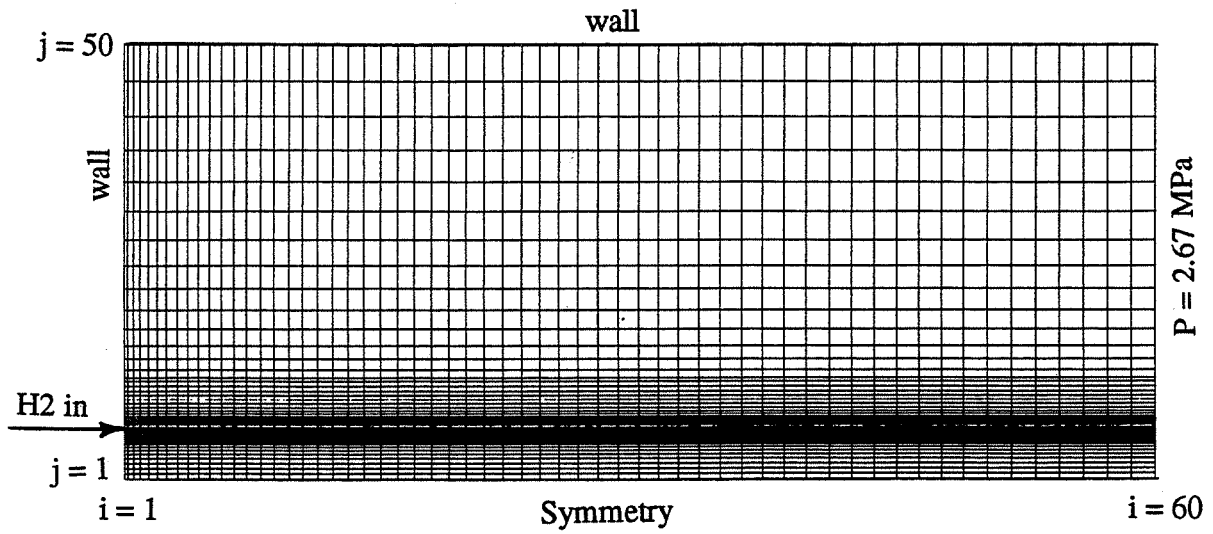
Fig. 1 Computational grid and boundary conditions for PSU injector simulation

Fig. 2 Spray parcel distribution for LOX injection only, t = 0.5 msec.
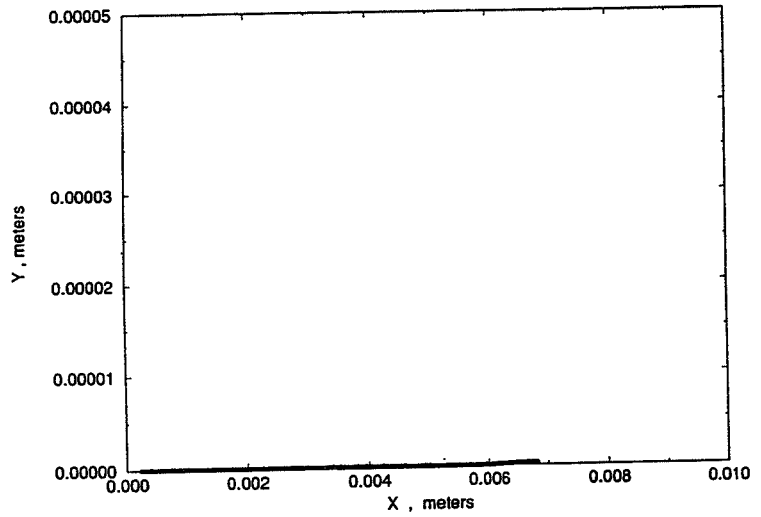
Fig. 3 Spray parcel distribution for GH2/ LOX injection, t = 0.5 msec.
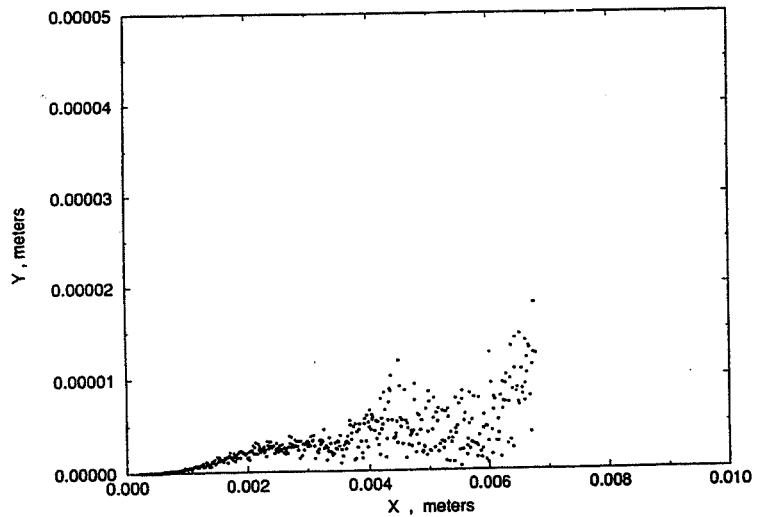
1993

NASA/ASEE SUMMER FACULTY FELLOWSHIP PROGRAM

MARSHALL SPACE FLIGHT CENTER
The University of Alabama

Structure in Gamma-Ray Burst Time Profiles:
Correlations with Other Observables

Prepared by: John Patrick Lestrade

Academic Rank: Associate Professor

Institution and Department: Mississippi State University
                                               Department of Physics and
                                               Astronomy

MSFC Colleague: G. J. Fishman

NASA/MSFC:

    Laboratory: Space Science

    Division: Astrophysics

    Branch: Gamma-Ray Astronomy

Introduction

One of the current debates raging in the world of gamma-ray burst physics is whether the sources of these enigmatic bursts arise from a single or from multiple distributions. Several authors contend that the histograms of GRB observables imply the latter. The two most-likely candidate components are galactic and cosmological. For example, Atteia et al. (1993) claim that a dip in the V/V_{max} distribution is a result of such a two-component source distribution. Lamb et al. (1993) have used a parameter called the 'burst variability' calculated by dividing the maximum count rate on the 64-msec timescale by that from the 1024-msec timescale to show that a correlation of this parameter with burst brightness implies a two-component model. Lamb's paper has met vigorous criticism.

We have developed two parameters that measure the variability or structure in the time profiles of BATSE gamma-ray bursts. Both parameters ("structure" and "spike height") are based on the statistics of "runs up" and "runs down" (Knuth, 1981). In short, the structure parameter is the observed number of runs (at several lengths) minus the number expected in a chance distribution. The "spike height" is the sum of all run heights minus the expected sum. These two are straight-forward to calculate, robust, and measure the variability over the complete profile – not just at the peak. For a full description of the algorithm, refer to Lestrade (1993).

We have applied this algorithm to the profiles of 156 GRB's. In this paper we present graphs of the two parameters as functions of 1) burst duration, 2) burst hardness ratio, 3) V/V_{max}, 4) source galactic longitude, and 5) source galactic latitude. We seek correlations as well as groupings in the data that might indicate a multi-component source distribution.

Correlations:

1) Duration: As a measure of duration we take the values of T_{90} in units of 64-msec bins. In this paper, we are considering only those bursts whose durations are longer than 12 seconds (i.e., 200 bins.) As Figure 1 shows, there are no apparent groupings nor significant correlations.

2) Hardness: For the hardness ratio, we use the value $h =$(chan 3+ chan 4)/(chan 1+ chan 2) from the BATSE DISCSC data. This is approximately equal to the flux above 100 keV divided by the flux below 100 keV (down to the threshold of roughly 25 keV). As before, Figure 2 shows no correlation nor any evidence of grouping.

3) V/V_{max}:   The quantity V/V_{max} measures the relative distance to a burst. Distant, weak bursts have values close to unity while the brightest have values close to zero. For a homogeneous distribution of sources, the distribution should show a uniform distribution between 0 and 1. As is well documented, the ensemble of

GRB's shows a paucity of weak bursts indicating a radial inhomogeneity. In effect, our instruments are seeing to the "edge" of the radial distribution.

Of course, we would expect to see a correlation between the amount of structure in a burst and the burst's distance (or V/V_{max}). This is seen in Figure 3 which shows that the more distant, i.e., weakest bursts, show less structure because the smaller spikes are lost in the background noise. Naturally, as seen in the right part of Figure 3, the more distant bursts have spikes which are less intense.
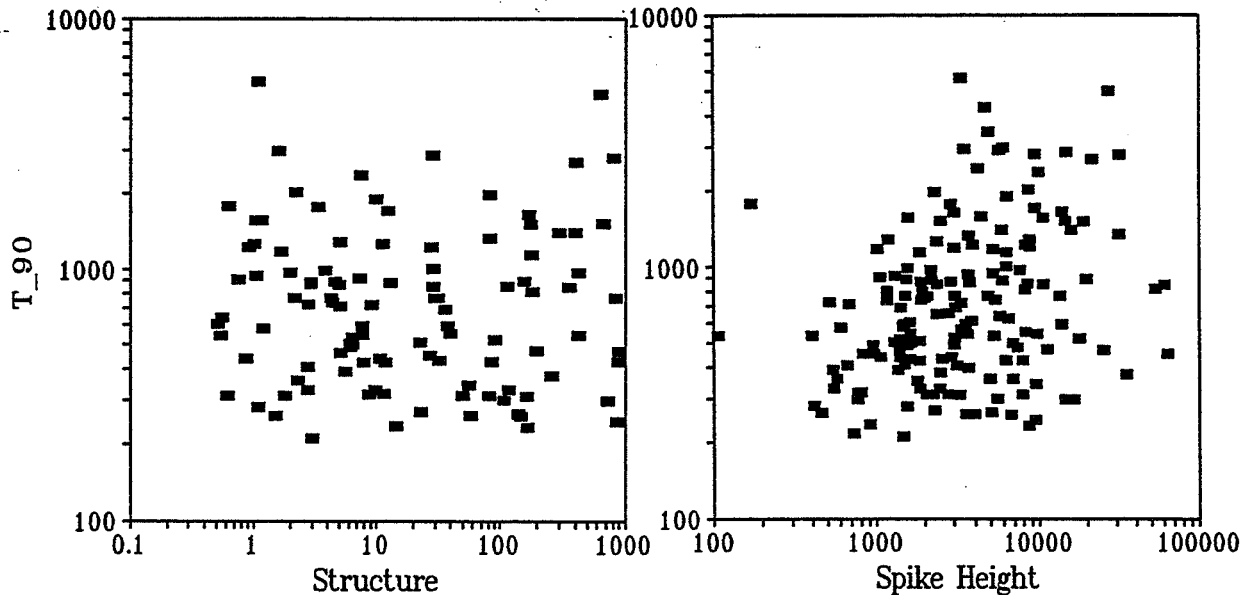
Figure 1. Burst Duration versus Structure and Spike Heights
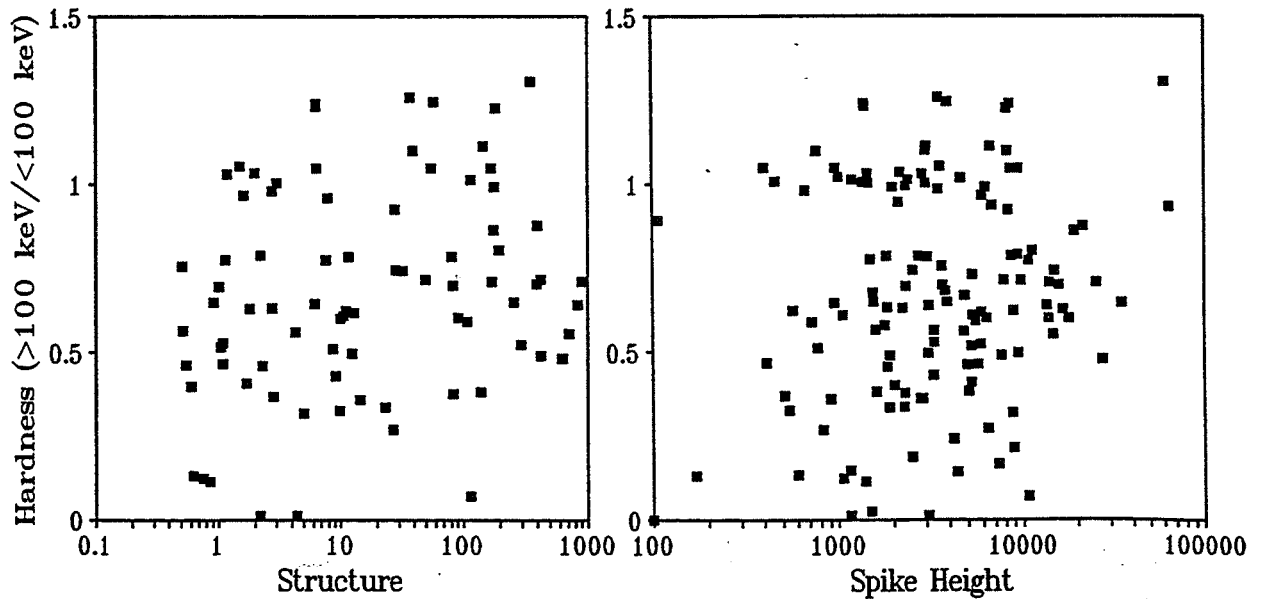
Figure 2. Burst Hardness Ratio versus Structure and Spike Heights
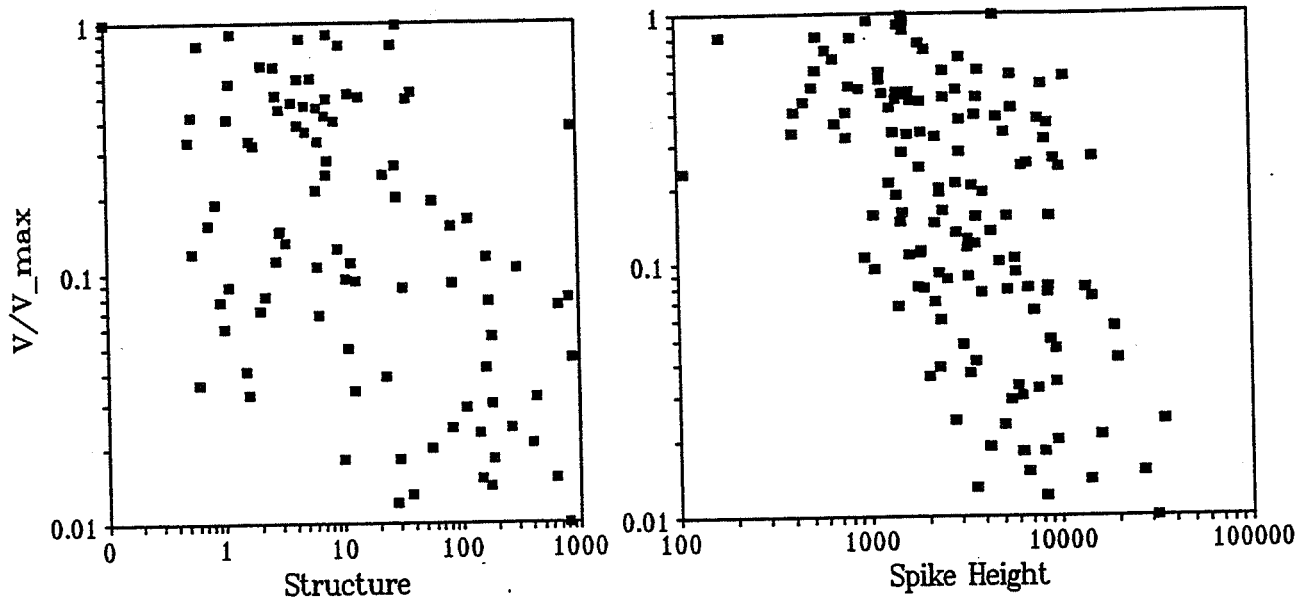
Figure 3. Burst V/V_{max} versus Structure and Spike Heights

4) Sky Position: Finally, Figures 4 and 5 present graphs of galactic longitude and latitude versus structure and spike height. Figure 4 shows no significant features in galactic longitude. However, Figure 5 shows that bursts that come from high latitudes (i.e., $> 45°$) show less variance in the spike height parameter than those that come from low latitudes (i.e., within $45°$ of the galactic plane).
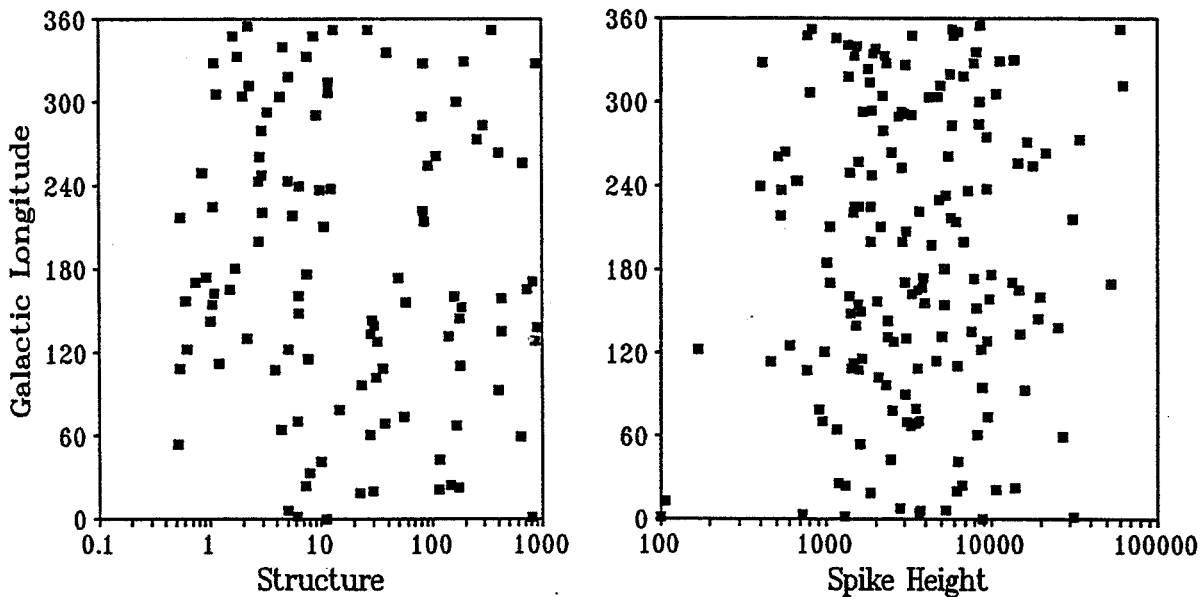
Figure 4. Burst Galactic Longitude versus Structure and Spike Heights
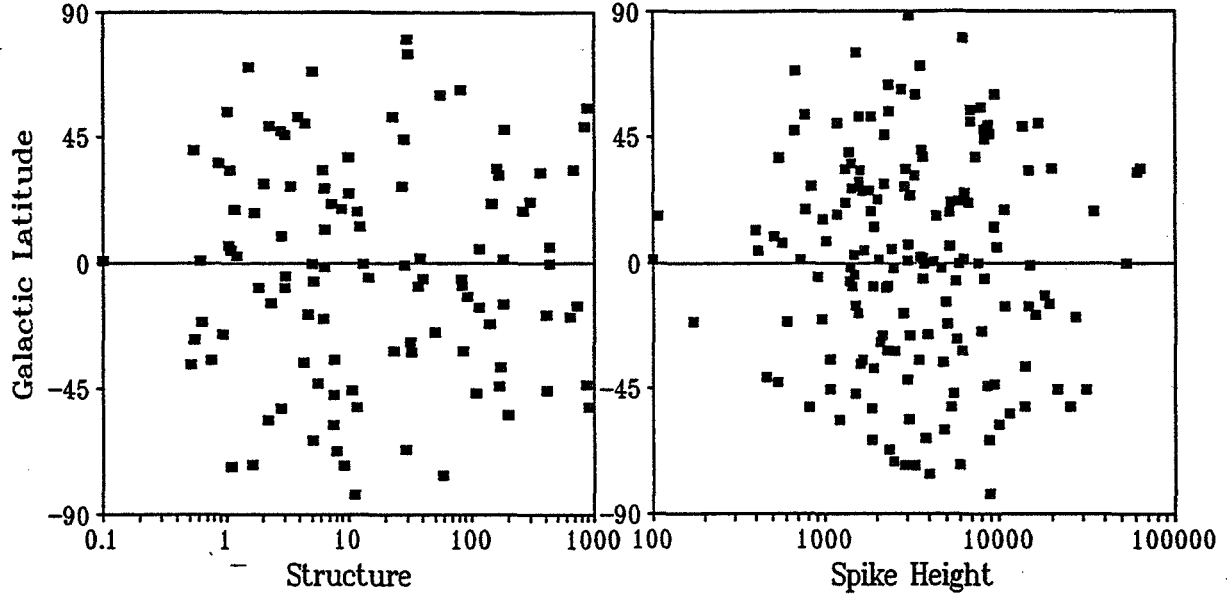
Figure 5. Burst Galactic Latitude versus Structure and Spike Heights

Conclusion:

The result seen in the Latitude-Height graph is not expected. It is possible that this is just a statistical anomaly. We will soon do a complete statistical analysis to determine its significance. If the result stands up under further scrutiny, it will certainly be adopted by the "galactic" modelers as evidence that at least some bursts arise from neutron stars which are confined to the plane of the galaxy.

References:

1. Atteia, J.-L. and Dezalay, J.-P., Gamma-Ray Bursters in the Galactic Disk *Astron. Astrop.* , in press, 1993.

2. Lamb, D. Q., Graziani, C. and Smith, I. A., Evidence for Two Distinct Morphological Classes of Gamma-Ray Bursts From Their Short-Timescale Variability *Ap. J.* , in press, 1993.

3. Knuth, D. E., The Art of Computer Programming, Seminumerical Algorithms, 2nd (Addison Wesley, Reading, Mass., 1981), p. 65.

4. Lestrade, J. P., The Statistics of Runs Up and Down for BATSE GRB Time Profiles *Ap. J.* , in prep., 1993.

1993

NASA/ASEE SUMMER FACULTY FELLOWSHIP PROGRAM

MARSHALL SPACE FLIGHT CENTER
THE UNIVERSITY OF ALABAMA IN HUNTSVILLE

SPATIAL INTERPRETATION OF
NASA'S MARSHALL SPACE FLIGHT CENTER
PAYLOAD OPERATIONS CONTROL CENTER
USING VIRTUAL REALITY TECHNOLOGY

Prepared By: Patricia F. Lindsey

Academic Rank: Lecturer

Institution and
School: East Carolina University,
                                School of Human Environmental
                                Sciences

MSFC Colleague: Joseph P. Hale

NASA/MSFC:

    Office: Missions Operations Laboratory
    Division: Operations Engineering Division
    Branch: Crew Systems Engineering Branch

SPATIAL INTERPRETATION OF NASA'S MARSHALL SPACE FLIGHT CENTER PAYLOAD OPERATIONS CONTROL CENTER USING VIRTUAL REALITY TECHNOLOGY

Introduction

In its search for higher level computer interface and more realistic electronic simulation for measurement and spatial analysis in human factors design, NASA at Marshall Space Flight Center is evaluating the functionality of virtual reality (VR) technology. Virtual reality simulation generates is a three dimensional environment in which the participant appears to be enveloped (Nugent, 1991). It is a type of interactive simulation in which humans are not only involved , but included (Helsel and Roth, 1991).

The military and entertainment industries along with the physical sciences have driven the development of computer equipment, programming, and presentation techniques used in the production and presentation of VR generated environments. The development of headsets, high resolution displays and position sensors have enabled the creation of the illusion of existing within a yet unconstructed space (Editorial, 1991).

The general purpose nature of VR technology makes it an intelligence amplifying (IA) tool--utilizing both the computer advantage in calculation and the human advantage in evaluation and putting ideas into context. These advantages are augmented with the use of input gloves, body suits, and display head gear that permits the user to utilize natural movement, rather than typed instruction or symbols and text picked from a menu (Rheingold, 1991).

Virtual reality technology is still in the experimental phase but it appears to be the next logical step after computer aided three-dimensional animation in transferring the viewer from a passive to an active role in experiencing and evaluating an environment (Eschelman and Tatchell, 1991). There is great potential for using this new technology when designing environments for more successful interaction, both with the environment and with another participant in a remote location. At the University of North Carolina, a VR simulation of a the planned Sitterson Hall, revealed a flaw in the building's design that had not been observed during examination of the more traditional building plan simulation methods on paper and on computer aided design (CAD) work station (Aukstankalnis, 1991). The virtual environment enables multiple participants in remote locations to come together and interact with one another and with the environment. Each participant is capable of seeing himself and the other participants and of interacting with them within the simulated environment.

Utilization

Three areas of utilization of VR technology in human factors design covered in this study are: (a) simulation tech-

niques, (b) behavioral settings, and
(c) human/computer interaction. Simulations provide a method
of presentation of the environment without necessitating on-
site visits, permit response to environments to manipulate the
prospective environment. Simulation is most useful in situa-
tions where observations or experimentation are not feasible
or ethical.

Behavioral settings are social and psychological situa-
tions in which human behavior occurs (Wicker, 1979). They are
both structural and dynamic (Barker, 1968) and include time
and place boundaries, duration of setting, number of times
setting occurred over a period of time, number of par-
ticipants, positions of responsibility, demographic group to
which participants belong, behavior patterns of participants,
and behaviors that occur in the setting (Wicker,1979). In or-
der to understand the behavior of individuals or groups, we
must examine the opportunities and constraints encompassed in
their environments.

Virtual reality enhances human/computer interaction. In-
teractive computer programs, using VR simulation take ad-
vantage of both the computer advantage in calculation and the
human advantage in evaluation and putting ideas into context.
Virtual reality weakens the barrier between man and machine by
permitting the user to use natural movement rather than symbol
or word commands.

Using VR for evaluation of behavioral settings enables
exploration of connections between specific environmental at-
tributes and users perceptions of those attributes. Com-
ponents within a behavioral settings control the range of
human behavior by promoting some actions and prohibiting
others, therefore observation and research should clarify and
supplement that which is known about relationships between
physical environments and human behavior.

The Study
Virtual reality simulation is promising but there are no
studies to verify that reaction to the VR environment ap-
proximates reaction to the "real world" environments. This
study compares responses of participants who viewed NASA's
Payload Operations Control Center (POCC) at Marshall Space
Flight Center with responses of the same participants who
viewed the same environment via VR simulation. This study in-
vestigates: (a) the potential for using VR to evaluate
human/environmental interaction, (b) whether observation of
environments using VR simulation provides the same information
about the characteristics of that environment as is provided
by observation of the "real world" environment, (c) the
reliability of using virtual reality to interpret the at-
tributes, deficiencies, and characteristics of an existing or
planned environment.

The study is a pretest-posttest design. The sample con-

sisted of 24 volunteers--12 NASA employees who have worked in
POCC console positions and 12 university and community college
faculty members who have never worked in the POCC. Six from
each group were male and six were female. Responses of par-
ticipants were recorded on a forced response questionnaire,
and a semantic differential questionnaire. In addition, six
members of the sample were asked to give verbal responses to a
moderately scheduled, open ended follow up questionnaire.
Responses were recorded on audio tape. The qualitative infor-
mation gathered from the semantic differential and the follow
up questionnaire will be used to clarify the quantitative in-
formation gathered from the forced response questionnaire.

Participants were seated at two specified points in both
the "real world" and VR POCCs. Questionnaires were completed
from these two locations. The participants' seat height was
adjusted so that their eye height approximated the eye height
of a 50th percentile male at one location and a 50th percen-
tile female at the other location (NASA, 1989). After one set
of questions was completed in the virtual POCC, changes were
made to the virtual environment and the questionnaire was com-
pleted again. Responses before and after the changes will be
compared. Questions concerned distance judgment, head rota-
tion, and perception. The sequence of observation was the
same from both consoles and in the "real world" and the VR
POCCs. The semantic differential questionnaire was completed
from the center back of the POCC from a standing position.

The equipment, hardware and software used to create the
virtual POCC environment included eye-phones and data glove by
VPL research, Inc. A Macintosh 2FX computer, 2 silicon
graphics computers--310 VGX and 320 VGX-B. The graphics
package is Swivel 3-D by VPL Research, Inc. Body Electric
Visual Programming Language connects input by the operator to
drive the simulator is translated by Isaac.

Since participants using VR equipment were unable to read
the questionnaire or designate the answers while wearing VR
gear, the questions and answer options must be read to the
participant and answers marked by a surrogate. The researcher
or research assistant acted as surrogate. In order that con-
ditions be as alike as possible in both settings, questions
were also read and answers marked by the surrogate in the
"real world" POCC.

Data from the questionnaires will be coded, entered into
the computer and verified for accuracy. Using SPSS, descrip-
tive statistics will be generated including frequencies,
means, and percentages. Analytical statistics for all
hypotheses will include a repeated measures multivariate
analysis of variance to test differences between groups.

Conclusion
Analysis of data has not yet begun but some anticipated
conclusions drawn from the data and from comments of par-

ticipants include a similarity in spatial analysis among groups. Some differences are apparent between participants who have worked at the POCC consoles and those who have not. It appears that there is some difference in responses between those who view the "real world" POCC first and those who view the VR POCC first. Estimation of distances in the VR POCC appear to be similar to estimation of distances in the "real world" POCC up to a distance of about 10 feet. Beyond that, however, the estimated distances in the VR POCC are greater than those in the "real world" POCC. Overall, the estimates of distance, head rotation, perception appear to be similar in both "worlds".

Acknowledgments

References

1. Aukstankalnis, G. Virtual reality and experiential prototypes of CAD models. DesignNet. (1992, January).
2. Barker, R.G. Ecological psychology. Stanford, CA.: Stanford University Press.
3. Editorial Being and believing-ethics in virtual reality. Lancet, 338(8762), 283-284. (1991).
4. Eshelman, P. & Tatchell, K. How beneficial a tool is computer-aided design? Forum. pp. 15-19. (1992).
5. Helsel, S.K. & Roth, J.P. (eds.). Virtual reality: Theory, practice, and promise. Westport, CN: Meckler Publishing. (1991).
6. National Aeronautics and Space Administration (NASA). Man-Systems Integration Standards: SA-STD-3000. National Aeronautics and Space Administration. pp. 3-11 - 3-25. (1989).
7. Nugent, W.R. Virtual reality: Advanced imagery special effects let you roam in cyberspace. Journal of the American Society for Information Science,42(8), 609-617. (1991).
8. Rheingold, H. Virtual reality. New York: Simon & Schuster. (1991).
9. Wicker, A.W. An introduction to ecological psychology. Belmont, CA: Wadsworth, Inc. (1979).

1993

NASA/ASEE SUMMER FACULTY FELLOWSHIP PROGRAM

MARSHALL SPACE FLIGHT CENTER
THE UNIVERSITY OF ALABAMA IN HUNTSVILLE

NEURAL NETWORK-BASED CONTROL USING LYAPUNOV FUNCTIONS

Prepared By: Leon A. Luxemburg, Ph.D.
 Academic Rank: Assistant Professor Institution and
Department: TAMU
                         Marine Engineering
MSFC Colleague: Henry B. Waites, Ph.D.
NASA/MSFC:
        Office: Structures and Dynamics Laboratory
        Division: Control Systems
        Branch: Precision Pointing Systems

Introduction

Consider a linear nonminimal phase plant given as follows:

$$\dot{x} = Ax + Bu \qquad (1)$$

$$y = Cx \qquad (2)$$

The goals of this research effort are:

1. To develop an algorithm for offline stabilization of linear and nonlinear plants with known parameters by using a neural network controller.

2. The results of stabilization procedure must be rigorously tested mathematically.

3. The obtained controller should become linear controller which also stabilizes the plant when linearization of the neural network is performed.

4. Tracking of step inputs must be achieved.

5. Provide unified treatment of plant and controller dynamics in terms of differential equations rather than considering a hybrid discrete-continuous system.

To stabilize (1) we propose a neural network described by the following equations:

$$\dot{z} = g(z, u, y) \qquad (3)$$

where the output of the net o is given by $o = w_1^T y + w_2^T z$ and $u = o + ref$, where ref is the reference input.

Definition of asymptotic stability of nonlinear system. Consider a plant-controller dynamical system given above in the phase space R^n with state vector $(x^T, z^T)^T$. Then this controller stabilizes the plant with the region of stability U, $0 \in U \subset R^n$ if and only if disconnecting external input ref results in convergence of any trajectory of combined plant-controller state space to 0.

The neural network consists of three layers: input layer, inner layer and the output layer with 5,4 and 2 nodes in these layers respectively. Sigmoid functions in the inner layers are chosen to be hyperbolic tangent functions $y(x) = (exp(x) - exp(-x))/(exp(x) + exp(-x))$. The layers are fully interconnected resulting in 28 weights. Additional weights are 4 weights for 2 two-dimensional vectors w_1, w_2 in the output o above totalling 32 unknown weights. The 5×4 matrix of weights connecting input to inner layer is denoted by E and the 4×2 matrix of weights connecting inner

layer to the output layer is denoted by D. The total 32-dimensional weight vector is denoted by r.

To fully explain our approach we need to formulate two well known results about Lyapunov functions:

Result A: Let $\dot{x} = p(x)$, $x \in R^n$ be a differential equation on a bounded open set $U \subset R^n$ and let $p(0) = 0 \in U$. Let $h(x)$ be a continuous function on U such that $h(x) > 0$ on U and $h(0) = 0$. Let $< \nabla h(x), p(x) > < 0$ for all $x \in U$, where $\nabla h(x)$ denotes gradient of h and $<,>$ denotes the scalar product in R^n. Then every trajectory of our differential equation with initial condition in U converges to 0 as $t \to \infty$.

Result B: All the eigenvalues of matrix T have negative real parts if and only if for any given positive definite symmetric matrix N the matrix equation $T^T M + MT = -N$ has a unique positive definite symmetric solution M.

The basic underlying idea of the solution of stabilization problem using neural network controller is as follows: find a 6×6 matrix M and the set of weights r with dimension of r being 32 such that $h(v) = v^T M v$ is the Lyapunov function in a neighborhood of 0 in a six dimensional state-space with the state vector $\left(\begin{smallmatrix} x \\ z \end{smallmatrix}\right)$. This would require that the time derivative of h , $\dot{h}(v) = v^T(T^T M + MT)v$ be a negative function on U where T is the Jacobian of the overall plant-controller dynamical system. Function $\dot{h}(x)$ depends altogether on 68 parameters: on vector r and on vector g which is such a vector that when arranged in a 6×6 matrix G will satisfy the equation $GG^T = M$.

Our approach then is to start with random vector r and random vector g and form a gradient descent equation

$$\dot{q} = -\alpha \partial \dot{h}/\partial q \tag{4}$$

where q is the six-dimensional state vector $q = \left(\begin{smallmatrix} x \\ z \end{smallmatrix}\right)$, α is not a constant but a vector and in the formula above we consider the Hadamard product of α with the partial derivative of $\dot{h}$ by q. Also, α changes with time as the function $\dot{h}$ decreases.

While simulating the gradient descent equation we modify vectors r and g until function $\dot{h}$ above is negative on a neighborhood of 0.

To check that we have designed the stabilizing controller with the linear plant we need only to check that the egenvalues of the matrix $MT + T^T M$ are all negative. However, in this section we extend our method to nonlinear plants and show how to verify the stability in this case.

Algorithm for stabilization of nonlinear plants:

1. Stabilization of Jacobian at the equilibrium is done first and proceeds as in the case of linear plants. (Here we assume that the nonlinear plant has an equilibrium and we stabilize around this equilibrium).

2. After obtaining some open region of stability around the equilibrium as in part 1 we select points at random lying on concentric expanding spheres around this stable equilibrium and adjust the weights of neural net to achieve the negativity of the derivative of Lyapunov function. Lyapunov function M is also given as a neural net.

Verification of stability of a given region for the given nonlinear plant and stabilizing neural net: Given the candidate for stability region U and the Lyapunov function h we can derive the upper bound K on the partial derivatives of $\dot{h}$ with respect to state vector:

$$\partial \dot{h}/\partial w < K \qquad (5)$$

where w is the arbitrary point in U. If for every point $w \in U$ we have $\dot{h}(w) < -\beta$, $\beta > 0$ then, as follows from the Taylor's formula for multivariable functions, in the open ball of of radius β/K the derivative $\dot{h}$ is negative. If we cover U with the balls of radius β/K then $\dot{h}$ is negative on U insuring stability. This can also give us an estimate on the number of training points to achieve the stability.

Definition. Given a differential equation $\dot{x} = f(x)$, $x \in R^n$ a point x_0 is an equilibrium of order k, $k \leq n$ if $f(x_0) = 0$ and the Jacobian $\partial f(x_0)/\partial x$ at x_0 is nondegenerate and has exactly k eigenvalues with positive real parts. By a stable manifold of x_0 we mean a union of all trajectories converging to x_0 as $t \to \infty$.

Definition. Consider the dynamical system $\dot{w} = f(w)$ described by a neural network-plant differential equations and having the Lyapunov function h. Let U be the maximal set such that U is connected, contains the origin of the state-space, h is positive on U and $\dot{h}$ is negative on U. Then U is called the maximal stability region.

Theorem. In the notations of previous two definions let $\dot{w} = f(w)$ be a differential equation describing plant-neural network dynamical system and let U be the maximal stability region for Lyapunov function h. Then

1. If U is bounded then on the boundary of U there are equilibria of all orders k, $0 \leq k \leq n$.

2. Under generic assumptions the boundary of U is the union of stable manifolds of equilibrium points lying on the boundary.

3. Every trajectory on the boundary of U converges to an equilibrium point as $t \to \infty$. If U is bounded the the same is true for $t \to -\infty$.

4. The point on the boundary where the minimum of h is achieved is an equilibrium point of order 1.

Conclusions

We have successfully demonstrated how the problem of stabilization of plants can be reduced to a problem of approximation of functions. Neural networks have been shown to have approximating and interpolating properties. This approach is good for linear and nonlinear plants. Software has been generated to demonstrate this approach.

Directions for further research:

1. Generate faster software to utilize parallel processing features.

2. Improve algorithms to increase success rate for ill-conditioned plants such as the one considered. The convergence is successful for a random linear plant all the time.

3. Generate efficient software for nonlinear plants stabilization and tracking.

4. Study regions of stability and phase portraits of plant-neural controller and gradient descent learning differential equations.

5. Develop techniques for pole placing of linearized version of plant-neural controller system and of shaping the stability region.

Acknowledgements

1993

NASA/ASEE SUMMER FACULTY FELLOWSHIP PROGRAM

MARSHALL SPACE FLIGHT CENTER
THE UNIVERSITY OF ALABAMA IN HUNTSVILLE

ACCESS TO SPACE STUDIES

Prepared by: James A. Martin, Sc.D.

Academic Rank: Associate Professor

Institution and
  Department: The University of Alabama,
                       Aerospace Engineering Department

MSFC Colleague: Robert F. Nixon

NASA/MSFC:

    Office: Space Transportaion and Exploration
    Group: Upper Stages

Access to Space Studies

James A. Martin
University of Alabama

Introduction

The National Aeronautics and Space Administration is currently considering possible directions in Earth-to-orbit vehicle development under a study called "Access to Space." This agency-wide study is considering commercial launch vehicles, human transportation, space station logistics, and other space transportation requirements over the next 40 years. Three options are being considered for human transportation: continued use of the Space Shuttle, development of a small personnel carrier (personnel logistics system, PLS), or development of an advanced vehicle such as a single-stage-to-orbit (SSTO). Several studies related to the overall Access to Space study are reported in this document.

Hydrogen Upper Stage for Delta

The Delta commercial launch vehicle has had a long and successful life. One of the possibilities for extending the capability of the Delta is to replace the storable second stage and solid third stage with a hydrogen/oxygen stage. A study was conducted to show the payload potential of such a stage with several engine options. The first step in the study was executing the trajectory optimization program Opguid to find the burnout weight for each engine design point. The inert weight of the stage was calculated from weight estimating relationships developed for such a stage, and the payload was found by subtracting the inert weight from the burnout weight. Several propellant weight cases were computed for each engine case.

The RL10C, which has not been developed but is a derivative of an existing RL10 engine, was analyzed at several thrust levels and exit areas. The RL10A4, which is an existing engine, and an advanced expander were analyzed. A new engine concept called the Advanced Technology Low Cost engine (ATLC) under consideration for development was analyzed. It would have a low-pressure staged combustion cycle and an uncooled chamber. The results are shown in the enclosed figure. Because the thrust level of the RL10C could be chosen at the optimum value for this application, it provided a somewhat better payload than the other candidate engines.

The results of this study indicate that a hydrogen upper stage can provide a payload increase from 4010 lb, the capability of the existing Delta, to about 5600 lb.

The inert weight calculations used in the analysis assume a stage with self-supporting tanks with convex bulkheads. The inert weight is approximately 6500 lb. An existing stage, Centaur, has pressure-stabilized tanks and a concave lower hydrogen tank bulkhead. With these features, it has an inert weight of about 4300 lb. Using such a stage would increase the payload to about 6800 lb, but the costs may be greater.

Advanced SSTO Engines

A current contract with Rocketdyne is considering advanced hydrogen engines for the SSTO vehicle option. After considering previous engine studies for SSTO vehicles, several engine designs were selected for analysis. This analysis will include engine calculations by Rocketdyne and vehicle analysis by NASA. Vehicle calculations at The University of Alabama may also be included. The engines will include full-flow staged-combustion engines, hybrid expander engines, and SSME-type engines. Mixture ratios of 6 and 7 will be included. Initial results indicate that the full-flow engine can reduce the vehicle dry mass from 232,000 lb to 159,000 lb.

Expendable Hydrogen Tank SSTO

The fully reusable SSTO being considered should have considerably lower recurring costs than the Space Shuttle or PLS options. There has been an assumption that a fully reusable vehicle would have the lowest recurring costs. To explore this assumption, a concept has been studied with an expendable hydrogen tank. Initial vehicle results indicate that the vehicle gross weight drops from about 2.4 million lb for the fully reusable vehicle to under 1.8 million lb with the expendable hydrogen tank. This is because returning the hydrogen tank for reuse increases the size of the vehicle, increasing the thermal protection weight, the wings, landing gear, etc. The number of SSME's is reduced from 7 to 5. The development, production, spares, and engine costs are therefore reduced. This reduction is balanced by the added cost of the expended tank which must be replaced each flight. Cost estimates show that the net result is essentially no change in the total costs, but the early costs are reduced, which would provide a net savings if the time value of money is included in the analysis.

Orbiter instead of PLS

The PLS option studies have discovered a vehicle concept with some promise. It uses a reusable propulsion and avionics (PA) module with expendable tanks. Each PA module has two SSME's. With three PA modules, a 65,000 lb payload can be launched to the space station. Six flight of this cargo vehicle per year can provide the space station logistics. The PLS can be launched to the space station on the same vehicle. The recurring costs are estimated to be significantly lower

than the current Space Shuttle costs, but the development costs that must be invested to get to this system are quite high. In an attempt to reduce these costs, a concept was developed that does not require the PLS development. The Space Shuttle orbiter is used with a small oxygen tank in the payload bay and a small set of expendable hydrogen tanks. This orbiter and small tank set is launched with the vehicle with three PA modules. Weight estimates and trajectory results indicate that a 21,700 lb payload can be delivered to the space station.

Russian Engine PA Module

There is a possibility that Russian engines could be used in a new launch vehicle. The existing RD-170 engine has been proven to be reliable and has excellent performance. A concept was developed which would use a PA module to reuse one RD-170 and another PA module to reuse two SSME's. This concept would have more payload than the concept with three PA modules with two SSME's each, and the tank would be smaller because most of the fuel would be kerosene rather than hydrogen. One alternative to this concept is to use two RD-180 engines, each in a PA module, instead of one RD-170. The two SSME's would still be used. The RD-180 is essentially half of an RD-170. Another alternative is to use three PA modules, each with one RD-701 engine. The RD-701 is a tripropellant derivative of the RD-170. In this alternative, no SSME's would be needed.

Engine Comparisons
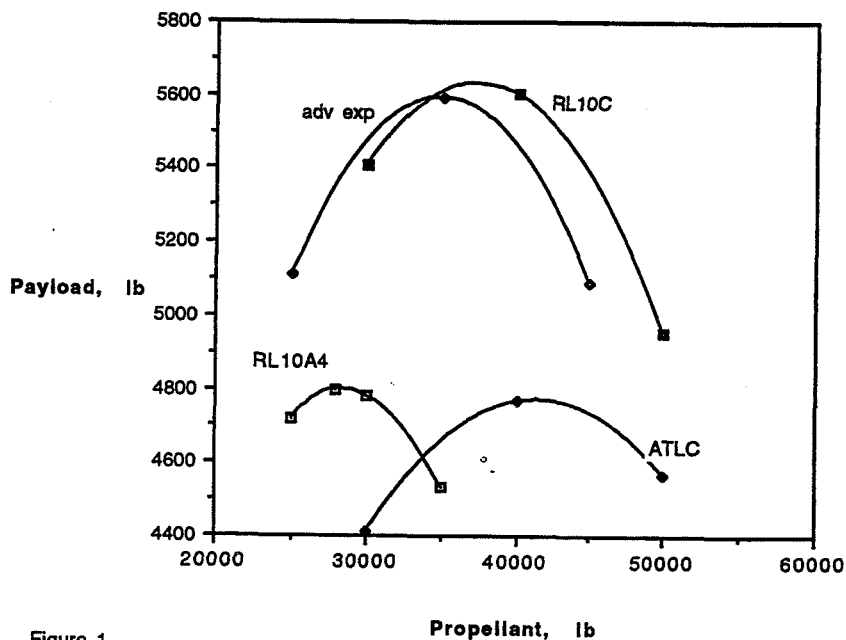
Figure 1

NASA/ASEE SUMMER FACULTY FELLOWSHIP PROGRAM

MARSHALL SPACE FLIGHT CENTER
THE UNIVERSITY OF ALABAMA

Flux Measurements Using the BATSE
Spectroscopic Detectors

Prepared by: Bernard McNamara

Academic Rank: Professor

Institution and   New Mexico State Universiy
Department: Astronomy Department

NASA/MSFC
    Office: Space Sciences Laboratory
    Division: High Energy Astrophysics
    Branch: Gamma-Ray and Cosmic Ray

MSFC Colleague   B.A. Harmon

Introduction

Among the Compton Gamma-Ray Observatory instruments, the BATSE Spectroscopic Detectors (SD) have the distinction of being able to detect photons of energies less than about 20 keV. This is an interesting energy range for the examination of low mass X-ray binaries (LMXBs). In fact, Sco X-1, the prototype LMXB, is easily seen even in the raw BATSE spectroscopic data. The all-sky coverage afforded by these detectors offers a unique opportunity to monitor this source over time periods never before possible.

The aim of this investigation was to test a number of ways in which both continuous and discrete flux measurements can be obtained using the BATSE spectroscopic datasets. A instrumental description of a SD can be found in the Compton Workshop of April 1989 (p 2-39), this report will deal only with methods which can be used to analyze its datasets. Many of items discussed below, particularly in regard to the earth occultation technique, have been developed, refined, and applied by the BATSE team to the reduction of BATSE LAD data. Code written as part of this project utilizes portions of that work. The following discussion will first address issues related to the reduction of SD datasets using the earth occultation technique. It will then discuss methods for the recovery of the flux history of strong sources while they are above the earth's limb. The report will conclude with recommended reduction procedures.

SD Fluxes Measured Using the Earth Occultation Technique

The earth occultation technique utilizes two source flux measurements per orbit: one obtained shortly after the source rises above the earth's limb and one shortly before the source sets behind the earth's limb. These fluxes are subtracted from background values taken near these times but when the source is behind the earth's limb. Since the background changes in a continuous fashion, a detailed background model is not needed to obtain source flux measurements using this method. This is the strongest positive attribute of the earth occultation method. The actual details of how the source and background fluxes are measured depend upon such things as the source strength, the presence of other sources, and the time over which the measurement takes place. These are discussed below.

Item 1): The source strength

The main complicating factor here occurs when the source is strong and exhibits random, short period, variations. Such sources are not common in SD datasets. In fact, only one celestial source, Sco X-1, has been observed to show this type of activity. In this case the slope of the least squares line on either side of the occultation step is normally quite different. If the same slope is assumed an inaccurate estimate of the step size can result.

In addition, if the source variability timescale is less than but comparable to the interval being fit, then the least squares slope and intercept can be influenced by activity somewhat removed in time from the step. This will also result in a difference in the source strength, depending on the integration time.

Item 2): Least squares based estimates of the background flux

The background flux reflects an approximate sinusoidal pattern governed by the amount of earth blockage as seen by the detector. Over time intervals exceeding a few hundred seconds the background flux can change in a nonlinear fashion. Incorporating a quadratic term into the background model to account for this departure can produce a better fit. An undesirable effect of this is that as one includes times further and further from the step, flux changes which occur close to the step have less and less of an impact on the model. This makes the estimate of the background flux located at the step suspect. A second problem is that as a wider time interval is included, other rising and setting sources may effect the background fit in undesirable ways.

Item 3): Using background fluxes measured close to the step

This might appear to solve the problem raised above. Unfortunately it also has problems. Generally the background level is not constant with time. One must therefore somehow correct the computed background flux to the value it would have had at the time when the (step + background) flux is measured. If the time interval over which the background is measured is short, the resultant flux level will be sensitive to noise fluctations since it will be based on relatively few points.

Item 4): Dealing with very noisy data

The data collected using a gain setting of 8X is normally quite noisy compared to that at 4X. To lessen the impact of noise, two types of filters can be employed. The first removes large cosmic ray spikes from the data. This can be accomplished by passing the data through a filter which removes datapoints which deviate from prior points by a user defined number of standard deviations. A second filter which removes high frequency noise (such as Butterworth filter) can then be applied. This procedure was tested with BATSE SD data an appears to work quite well. The selection of filter parameters involves a subjective decision but reasonable variations in their values only change the step sizes by small amounts i.e. 1-2 cnts/sec.

SD Light Curves Obtained During a Single Orbit

In many cases it is desirable to obtain the entire light curve of a source while it is above the earth's limb. To do this one must have a model which accounts for the background

during this entire time period. Two models have been developed and tested which, at least to first order, allow this to be done. The first fits the background to a second order polynomial in terms of the cosine of the earth angle. The second model attempts to remove the background by subtracting a nearby orbit which not only includes background but the primary and/or other sources. This latter model assumes that the secondary sources have an identical level of activity in the reference and program orbit. These two models are more fully described below.

Model 1: Background Removal Using a Polynomial Earth Angle Fit

For this model to work one must have background data from a substantial portion of an orbit. Lack of TDRSS communication, SAA passages, and the short term decay of radioactive isotopes all combine to make this condition difficult to meet. It is also not intended to track subtle changes in the background. Increasing the order of the polynomial to account for these changes generally results in a poorer overall background fit. A much more detailed, physically based, background model is currently being developed by the BATSE team but is not yet available. A second complicating feature which this model does not address is the presence of multiple sources. In the case of Sco X-1 the galactic center region can rise and set shortly after Sco X-1. Obviously when this situation occurs, results based upon this simple model will be incorrect.

Model 2: Subtraction of an Inactive Nearby Orbit

This technique assumes that orbits exist in which the presence of a source can be treated as a constant additive term to the background. Orbits which appear to meet this condition occur often in the SD datasets of Sco X-1. This type of behavior is associated with Sco X-1 when it is located on its normal branch in a two color x-ray diagram. Even when this source is active, orbits which show a constant level of activity are not uncommon. The equality of step sizes at earth rise and set can be used to help locate orbits of constant activity as can a visual inspection of a flux versus time plot of the data. The subtraction of two orbits which meet these criteria can also be used to reveal subtle, longer term variations that are difficult to see in the unprocessed data. The advantage of this technique is that other sources, which exhibit constant emission over a few orbits, are subtracted out of the signal. The disadvantage of the technique is that slight trends may be introduced into the orbit of interest from the reference orbit. In cases where high precision is needed, the presence of these trends can be determined by differencing the reference orbit to another nearby orbit which meets the above criteria.

<div align="center">

Adopted Analysis Techniques

Earth Occultation Method

</div>

A compromise between the various issues raised above which appears to work well is to

model the background with a linear least squares fit extending 100-150 seconds prior to the step. Longer time periods run the danger of 1) incorporating other sources, 2) violating the linear assumption, and 3) not adequately modeling the region close to the step. For measurement of the source, two different approaches are used. The first measures the average (source + background) flux over a time period of 40-60 seconds immediately after/preceding the step. The 60sec interval yields a slightly smaller step error. The second approach models this region with a linear least squares fit. In both cases the background flux is extrapolated to the time of the step. If the source is relatively inactive, both methods give, to within the step error, identical results. If the source is active, the average value is believed to give a better value of the instantaneous step size. The computer programs written to perform these tasks were tested by running a LAD dataset and then comparing the step sizes with those obtained with the BATSE LAD earth occultation software. The LAD step sizes from both programs were found to be in agreement.

SD datasets collected using gain settings near 8X are very noisy. A significant improvement in the value of a step size can result with the aid of the filtering techniques mentioned earlier. The application of these filters may be a necessary condition in order to obtain meaningful results with a gain setting of 8X. Depending on the source energy distribution and strength some additional higher energy information may be available from channel 2 data when the gain is set at either 4X or 8X. The sensitivity of a SD increases by a factor of about 2.5 from 16 to 40 keV . In the case of Sco X-1 this helps compensate for the fact that the flux emitted by this source drops off steeply above 10 keV.

Orbital Light Curves

At the present time I would recommend the subtraction of a quiescent orbit from a nearby orbit to obtain an orbital light curve. The main assumption inherent in this technique is that occassionally one can find orbits where the source emission is relatively constant. A second but less severe assumption is that the earth modulated x-ray background is also repeatable over at least a few orbits. The former assumption can be tested by viewing the raw orbital data and by comparing the step sizes at earth rise and set for each orbit. If the source is indeed stable during an orbit, its rise and set step sizes should to equal. In the case of Sco X-1 periods of activity are easily distinguishable even in the raw data. The assumption dealing with the repeatable nature of the background was tested by computing its least squares determined slope near a Sco X-1 step during the course of a day. The slope was found to be unchanged over time intervals of approximately 30,000 sec. This implies that the earth modulated x-ray background changes slowly: overtime frames of many hours. A significant advantage that the orbital subtraction model enjoys over that discussed above is that it automatically accounts for other sources that have constant emission over this time period.

NASA/ASEE SUMMER FACULTY FELLOWSHIP PROGRAM

MARSHALL SPACE FLIGHT CENTER
THE UNIVERSITY OF ALABAMA IN HUNTSVILLE

INTEGRATION AND EVALUATION OF A SIMULATOR DESIGNED TO BE USED
WITHIN A DYNAMIC PROTOTYPING ENVIRONMENT

Prepared by: Loretta A. Moore

Academic Rank: Assistant Professor

Institution and
  Department: Auburn University
                    Department of Computer Science and Engineering

MSFC Colleague: Joseph P. Hale

NASA/MSFC:

       Laboratory: Mission Operations
       Division: Operations Engineering
       Branch: Crew Systems Engineering

Introduction

The Human Computer Interface (HCI) prototyping environment is designed to allow developers to rapidly prototype systems so that the interface and functionality of a system can be evaluated and iteratively refined early in the development process. This keeps development costs down by modifying the interface during the requirements definition phase, thus minimizing changes that need to be made during and after flight code development. Problems occur within a system when the user interface is not adequately developed and when designers and developers have an incomplete understanding of the system requirements.

A process has been developed for prototyping on-board payload displays for *Space Station Freedom* (Moore, 1992). This prototyping process consists of five phases: identification of known requirements, analysis of the requirements, development of a formal design representation and specification, development of the prototype, and evaluation of the prototype. The actual development of the prototype involves prototyping the displays, developing a low fidelity simulator, building of an interface (or communication) between the displays and the simulator, integration of these components, and testing to ensure that the interface does what the developer expects.

This research integrates and evaluates a software tool which has been developed to serve as a simulator within the prototyping environment. The tool is being evaluated to determine whether or not it meets the basic requirements which are needed for a low fidelity simulator within this environment. In order to evaluate the architecture and its components, a human computer interface for and a simulator of an automobile have been developed as a prototype. The individual components (i.e., the interface and simulator) have been developed (Moore, 1993), and the current research was designed to integrate and test the complete working system within the prototyping environment. The following sections will describe the architecture and components of the rapid prototyping environment, the development of a system to assess the environment, and the integration and evaluation of PERCNET.

Architecture of the Environment

The architecture for building prototypes of systems consist of four major components: a interface development tool, a test and evaluation simulator development tool, a dynamic, interactive interface which links the interface and the simulator, and an embedded evaluation capability. The interface development tool allows the designer to dynamically develop graphical displays. The test and evaluation simulator development tool will allow the functionality of the system to be implemented and will act as driver for the displays. The dynamic, interactive interface will handle communication between the HCI prototyping tool and the simulation environment. This component consists of a server which sends and receives messages between the other components. The embedded evaluation capability will collect data while the user is interacting with the system and will evaluate the adequacy of an HCI based on a user's performance.

Human Computer Interface Development Tool. Sammi by Kinesix has been chosen as the Human Computer Interface (HCI) development tool. Sammi is a graphical user

environment which allows user interfaces to be built which can manage networked information graphically. Sammi combines the functions of a graphical user interface with full network communication support. Within Sammi the user interface and the networked data access can be defined independently of the actual data source or application. This will allow an interface developed under Sammi and communicating with the low fidelity simulator, to later be connected to a high fidelity simulator such as those in the Payload Crew Training Complex (PCTC), and later to the actual on-board flight software. Sammi has a distributed architecture which means that the user interface and the application code are separate, that is, the user interface is no longer embedded within the application code. With this separation users can easily create and modify the human computer interface without affecting the datasource, and vice versa. This will allow concurrent development of the application and the interface. Sammi developed applications can use remote procedure calls to access information from a variety of nodes and servers on an Ethernet network.

Simulator Development Tool. A simulator is a computer program that models a system or process in order to enable people to study it. The simulator development tool should provide the capability to develop a low fidelity simulation of a system or process. The development of a simulator has two important functions. First, the simulator helps the developer to identify and define basic system requirements. Second, potential users can evaluate both the look (in terms of the screen layout, color, objects, etc.) and feel (in terms of operations and actions which need to be performed) of a system. During the requirements definition phase, a high-fidelity simulation of the system will not yet have been developed, so it is important to build a low fidelity simulator, so that the iterative cycle of refining the human computer interface based upon a user's interactions can proceed.

For a piece of software to function as a simulator within this environment there are several requirements which must be met in addition to it just being a simulation tool. These requirements include the ability of the process to communicate with UNIX processes using the TCP/IP protocol; real-time simulation execution, the execution engine must be tied to a real time clock to assure that simulation timing and data collection are accurate; an option for a variable communications mode during execution (i.e., with and without external communication); real time communication with Sammi on a separate platform, via Ethernet; the ability to receive data from Sammi to dynamically control scenario events, modify blackboard variables, trigger scenario events, and track operator actions for post-hoc analysis; the ability to specify and send commands and data to Sammi; and the ability to receive data and commands from multiple Sammi applications/stations. The multiple Sammi stations may include one or more display prototype stations and a monitoring station. A Simulator Director should be able to send commands to this software from a monitoring station (e.g., start simulation, trigger scenario event). Sammi subroutines must be provided that have been developed for the Simulator-Sammi communication and the software must be tested and validated with documentation provided. PERCNET is designed to be used as a knowledge-based graphical simulation environment for modeling and analyzing human-machine tasks. Within PERCNET task models are developed using modified petri nets, a combination of petri nets, frames, and rules. This research evaluated PERCNET to determine whether or not it met the basic requirements which were listed above.

Dynamic, Interactive Interface. This interface will handle communication between the HCI prototyping tool and the simulation environment during execution. This interface is a server which has been developed using the Sammi Application Programmer's Interface (API). It will be a peer-to-peer or asynchronous server which means that messages and commands can be sent and received both ways between Sammi and the application. Once the embedded evaluation tool has been developed, the server can also service requests from this process providing information as to which functions the user has used, errors which have been made, and so forth.

Embedded Evaluation Capability. The embedded evaluation capability will include a capture/playback component and an analysis component. The Capture feature will capture a user's session and save this information to a log. This log can later be "played" back or analyzed. The analysis component will analyze the user's session and provide guidelines for the redesign of the system. Some of the measures will include: frequency of use of specified features, task completion time, error counts, requests for help, amount of work/errors per unit time, and response time to different activities and events.

Development of a prototype within the Architecture

In order to assess the individual components of the architecture a system was chosen and developed (Moore, 1993). The system chosen for pathfinding and initial empirical evaluation of the project was an automobile. An automobile has sufficient complexity and subsystems' interdependencies to provide a moderate level of operational workload. Further, potential subjects in the empirical studies would have a working understanding of an automobile's functionality, thus minimizing pre-experiment training requirements. There were four basic tasks which were completed: (1) requirements were developed for the automobile simulator, (2) the automobile simulator was developed using PERCNET, (3) a human computer interface for operating the automobile simulator was developed using Sammi, and (4) evaluation criteria for the operation of the automobile simulator were developed (Moore, 1993).

Integration and Evaluation of PERCNET

The initial design provided by Perceptronics presented a potential problem. The dynamic, interactive interface component was designed to be embedded within the PERCNET process. This would allow Sammi and PERCNET to communicate, however, there would be no way for other processes to communicate with Sammi and PERCNET. This was a real problem within our environment because the embedded evaluation capability would be a separate process that needed to send messages and receive information from this process during the execution. Once this problem was identified and the importance of this function was understood, the developers from Perceptronics changed the architecture.

PERCNET provides the basic functionality of a tool which can act as a simulator with the changes made in its architecture. However, there are some remaining issues which need to be addressed and major problems with the current system which need to be fixed. One problem concerns the system running out of swap space and exiting because it can no longer

allocate memory. A minimal configuration of this tool needs to be presented and the the system should be able to run with this configuration without the system exiting. A second problem involves the tendency of the system to core dump, sometimes in response to specific features (such as trying to use an option from the menu which has not been implemented or is not currently working) and sometimes randomly. A third problem, is that the screen and the keyboard lock up and the system has to be rebooted. It is not clear whether the problem can be attributed to PERCNET or the second screen (a Plasma display) which is attached to the SunSPARC station on which we are running PERCNET. This item needs further investigation. There have been other problems with several features of the system and most of these have been fixed by the developers at Perceptronics. However, there are several functions of the system which have not yet been evaluated yet, such as, communication across the network, having multiple Sammi displays communicate with a single PERCNET model, and being able to start and stop the simulation from the second Sammi window.

Conclusions and Future Work

PERCNET has been integrated within the human computer interface prototyping environment; however, it is recommended that further testing and evaluation be conducted using the automobile interface and simulator to resolve the issues previously discussed. Most requirements have been met but there needs to be a more thorough evaluation of the simulator tool and the architecture of the environment.

Following the automobile prototype development, a second system, based on a Spacelab/Space Station payload should be developed for further evaluation of the environment. This should involve development of the payload simulator requirements from existing experiment simulator requirement documents, development of the payload simulator using PERCNET, development of an interface for the payload using Sammi, and integration and testing of the payload simulator and interface.

References

Moore, L. A. (1993). Assessment of a Human Computer Interface Prototyping Environment (Contract No. NAS8-39131). MSFC, AL: NASA, George C. Marshall Space Flight Center.

Moore, L. A. (1992). A Process for Prototyping Onboard Payload Displays for Space Station Freedom. In M. Freeman, R. Chappell, F. Six, & G. Karr (Eds.), Research Reports - 1992 NASA/ASEE Summer Faculty Fellowship Program (Report No. NASA-CR-184505, pp. XXXVI.1 - XXXVI.4). MSFC, AL: NASA, George C. Marshall Space Flight Center.

Perceptronics User's Manual. (1992). Woodland Hills, California: Perceptronics, Inc.

Sammi User's Guide. (1992). Houston, Texas: Kinesix Corporation.

1993

NASA/ASEE SUMMER FACULTY FELLOWSHIP PROGRAM

MARSHALL SPACE FLIGHT CENTER
THE UNIVERSITY OF ALABAMA IN HUNTSVILLE

EVALUATION OF OVOSTATIN AND OVOSTATIN ASSAY

Prepared By: Debra M. Moriarity, Ph.D.

Academic Rank: Associate Professor

Institution and
  Department: University of Alabama in
                                Huntsville,
                                Department   of   Biological
                                Sciences

MSFC Colleague: Marc L. Pusey, Ph.D.

NASA/MSFC:

    Office: ES 76
    Division: Microgravity   Science   and
                                Applications
    Branch: Biophysics

INTRODUCTION

Ovostatin is a 780,000 MW protein, originally isolated from chicken egg white, which is active as a protease inhibitor (1). Structural studies indicate that the protein is a tetramer of identical subunits of 165,000 MW which can be separated upon reduction with β-mercaptoethanol. Chicken ovostatin is an inhibitor of metalloproteases such as collagenase and thermolysin, and of acid proteases such as pepsin and rennin (2). Ovostatin isolated from duck eggs (3) and from crocodile eggs (4) appears to be similar to chicken egg ovostatin, but with significant differences in structure and function. Duck ovostatin contains a reactive thiol ester which is not found in the chicken protein, and duck and crocodile ovostatin inhibit serine proteases such as trypsin and chymotrypsin, while chicken ovostatin does not. Electron microscopy (4,5) of ovostatin indicates that two subunits associate near the middle of each polypeptide to form a dimer with four arms. Two of these dimers then associate to produce a tetramer with eight arms, with the protease binding site near the center of the molecule. Upon binding of the protease, a conformational change causes all eight arms to curl toward the center of the molecule, effectively trapping the protease and sterically hindering access of the substrates to its active site. The structural organization and mechanism of action proposed for ovostatin are nearly identical to that proposed for α_2-macroglobulin, a serum protease inhibitor (6) which may play an important role in regulation of proteases in animal tissues.

Although the general arrangement of subunits appears to be the same for all ovostatins studied, some differences have been observed, with chicken ovostatin more closely resembling reptilian ovostatin than the duck protein. This is a surprising result, given the evolutionary relatedness of chickens and ducks. It is possible that the difference in structures may be due to deformed subunit arrangements which occur during the processing and fixing necessary for electron microscopy (4). Examination of the native structure of these proteins using X-ray crystallography would help clarify these discrepancies.

BODY

Obviously, it is necessary to have good quality crystals of ovostatin if x-ray crystallography is to be performed. Such crystals could also be used as a model system to study and understand numerous aspects of crystal growth for such a large protein. For these reasons, attempts have been made at MSFC to prepare crystals of chicken egg white ovostatin. Ovostatin has been purified using slight modifications of published procedures. SDS-gel electrophoresis under reducing conditions

indicated a large band of MW 165,000 and a smaller band at MW
88,000. This smaller band has been reported to be a fragment
produced by action of the bound protease on the ovostatin (7)
and has also been found to occur due to autolytic degradation
of duck ovostatin. Such autolytic degradation had not
previously been observed for chicken ovostatin (7). Attempts
to crystallize the ovostatin preparations have had limited
success, with reasonable size crystals only occurring on a few
occasions. For this reason, it was deemed necessary to
investigate the protease inhibitory activity of the ovostatin
preparations to determine if native, active molecules were in
fact being purified.

One assay for ovostatin employs the metalloprotease
thermolysin and uses azocasein as its substrate in a reaction
carried out at 23°C. Nagase et al. (1) have reported that
using this assay, they have observed a 1:1 stoichiometric
relationship between thermolysin and ovostatin. Thus, when
there is a molar ratio of ovostatin:thermolysin of 0.5 one
should observe 50% inhibition of the protease. Initial trials
using this assay at MSFC resulted in absorbance differences
between the blanks and the positive controls of only 0.3 - 0.6
absorbance units. Also, the azocasein substrate gave higher
readings with increasing storage time at 4°C. Hemoglobin was
tried as an alternate substrate for the thermolysin, but was
not a good substrate for the enzyme. After several
preparations of new azocasein solutions it was found that
storing the azocasein solution at -20°C gave more stable, low
blank values for the assay. Increasing the assay temperature
from 23°C to 37°C increased the activity of the thermolysin
and hence, the absorbance readings, as expected. However, it
was observed that ovostatin inhibition of thermolysin was
decreased at molar ratios of ovostatin:thermolysin less than
1.0. The observed temperature dependence of the assay is
shown in Figure 1. Since ovostatin is expected to be a
physiologically important inhibitor of bacterial proteases in
the egg at the normal chicken body temperature of 42° C these
results are curious and warrant further investigation.

Figure 1.

Ovostatin Inhibition of Thermolysin
Temperature Dependence

25 C 30 C 37 C 42 C
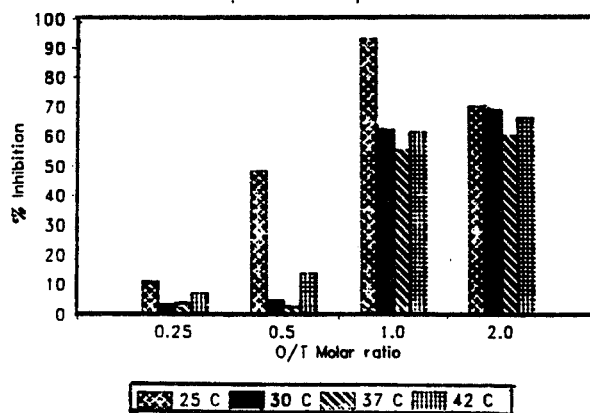
Several ovostatin preparations were assayed and found to yield less than a 50% inhibition of the thermolysin when used at a 0.5 molar ratio of ovostatin:thermolysin. These preparations were analyzed by SDS-polyacrylamide electrophoresis, and all but one appeared to be quite pure, except that the 88K MW degradation product was visible in nearly all the lyophilized, stored preparations. Assay and gel electrophoresis were then performed on freshly prepared ovostatin at several key steps during the purification procedure. The preparation did not have much of the 88K band present and seemed to be nominally active through the ion exchange column portion of the isolation procedure. At this point it was also observed that the ovostatin solutions stored at 4°C appeared to lose activity with time. Thus, preparations of ovostatin that required more than 5-6 days to complete could be becoming less active during the isolation.

Many of the blood coagulation factors are proteases and it was of interest to determine whether ovostatin might inhibit one or more of these. Thrombin, which acts near the end of the blood clotting cascade, is readily available commercially, so ovostatin was examined for its ability to inhibit the action of thrombin on fibrinogen and the subsequent formation of a fibrin clot. Assays at 37°C with up to a 2 fold molar excess of ovostatin over thrombin did not indicate any inhibition. Native polyacrylamide gels of ovostatin incubated with thermolysin or with thrombin indicated that the thermolysin bound to ovostatin and changed its electrophoretic mobility, but the thrombin did not.

Assays of ovostatin performed at both high (1.0 mg/ml) and low (0.025 mg/ml) concentrations gave conflicting and irreproducible results. It was thought that perhaps there was either an as yet unreported requirement for some cation for ovostatin activity, or that some cation could inactivate the ovostatin. To test this hypothesis, ovostatin was incubated with 1 mM EDTA prior to incubating it with thermolysin. The results of this experiment indicated that this treatment may have produced a slight increase in the activity of the ovostatin when assayed at a molar ratio of 0.5. However, incubation of ovostatin with 5 mM EDTA resulted in the opposite effect, decreasing the ovostatin activity at a 0.5 molar ratio.

Several attempts were made to crystallize different ovostatin preparations that had been stored lyophilized at -20°C, but none were successful.

CONCLUSIONS

As is often the case in science, these results have

raised more questions than they have answered. While it appears that ovostatin prepared at MSFC has some inhibitory activity towards thermolysin, it may not have optimal activity. This may or may not be the reason for the difficulty in crystallizing these preparations. Although the crystallization problem was not solved, several important observations were made:

1)   Azocasein solutions must be stored at -20° C.

2)   Thermolysin solutions should be made up as concentrated solutions in 50% glycerol, stored at -20° C and diluted to the appropriate concentration immediately before use.

3)   Hemoglobin is not a good substrate for this assay.

4)   Chicken ovostatin does not inhibit thrombin.

5)   The inhibition of thermolysin by ovostatin is temperature dependent at low ovostatin:thermolysin ratios, and decreases as one approaches physiological temperatures.

6)   It appears that there are as yet undefined variables in the purification of active chicken ovostatin.

More work needs to be done to identify the reason for the appearance of the 88K MW band in the ovostatin preparations and to discern the appropriate conditions to produce ovostatin crystals.

REFERENCES

1. Nagase, H. and Harris, E.D., Jr. (1983) *J. Biol. Chem.* **258,** 7481-7489

2. Kato, A, Kanemitsu, T. and Kobayashi, K. (1991) *J. Agric. Food Chem.* **39,** 41-43

3. Nagase, H., Harris, E.D., Jr. and Brew, K. (1986) *J. Biol. Chem.* **261,** 1421-1426

4. Ikai, A., Kikuchi, M. and Nishigai, M. (1990) *J. Biol. Chem.* **265,** 8280-8284

5. Ruben, G.C., Harris, E.D., Jr. and Nagase, H. (1988) *J. Biol. Chem.* **263,** 2861-2869

6. Sjoberg, B. and Sarolta, P. (1989) *J. Biol. Chem.* **264,** 14686-14690

7. Nagase, H. and Harris, E.D., Jr. (1983) *J. Biol.Chem.* **258,** 7490-7498

1993

NASA/ASEE SUMMER FACULTY FELLOWSHIP PROGRAM

MARSHALL SPACE FLIGHT CENTER
THE UNIVERSITY OF ALABAMA IN HUNTSVILLE

EVALUATION OF COMPUTER-AIDED INSTRUCTION TECHNIQUES
FOR THE CREW INTERFACE COORDINATOR POSITION

Prepared By: Gary P. Moynihan

Academic Rank: Assistant Professor

Institution and Department: The University of Alabama
                                      Department of Industrial Engineering

MSFC Colleague: Beth Skidmore

NASA/MSFC:
        Division: Mission Operations Laboratory
        Branch   Crew Training and Support

The Crew Interface Coordinator (CIC) is responsible for real-time voice and procedural communication between the payload crew on the orbiter and the payload operations team on the ground. This function is dedicated to science activities and operations, and may also include some responsibilities for crew training. CIC training at Marshall Space Flight Center (MSFC) consists of mission-independent training, mission simulations, and line-organization training. As identified by Schneider, the program provides very good generic training, however position-specific training may be obtained in a very unstructured way. (4) A computer-based training system, identified as Mac CIC is currently under development to address this issue. Mac CIC is intended to provide an intermediate level of training in order to prepare the CIC for the more intensive mission simulations. Although originally intended as an Intelligent Tutoring System, Mac CIC currently exists as a hypertext-based application. The objectives of this research is to evaluate the current system, and to provide both recommendations and a detailed plan for Mac CIC's evolution into an Intelligent Tutoring System.

The goal of the Mac CIC system is to provide training on integrating CIC-specific knowledge and skills in an interactive environment. The system is executed on a Macintosh IIci microcomputer and utilizes text, graphics, video and digitized audio to present information to the user. The initial system design identified the following major modules: (4)

1) "Teach Me About" - provides a library of CIC-specific knowledge, · including: Payload Operations Overview, Communications, Mission Timeline, Documentation and CIC Overview,

2) "Skills" (also referred to as "Practice") - allows the trainee to practice CIC-specific skills one topic at a time. It is intended to provide tutoring capabilities in addition to conventional Question/Answer drills.

3) "Scenarios" - provide a means for the CIC trainee to practice making decisions which require integrated knowledge and skills.

At the time of this writing, the major portion of the Teach Me About module has been constructed using SuperCard (Version 1.6). Little programming has been done regarding the remaining modules. The initial design envisioned the utilization of the NEXPERT OBJECT expert system shell as a platform for the Skills and Scenario modules. NEXPERT would be linked to the SuperCard application via its HyperBridge facility.

According to Dumslaff and Ebert, the three primary methodologies of computer-based training systems are traditional computer-assisted instruction, hypertext and intelligent tutors. (1) A large variety of hypertext-based training systems have been developed, and the present trend appears to favor this approach over the highly structured computer-assisted instruction. (2,) The decision to utilize SuperCard as the basis for the Teach Me About module is consistent with current work in the field.

Intelligent tutoring systems differ from the other methods of computer-based instruction by incorporating artificial intelligence techniques. The utilization of expert systems is a well-established means of doing this. (3) Although symbolic languages (e.g. LISP, PROLOG) or even conventional languages (e.g. C, PASCAL) may be used to develop an expert system, the selection of an expert system shell for the Mac CIC project was a correct decision. Expert system shells are pre-packaged inferencing mechanisms with auxiliary features so as to facilitate systems development. Essentially, they are expert systems without the domain-specific knowledgebase. The advantage of this approach is that it allows the project team to focus effort on establishing the knowledgebase, and not on constructing supporting software facilities. NEXPERT OBJECT is a multiparadigm expert system shell capable of using both objects and rules. It also provides both forward and backward search mechanisms along its inference net. NEXPERT's hybrid method of chaining tends to be an extremely efficient processor, as is found in most true expert system environments. Selection of of NEXPERT OBJECT provided the best balance of cost versus capabilities for this project. It is important to note that NEXPERT is a complicated application, and as with most other environments, training is not trivial. (3)

Although the overall design approach to Mac CIC appears to be correct, considerable work remains regarding the existing module and those still to be developed. The initial step in the development of these recommendations was to obtain feedback from actual CICs. A preliminary review of the existing Mac CIC system was conducted from June 7 to 9. The group included both experienced and novice CICs, thus providing a broad perspective. Suggestions were reviewed, and many form the foundation of the subsequent recommendations in this report.

It is envisioned that aspects of the Mac CIC system could be migrated in order to support the training of other POCC positions. (e.g. Data Management Coordinator (DMC), Operations Controller (OC), Payload

Activities Planner (PAP)). Analysis of the system indicates that most of the Teach Me About module is suitable for migration to these POCC positions, The CIC Overview and still to be developed CIC Golden Rules, however, are position-specific, as will be the Skills and Scenario modules. The approach taken for each of these, however, can be used for migration. This would essentially provide the framework around which domain-specific knowledge could be applied. This is particularly true if the recommended modular approach (separation of domain-dependent rules from instructionally oriented ones) is used for the construction of the knowledgebases.

The underlying strategy, behind this development plan, is to deploy an initial version of Mac CIC as soon as possible. Subsequent versions, each with additional functionality, would be phased in. This incremental approach is strongly recommended in the literature. While permitting the earliest possible deployment, this approach also allows post-implementation feedback from the students to be incorporated into later versions.

Implicit in the plan is the need to focus effort on a prioritized work list, based on what is directly applicable to the CIC function. Early in Phase 1, a management decision, on these priorities, is scheduled. This decision would be based on a review of the documented SuperCard linkages and the omissions identified. It is recommended that any further work on the Documentation and CIC Golden Rules components be deferred. Review of these indicates that much of this material has already been incorporated into other module components. The priorities should then list actual system corrections first, then modifications to existing functionality, again within the perspective of what is relevant to the CIC. The prioritized list would then be worked within the 4 1/2 week window allocated to reprogramming.

New facilities would then be developed for the Teach Me About module. The query capability would simply be a series of questions that would test the trainee's understanding of the material. The debriefing facility would provide both a series of questions, and a free-form display for eliciting the student's comments regarding the Mac CIC method of instruction. The preliminary student model would be an individualized file for maintaining a history of the student's comments and test answers. File update would be provided by the XCMD function resident in SuperCard. After undergoing verification and validation, the Teach Me About module would be available

for student use. Post-implementation documentation of any changes to the SuperCard linkages. would then follow.

Knowledge acquisition may begin upon completion of Phase 1. Since knowledge will be drawn from mission-specific videotapes and documents, these sources need to be made available by this date. Identification of the Specific Behavioral Objectives (SBO), i.e. the trainee learning goals, should occur early in the knowledge acquisition process. A Functional System Design of the module can then be derived based upon these goals. Programming, verification, validation and implementation of the module follow, based upon the agreed design. Teach Me About module test cases are rerun at this point to ensure that there are no unforeseen implications of installing the new module. Documentation of the SuperCard linkages is then updated to reflect integration with the NEXPERT knowledgebase.

Phase 3, development of the Scenario module, follows the same sequence of activities as Phase 2. The duration of Phase 3 is anticipated to be significantly less than Phase 2, since it primarily integrates knowledge previously acquired, and functions previously programmed. The scenarios developed initially would be "canned", i.e. all trainees would execute them.As a history of student responses is built up, the student model can be progressively refined and validated. Future iterations of the Mac CIC scenarios would be intelligently selected by the system based on the specific levels of proficiency, and the specific problems indicated in the enhanced student model.

REFERENCES

1) Dumslaff, U. and Ebert, J., "Structuring the Subject Matter" in Proceedings of the Fourth International Conference on Computers and Learning, Wolfville, Nova Scotia, Canada, June 17 - 20, 1992, P. 174 - 186.

2) Farrow, M., "Knowledge Engineering Using Hypercard: A Learning Strategy for Tertiary Education", Journal of Computer-Based Instruction, Vol. 20, No. 1, Winter 1993, P. 9 - 14.

3) Ignizio, J.P., Introduction to Expert Systems ,McGraw-Hill, New York, 1991.

4) Schneider, M.P., "An Intelligent Position-Specific Training System for Mission Operations",NASA Technical Memorandum 108381, October, 1992.

1993
NASA/ASEE SUMMER FACULTY FELLOWSHIP PROGRAM
MARSHALL SPACE FLIGHT CENTER

THE UNIVERSITY OF ALABAMA OF HUNTSVILLE

ERROR CODING SIMULATIONS

Prepared by: Viveca K. Noble

Academic Rank: Instructor

Institution and   Tuskegee University
Department:

MSFC Colleague(s):   Bernd Seiler
                                Helen L. Thomas

NASA/MSFC:

Office: Astrionics Laboratory
Division: Computers and Communications
Branch: Flight Data Systems

Introduction

There are various elements such as radio frequency interference (RFI) which may induce errors in data being transmitted via a satellite communication link. When a transmission is affected by interference or other error-causing elements the transmitted data becomes indecipherable. It becomes necessary to implement techniques to recover from these disturbances. The objective of this research is to develop software which simulates error control circuits and evaluate the performance of these modules in various bit error rate environments. The results of the evaluation provides the engineer with information which helps determine the optimal error control scheme.

The Consultative Committee for Space Data Systems (CCSDS) recommends the use of Reed-Solomon (RS) and Convolutional encoders and Viterbi and RS decoders for error correction (Reference [2]). The use of forward error correction techniques greatly reduces the received signal-to noise needed for a certain desired bit error rate. The use of concatenated coding, e.g. inner convolutional code and outer RS code, provides even greater coding gain. The 16-bit Cyclic Redundancy Check (CRC) code is recommended by CCSDS for error detection (Reference [2]).

Evaluation and Implementation

The initial development phase of the simulator required evaluation of custom error correction software generated for Goddard Space Flight Center (GSFC) to determine what modules were applicable to Marshall Space Flight Center's (MSFC) planned laboratory capabilities as illustrated in Figure 1. A block diagram which illustrates the operation of the GSFC software is shown in Figure 2.
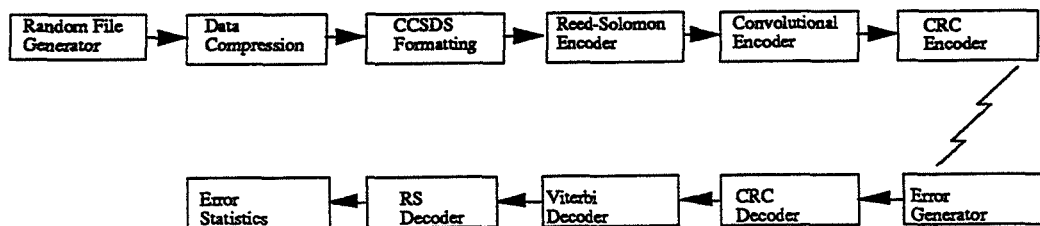
Figure 1
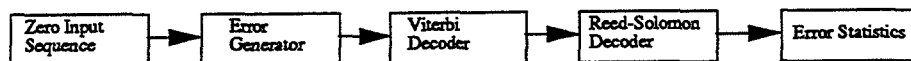
Figure 2

Since the software assumes an all zero input sequence, there is no need for an encoder because the encoded sequence will still be all zeros. This makes the task of determining the error rate a matter of only determining the percentage of non-zero decoder outputs (Reference [5]). Since MSFC's desired system requires random or user-specific data the software from Goddard is unusable in its present form. In order to provide error control capabilities for the Solar Xray Imager (SXI), the remaining modules of the CCSDS telemetry system simulator were developed. These modules include a multiplicative congruential random number generator (RNG), a random error generator, a CCSDS formatter and a CCSDS recommended CRC error detection encoder/decoder. The error statistics generator is currently being developed.

The RNG uses Equation 1 (Reference [3]):

$$X_{n+1} \equiv X_n p \pmod{2^k} \tag{1}$$

where $X_n = 1$, $p = 37$ and $k = 15$. These variables may be assigned any value but X_n and p must be odd. The RNG produces 8968 (8920 bits, maximum transfer frame length plus 48 bits, primary header length) decimal values ranging form 0 to 8191 with a period of 2^{k-2}. Binary values are generated by dividing the decimal values by 4000 and assigning 1 to resulting values greater than 0.5 and 0 to resulting values less than or equal to 0.5. The binary values are used as the random input data and the decimal values are used to access elements in the CRC-encoded message to generate errors in random order.

The CCSDS formatter inserts the sync marker $1ACFFC1D_{hex}$ (Reference [1]) at the beginning of the binary data file to conform to the CCSDS transfer frame format shown in Figure 3 (Reference [2]).

					TRANSFER FRAME PRIMARY HEADER							
ATT. AYNC MARK	FRAME IDENTIFICATION				MASTER CHANNEL FRAME COUNT	VIRTUAL CHANNEL FRAME COUNT	FRAME DATA FIELD STATUS					
	VER #	S/C ID	VIRT CHAN ID	OPER CTRL FIELD FLAG			SEC. HEADER FLAG	SYNC FLAG	PACKET ORDER FLAG	SEGMENT LENGTH ID	FIRST HEADER POINTER
	2	10	3	1			1	1	1	2	11
32	16				8	8	16				
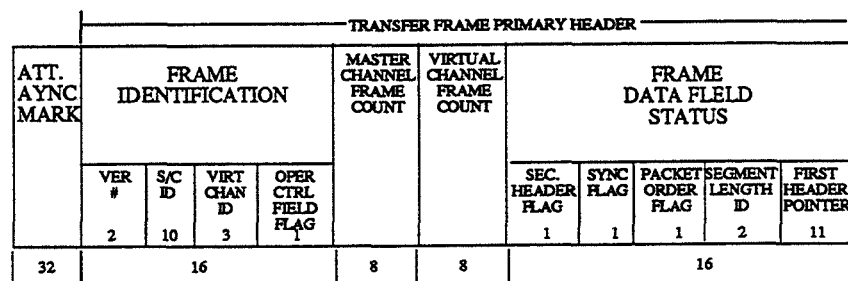
Figure 3

The CRC encoder looks for the 32-bit sync marker, encodes the remaining information bits after synchronization is established and stores the first forty-eight (48) bits of the remaining bits in a header array. The error detection encoder module is the software implementation of the circuit in Figure 4 (Reference [2]).
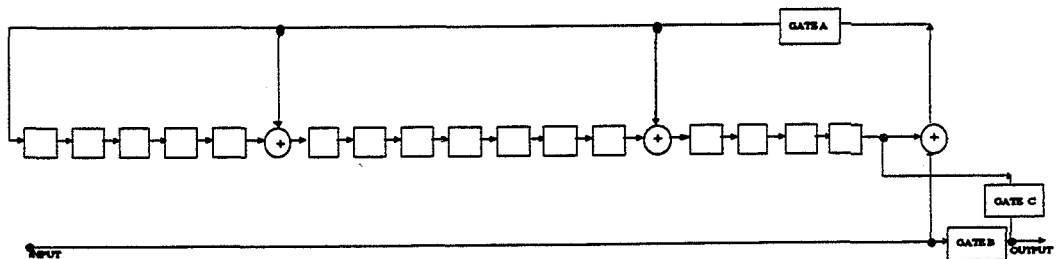
Figure 4

This procedure generates a (n, n-16) code where n is the number of bits in the encoded message and n-16 is the unencoded message. Equation 2 is the 16-bit Frame Check Sequence (FCS)

$$FCS = [X^{16} \cdot M(X) + X^{(n-16)} \cdot L(X)] \text{ modulo } G(X) \tag{2}$$

where $M(X)$ is the unencoded message in the form of a polynomial, $L(X)$ is the polynomial

used to set the 16-bit register to the all 1 state and is given by Equation 3:

$$L(X) = \sum_{i=0}^{15} X_i \qquad [3]$$

and G(X) is the generating polynomial given by Equation 4:

$$G(X) = X^{16} + X^{12} + X^5 + 1 \qquad [4]$$

The generator polynomial has a Hamming distance of 4 therefore it is guaranteed to detect error sequences composed of one, two or three bit errors (Reference [4]). When this code is applied to a block of less than 32768 (2^{15}) bits, it also has the capability to detect all odd number of bit errors, to detect at most two bit errors, to detect all single burst errors with a length of 16 bits or less as long as there are no other errors in the block and has an undetected error probability of 2^{-15} (or 3×10^{-5}) for a random error sequence containing an even number of bit errors greater than or equal to 4.

The error detection decoder module is the software implementation of Figure 5 (Reference [2]).
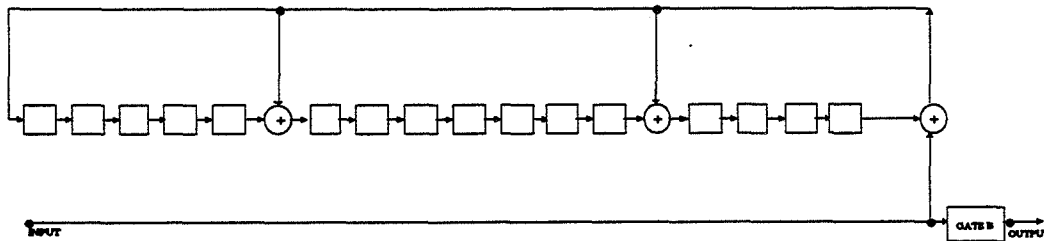
Figure 5

Equation 5 gives the error detection syndrome.

$$S(X) = [X^{16} \cdot C^*(X) + X^n \cdot L(X)] \bmod G(X) \qquad [5]$$

where $C^*(X)$ is the received block in polynomial form and $S(X)$ is the syndrome polynomial. The 16-bit register will contain all zeros if no error is detected and will contain non-zero values if an error is detected. The decoder also attempts to establish synchronization, but if a sync marker error occurs, a message will be generated to indicate this occurence and zeros will appear in the syndrome polynomial to reflect this error.

The decoder's performance has been verified for up to 3 random errors. Tests will be performed to verify the additional performance characteristics. In generating statistics on the error detection capability, various bit error rate environments will be created and decoded for a number of successive runs. The error statistics generator will assign a one for each non-zero syndrome and a zero for each zero syndrome. It will determine the error statistics based on the percentage of non-zero terms.

Conclusion and Future Tasks

All of the previously discussed software is written in FORTRAN 77. Due to the inflexible nature of this language, e.g. input data arrays must be given a declared size, it is recommended that the code be converted to C and all future code be written in C. Appropriate error distributions must be determined so that customized error control environments may be developed. The current error correction portion of the system must be written for use with random data and user specific data. Convolutional and RS encoders and a more refined and flexible error generator must be developed. Data compression modules need to be added for the handling of "housekeeping" data. Testing of the code for various bit error rates must be continued in order to gather statistical data on the performance of the code. The process presented above provides a modular, inexpensive error control environment. Its use will allow an engineer to create an optimal error control environment for a given error distribution prior to implementing the procedure in hardware.

References

[1]   *Telemetry Channel Coding,* Recommendation CCSDS 101.0-B-3, Issue 3, Blue Book, Consultative Committee for Space Data Systems,   May 1992 or later issue, p. 5- 1.

[2]   *Telemetry,* Recommendation CCSDS 100.0-G-1, Issue 1, Green Book, Consultative Committee for Space Data Systems, December 1987 or later issue, pp. 3-19 - 3-20 and pp. D-1 - D-4.

[3]   Hamming, R. W., *Numerical Methods for Scientists and Engineers,* Dover Publications, Inc., New York, 1986

[4]   Jain, Raj, *Error Characteristics of Fiber Distributed Data Interface (FDDI) ,* IEEE Transaction on Communications, Vol. 38, No. 8, August 1990, p. 1249.

[5]   Odenwalder, Joseph P., *Error Control Coding Handbook,* Final   Report, Contract F44620-76-C-0056, July 15, 1976, p. 4 and p. 122.

1993

NASA/ASEE SUMMER FACULTY FELLOWSHIP PROGRAM

MARSHALL SPACE FLIGHT CENTER
THE UNIVERSITY OF ALABAMA IN HUNTSVILLE

SIMULATION OF CRYOGENIC TURBOPUMP ANNULAR SEALS

Prepared By: Alan B. Palazzolo, Ph. D., P.E.

Academic Rank: Associate Professor

Institution and
 Department: Texas A&M University,
                            Mechanical Engineering Department

MSFC Colleague(s):   Dr. Steve Ryan,
                            Donald P. Vallely

NASA/MSFC:

       Office: Structures & Dynamics Laboratory
       Division: Control Systems Division
       Branch: Mechanical Systems Control Branch

In reference (1) San Andres employs the NBS software package MIPROPS to account for density's dependence on pressure in the simulation of liquid annular seals. His example on a LH_2 seal showed a significant change in the mass coefficient compared to a constant density model. San Andres Yang and Childs (2,3) extended this analysis by including the pressure and temperature dependence of density, specific heat, viscosity, volumetric expansion and thermal conductivity in a coupled solution of the energy, momentum and continuity equations. Their example showed very significant changes in stiffness and inertia for a high speed (38,000 rpm), large L/D ratio (0.5) LOX seal, as compared to their constant temperature results.

The current research rederived the San Andres-Yang-Childs (SYC) analysis and extended it to include not only the Moody friction model of SYC but also the Hir's friction model. The derivation begins with obtaining the local differential equations of continuity, momentum and energy conservation in the seal. These equations are averaged across the film thickness to obtain the resulting "bulk flow" differential equations. Shear stress and convective heat loss through the stator (seal) and rotor are related to the Moody and Hir's friction factor model. The Holman analogy is employed to relate heat conduction in or out of the fluid film's boundary layer to the friction induced shear stress.

The steady state problem (d/dt=0) was solved using a shooting algorithm for the two-point boundary value problem. This require a simultaneous integration of the two momentum equations and the continuity and energy equation. The results for temperature increase through the seal shows excellent agreement with the SYC model results as shown in figure 1. The SYC papers also describes an approximate solution algorithm which assumes constant properties and friction factors along the length of a concentric, straight seal. This model was deciphered and programmed and shows excellent agreement with the published SYC approximate solution results, a comparison of which is shown in figure 1.

The linearization coefficient expressions were derived to solve the first order (perturbation) problem for the dynamic coefficients. This linearization procedure was performed for both the Hir's and Moody models and revealed two errors in the SYC linearization coefficients for the viscosity and density in the circumferential momentum equations, and a missing convective heat flux term in the energy equation. The results showed that the Hir's model linearization coefficients were quite different from their Moody counterparts, while maintaining a similar form as regards to programming.

The non-dimensional equations employed in the preceding analysis were used to derive similarity conditions and expressions to infer LOX seal characteristics from those of a similar water seal. The branch is currently developing this tester and required sizing information along with equations which relate characteristics of the two seals. The similarity analysis was confirmed by running the TAMUSEAL code for a LOX seal and for its "similar" water seal. The results of these two runs showed nearly perfect agreement with those predicted by the similarity equations. This

numerical check was performed for both a Hir's and a Moody model type seal. The same study identified non-dimensional dynamic coefficients which remain invariant for seals that are mutually similar, i.e., obey the same conditions of similarity.

The detailed analysis and results of this work may be found in the 430 page report, "Thermal and Similarity Studies for Cryogenic Liquid Annular Seals" issued by the Summer Faculty Fellow to the Mechanical Systems Controls Branch. Future work includes programming the first order solution to the thermohydrodynamic problem to obtain the resulting dynamic coefficients, including seal housing flexibility and extending the bulk flow model to include impeller forces.

The Fellow also planned an installation of an impact damper on the TTB-ATD-HPOTP. The proposed location of the impact damper is shown in figure 2. This device will consist of 12-20 specially designed, cylindrical impactors contained in a ring type fixture. This type of damper has been successfully employed in LN_2 at Texas A&M. Testing of the impact damper may begin as early as Summer '94 if approved by the TTB Review Panel.

REFERENCES

1. San Andres, L.A., "Analysis of Variable Fluid Properties, Turbulent Annual Seals," <u>ASME Journal of Tribology</u>, Vol. 113, October, 1991, pp. 694-702.

2. San Andres, L.A., "Thermal Effects in Cryogenic Liquid Annular Seals - Part II: Numerical Solution and Results," <u>ASME/STLE Joint Tribology Conference</u>, Paper No. 92-Trib-5, pp. 1-8.

3. Yang, Z., San Andres, L., and Childs, D., "Thermal Effects in Cryogenic Liquid Annular Seals - Part I: Theory and Approximate Solution," <u>ASME/STLE Joint Tribology Conference</u>, Paper No. 92-Trib-4, pp. 1-10.

4. Yang, Z., San Andres, L.A., and Childs, D., "Importance of Heat Transfer from Fluid Film to Stator in Turbulent Flow Annular Seals," <u>WEAR</u>, Vol. 160, 1993, pp. 269-277.
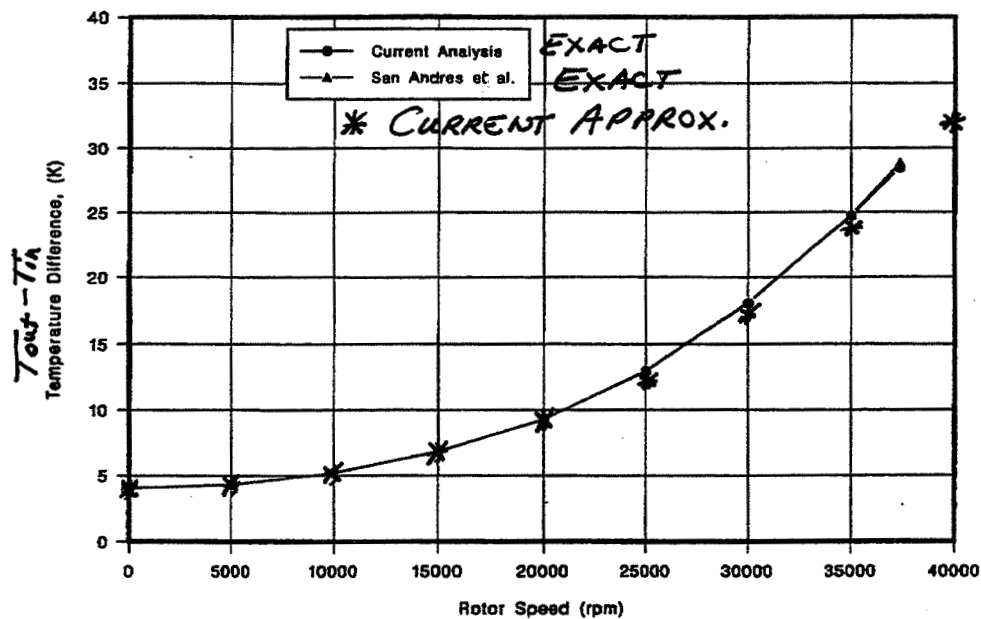
FIGURE 1 – COMPARISON BETWEEN THE EXACT AND APPROXIMATE
TEMPERATURE RISES
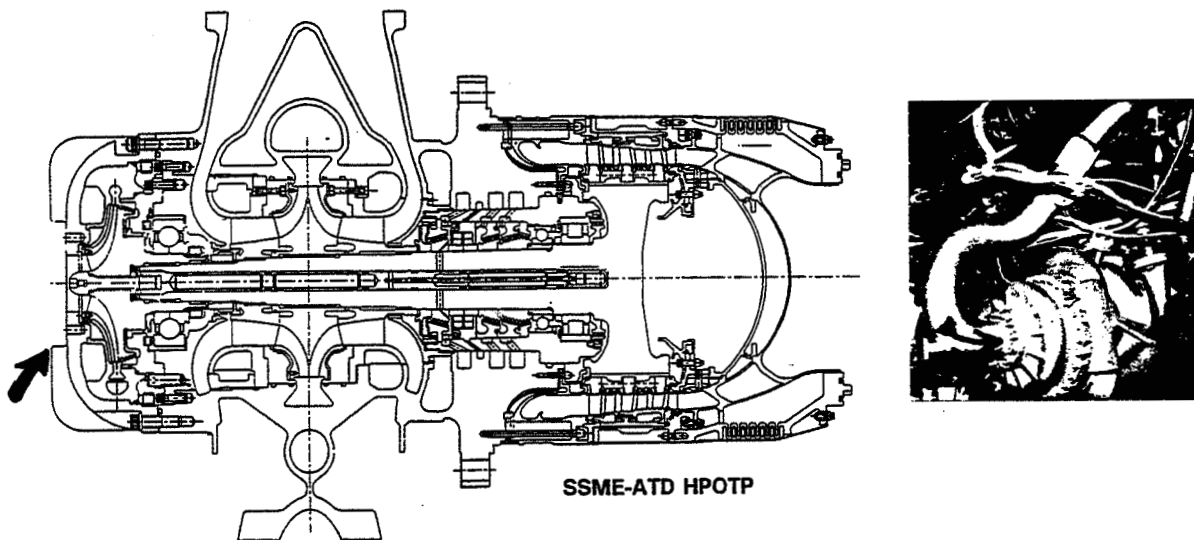
SSME-ATD HPOTP

FIGURE 2 – PROPOSED LOCATION OF THE SSME-ATD-HPOTP
IMPACT DAMPER

1993
NASA/ASEE SUMMER FACULTY FELLOWSHIP PROGRAM

MARSHALL SPACE FLIGHT CENTER
THE UNIVERSITY OF ALABAMA IN HUNTSVILLE

CONTROLLER MODELING AND EVALUATION FOR PCV ELECTRO-MECHANICAL
ACTUATOR

Prepared By: Joey K. Parker

Academic Rank: Associate Professor

Institution and
  Department: The University of Alabama,
                               Department of Mechanical Engineering

MSFC Colleagues: Martha Cash
                               Charles Cornelius

NASA/MSFC:

        Laboratory: Propulsion
        Division: Component Development
        Branch: Control Mechanisms

Background

Hydraulic actuators are currently used to operate the propellant control valves (PCV) for the Space Shuttle Main Engine (SSME) and other rocket engines. These actuators are characterized by large power-to-weight ratios, large force capabilities, and rapid accelerations, which favor their use in control valve applications. However, hydraulic systems are also characterized by susceptibly to contamination, which leads to frequent maintenance requirements. The Control Mechanisms Branch (EP34) of the Component Development Division of the Propulsion Laboratory at the Marshall Space Flight Center (MSFC) has been investigating the application of electro-mechanical actuators as replacements for the hydraulic units in PCV's over the last few years. This report deals with some testing and analysis of a PCV electro-mechanical actuator (EMA) designed and fabricated by HR Textron, Inc. This prototype actuator has undergone extensive testing by EP34 personnel since early 1993. At this time, the performance of the HR Textron PCV EMA does not meet requirements for position tracking.

Hardware

Dual 14 hp brushless DC motors are mounted to common valve shaft. Two motors are used to provide redundancy, but only one motor operates at any given time. A single rotary variable differential transformer (RVDT) is used for shaft position sensing, while dual resolvers are used for motor position sensing. A triple pass gear arrangement with an overall ratio of 85:1 couples the motor shaft to the valve. A pneumatic cylinder backup system is also provided to close the valve completely in case of control system failure.

A combined analog/digital electronic controller board is used to operate the brushless DC motors. The HR Textron EMA controller sequences the current flow to the coils through three integrated gate bipolar transistors (IGBT's). A resolver-to-digital interface chip uses the resolver position feedback to determine which IGBT and coil to energize next. The resolver-to-digital chip also provides an analog voltage proportional to the motor velocity, which is used as an additional feedback signal in the controller circuitry. The output signal from the RVDT is used to provide a conventional position control loop as well. The controller board is designed to be a "drop-in" replacement for the current hydraulic PCV actuator controllers. The interface is designed to be transparent to the Honeywell SSME engine controller, i.e., the engine controller is unchanged and operates as if a hydraulic actuator were in place.

Objectives

In the current state, the PCV EMA actuator and controller is not able to meet the desired position tracking performance. To address this problem, the goals and objectives of this summer's project were:

a) develop an analytical model to predict PCV EMA performance,
b) verify the model with experimental results,
c) modify the modeled controller to reduce tracking errors,
d) incorporate controller changes in prototype hardware, and
e) test the modified controller for acceptable performance.

The remainder of this report will focus primarily on the first two items, with some discussion of the last three.

PCV EMA Controller Model

The simplified model (shown below in Figure 1) was developed for the PCV EMA which assumed a conventional permanent magnet DC motor and a lumped inertia due to the motor shaft, gearbox, and valve. This model uses the same controller structure as the prototype hardware, for example the position and velocity feedback's and both voltage and current limits. The final version of the model was developed by adjusting parameter values to fit the experimental results.

Most of the parameter values were developed from a step response of the prototype. The initial slope of the step response gives the maximum acceleration capabilities of the system, which is determined by $\dot{\omega}_{max} = K_t\, i_{a,max}/J = 2600\,\text{rad}/\text{sec}^2$. Since $i_{a,max}$ is assumed to be known, the values for K_t and J were adjusted to give the appropriate values. With an ideal DC motor, the torque constant is related to the back EMF constant, so these two values were adjusted together to give the maximum velocity shown in the step response. The motor resistance and inductance were adjusted to give approximately the same "curved" response near the maximum velocity.
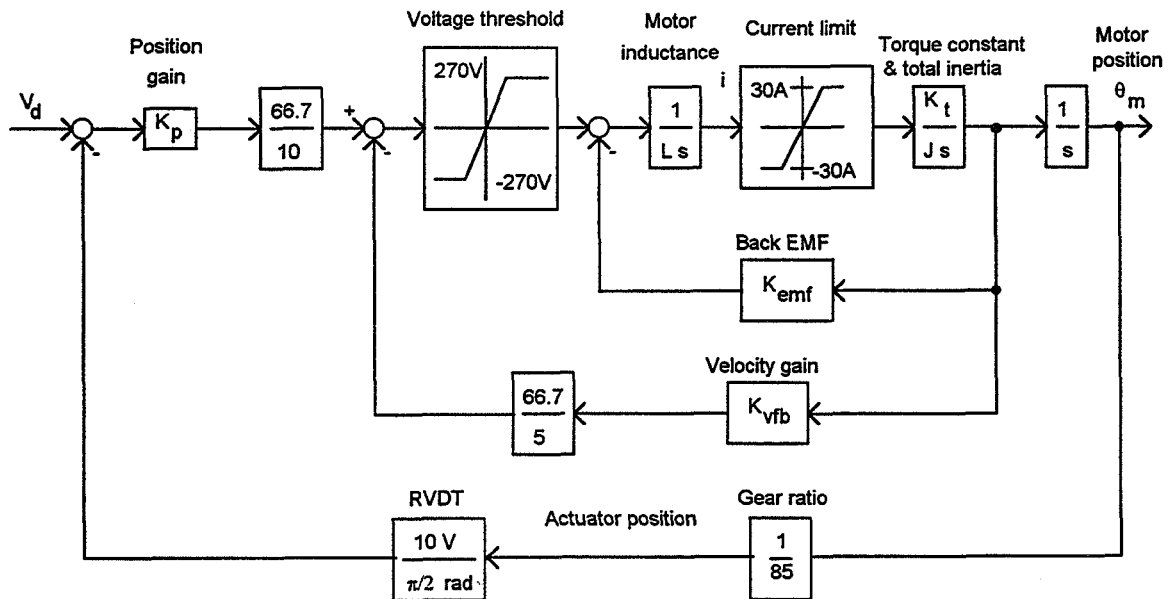
Figure 1 - Simplified Model for PCV EMA

Model Performance and Results

Experimental and simulation results are availiable for the nominal position gain of 5.8 as well as gains of 4.8 and 6.8. Space limitations prevent their display in this report. Note that all testing and simulation of the PCV EMA system was done in the unloaded state. The simulation results closely match the experimental output, particularly while the valve is opening (position increasing). Frequency response tests for both the simulation and experimental hardware were also conducted. The analytical or simulation results were

obtained by applying discrete sine wave inputs to the model and continuing until steady-state was reached. The experimental results were obtained from a sine sweep (from a function generator) applied to the hardware. Although the data for the two curves (simulation and experimental) were obtained differently, the general trends appear to match. The close match between the simulation and experimental results indicates that the model is a reasonable representation of the experimental system. The modeled controller can be easily modified for improvements in tracking error which could be tested later on the prototype hardware.

Controller Improvements

From the simplified controller model, the steady-state error for a ramp input is given by the following equation

$$\text{Tracking Error} = \left(\frac{2\,N\,K_{vfb}}{K_p K_{RVDT}} \right) (\text{Ramp Magnitude})$$

where K_{RVDT} is the fixed gain of the RVDT position transducer, and the other terms are defined below. Since the gear ratio N is also fixed, the tracking error for a constant ramp magnitude can be reduced by one of three ways: increasing the position gain, K_p, decreasing the velocity gain, K_{vfb}, or add a compensator (integrator, phase lag/lead, etc.).

Step responses of the model with different position loop gains K_p were determined. With a small step of ± 1 degree applied, no overshoot was apparent, even at the large gains of 15 and 20. With a larger step of ± 5 degrees applied, the response associated with a gain of 20 showed a pronounced overshoot, while the remaining gains did not. Finally, the responses to a ± 30 degree step were found. Essentially all of the gains (except the nominal value of 5.8) cause some overshoot. The overshoot responses would be a problem if the PCV were operated near one of the position limits (approximately 0 and 85 degrees). However, the Honeywell SSME engine controller reportedly limits its outputs to 3% of full stroke per 20 millisecond sampling period. This would prevent the system from requesting large step changes in the PCV.

The analytical model indicates that increasing the position control gain to 15-20 is a simple means of improving the PCV EMA controller performance. However, excessive overshoot occurs for large step inputs (which do not occur with the Honeywell engine controller). Unfortunately, attempts to verify the analytical results led to an electrical failure in the prototype controller. Two of the three IGBT power transistors were "blown" during a test with large (+/- 30 degree) step inputs. Several other circuit components associated with the IGBT drivers were also destroyed during the mishap. Since only a single PCV EMA controller circuit board exists, a repair effort was begun.

Controller Debugging

The prototype EMA PCV controller board was difficult to repair due to a variety of reasons including inconsistent documentation, inaccurate circuit diagrams, and uncommon (or not readily available) circuit components. For example, the written documentation which accompanied the PCV EMA hardware was evidently for an earlier version of the controller which had since been changed. The latest set of circuit schematics were in general agreement with the actual hardware, but many significant differences existed. Finally, many of the

electronic components on the controller board were not readily available from NASA sources. Some damaged components were replaced with the nearest equivalent part which was available. For example, the original Toshiba #MG100J2YS9 IGBT's were replaced with Powerex #CM100DY-12E models which were of similar, but not identical rating. Instrumentation and technical assistance from EB24 personnel (particularly Justino Montenegro) was invaluable in repairing the damaged controller board.

The efforts to "debug" the PCV EMA controller board were undertaken for two reasons; to repair the system so testing could continue, and to determine the cause of failure. Since the original failure occurred during large (± 30 degree) step inputs, early speculation was that voltage spikes on the power lines caused the IGBT's to fail. However, testing during the first week of August indicated that the existing system maintains voltages of less than 300 volts (with a nominal voltage of 270 volts). Since the IGBT's are rated at 600 volts and the system does not suffer from voltage spikes, it is unlikely that this is the source of the system failure, or that additional "snubber" networks would prevent future failures.

The most likely cause of the system failure was the electrical design and/or the power dissipation capability of the IGBT's themselves. The safe operating area for the Toshiba #MG100J2YS9 IGBT's depends on both collector current (which goes to the motor coils) and the collector-emitter voltage. Although these IGBT's are "rated" at 600 volts and 100 amps, clearly these two values do not apply simultaneously. The operating level for the current PCV EMA controller appears to be marginal for continuous operation over a 0.25 second period. If the power dissipation capabilities of the IGBT did not cause the system failure, then the most likely cause is the physical construction of the prototype circuit board. The overall appearance of the controller gives it an experimental "look" which does not inspire confidence in its performance or longevity.

Conclusions
1) A simple analytical model which treats the brushless DC motor as a conventional permanent magnet DC motor has been developed which matches the prototype PCV EMA performance. A computer program is available for simulating this model's performance with a variety of commanded inputs.
2) The simulations and initial testing results indicate that increasing the position gain to the level of 15-20 should provide acceptable performance for typical ramp type inputs. Excessive overshoot will be a problem at these gain levels if large step inputs (of ± 5 degrees or more) are applied.
3) It is unlikely that additional "snubber" networks placed on the IGBT's of the prototype controller board would prevent system failure if large step inputs were applied.
4) The power dissipation capability of the IGBT is the most likely cause of the system failure. Large step inputs cause an excessively long series of relatively long duration (100-200 μsec) pulses to be applied to the IGBT's. Manufacturer's data indicates that these pulses may cause the IGBT's to operate outside their safety margin.

Acknowledgements

THE MEASUREMENT AND ANALYSIS OF LEAF SPECTRAL REFLECTANCE OF TWO STANDS OF LOBLOLLY PINE POPULATIONS

Prepared By: Anthony D. Paul

Academic Rank: Assistant Professor

Institution and
 Department: Oakwood College,
                        Biology Department

MSFC Colleague: Jeff Luvall

NASA/MSFC:

    Office: Space Science Laboratory
    Division: Earth Science & Applications
    Branch: Earth System Processes & Modeling

My research was under the mentorship of Dr. Jeff Luvall. I worked at Marshall from June 1 through August 6, 1993. My proposal titled "The Measurement and Analysis of Leaf Spectral Reflectance of Two Stands of Loblolly Pine Populations." The populations for this study were chosen from a larger population of 31 families managed by the International Forest Seed Company, Odenville, Alabama. The technology for mobile ground base spectral detecting is new and therefore the majority of time, June 2 through July 9, this summer was spent on learning the techniques of the Spectrometer II spectroradiometer used in the gathering of spectra information. The activities included in the learning process were as follows:

- calibration of the equipment
- programming the associated computer for data management
- operation of the spectral devices
- input and output of data

From July 12 through August 3 the time was spent on learning the 'STATGRAP' computer software. This software will be used in the analysis of the data retrieved by the Spectrometer II spectroradiometer.

Dr. Greg Carter, at Stennis, a colleague of Dr. Luvall, has been conducting similar work with different instruments and procedures and has agreed to host us for a training session on data gathering and analysis. This visit, which was previously planned for July 9, 1993, but had to be postponed because of schedule conflicts, is now confirmed for August 18-22, 1993. This trip to Stennis will provide the knowledge for conducting the field operations in my study, i.e., gathering of data and file conversions.

1993
NASA/ASEE SUMMER FACULTY FELLOWSHIP PROGRAM

MARSHALL SPACE FLIGHT CENTER
THE UNIVERSITY OF ALABAMA IN HUNTSVILLE

LRAT: LIGHTNING RADIATIVE TRANSFER

Prepared by: Dieudonné D. Phanord

Academic Rank: Assistant Professor

Institution and
  Department: University of Alabama in Huntsville
                            Department of Mathematical Sciences

MSFC Colleagues: William Koshak, Ph.D.
                            Richard Blakeslee, Ph.D.
                            Hugh Christian,Ph.D.

NASA / MSFC:
    Laboratory: Space Science
    Division: Earth Sciences /Applications
    Branch: Remote Sensing

I. INTRODUCTION

In this report, we extend to cloud physics the work done in (5–9) for single and multiple scattering of electromagnetic waves. We consider the scattering of light (visible or infrared) by a spherical cloud represented by a statistically homogeneous ensemble of configurations of N identical spherical water droplets whose centers are uniformly distributed in its volume V. The ensemble is specified as in (8), by the average number ρ of scatterers in unit volume, and by $\rho f(\mathbf{R})$ with $f(\mathbf{R})$ as the distribution function for separation $\mathbf{R}$ of pairs. The incident light, $\vec{\phi}_0 = \hat{\mathbf{a}}_0 e^{i\vec{k}_0 \cdot \mathbf{r}}$, a plane electromagnetic wave with harmonic time dependence, is from outside the cloud. The propagation parameter k_0 and the index of refraction η_0 determine physically the medium outside the distribution of scatterers.

We solve the interior problem separately to obtain the bulk parameters for the scatterer equivalent to the ensemble of spherical droplets (2–5). With the interior solution or the equivalent medium approach, the multiple scattering problem is reduced to that of an equivalent single scatterer excited from outside illumination. A dispersion relation which determines the bulk propagation parameter K and the bulk index of refraction η of the cloud is given in terms of the vector equivalent scattering amplitude $\vec{\mathcal{G}}$ and the dyadic scattering amplitude $\tilde{\mathbf{g}}$ of the single object in isolation.

Based on this transfer model we will have the ability to consider clouds composed of inhomogeneous distribution of water and/or ice particles and we will able to take into account particle size distributions within the cloud. We will also be able to study the effects of cloud composition (i.e., particle shape, size, composition, orientation, location) on the polarization of the single or the multiple scattered waves. Finally, this study will provide a new starting point for studying the problem of lightning radiative transfer (3–4).

In general, we work in spherical coordinates. We use bold face or an arrow to denote a vector or a vector operator. A circumflex indicates a vector of unit magnitude. A tilde on the top of a letter denotes a dyadic (second rank tensor). For brevity, we use [5:4] for equation 4 of Ref. (5) etc.

II. MATHEMATICAL MODELING/SOLUTION INSIDE THE CLOUD FOR OUTSIDE INCIDENCE

The solution inside the cloud for outside illumination corresponds to the multiple scattering of a plane electromagnetic wave by an ensemble of configurations of N identical spherical water droplets. To obtain the solution inside the cloud, we consider first the single scatterer in isolation, second a fixed configuration of N identical scatterers, and third an ensemble of the above-mentioned configurations.

For an incident plane electromagnetic wave $\vec{\phi} = \hat{\mathbf{a}}_1 e^{i\vec{\kappa}_1 \cdot \mathbf{r}}$, $\kappa_1 = k_0 \eta_1$, and η_1 being the complex relative index of refraction for the host medium inside the cloud but outside each droplet, the total outside solution for the single scatterer in isolation (outside the single water droplet but still inside the host medium) $\vec{\psi} = \vec{\phi} + \mathbf{u}$ satisfies the following differential equation obtained from Maxwell's equations after suppressing the

harmonic time dependence factor $e^{-i\omega t}$

$$\left[\vec{\nabla} \times \vec{\nabla} \times + \kappa_1^2\right]\vec{\psi} = 0, \vec{\nabla} \cdot \vec{\psi} = 0. \tag{1}$$

The solution inside the single spherical water droplet in isolation $\vec{\psi}_{in}$ satisfies [1] with κ_1 replaced by κ_2. Here, $\kappa_2 = \kappa_1 \eta_2 = k\eta_1\eta_2$, with η_2 being the complex relative index of refraction for the medium inside the spherical water droplet. The propagation parameters κ_1 and κ_2 correspond (within the distribution of identical spheres) to the media outside and inside the water droplet respectively.

Similar to Twersky (7), we have

$$\vec{\psi} = \hat{a}_1 e^{i\vec{\kappa}_1 \cdot \mathbf{r}} + \left\{\tilde{h}(\kappa_1|\mathbf{r} - \mathbf{r}'|), \mathbf{u}(\mathbf{r}')\right\}, u(r) = \left\{\tilde{h}, \mathbf{u}\right\} \equiv$$
$$-\frac{\kappa_1}{i4\pi}\int\left[\left(\tilde{h} \times \hat{n}\right) \cdot \left(\vec{\nabla} \times \mathbf{u}\right) - \left(\vec{\nabla} \times \tilde{h}\right) \cdot \left(\hat{n} \times \mathbf{u}\right)\right]dS(\mathbf{r}'). \tag{2}$$

Here, $\tilde{h} = \left(\tilde{I} + \frac{\vec{\nabla}\vec{\nabla}}{\kappa_1^2}\right)h(\kappa_1|\mathbf{r} - \mathbf{r}'|)$, $h(x) = \frac{e^{ix}}{ix}$, and $\tilde{I}$ being the identity dyadic. It is important to note that $\mathbf{r}$, and $\mathbf{r}'$ denote the observation point and a point on the surface S or in the volume v of the water droplet respectively.

Asymptotically $(\kappa_1 r >> 1)$ we can write

$$\mathbf{u}(\mathbf{r}) = h(\kappa_1 r)\mathbf{g}(\hat{r}, \hat{\kappa}_1 : \hat{a}_1), \quad \mathbf{g}(\hat{r}) = \tilde{I}_* \cdot \mathbf{g}(\hat{r}). \tag{3}$$

Here, $\tilde{I}_* = \left(\tilde{I} - \hat{r}\hat{r}\right)$ is the transverse identity dyadic and $\hat{a}_1 \cdot \vec{\kappa}_1 = 0$. The spectral representation of $\mathbf{u}$ is

$$\mathbf{u}(\mathbf{r}) = \frac{1}{2\pi}\int_c e^{i\vec{\kappa}_{1c} \cdot \mathbf{r}'}\mathbf{g}(\hat{r})d\Omega(\theta_c, \varphi_c), \quad r > \left(\hat{r} \cdot \mathbf{r}'\right), \vec{\kappa}_{1c} = \kappa_{1c}\hat{r}_c(\theta_c, \varphi_c), \tag{4}$$

and the single scattering amplitude $\mathbf{g}(\hat{r}, \hat{\kappa}_1 : \hat{a}_1) = \left\{\tilde{I}_t e^{-i\vec{\kappa}_1 \cdot \mathbf{r}'}, \mathbf{u}(\mathbf{r}')\right\}$ can also be evaluated from Mie scattering theory.

Now, we consider a fixed configuration of N identical scatterers with centers located by $\mathbf{r}_{m(m=1,2,3,...,N)}$. The total outside field

$$\mathbf{\Psi}(\mathbf{r}) = \vec{\phi}(\mathbf{r}) + \sum_{m=1}^{N} \mathbf{U}_m(\mathbf{r} - \mathbf{r}_m), \mathbf{U}_m(\mathbf{r} - \mathbf{r}_m) \sim h(\kappa_1|\mathbf{r} - \mathbf{r}_m|)\mathbf{G}_m, |\mathbf{r} - \mathbf{r}_m| \to \infty. \tag{5}$$

Equivalently, for the scatterer located at $\mathbf{r}_t$, we use the self-consistent approach of (6–7) to obtain the total outside configurational field

$$\mathbf{\Psi}_t(\mathbf{r}) = \vec{\phi}(\mathbf{r}) + \sum\nolimits' \mathbf{U}_m(\mathbf{r} - \mathbf{r}_m) + \mathbf{U}_t(\mathbf{r} - \mathbf{r}_t), \sum\nolimits' = \sum_{m=1, m \neq t}. \tag{6}$$

Using [6] and the general reciprocity relation $\left\{ \mathbf{\Psi}, \, \vec{\psi}_{\hat{\mathbf{a}}_1} \right\}_t = 0$ for any arbitrary direction of incidence and polarization $\hat{\mathbf{a}}_1$, we derive as in (2) the self-consistent integral equation for the multiple configurational scattering amplitude

$$\mathbf{G}_t(\hat{\mathbf{r}}) = \tilde{\mathbf{g}}_t(\hat{\mathbf{r}}, \hat{\kappa}_1) \cdot \hat{\mathbf{a}}_1 e^{i\vec{\kappa}\cdot\mathbf{r}_t} + \sum' \int_c \tilde{\mathbf{g}}_t(\hat{\mathbf{r}}, \hat{\mathbf{r}}_c) \cdot \mathbf{G}_m(\hat{\mathbf{r}}_c) e^{i\vec{\kappa}_{1c}\cdot\mathbf{R}_{tm}}, \qquad [7]$$

with $\mathbf{R_{tm}} = \mathbf{r}_t - \mathbf{r}_m$, $\int_c = \frac{1}{2\pi} \int d\Omega_c$, $\tilde{\mathbf{g}}(\hat{\mathbf{r}}, \hat{\kappa}_1) \cdot \hat{\mathbf{a}}_1 = \mathbf{g}(\hat{\mathbf{r}}, \hat{\kappa}_1 : \hat{\mathbf{a}}_1)$, and the magnitude of the separation distance $|\mathbf{R_{tm}}|$ is bounded above by the diameter D of the cloud.

We take the ensemble average of [7], use the quasi-crystalline approximation of Lax (2), the equivalent medium approach and Green's theorems, to obtain (7) the dispersion relation determining the bulk parameters

$$\vec{\mathcal{G}}\left(\hat{\kappa}_1 \middle| \vec{\mathbf{K}}\right) = -\frac{\rho}{c_0(\mathbf{K}^2 - \kappa_1^2)} \left\{ \left[e^{-i\vec{\mathbf{K}}\cdot\mathbf{R}}, \, \vec{\mathbf{U}} \right] \right\} + \rho \int_{V_D - v} [f(\mathbf{R}) - 1] e^{-i\vec{\mathbf{K}}\cdot\mathbf{R}} \vec{\mathbf{U}} d\mathbf{R}, \qquad [8]$$

where $d\mathbf{R}$ denotes volume integration over $(V_D - v)$. Here, $\vec{\mathcal{G}}$ is the equivalent scattering amplitude and $\vec{\mathbf{U}}$ is a radiative function defined by $\vec{\mathbf{U}} = \int_c \tilde{\mathbf{g}}(\hat{\mathbf{r}}, \hat{\mathbf{r}}_c) \cdot \vec{\mathcal{G}}\left(\hat{\kappa}_{1c} \middle| \vec{\mathbf{K}}\right) e^{i\vec{\kappa}_{1c}\cdot\mathbf{R}}$, and $c_0 = \kappa_1/4\pi i$. The bulk propagation parameter $\mathbf{K} = \kappa_1 \eta$ with η being the bulk index of refraction, and $\{[f, g]\} = \int_S [f \partial_n g - g \partial_n f] dS$ is the Green surface operator with outward unit normal from v. Equation (16) solves formally the interior problem for the cloud with outside illumination.

III. BULK PARAMETERS AND LEADING TERM APPROXIMATIONS

To simplify [8], we force the model to neglect all phase transition effects (1), and to take only into account pair interaction due to central forces. If the inter-droplet potential is negligeable, we can choose $f(\mathbf{R})$ to be always equal to unity. Hence, [8] is reduced to

$$\left[(\mathbf{K}^2 - \kappa_1^2)\tilde{\mathbf{I}}_* + \left(\frac{\rho}{c_o}\right) \tilde{\mathbf{g}}\left(\hat{\mathbf{r}}, \hat{\mathbf{K}}\right) \right] \cdot \vec{\mathcal{G}}\left(\hat{\kappa}_1 \middle| \vec{\mathbf{K}}\right) = 0. \qquad [9]$$

In [9], let $\hat{\mathbf{r}} = \hat{\mathbf{K}}$. In addition, because optical scattering from a cloud is highly forward peaked (7), we neglect back scattering and reduce [9] to

$$\left[(\mathbf{K}^2 - \kappa_1^2)\tilde{\mathbf{I}}_*\left(\hat{\mathbf{K}}\right) + \left(\frac{\rho}{c_o}\right) \tilde{\mathbf{g}}\left(\hat{\mathbf{K}}, \hat{\mathbf{K}}\right) \right] \cdot \vec{\mathcal{G}}\left(\vec{\mathbf{K}} \middle| \vec{\mathbf{K}}\right) = 0. \qquad [10]$$

If the scatterers preserve the incident polarization (7:68), we have from [10]

$$(\mathbf{K}^2 - \kappa_1^2) = -\left(\frac{\rho 4\pi i}{\kappa_1}\right) \tilde{\mathbf{g}}\left(\hat{\mathbf{K}}, \hat{\mathbf{K}}\right), \quad \eta^2 - 1 = -\left(\frac{\rho 4\pi i}{\kappa_1^3}\right) \tilde{\mathbf{g}}\left(\hat{\mathbf{K}}, \hat{\mathbf{K}}\right). \qquad [11]$$

Equation [11] determines the bulk propagation parameter K and the bulk index of refraction η of the equivalent medium for the bounded distribution of the spherical water droplets.

IV. CONCLUSION

The multiple scattering problem has been reduced to that of a single equivalent scatterer in isolation. Formulae are given for the bulk propagation parameter K and the bulk index of refraction η of the equivalent medium. The results are quite general in nature and can be extended to non-spherical geometries. Also, they can be applied immediately to the problem of pulsating optical point sources arbitrarily distributed throughout a scattering medium. When $f(\mathbf{R}) - 1 \neq 0$, [8] can be approximated or solved numerically.

References

1. H. Eyring, D. Henderson, and W. Jost, Physical Chemistry, An Advance Treatise, Volume VIIIA (Academic Press, New York, 1971).
2. Lax . M., "Multiple Scattering of Waves." , Rev. Modern Phys. 23, (1951), 287–629.
3. Solakiewicz. R., "Electromagnetic Scattering in Clouds" NASA-MSFC, Summer (1992), XLVIII.
4. Thomason, L. W., and E. P. Krider, "The effects of clouds on the light produced by lightning." J. Atmos. Sci., 39, (1982), 2051–2065.
5. Twersky, V., 1962: " On a General Class of Scattering Problems.", J. Math. Phys. 3, 4, (1962), 716–723.
6. Twersky, V., "Coherent scalar field in pair-correlated random distributions of aligned scatterers." J. Math. Phys., 18, 12, (1977), 2468–2486.
7. Twersky, V., "Coherent electromagnetic waves in pair-correlated random distributions of aligned scatterers." J. Math. Phys., 19, 1, (1978), 215–230.
8. Twersky, V., Multiple Scattering of Waves by correlated distributions. In (Mathematical Methods and Applications of Scattering Theory, Springer-Verlag, New York, 1980).
9. Twersky, V., "Propagation in correlated distributions of large-spaced scatterers." J. Opt. Soc. Am., 73, (1983), 313–320.

1993

NASA/ASEE SUMMER FACULTY FELLOWSHIP PROGRAM

MARSHALL SPACE FLIGHT CENTER
THE UNIVERSITY OF ALABAMA IN HUNTSVILLE

SPACE SHUTTLE MAIN ENGINE PERFORMANCE ANALYSIS

Prepared By: L. Michael Santi, Ph.D.

Academic Rank: Associate Professor

Institution and
  Department: Christian Brothers University
                           Mechanical Engineering Department

MSFC Colleague: John P. Butas

NASA/MSFC

      Laboratory: Propulsion
      Division: Motor Systems
      Branch: Performance Analysis

I. BACKGROUND

For a number of years, NASA has relied primarily upon periodically updated versions of Rocketdyne's Power Balance Model (PBM) to provide Space Shuttle Main Engine (SSME) steady-state performance prediction. A recent computational study (1) indicated that PBM predictions do not satisfy fundamental energy conservation principles. More recently, SSME test results provided by the Technology Test Bed (TTB) program have indicated significant discrepancies between PBM flow and temperature predictions and TTB observations (2). Results of these investigations have diminished confidence in the predictions provided by PBM, and motivated the development of new computational tools for supporting SSME performance analysis.

A multivariate least squares regression algorithm was developed and implemented during this effort in order to efficiently characterize TTB data. This procedure, called the "gains model", was used to approximate the variation of SSME performance parameters such as flow rate, pressure, temperature, speed, and assorted hardware characteristics in terms of six assumed independent influences. These six influences were engine power level, mixture ratio, fuel inlet pressure and temperature, and oxidizer inlet pressure and temperature. A BFGS optimization algorithm (3) provided the base procedure for determining regression coefficients for both linear and full quadratic approximations of parameter variation. Statistical information relative to data deviation from regression derived relations was also computed.

A new strategy for integrating test data with theoretical performance prediction was also investigated. The current integration procedure employed by PBM treats test data as pristine and adjusts hardware characteristics in a heuristic manner to achieve engine balance. Within PBM, this integration procedure is called "data reduction". By contrast, the new data integration procedure, termed "reconciliation", uses mathematical optimization techniques, and requires both measurement and balance uncertainty estimates. The reconciler attempts to select operational parameters that minimize the difference between theoretical prediction and observation. Selected values are further constrained to fall within measurement uncertainty limits and to satisfy fundamental physical relations (mass conservation, energy conservation, pressure drop relations, etc.) within uncertainty estimates for all SSME subsystems. The parameter selection problem described above is a traditional nonlinear programming problem. The reconciler employs a mixed penalty method to determine optimum values of SSME operating parameters associated with this problem formulation.

The new data reconciliation procedure was used to analyze performance characteristics of two SSME subsystems, the high pressure fuel turbopump and fuel preburner subsystem (HPFTP), and the high pressure oxidizer turbopump and oxidizer preburner subsystem (HPOTP). Reconciliation results for these subsystems were compared to data from TTB test sequence 25 and to PBM data reduction analysis predictions. Typical comparison results are presented in the next section of this report.

II.   ANALYSIS RESULTS

Gains model regression analyses were performed using HPFTP data from TTB-25, a 205 second duration SSME firing. Data from 59 time slices were used to obtain both linear and quadratic fits to operating parameter variation. Results for three such parameters are plotted relative to data slice start time in Figures 1 through 3. Multivariate linear fits provided excellent agreement with both high pressure fuel turbine flow and discharge temperature data as exhibited in Figures 1 and 2. For these parameters, the standard deviation of data from functional fit was 0.23 lb/sec and 3.81 degrees Rankine respectively. A multivariate quadratic fit accurately (σ=0.0018 mru) described fuel preburner O_2/H_2 mixture ratio as shown in Figure 3. The gains model used in this study was uniformly efficient and reliable in identifying performance influences for all test data examined.

Comparisons of TTB-25 test data, PBM reduction analysis predictions, and reconciliation analysis results are presented in Figures 4 through 6. Regarding high pressure oxidizer turbine flow, alarming differences, both in magnitude and trend, exist between PBM prediction and TTB-25 data as displayed in Figure 4. Reconciliation results for HPOT flow are seen to agree well with TTB-25 data. Large differences, on the order of 100-160 degrees R, are observed between PBM prediction and TTB-25 data for the oxygen preburner combustion temperature, as displayed in Figure 5. Reconciliation analysis results are seen to lie between test data and PBM predictions, approximately 60-100 degrees greater than PBM predictions. TTB-25 data for high pressure oxidizer turbine temperature drop are significantly greater than both PBM and reconciliation predictions as displayed in Figure 6. In general, the reconciliation procedure appears to provide a reasonable integration of flow thermo-physics and test data. In addition, it provides a logical scheme for indicating test data integrity.

III.   RECOMMENDATIONS

1.   Gains model regression fits should be extended to a larger range of engine operating conditions and/or multiple engine tests to determine range and order limitations.
2.   The gains model should be expanded to support decisions regarding the health and operation of the SSME.
3.   Development of the reconciliation strategy should be continued.
4.   Assumptions underlying PBM predictions should be evaluated.

IV.   REFERENCES

1.   Santi, L. M., "Validation of the Space Shuttle Main Engine Steady State Performance Model," NASA Contractors Report CR-18404-XLI, October, 1990.
2   "Technology Test Bed Program - Engine 3001 - with Instrumented Turbopumps - First Test Series Test Report," NASA report TTB-DEV-EP93-001, January 15, 1993.
3.   Fletcher, R., "A New Approach to Variable Metric Algorithms,"
      Comput. J., Vol. 13, 1970, pp. 317-322.

FIGURE 1. HPFT FLOW FROM TTB-25
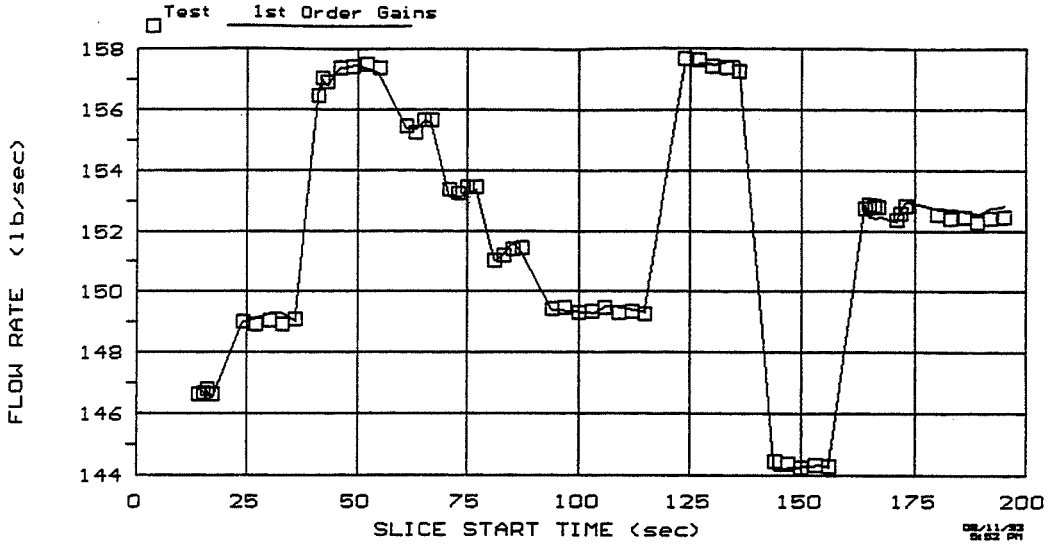
FIGURE 2. HPFT DISCHARGE TEMPERATURE – AVG FROM TTB-25
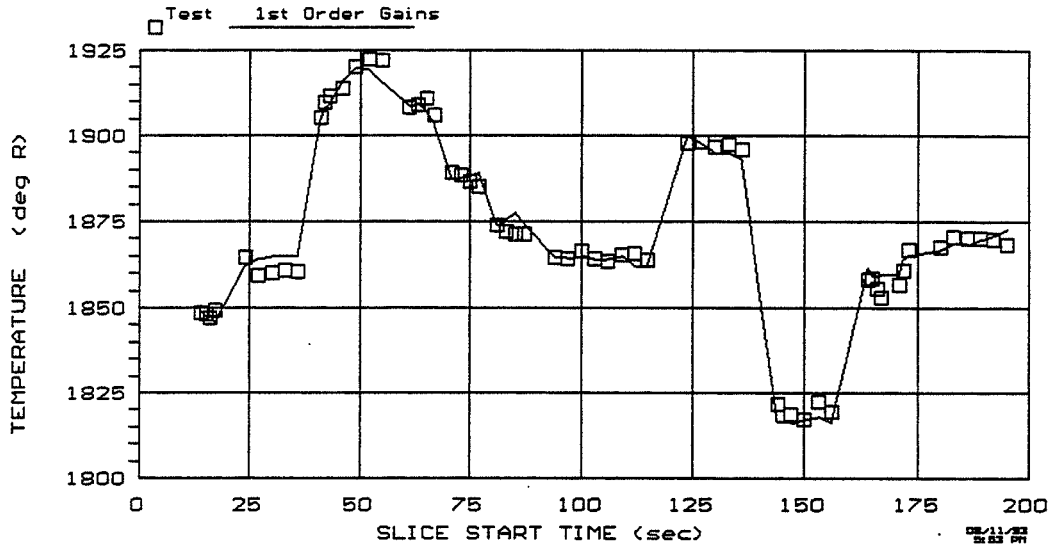
FIGURE 3. FPB MIXTURE RATIO FROM TTB-25

XXXIX-3
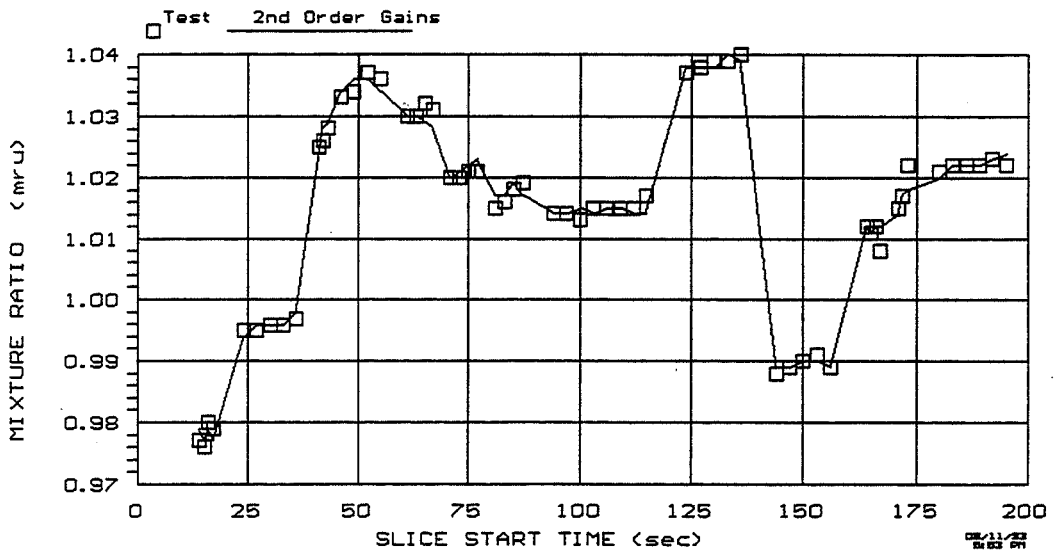
FIGURE 4. HPOT FLOW FROM TTB-25
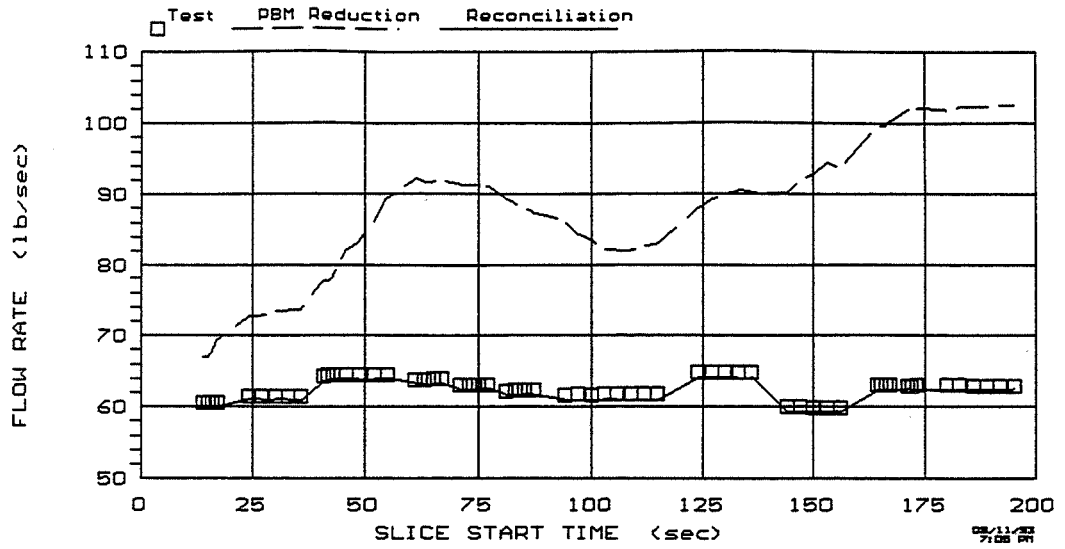
FIGURE 5. OPB COMBUSTION TEMPERATURE FROM TTB-25
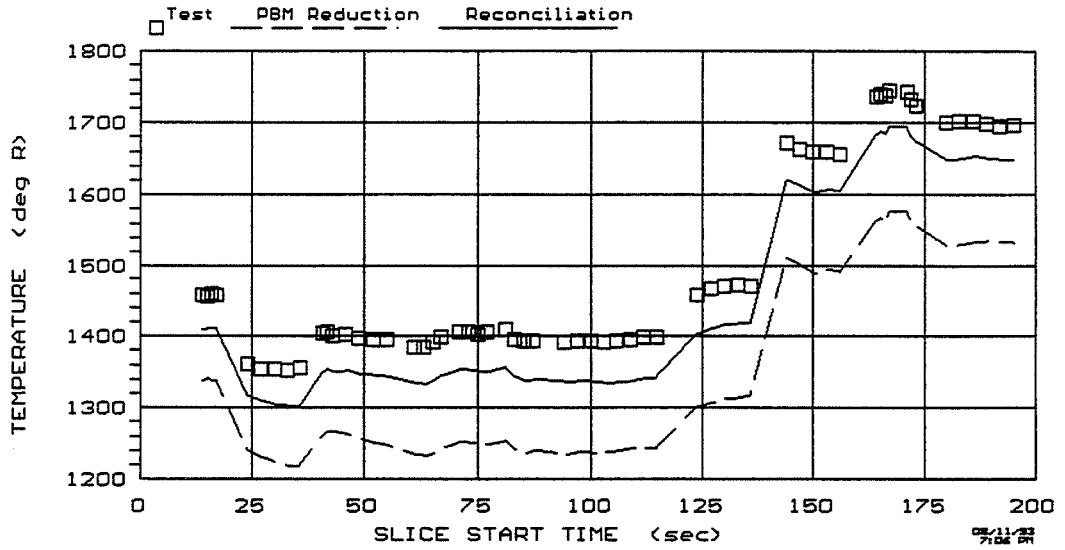
FIGURE 6. HPOT TEMPERATURE DROP FROM TTB-25
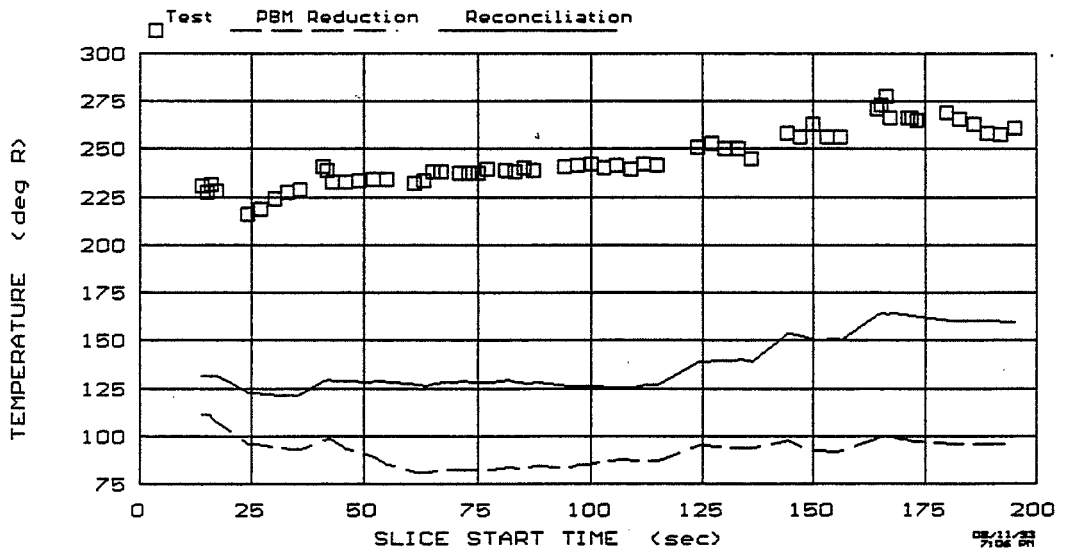
1993

NASA/ASEE SUMMER FACULTY FELLOWSHIP PROGRAM

MARSHALL SPACE FLIGHT CENTER
THE UNIVERSITY OF ALABAMA IN HUNTSVILLE

EVALUATION OF THE EFFICIENCY AND FAULT DENSITY OF SOFTWARE
GENERATED BY CODE GENERATORS

Prepared by: Barbara Schreur, Ph.D.

Academic Rank: Associate Professor

Institution and
 Department: Texas A&I University
                                Department of Electrical
                                 Engineering and Computer Science

MSFC Colleague: Kenneth S. Williamson

NASA/MSFC:

        Office: Astrionics Laboratory
        Division: Software Division
        Branch: Systems Engineering

Introduction

Flight computers and flight software are used for GN&C (Guidance, Navigation and Control), Engine Controllers and Avionics during missions. The software development requires the generation of a considerable amount of code. The engineers who generate the code make mistakes and the generation of a large body of code with high reliability requires considerable time.

Computer-Aided Software Engineering (CASE) Tools are available which generate code automatically with inputs through graphical interfaces. These tools are referred to as code generators. In theory, code generators could write highly reliable code quickly and inexpensively. The various code generators offer different levels of reliability checking. Some check only the finished product while some allow checking of individual modules and combined sets of modules as well. Considering NASA's requirement for reliability, an in house comparison of the reliability of automatically generated code and of manually generated code is needed.

Furthermore, automatically generated code is reputed to be as efficient as the best manually generated code when executed (2). In house verification is warranted.

Evaluation of CASE Tools

A software project of suitable complexity has yet to be provided for evaluation. When delivered, in the form of hardware and software requirements, this project will lead to a segment of software with

1. a length of at least 2000 lines.
2. a minimum of three levels of hierarchy.
3. one level having a minimum of two routines.
4. minimal complexity.

The plan is to develop the software package using two developers each using a CASE Tool and standard methods (4). Two candidate CASE Tools are ASTER and MATRIX$_x$.

CASE Tools are rigid in how they generate programs. They may, for instance, make extensive use of nested ifs rather than case statements. In some applications, this rigidity may produce inefficient code outright or may not mesh well with the characteristics of the compiler thereby causing inefficient execution. The generated code will be examined for such characteristics and the effects of any such characteristics will be investigated.

The spiral model of the software process is characteristic of CASE Tools. They also allow program changes without using patches because the code is regenerated as an internally consistent whole (1). Additionally, the blocks of code in the CASE Tool libraries are reputedly highly reliable. The principal question is whether a combination of many such blocks retains the high reliability or whether the way they interact is capable of producing faults (2). The generated code will be tested for the existence of faults as the modules are completed, if that is allowed by the CASE Tool. This will be followed by testing of the completed segment.

The metrics selected are those contained in MM 8075.1A (3), which may be tailored. A database will be developed to serve as a collector of the measures. These measures will be provided by metrics generating tools available in the public domain and by tools to be acquired for

this project. The metrics will include the following:

1. Software size: The number of lines of code that must be maintained.
2. Software Staffing: The number of software engineers and immediate supervisor involved in the development.
3. Requirements Stability: The total number of requirements that must be implemented.
4. Development Progress: The number of successfully completed modules.
5. Computer Resource Utilization: Percent utilization of CPU, disk, and I/O channel.
6. Test Case Completion: Percent of successfully completed test cases.
7. Discrepancy Report Open Duration: The time between the report of a problem and the resolution of the problem.
8. Fault Density: The number of open Discrepancy Reports and the total defect density normalized by the software size over time.
9. Test Focus: Percentage of problem reports resolved through software solutions.
10. Software Reliability: Probability that the software works under specified conditions for a specified time.
11. Design complexity: Number of modules that have a complexity greater than a predetermined number.
12. Ada Instantiations: Size and number of generic subprograms developed and the number of times they are used. (For C++, the number of object invocations.)

In addition to the metrics, the effectiveness of the CASE tools will be evaluated using the following criteria:

1. The languages available for code generation.
2. The ability to test modules as they are developed both individually and as part of the system.
3. The language the code generator is written in.
4. The libraries, including icons, that are available.
5. The ability to import code from other files and/or projects.
6. The ability to trace variables through the code and determine the effects they have.
7. The documentation of the software created by the code generator.
8. Check on the ability of the tool to "reverse" engineer a section of code for reusability.

A requirements document and test procedures will be developed for typical flight modules.

The original plan was to begin training on ASTER starting with week five. ASTER has not yet been delivered. When it became apparent that ASTER would not be delivered, training was started on MATRIX$_X$. Training in MATRIX$_X$ is progressing and should be completed by week ten. Draper Labs will conduct a two week training session on ASTER in October, 1993 so training on ASTER cannot begin until then.

Future Analysis

Recommendations for future work include the following:
1. The use of at least three Code Generators using non-trivial complex GN&C source code or the equivalent.
2. Analyzing the source code with respect to McCabe complexity, fault density (per 1000 Lines of Code), and efficiency.

3. Performing Software Verification and Validation (V&V).
4. Recommending V&V Methodology and Work-Arounds for Software Source Code Generators.

Conclusion

The project is ambitious. Training is required with several tools as they become available. This report is a delineation of the project and a substantial portion of the training. It is true that a great deal about CASE Tools and metrics has been learned by this Summer Fellow. Whether this work is continued by this Fellow or another, this report provides the basis for an evaluation of the CASE Tools.

References

1. Billmann, L., Mirab, H. and Winkler, U., "CASCSD-CASE Tools", Measurement and Control, Vol. 25, June 1992, pp. 137-143.

2. Dellen, C. and Liebner, G., "Automated Code Generation from Graphical, Reusable Templates", 10th IEEE/AIAA Digital Avionics Systems Conference Proceedings, IEEE, 1991, pp.299-304.

3. MSFC,"MSFC Software Management and Development Requirements Manual", MM 8075.1A, NASA, August 1993.

4. Williamson, K., "The ASTER Code Generator CASE Tool Evaluation", Internal Report, MSFC, May 12, 1993.

1993

NASA/ASEE SUMMER FACULTY FELLOWSHIP PROGRAM

MARSHALL SPACE FLIGHT CENTER
THE UNIVERSITY OF ALABAMA IN HUNTSVILLE

MICROMECHANICAL SIMULATION OF DAMAGE PROGRESSION IN CARBON
PHENOLIC COMPOSITES

Prepared By:	Kerry T. Slattery, Ph.D.
Academic Rank:	Assistant Professor
Institution and Department:	Washington University in St. Louis Department of Civil Engineering
MSFC Colleagues:	Raymond G. Clinton, Ph.D. Roy M. Sullivan, Ph.D.

NASA/MSFC:

Office:	Materials and Processes Laboratory
Division:	Nonmetallic Materials
Branch:	Ceramics and Coatings

INTRODUCTION

Carbon/phenolic composites are used extensively as ablative insulating materials in the nozzle region of solid rocket motors. The current solid rocket motor (RSRM) on the space shuttle is fabricated from woven rayon cloth which is carbonized and then impregnated with the phenolic resin. These plies are layed up in the desired configuration and cured to form the finished part. During firing, the surface of the carbon/phenolic insulation is exposed to 5000°F gases from the rocket exhaust. The resin pyrolizes and the material chars to a depth which progresses with time. The rate of charring and erosion are generally predictable, and the insulation depth is designed to allow adequate safety margins over the firing time of the motor. However, anomalies in the properties and response of the carbon/phenolic materials can lead to severe material damage which may decrease safety margins to unacceptable levels. Three macro damage modes which have been observed in fired nozzles are: ply lift, "wedge out", and pocketing erosion. Ply lift occurs in materials with plies oriented nearly parallel to the surface. The damage occurs in a region below the charred material where material temperatures are relatively low -- about 500°F. Wedge out occurs at the intersection of nozzle components whose plies are oriented at about 45°. The corner of the block of material breaks off along a ply interface. Pocketing erosion occurs in materials with plies oriented normal to the surface. Thermal expansion is restrained in two directions resulting in large tensile strains and material failure normal to the surface. When a large section of material is removed as a result of damage, the insulation thickness is reduced which may lead to failure of the nozzle due to excessive heating of critical components. If these damage events cannot be prevented with certainty, the designer must increase the thickness of the insulator thus adding to both weight and cost.

One of the difficulties in developing a full understanding of these macro damage mechanisms is that the loading environment and the material response to that environment are extremely complex. These types of damage are usually only observed in actual motor firings. Therefore, it is difficult and expensive to evaluate the reliability of new materials. Standard material tests which measure mechanical and thermal properties of test specimens can only provide a partial picture of how the material will respond in the service environment. The development of the ANALOG test procedure (2) which can combine high heating rates and mechanical loads on a specimen will improve the understanding of the interactive effects of the various loads on the system. But a mechanistic model of material response which can account for the heterogeneity of the material, the progression of various micromechanical damage mechanisms, and the interaction of mechanical and thermal stresses on the material is required to accurately correlate material tests with response to service environments. A model based on fundamental damage mechanisms which is calibrated and verified under a variety of loading conditions will provide a general tool for predicting the response of rocket nozzles. The development of a micromechanical simulation technique has been initiated and demonstrated to be effective for studying across-ply tensile failure of carbon/phenolic composites.

APPROACH

The finite element method is used to simulate the progression of micromechanical damage mechanisms in the carbon/phenolic material. Two damage mechanisms are considered: fiber/matrix interface debonding and matrix cracking. The failure process in across-ply tension appears to initiate at the fiber/matrix interface and progress to adjacent fibers. A crack eventually reaches the interface between two plies and propagates along that interface resulting in specimen rupture. Fiber breakage is observed where yarns are severely kinked, but this damage mode is assumed to occur after the development of a critical flaw and is not currently accounted for in the model.

A two-dimensional finite element model is created to simulate the failure of a section of the composite. A typical model consists of one yarn end along with parts of the surrounding in-plane yarns. A sketch of a typical model is shown in Fig. 1. The model consists of three types of finite elements: out-of-plane fiber (OPF), in-plane fiber (IPF), and matrix (MAT). The elements are square with four-nodes and eight-degrees-of-freedom. The OPF element represents a fiber end surrounded by a small amount of matrix. The IPF element has the same dimensions and represents a composite oriented at the yarn angle at the element location. The MAT element is pure matrix and is placed in resin-rich areas. The OPF, IPF, and MAT are "superelements" whose properties are determined from detailed finite element analyses of the constituent materials. Stiffness, thermal expansion, and crack-tip displacement properties are tabulated for many possible damage states for each superelement type. For example, damage in the OPF element is characterized by the location and length of debonds along the fiber/matrix interface. Finite element models are generated and analyzed for approximately 1000 different debond configurations. The results are stored and used to determine superelement properties in the simulation based on the initial interface flaws and the progression of those flaws. This method allows efficient simulation of micromechanical damage progression on models of significant sections of composite.
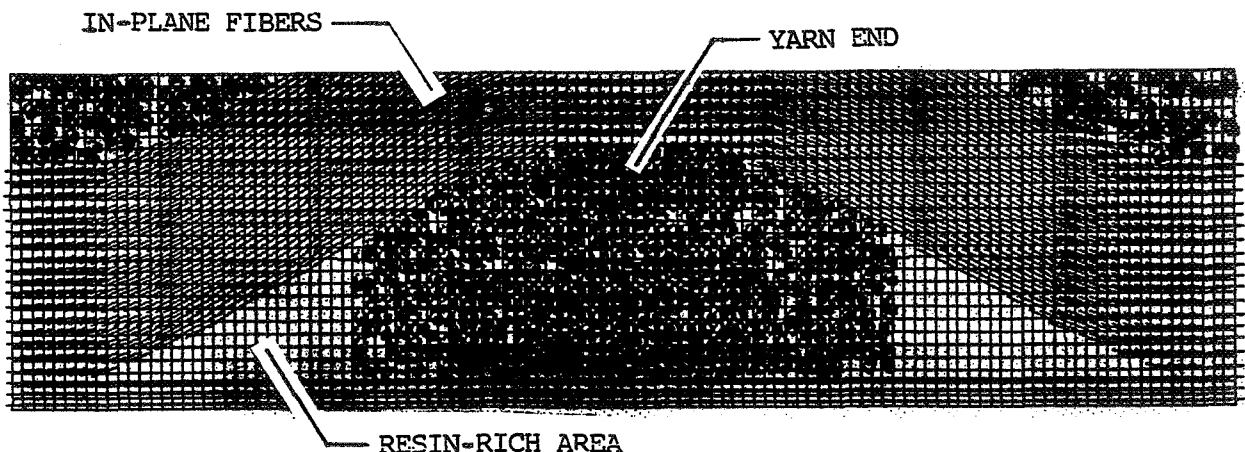

Figure 1. Micromechanical Simulation Model of Woven Carbon/Phenolic Composite

The damage growth model is based upon fracture mechanics principles. A simple model for initial flaws is assumed at the beginning of the simulation. All initial flaws are on the fiber/matrix interface. In the detailed finite element model of the OPF, there are 32 nodes on the interface. An interface flaw is modeled by "disconnecting" the fiber from the matrix at a node. A large debond is formed when several adjacent nodes are disconnected. Flaw distribution schemes are usually random. The simulation method allows the flexibility to investigate are variety of flaw configurations. The two used in this work were placing a fixed length debond (e.g. 45 degrees) on some percentage of randomly selected fibers and specifying a percentage of disconnected nodes on the fiber/matrix interface. Flaw growth is determined using the crack closure method. This method has been used to study failure modes in metal matrix composites (1). Each existing flaw in a superelement is analyzed in several possible propagated states given the current nodal displacement. Tabulated data on crack tip displacements are used to determine the distance between the nodes at the current crack tip and the displacement caused by a unit force at those nodes. The amount of work required to close the crack to its current state from the assumed, propagated state is calculated and compared with the amount of energy required to create the new surface. The crack propagates if the work exceeds the surface energy. The model is idealized since the fibers, which are modeled as circular, actually have irregular shapes and since the quality of the bond between the fiber and matrix also varies around and along the fiber; however, the interface model should provide sufficient flexibility to adequately match the response of the interface by varying the surface energy and the flaw distribution.

A material configuration is selected based on photomicrographs of the composite. A simple mesh generation subroutine is written to define the distribution of the three types of elements and the direction of the IPF elements in the finite element simulation. The nodes on the bottom of the model are fixed, and a uniform tensile stress is applied to the opposite face. The stress level is increased in small increments, and the model is analyzed. After each load step, the properties of each element are updated based upon the crack propagation models. The simulation continues until a maximum stress is reached and severe damage occurs in the model.

RESULTS

Figure 2 shows the progression of damage in a simple section of out-plane fibers with some pure matrix elements. Initial flaws on the fiber/matrix interface are represented by thick lines in Fig 2a. These initial flaws begin to progress at about 0.07% strain as shown in Fig. 2b. The interface flaws propagate to adjacent fibers and eventually coalesce to form a critical flaw which leads to specimen rupture as shown in Fig. 2c. The technique was also applied to a more complex model such as that shown in Fig. 1. The results of many simulations using a range of values for various parameters demonstrated that the response of carbon/phenolic materials can be simulated effectively using this technique.
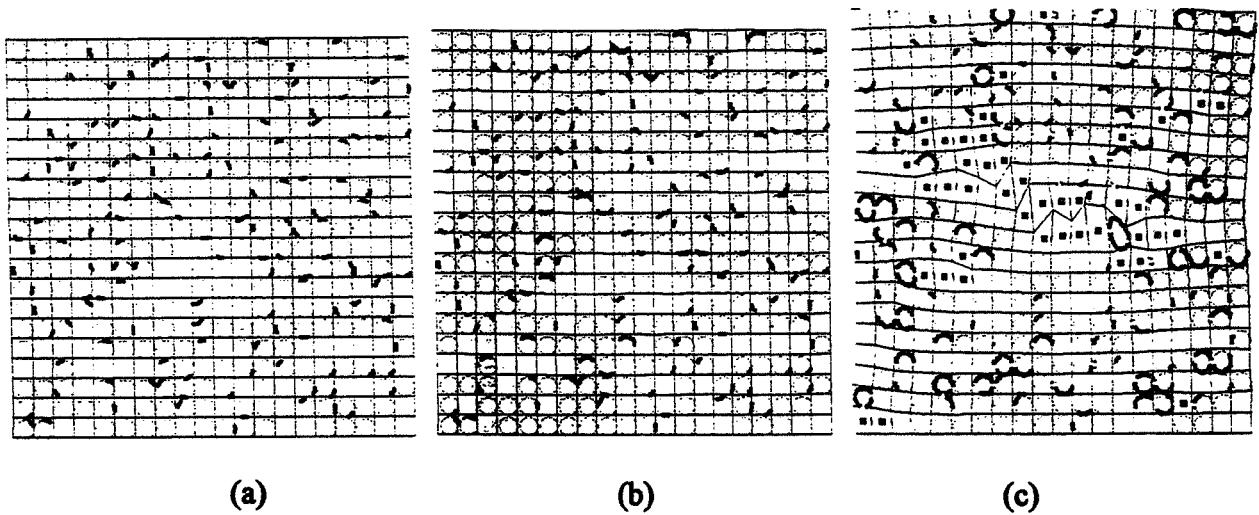
| (a) | (b) | (c) |

Figure 2. Damage Progression in Composite Loaded in Transverse Tension

CONCLUSIONS

A technique to perform micromechanical simulations of damage progression in carbon/phenolic composites has been developed. The technique is effective at modeling across-ply tensile response although additional calibration and verification based on damage in tested specimens must be performed to refine the estimates of critical parameters. Thermal loads can also be applied in the simulation, and preliminary results demonstrate that cracking during post-cure cooldown can be predicted using this technique. Given values for the three principle model parameters: fiber/matrix interface surface energy, interface flaw distribution, and matrix surface energy, along with standard material properties for the constituent materials, any loading condition can be easily simulated. Of course, some of these properties cannot be measured directly, so the simulation technique can aid in determining these values by performing simulations of the material response under a variety of loads and finding the optimum values for the parameters which yield the best results for most conditions. This method can also be extended to three-dimensions if extensive computer resources are available, but two-dimensional simulations can provide substantial new insights into the behavior of carbon/phenolic composites.

REFERENCES

1. Mital, S.K., Caruso, J.J., and Chamis, C.C., "Metal Matrix Composites Microfracture: Computational Simulation," *Computers & Structures*, Vol. 37, No. 2, February, 1990, pp. 141-150.

2. Poteat, R.M., Ohler, H.C., Koenig, J.R., Wendel, G.M., Crose, J.G., and Marx, D.A., "Nozzle Ablative Simulation Apparatus Development," *Proceeding of JANNAF Rocket Nozzle Technology Subcommittee Meeting*, December 1992.

1993

NASA/ASEE SUMMER FACULTY FELLOWSHIP PROGRAM

MARSHALL SPACE FLIGHT CENTER
THE UNIVERSITY OF ALABAMA IN HUNTSVILLE

A CHEMICAL SENSOR AND BIOSENSOR BASED TOTALLY AUTOMATED WATER
QUALITY MONITOR FOR EXTENDED SPACE FLIGHT: STEP ONE

Prepared by: Robert S. Smith, Ph.D.

Academic Rank: Assistant Professor

Institution: St. John Fisher College
Department: Chemistry Department

MSFC Colleague: Layne Carter

NASA/MSFC:

Office: Structures and Dynamics
Laboratory
Division: Thermal Engineering and Life
Support
Branch: Life Support Systems

This report is the result of a literature search to consider what technologies should be represented in a totally automated water quality monitor for extended space flight. It is the result of the first summer in a three year JOVE project.

The next step will be to build a test platform at the Authors' school, St. John Fisher College. This will involve undergraduates in NASA related research. The test flow injection analysis system will be used to test the detection limit of sensors and the performance of sensors in groups. Sensor companies and research groups will be encouraged to produce sensors which are not currently available and are needed for this project

A ground base water lab follows standard methods (4). As technology evolves there is a lag time incorporating the new technologies into standard methods since new methods must be validated and approved by the appropriate government agencies. The priorities for method development for a ground based system vs a space system are almost diametrically opposed, e.g, throughput is a major concern for a ground based system but the sample load will be relatively small in the extended flight system.

A totally automated water quality monitor for extended space flight, e.g., use on the Space Station Freedom, needs to meet the criteria shown in Table 1. It must have sufficient detection limits to analyze for the parameters listed in Table 2 to NASA specifications. Design of a system is aided if an exact list of Organic Toxicants is given rather than general categories, e.g., organic acids. NASA performs evaluations of all materials used in spacecraft to determine candidate compounds, e.g., plasticizer offgases.

Table 1

Water Quality Monitor Criteria

Totally Automation for routine operation
Minimal maintenance requirements
Low power usage
Low weight
Low space requirement
Low use of expendable items
Low use of reagents
Minimal sample size
Work in Microgravity
Withstand Launch
Meet NASA material limitations
Méet NASA safety criteria
Provide data directly to main computer system
Analyze for parameters listed in Table 2

Table 2

pH
Conductivity
Color
Bactericide
Turbidity
Dissolved Gas
Free Gas
Inorganic Anions
Inorganic Cations
Total Organic Carbon
Organic Toxicants

Till recently the development of a totally automated water quality monitor would have been built around the same instruments found in earth based analytical laboratories. Methods would evolve around separation based instruments, e.g., liquid and gas chromatography, which use non-specific detectors unless hyphenated system are used such as gas chromatography-Mass spectroscopy where the separation is performed by the first instrument and specific peak identification is done by the second. These instruments are complex, heavy, have relatively high power requirements and require a moderate amount of skill to service and maintain. Figure 1 shows the revolution in water quality related sensor research that has occurred in the late 80's and early 90's.
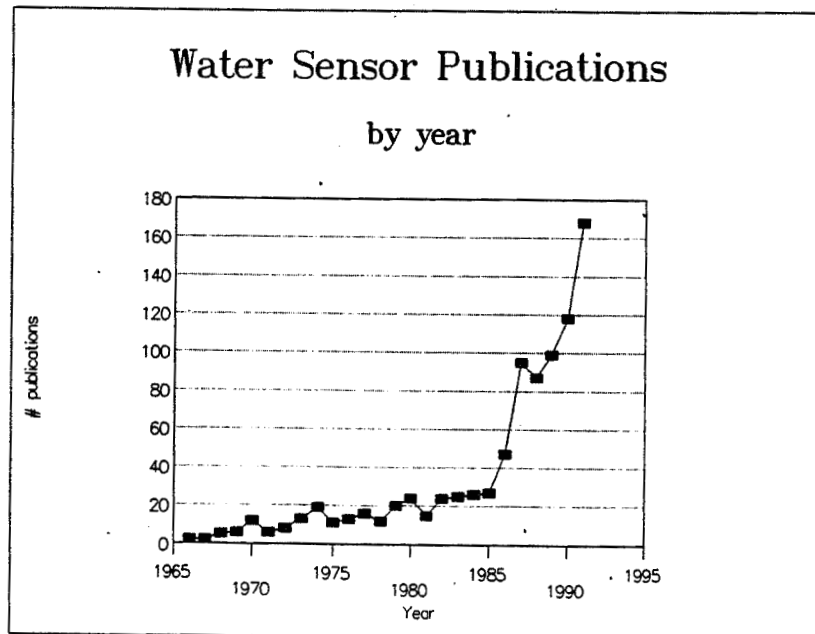

Water Sensor Publications by year

Figure 1

The chemical sensor or biosensor is a link between a chemical system and a computer. The computer handles only numbers in its digital world. Information in the analog world must be converted from voltages to numbers. The chemical sensor provides a link between analyte concentration and a voltage. This completes the chain to get from changing analyte concentration to changing numbers in the computer.

The transducer in a sensor may be potentiometric, amperometric, conductimetric, impedimetric, optical, calorimetric, acoustic, or mechanical (3). A biosensor links one or more of these with a biological material that may be, for example, organisms, tissues, cells, organelles, membranes, enzymes, receptors, antibodies, or nucleic acids. Polymeric materials play an important role in the mating of biomaterials and transducers. They place structural roles as well as active roles in time release of materials and conduction of signals.

Some examples of sensors are ion sensitive electrodes, enzyme electrodes, immunosensors, quartz crystal microbalance, chemically sensitive field-effect transistors, fiber optic, slab waveguide, bioluminescence, and electrochemical. Many variations of sensors have been reported (1).

Ion sensitive electrodes may be used for the inorganic anions, non-metal cations and dissolved gas. The metals can be determined using potentiometric stripping analysis. A diode array spectrometer can determine color, bactericide, turbidity, and free gas. A conductivity cell will be used for conductivity determination. TOC can be determined by commercially available TOC detector. Organic Toxicants can be determined by immunosensors and enzyme based sensors (2).

An extensive list of literature references of sensors for water quality management is available from the author via internet at rss@sjfc.edu. A macro written in Microsoft Word was used to prepare the output from STN searches for entry into Borland's Paradox database program. This allowed offline searches and sorting of the reference material.

The ultimate flow injection system can be envisioned with a backplane for power, signals, reagents, and sample. Ultimately electronic components and sensors will be fabricated on the same wafers to the extent that the output of the sensor package will be network compatible. Sensor modules would plug into this backplane to receive their input needs and give their output on the computer network. The modules could contain their own diagnostics and notify ground control or the astronauts when they need replacing. The astronauts would simple unplug a module that might be the size of a 35mm slide and plug in a new one.

This system would make an ideal candidate for a technology reinvestment or transfer program to be developed as a water quality monitor for home/industrial use. As sensors useful for water quality monitoring are mass produced their cost should drop dramatically. The system could monitor raw water quality to a house and direct the water to in-house purification on a as need basis. It could also monitor the performance of the in-house water purification system. A version of the system could be used for those using unfamiliar water, e.g., travelers, campers, hikers, etc.

Acknowledgement

References

1. Biosensors and Chemical Sensors ACS Symposium Series 487; Edelman, P.G.; Wang, J.W., Eds.; American Chemical Society: Washington D.C., 1992.

2. Bonting, S.L.; "Utilization of Biosensors and Chemical Sensors for space applications"; Biosensors and Bioelectronics; 7(8),1992; 535-548.

3. Carstens, J.R.; Electrical Sensors and Transducers; Regents/Prentice Hall: Englewood Cliffs, N.J., 1993.

4. Standard Methods for the Examination of Water and Wastewater; Greenberg, A.E.; Clesceri, L.S.; Eaton, A.D., Eds.; American Public Health Assoc.: Washington D.C., 1992; 18th Ed.

1993

NASA/ASEE SUMMER FACULTY FELLOWSHIP PROGRAM

MARSHALL SPACE FLIGHT CENTER
THE UNIVERSITY OF ALABAMA IN HUNTSVILLE

MICROSTRUCTURAL ANALYSIS OF
THE 2195 ALUMINUM-LITHIUM ALLOY WELDS

Prepared by: George E. Talia, Ph.D.

Academic Rank: Associate Professor

Institution and
Department: The Wichita State University
                            Department of Mechanical Engr.

MSFC Colleague: Arthur C. Nunes,Jr.,Ph.D.

NASA/MSFC:

    Office: Materials & Processes Laboratory
    Division: Metallic Materials & Processes
    Branch;   Metallurgical Research

Introduction

The principal objective of this research was to explain a tendency of 2195 Al-Li alloy to crack at elevated temperature during welding. Therefore, a study was made on the effect of welding and thermal treatment on the microstructure of Al-Li Alloy 2195. The critical roles of precipitates, boundaries, phases, and other features of the microstructure were inferred from the crack propagation paths and the morphology of fracture surfaces of the alloy with different microstructures. Particular emphasis was placed on the microstructures generated by the welding process and the mechanisms of crack propagation in such structures. Variation of the welding parameters and thermal treatments were used to alter the micro/macro structures, and they were characterized by optical and scanning electron microscopy. A theoretical model is proposed to explain changes in the microstructure of welded material. This model proposes a chemical reaction in which gases from the air (i.e., nitrogen) release hydrogen inside the alloy. Such a reaction could generate large internal stresses capable to induce porosity and crack-like delamination in the material.

Experimental Procedures

2195 Al-Li alloy plates were produced by the Reynolds Metals Company, one pass (root pass) and two passes (root pass and cover pass) welds were performed at the Marshall Space Flight Center. Transverse and longitudinal sections of the welds were analyzed by optical micrographic techniques. Each metallographic sample was prepared for examination using standard polishing preparation techniques and etched with Keller's reagent. Optical microscopy observations were performed using a Nixon inverted microscope. One pass autogenous welds were selected for further thermal processing, i.e., heat treatment at different temperatures in vacuum, air, or Helium atmosphere.

Results

Optical micrographs of the fusion zone of a single pass and two-pass welds in 2195 Al-Li alloy are shown in Figure 1. The initial metallographic analysis of the single pass weld revealed a well formed grain structure with a small amount of porosity. This porosity compares with the initial porosity of the parent metal. See Figure 1-a. For two pass welds a large amount of porosity is observed in the first pass fusion zone (but not in the second or cover pass) and some of the pores take a crack-like shape as shown in Figure 1-b.

To separate the temperature effects from stresses effects generated by the second pass weld some of single pass welded material was furnace heat treated at 450 C for a minute in air and in vacuum. A comparison of the different structures is made

(a)
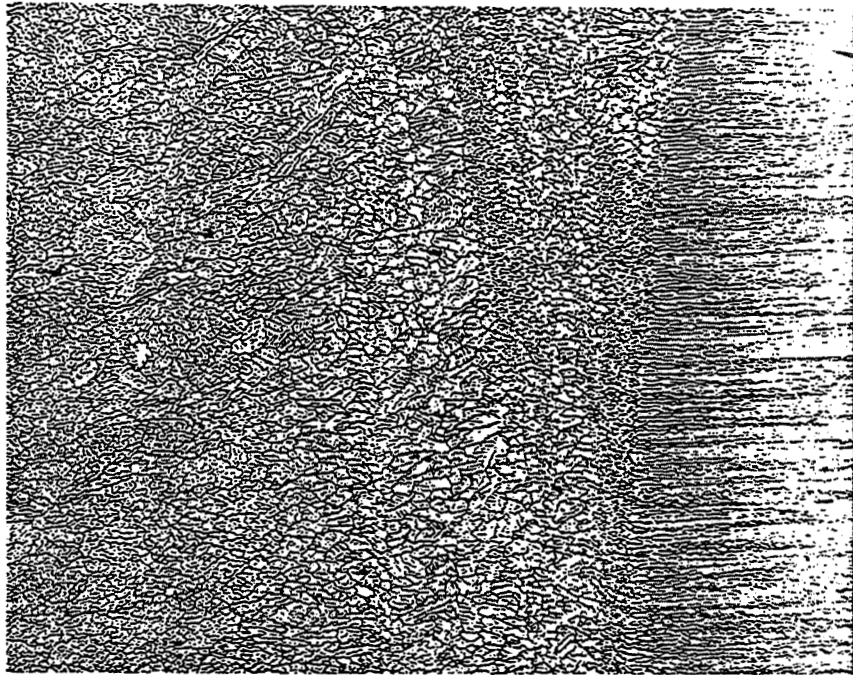
.5 mm

(b)

Figure 1.- Optical micrographs of 2195 Al-Li alloy subjected to
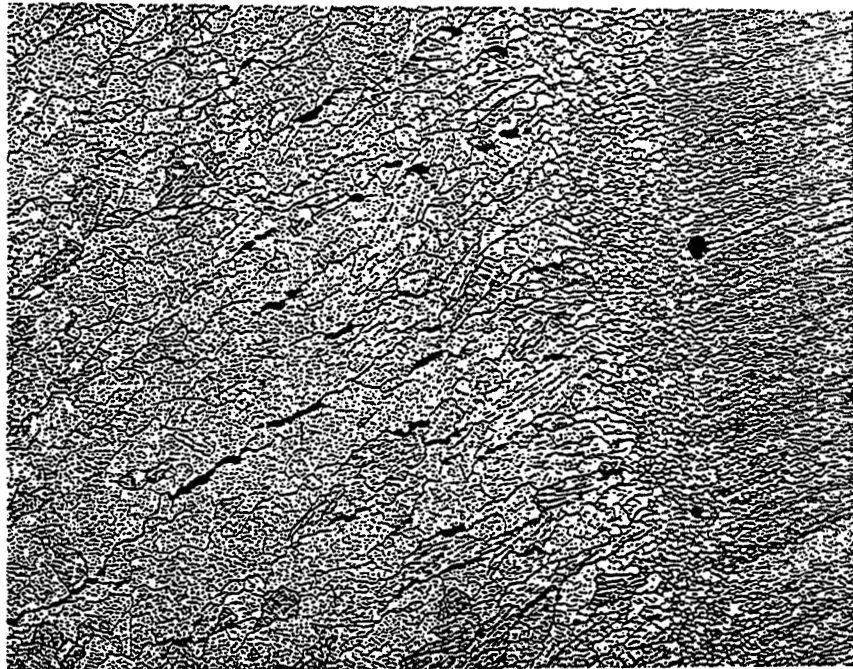(a) a fusion pass weld and (b) a fusion pass plus a heating (but
not melting) cover pass.

in Figure 2. Figure 2-a presents a microstructure similar to the as-welded materials. In contrast, the air-heated Al-Li alloy shows evidence of a dendritic or grain boundary reaction. See Figure 2-b. In addition to the solid state boundary reaction, an increases in the porosity was observed in the air-heated material.

Furthermore, 1.2 % nitrogen contamination of the helium shield gas of a weld pass was observed to generate a large amount of porosity while, in contrast, electron beam (EB) welds performed in vacuum or welds thermally treated in helium present a porosity similar to that of the parent metal. All these results support nitrogen as a cause of the porosity observed in welds in Al-Li Alloy.

Discussion

Chemical analysis of Al-Li alloy 2195 base and weld metal indicated hydrogen contamination at levels much higher than expected for Alloy 2219, which lacks lithium. It is conjectured that the hydrogen is present in the form of a lithium compound. When the welds are heated in air, nitrogen penetrates rapidly into the material along dendritic boundaries. Then it begins to diffuse into the solid metal. When it encounters a hydrogen-lithium compound, replaces and releases hydrogen as a gas. At elevated temperatures high gas pressure form porosity and promote cracking.

Conclusions and Recommendations

Initial results have led to the following tentative conclusions:

a) Reheating (e.g., by a cover pass) generates both round porosity and crack-like porosity observed in 2195 Al-Li Alloy welds.

b) A tentative model has been developed to predict and understand the porosity formation.

c) Additional work is necessary to verify the proposed model and the mechanical properties of the 2195 Al-Li welds. Microhardness tests at room temperature should be employed to characterize the mechanical properties of the different features observed in the microstructure, especially in the welding zone. Hot tensile tests should also be performed to evaluate the welding zone strength and the effect of the temperature variation on the integrity of the welding.

Acknowledgments

The authors are extremely grateful to Dr. J. Singh for helpful discussions and experimental assistance.

(a)
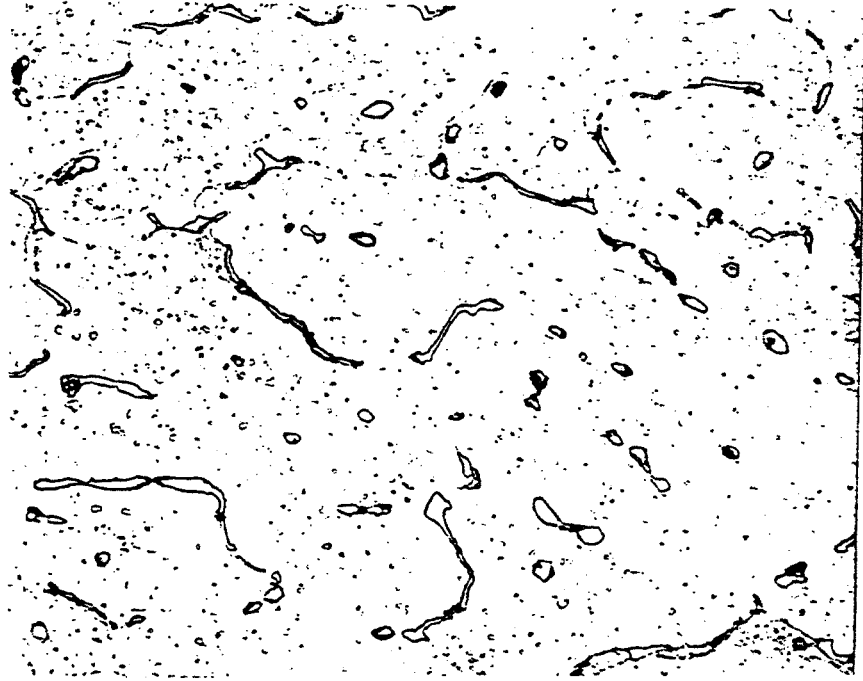
25 μm

(b)
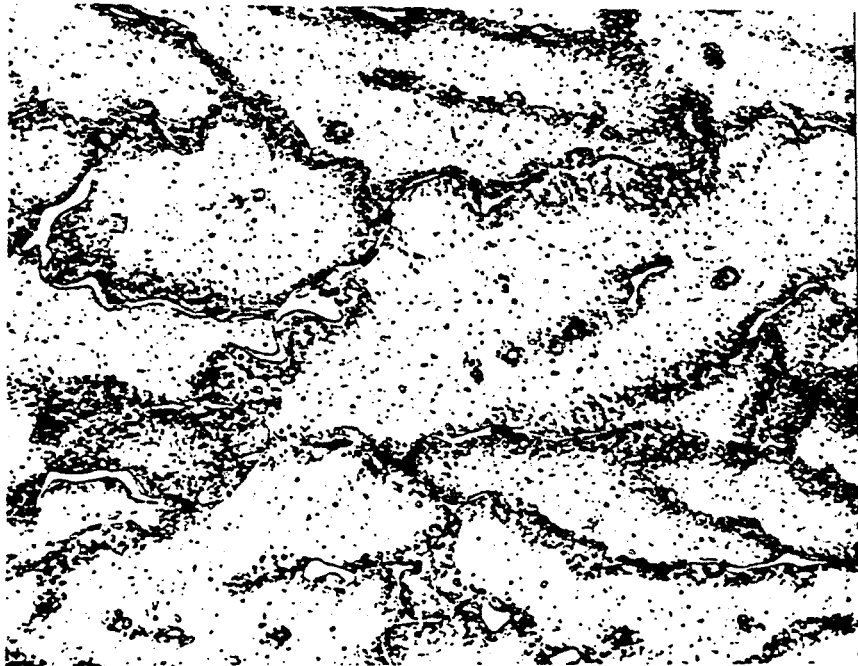
Figure 2.- Micrographs showing the effect of the heating at
450 C for a minute in vacuum (a) and in air (b).

1993

NASA/ASEE SUMMER FACULTY FELLOWSHIP PROGRAM

MARSHALL SPACE FLIGHT CENTER
THE UNIVERSITY OF ALABAMA

TORQUE EQUILIBRIUM ATTITUDES
FOR THE SPACE STATION

Prepared by:	Roger C. Thomspon, Ph.D.
Academic Rank:	Assistant Professor
Institution and Department:	The Pennsylvania State University Department of Aerospace Engineering
MSFC Colleague:	Connie Carrington, Ph.D.

NASA/MSFC:

Office:	Program Development
Division	Subsystems Design
Branch:	Guidance, Navigation, and Control

Introduction

All spacecraft orbiting in a low earth orbit (LEO) experience external torques due to environmental effects. Examples of these torques include those induced by aerodynamic, gravity-gradient, and solar forces. It is the gravity-gradient and aerodynamic torques that produce the greatest disturbances to the attitude of a spacecraft in LEO, and large asymmetric spacecraft, such as the space station, are affected to a greater degree because the magnitude of the torques will, in general, be larger in proportion to the moments of inertia. If left unchecked, these torques would cause the attitude of the space station to oscillate in a complex manner and the resulting motion would destroy the micro-gravity environment as well as prohibit the orbiter from docking. The application of control torques will maintain the proper attitude, but the controllers have limited momentum capacity. When any controller reaches its limit, propellant must then be used while the device is reset to a zero or negatively-biased momentum state. Consequently, the rate at which momentum is accumulated is a significant factor in the amount of propellant used and the frequency of resupply necessary to operate the station.

A torque profile in which the area under the curve for a positive torque is not equal to the area under the curve for a negative torque is "biased," and the consequent momentum build-up about that axis is defined as secular momentum because it continues to grow with time. Conversely, when the areas are equal, the momentum is cyclic and bounded. A Torque Equilibrium Attitude (TEA) is thus defined as an attitude at which the external torques "balance" each other as much as possible, and which will result in lower momentum growth in the controllers. Ideally, the positive and negative external moments experienced by a spacecraft at the TEA would exactly cancel each other out and small cyclic control torques would be required only for precise attitude control. Over time, the only momentum build-up in the controllers would be due to electro-mechanical losses within the device. However, the atmospheric torques are proportional to the density of the atmosphere and the density varies with the orbital position, time of day, time of year, and the solar cycle. In addition, there are unmodeled disturbances and uncertainties in the mass and inertias. Therefore, there is no constant attitude that will completely balance the environmental torques and the dynamic TEA cannot be solved in closed form. The objective of this research was to determine a method to calculate a dynamic TEA such that the rate of momentum build-up in the controllers would be minimized and to implement this method in the MATRIX$_X$ simulation software by Integrated Systems, Inc.

Description of Research

Previous methods for calculating TEAs have relied upon approximations of the atmospheric density and have assumed that the atmosphere was constant with respect to the orbital path of the spacecraft. The TEA calculation was reduced to a quasi-closed-form method in which the approximate torques were substituted into the equations of motion, and the resulting system was solved numerically. It was decided to research the possibility of determining dynamic TEAs for the space station while using accurate models of the atmosphere and including all six of the rigid-body degrees-of-freedom (DOF) in the numerical simulations.

A TEA is essentially the "optimal" attitude where the moments required of the controllers are zero-biased, and the research focused on formulating the optimization problem. Although

MATRIX$_X$ has an optimization module available, this feature was not included in the license of the Program Development Office. Consequently, minimization routines for single and multiple variables were adapted from Fortran codes collected by Press et al. (4). The appropriate algorithms were then translated into MATRIX$_X$ executable files.

To determine the feasibility of the optimization approach, a one DOF model was the first case to be tested. The inertia, aerodynamic moment, and gravity-gradient moment coefficients used in the model were taken from space station data so that the numerical results would be of the same order. The aerodynamic moment was given the form

$$M_{aero} = (\alpha - \varepsilon \sin \omega t) \theta \qquad [1]$$

to simulate the variable atmosphere. The equation of motion for this system is essentially Mathieu's equation (3) with a constant forcing function and has the form

$$I\ddot{\theta} + [(mgr - \alpha) + \varepsilon \sin \omega t] \theta = mgr\theta_0 \qquad [2]$$

where I is the inertia, $mgr\theta$ is the gravity-gradient moment, and θ_0 is the angle at which the gravity-gradient moment is zero. The cost function used in the optimization algorithm was

$$J = \left| \int M dt \right| \qquad [3]$$

where M is the sum of the environmental torques. This cost function allows the positive moments to cancel the negative moments, but returns a positive-definite value for all possible solutions.

Because this problem can be solved in closed form, the solution from the optimization algorithm could be compared to the analytical solution; the results were very good but also quite surprising. The TEA was successfully calculated with negligible error, but the unexpected result was in the torque profile. A very strong beat phenomenon was displayed where the low frequency component had a period of 20 orbits and the high frequency occurred at the orbital period. Further investigations indicated that the beat is very sensitive to the interaction between the forcing term (the gravity-gradient null position) and the amplitude of the time-varying component of the aerodynamic torques. The beat occurred only when the parameters had a certain proportional value and the range of the proportional constant at which the beat occurred was very small. However, this would seem to indicate that a given spacecraft configuration would exhibit this kind of motion at a certain atmospheric density and this subject will be investigated further.

The next test case was a three DOF model in which the attitude equations were implemented with the simplified gravity-gradient and aerodynamic torques. The environmental torques about each axis had different magnitudes and were completely independent of each other. The attitude dynamics, however, were coupled through Euler's Equations and the equations of motion governing the attitude of the spacecraft (1). With this model, the multi-variable optimization algorithm could be tested with the coupled, nonlinear attitude dynamics but without the complexity of the six DOF simulations. This system could not be solved in closed

form, but the attitude at which the torques about each axis are statically balanced could be determined and the TEA would be expected to be somewhere in the neighborhood of this attitude.

The cost function and the MATRIX$_x$ simulation for this system were substantially different from the simple form used in the previous case. The attitude of a spacecraft will vary as the spacecraft reacts to the external torques, but to maintain the micro-gravity environment, a fixed attitude (the TEA) is desired. Therefore, when the actual attitude and the fixed attitude coincide, no control torques are required even though the spacecraft is experiencing external torques at that attitude. When the actual attitude differs from the fixed attitude, the corresponding external torques will differ, and it is this difference that should be zero-biased. The simulation must therefore simultaneously integrate the motion of a spacecraft flying at a fixed attitude and a spacecraft allowed to react to the external moments. The moments are calculated for each spacecraft and the difference is the integrand of the cost function. The cost function is the magnitude of the vector resulting from the integration and is represented mathematically by

$$J = \sum_{i=1}^{3} \left| \int (M_{actual}^{(i)} - M_{fixed}^{(i)}) \, dt \right|$$ [4]

where the superscript indicates the ith element of the moment vector.

The optimization algorithm was able to find a TEA that drove the cost function to zero and this TEA was indeed very close to the static equilibrium attitude in the pitch and yaw axes, but differed significantly in the roll axis as shown in Table 1. Additional calculations proved that there was no other TEA in the neighborhood of the static equilibrium attitude and the large roll angle, necessary to obtain the zero-biased torques, was a consequence of the coupling between the axes. The beat phenomenon was again clearly displayed in the torque profiles.

Table 1: TEA for the 3 DOF model

Angles (rad)	Torques Balance Statically	TEA from optimization
Yaw	0.1048	0.0994
Pitch	0.1746	0.1761
Roll	0.0499	0.1899

The next stage of the research was to implement this method of calculating TEAs in the space station simulations. The procedure is essentially the same as that used in the three DOF example. The simulations were changed such that a fixed attitude model was integrated simultaneously with a free-flying model, but the simulations now included all six rigid-body degrees-of-freedom, an accurate atmospheric density model, and detailed atmospheric drag/moment calculations. The cost function remained exactly the same as used in the three DOF model. Examples of the Human Tended Configuration (HTC) and the International Human Tended Configuration (IHTC) were completed.

The results for both configurations were unexpected and were thought, at first, to be in error. Neither configuration had a TEA that resulted in zero-biased torques, and in both cases, the yaw torque was the only one that did not reduce to a zero bias. Additional calculations proved that the result returned from the optimization algorithm was indeed the minimum of the cost function. The explanation for this result is due to the coupling between the axes; an arbitrary body may have an equilibrium condition in which a biased torque about one axis is necessary to produce a zero-biased stable attitude about the other two. The yaw axis is the biased axis because the gravity-gradient torque about the yaw axis is extremely weak.

This type of behavior has been observed in previous studies (2) where yaw-biasing was necessary to provide a stable attitude. Previous attempts to determine the proper yaw bias were accomplished through trial and error methods. A yaw bias was chosen, the optimal attitude was determined for the roll and pitch axes, and the total momentum was calculated. The procedure was repeated for several different yaw angles and the momentum was plotted as a function of the yaw angle. The yaw bias was finally chosen at the point where the momentum was minimized. The calculation of TEAs using the method developed in this research seeks a solution in which the external torques are zero-biased. If such a solution does not exist, however, the optimization algorithm still seeks the minimum bias which in most cases will be the yaw biased attitude.

Conclusions

Calculating TEAs through minimizing the bias of the external torques was shown to be very promising. The method has distinct advantages over quasi-closed-form approaches used in the past because no assumptions about the mathematical behavior of the torques is required. The numerical simulations may contain any degree of complexity in the nonlinear dynamics and calculation of the external torques. The method is very robust, and with the proper optimization routine, can incorporate equality and inequality constraints. Finally, the method will find the zero-bias TEA if such a solution exists, or reduce to the yaw-biased solution. The method was tested on two simple models and several of the space station configurations with excellent result returned in all cases.

References

1. Hughes, Peter C., "Spacecraft Attitude Dynamics," John Wiley and Sons, New York, New York, 1986.
2. Kelly. J. J., "Optimum Yaw-Biasing for Arrow Mode," Memorandum A95-J845-M-9102083, 15 May 1991.
3. Pearson, Carl E., ed., "Handbook of Applied Mathematics, 2nd Ed.," Van Nostrand Reinhold Co., New York, New York, 1983, pp. 712-717.
4. Press, William H., Brian P. Flannery, Saul A. Teukolsky, and William T. Vetterling, "Numerical Recipes: The Art of Scientific Computing," Cambridge University Press, New York, New York, 1986, pp. 274-301.

1993

NASA/ASEE SUMMER FACULTY FELLOWSHIP PROGRAM

MARSHALL SPACE FLIGHT CENTER
THE UNIVERSITY OF ALABAMA IN HUNTSVILLE

PROPERTIES AND PROCESSING CHARACTERISTICS OF LOW DENSITY CARBON CLOTH PHENOLIC COMPOSITES

Prepared By:	C. JEFF WANG
Academic Rank:	Assistant Professor
Institution and Department:	Tuskegee University, AL, Chemical Engineering Department
MSFC Colleague:	Corky Clinton, Ph.D.
NASA/MSFC	
Office:	Materials and Processes Laboratory
Division:	Non-Metallic Materials
Branch:	Ceramics and Coatings

I. INTRODUCTION

Ply-lift and pocketing are two critical anomalies of carbon cloth phenolic composites (CCPC) in rocket nozzle applications [1]. Ply lift occurs at low temperatures when the A/P and in-plane permeabilities of the composite materials are still very low and in-plane porous paths are blocked. Pocketing occurs at elevated temperatures when in-plane permeability is reduced by the A/P compressive stress. The thermostructural response of CCPC in a rapid heating environment involves simultaneous heat, mass, and momentum transfers along with the degradation of phenolic resin in a multiphase system with temperature- and time-dependent material properties as well as dynamic processing conditions [2]. Three temperature regions represent the consequent chemical reactions, material transformations, and property transitions, and provide a quick qualitative method for characterizing the thermostructural behavior of a CCPC.

In order to optimize the FM5939 LDCCP (low density carbon cloth phenolic) for the nozzle performance required in the Advanced Solid Rocket Motor (ASRM) program, a fundamental study on LDCCP materials has been conducted [3]. The cured composite has a density of 1.0 ± 0.5 gm/cc which includes 10 to 25 % void volume. The weight percent of carbon microballoon is low (7-15 %). However, they account for approximately one third of the volume and historically their percentages have not been controlled very tightly. In addition, the composite properties show no correlation with microballoon weight % or fiber properties (e.g. fiber density or fiber moisture adsorption capacity. Test results concerning the ply-lift anomaly in the MNASA motor firings were [3]:
- Steeper ply angle (shorter path length) designs minimized/eliminated ply lifting
- Material with higher void volume ply lifted less frequently
- Materials with high (>9%) microballoon content had a higher rate of ply lifting
- LDCCP materials failed at microballoon-resin interfaces.

The objectives of this project are:
1. To investigate the effects of carbon microballoon and cabosil fillers as well as fiber heat treatment on plylift-related mechanical properties.
2. To develop a science-based thermostructural process model for the carbon phenolics. The model can be used in the future for the selection of the improved ASRM materials.
3. To develop the micro-failure mechanisms for the ply-lift initiation and propagation processes during the thermoelastic region of phenolic degradation, i.e. postcuring and devolatilization.

II. FILLER-RESIN INTERACTION AND FIBER HEAT TREATMENT

Six lots of LDCCP (Table 1) were fabricated by varying the fiber heat treatment condition, type of carbon microballoon, and the use of silica filler. Parameters governing the across-ply tensile properties, interlaminar shear strength, and plylift failure modes will be examined. The effects of the resin-filler interaction on gas permeability and thermal expansion behavior will also be investigated.

Table 1. Material Description

Prepreg Material	Fabric	Resin	Microballoon	Cabosil
FM5939 LDC 1722	BP CCA-8+	Ironsides 91LD	T	No
FM5939 LDC-X1 1723	BP CCA-8+	Ironsides 91LD	T	Yes
FM5055 LDC 1724	BP CCA-8	Ironsides 91LD	A	Yes
FM5055 LDC-X2 1725	BP CCA-8	Ironsides 91LD	T	Yes
FM5055 LDC-X3 1726	BP CCA-8	Ironsides 91LD	T	No
FM5939 LDC-X1 1727	BP CCA-8+	Ironsides 91LD	T	Yes

The FM5055 LDC material, fabricated with a carbon microballoon type A, is a "historical" LDCCP material, and FM5939 LDC, with a CCA-8+ carbon fabric and carbon microballoon type T, is under development for the ASRM program. The effects of microballoon type and the presence of cabosil on the specific gravity and volatile content are shown in Table 2.

Table 2. Composite density and volatile content, preliminary data

Prepreg material	Specific gravity[1]	Residual volatile, %[2]
FM 5939 LDC 1722	1.076	1.684
FM 5939 LDC X1 1723	1.071	1.850
FM 5939 LDC X1 1727	1.063	1.834
FM 5055 LDC 1724	1.034	2.405
FM 5055 LDC X2 1725	1.064	2.387
FM 5055 LDC X3 1726	1.073	2.260

1. - ASTM D 792: Standard Test Methods for Specific Gravity (Relative Density) and Density of Plastics by Displacement
2. - Thiokol Specification for RSRM, STW 5-2845E: Nozzle Reinforced Plastic Component Testing and Accepting Criteria

III. Polymer Degradation Model: An Initial Model Framework

Following the work published in wood pyrolysis [4], a one-dimensional material balance equation for the gases generated in the composite is given as:

$$\frac{\partial(\epsilon \rho z_g)}{\partial t} + \frac{\partial(\rho_g u)}{\partial x} = R_g \qquad (1)$$

where ρ_g = density of gas, u = superficial gas velocity, ϵ = porosity, and R_g = gas generation rate. Using Darcy's law for a porous medium, the momentum balance equation on gases permeation can be expressed as:

$$u + \frac{K}{\mu} \frac{\partial p}{\partial x} = 0 \qquad (2)$$

where K = permeability, μ = viscosity of gas. By defining an effective thermal conductivity, the energy balance equation on the solid phase is:

$$(1-\epsilon)\rho_s C_s \frac{\partial T}{\partial t} = \frac{\partial}{\partial x}[k^* \frac{\partial T}{\partial x}] - \rho_s u C_g \frac{\partial T}{\partial x} + h_R R_s \qquad (3)$$

where $k^* = (1-\epsilon)k_s + k_g$, C_s = heat capacity of solid, C_g = heat capacity of gas, h_R = heat of reaction, R_s = solid generation rate ($=-R_g$). In the material balance equation, the rate of polymer degradation is defined as:

$$R_s = -R_s = \frac{\partial}{\partial t}[(1-\epsilon)\rho] = \frac{\Delta M_R}{V} \frac{d\alpha}{dt} \qquad (4)$$

$$\frac{d\alpha}{dt} = \Sigma w_i \frac{d\alpha_i}{dt} \qquad (5)$$

where R_s = solid generation rate, w_i = weight fraction of volatile, pyrolysis gases, and carbon char, respectively, and α_i = degree of degradation for devolatilization, pyrolysis, and charring, respectively.

In the above equations, the material properties, e.g. thermal conductivity, heat capacity, and permeability, have to be estimated as functions of temperature, degree of degradation, and fiber or resin volume fraction. The rate of degree of degradation, $d\alpha/dt$, will be determined from the experimental data.

IV. Microscopic Analysis of Residual Thermal Stress in a Single Fiber-Matrix System

Efforts have been made to develop analytical tools for predicting stresses and internal pressure created when the composite is heated rapidly [1]. These models provide good insight into the thermal and mechanical responses of composites. However, the fracture mechanics of these models was based on macro-mechanics. In this section, a model framework for polymer thermal degradation and composite micro-mechanics will be presented.

Consider a single fiber embedded in a matrix, and the system is cooled by ΔT. Due to the differential thermal contraction a contact pressure, p, is developed at the fiber-matrix interface. The fiber is subjected to an external pressure, p, at r_f (radius of fiber) and resin is subjected to an internal pressure, p. Based on this thick cylinder model, the radial displacements and residual thermal stress can be calculated by the following equations [4].

$$u_f = \frac{(1-v_f)}{E_f} r_f P \qquad (6)$$

$$u_m = \frac{r_f P}{E_m} \left(\frac{r_f^2 + r_m^2}{r_m^2 - r_f^2} + v_m \right) \qquad (7)$$

where u_f, u_m are radial displacements of fiber and matrix, E_f, E_m are elastic modulus of fiber and matrix, r_m is the radius of matrix, and v_f, v_m are volume fraction of fiber and matrix. Compatibility at the fiber-matrix interface requires that

$$u_m - u_f = (\alpha_m - \alpha_f) r_f \Delta T \qquad (8)$$

Combining Eqs. (6)-(8), the residual thermal stress at the microscopic level is:

$$P/\Delta T = \frac{(\alpha_m - \alpha_f)}{\frac{1}{E_m} \left(\frac{r_f^2 + r_m^2}{r_m^2 - r_f^2} + v_m \right) + \frac{1-v_f}{E_f}} \qquad (9)$$

The typical values of E_m and α_m for phenolic resin are 5 GPa and $70 \times 10^{-6}/°C$, and E_f and α_f for medium-modulus carbon fibers are 270 GPa and $3.5 \times 10^{-6}/°C$, respectively. In the case of $v_f = 0.6$ and $r_f^2/r_m^2 = 0.6$, the value of $P/\Delta T$ in Eq. (9) will be equal to around 70 KPa/°C. When the phenolic composite is cooled from a curing temperature of 160°C to a room temperature of 25°C, the micro-level residual thermal stress is -9.4 MPa.

V. Acknowledgements

REFERENCES

1. R. M. Sullivan and N. J. Salamon, "A Finite Method for the Thermochemical Decomposition of Polymeric Materials - II. Carbon Phenolic Composites," Jnt. J. Engng Sci. 30, 939, 1992.
2. M. R. Tant and J. B. Henderson, "Thermochemical Expansion of Polymer Composites," Handbook of Ceramics and Composites, Vol. 1, Chap. 13, 1990.
3. A. Canfield, R. G. Clinton, S. Brown, and J. Koenig, "Fundamental Understanding of LDC Materials/Ply Lifting," JANNAF/RNTS Meeting, December 1992.
4. E. J. Kansa, H. E. Perlee, and R. F. Chaiken, "Mathematical Model of Wood Pyrolysis Including Internal Forced Convection," Combustion and Flame 29, 311 (1977).
5. L.-R. Hwang, "Processing-Structure-Property Relationships of Ceramic Fiber Reinforced Si-C-O Matrix Composites," Ph.D. Dissertation, Auburn University, AL, 1991.

1993

NASA/ASEE SUMMER FACULTY FELLOWSHIP PROGRAM

MARSHALL SPACE FLIGHT CENTER
THE UNIVERSITY OF ALABAMA IN HUNTSVILLE

Effects of Thermal-Solutal Convection on Temperature
and Solutal Fields under Various Gravitational Orientations

Prepared By: Jai-Ching Wang, Ph. D.

Academic Rank: Associate Professor

Institution and
Department: Alabama A&M University
                         Department of Physics

MSFC Colleague(s):   Sandor L. Lehoczky, Ph. D.
                         Dale Watring
                         Frank Szofran, Ph. D.

NASA/MSFC

        Office: Space Science Laboratory
        Division: Microgravity Science & Application Division/ES 71
        Branch: Electronic & Photonic Materials Branch/ES 75

Introduction

Semiconductor crystals such as $Hg_{1-x}Cd_xTe$ grown by unidirectional solidification Bridgmann method have shown compositional segregations in both the axial and radial directions (Lehoczky et. al..1980, 1981, 1983). Due to the wide separation between the liquidus and the solidus of its pseudobinary phase diagram (Lehoczky and Szofran 1981), there is a diffusion layer of higher HgTe content built up in the melt near the melt-solid interface which gives a solute concentration gradient in the axial direction. The value of effective diffusion coefficient calculated from fitting of the data to 1D model varies with $Hg_{1-x}Cd_xTe$ growth conditions (Szofran 1984).This indicates that the growth condition of the $Hg_{1-x}Cd_xTe$ is not purely diffusion controlled. Because of the higher thermal conductivity in the melt than that in the crystal in the growth system, there is a thermal leakage through the fused silica crucible wall near the melt-solid interface. This gives a thermal gradient in the radial direction. Hart (1971), Thorpe, Hutt and Soulsby (1969) have shown that under such condition a fluid will become convectively unstable as a result of different diffusivities of temperature and solute. It is quite important to understand the effects of this thermosolute convection on the compositional segregation in both axial and radial directions in the unidirectionally solidified crystals under various gravitational directions. To reach this goal, we start with a simplified problem to study the effects of thermal-solutal convection on the temperature and solutal fields under various gravitational orientations. We begin by reviewing model governing equations.

Governing Equations

In this study we adopt the Boussinesq approximation; The equation of state takes the form that density is constant except that in the presence of the gravitational field a buoyancy force exists due to density variations which is caused by the temperature variation and concentration variation in the melt.

Under the Boussinesq approximation and axial symmetric boundary conditions, the governing equations in cylindrical coordinates for incompressible fluid flow of the system are:

$$\frac{\partial u}{\partial t} + u\frac{\partial u}{\partial r} + \omega\frac{\partial u}{\partial z} = -\frac{1}{\rho}\frac{\partial p}{\partial r} + \upsilon\left(\frac{\partial^2 u}{\partial r^2} + \frac{1}{r}\frac{\partial u}{\partial r} + \frac{\partial^2 u}{\partial z^2} - \frac{u}{r^2}\right) \quad . \tag{1}$$

$$\frac{\partial \omega}{\partial t} + u\frac{\partial \omega}{\partial r} + \omega\frac{\partial \omega}{\partial z} = -\frac{1}{\rho}\frac{\partial p}{\partial z} + \upsilon\left(\frac{\partial^2\omega}{\partial r^2} + \frac{1}{r}\frac{\partial \omega}{\partial r} + \frac{\partial^2 \omega}{\partial z^2}\right)$$
$$+ g(\beta_T(T - T_0) + \beta_C(C - C_0)), \tag{2}$$

$$\frac{u}{r} + \frac{\partial u}{\partial r} + \frac{\partial \omega}{\partial z} = 0 \tag{3}$$

$$\frac{\partial T}{\partial t} + u\frac{\partial T}{\partial r} + \omega\frac{\partial T}{\partial z} = + \alpha_T\left(\frac{\partial^2 T}{\partial r^2} + \frac{1}{r}\frac{\partial T}{\partial r} + \frac{\partial^2 T}{\partial z^2}\right), \text{and} \tag{4}$$

$$\frac{\partial C}{\partial t} + u\frac{\partial C}{\partial r} + \omega\frac{\partial C}{\partial z} = \alpha_C\left(\frac{\partial^2 C}{\partial r^2} + \frac{1}{r}\frac{\partial C}{\partial r} + \frac{\partial^2 C}{\partial z^2}\right). \tag{5}$$

Scale the dimensional variable

The equations can be nondimensionalized by scaling the variables by a factor F; i. e $V = FV^*$. Scaling length by R_C, velocity by ν/R_C, time by R_C^2/ν, pressure by $\rho g \beta_T \Delta TR$, nondimensionalize temperature by setting $\Theta = \frac{T - T_m}{T_m}$ and nondimensionalize solute concentration by setting $\phi = \frac{C - C_0}{C_0}$. After the scaling and dropping all the *, the dimensionless equations become:

$$\left(\frac{\partial u}{\partial t} + u\frac{\partial u}{\partial r} + \omega\frac{\partial u}{\partial z}\right) = -\frac{\partial p}{\partial r} + \left(\frac{\partial^2 u}{\partial r^2} + \frac{1}{r}\frac{\partial u}{\partial r} + \frac{\partial^2 u}{\partial z^2} - \frac{u}{r^2}\right), \tag{6}$$

$$\left(\frac{\partial \omega}{\partial t} + u\frac{\partial \omega}{\partial r} + \omega\frac{\partial \omega}{\partial z}\right) = -\frac{\partial p}{\partial z} + \left(\frac{\partial^2 \omega}{\partial r^2} + \frac{1}{r}\frac{\partial \omega}{\partial r} + \frac{\partial^2 \omega}{\partial z^2}\right)$$

$$+ Gr_T^{1/2}\left(T + (Gr_C/Gr_T)C\right), \tag{7}$$

$$Pr\left(\frac{\partial T}{\partial t} + u\frac{\partial T}{\partial r} + \omega\frac{\partial T}{\partial z}\right) = K\left(\frac{\partial^2 T}{\partial r^2} + \frac{1}{r}\frac{\partial T}{\partial r} + \frac{\partial^2 T}{\partial z^2}\right), \text{ and } \quad K = \frac{K_i}{K_s}; \text{ i=melt, s=solid} \tag{8}$$

$$\frac{\partial C}{\partial t} + u\frac{\partial C}{\partial r} + \omega\frac{\partial C}{\partial z} = \frac{1}{S_c}\left(\frac{\partial^2 C}{\partial r^2} + \frac{1}{r}\frac{\partial C}{\partial r} + \frac{\partial^2 C}{\partial z^2}\right) \tag{9}$$

Where the thermal and solutal Grashof numbers respectively , Gr_T, Gr_C are defined by:

$$Gr_T = \frac{g\beta_T\Delta TR^3}{\nu^2} \quad \text{and} \quad Gr_C = \frac{g\beta_C\Delta CR^3}{\nu^2}. \tag{10}$$

The Prandtl number, Pr, and Schmidt number, Sc, are defined by:

$$S_C = \nu/\alpha_C \quad \text{and} \quad P_r = \nu/\alpha_T. \tag{11}$$

Compare the nondimensionalized equations with the FIDAP equations, we use the following inputs to the FIDAP for strongly coupled equations

Quantity	Setting		Values used
Density	1		1
Viscosity	1		1
Specific Heat, C_p	P_r	$P_r = \nu/\alpha$	0.233
Conductivity	K_i/K_s or 1		2
Capacity, C_{ps}	1		1
Diffusivity, D	$1/S_c$	$S_c = \nu/D$	0.0143
Thermal Volume Expansion, β_T	G_{rT}	$G_{rT} = g\beta_T \Delta T\, R_c^3/\nu^2$	
Solutal Volume Expansion, β_s	G_{rs}	$G_{rs} = g\beta_s \Delta C\, R_c^3/\nu^2$	

These governing equations show that the flow characteristic are determined uniquely by G_{rT}, G_{rc}, P_r and Sc. These equations have been solved by the FIDAP program developed by Fluid Dynamics International, Inc. The boundary conditions on the velocity field are no slip at all walls. The boundary conditions on the solute field are constant at the top of the melt and satisfy segregation condition at the growth interface.

Conclusions

Preliminary simulation results for the input values listed above and $G_{rC} = 0$ with $G_{rT} = 0$ reveal that CdTe compositional profile under 1D diffusion controlled growth condition agree well with the result obtained by Han et. al. (Han et. al. 1992). Fixed grid simulation for $G_{rC} = 0$ with $G_{rT} = 10^4$ has also been obtained. Results indicated that CdTe concentration profiles has been effected by convection due to horizontal thermal gradients.(Figs 2). Although a great effort has been applied, the steady state simulations for the effects of concentration profiles under deformed grids has never been converged. The planed studies will be continued by doing transient simulations.
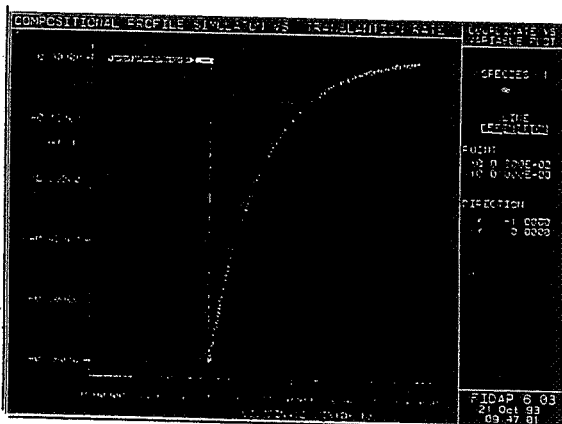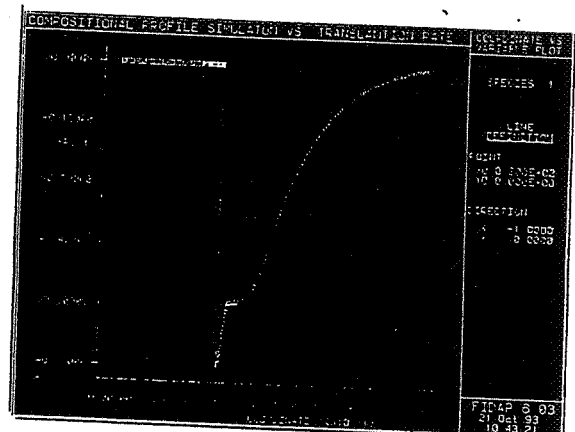

Fig.1. $G_{rC} = 0$, $G_{rT} = 0$.

Fig.2 $G_{rC} = 0$, $G_{rT} = 10^4$

Acknowledgment

I would like to express my sincere appreciation to the NASA/ASEE Summer Faculty Fellowship Program Administrators Drs. Gerald Karr and Frank Six for providing me the opportunity to participate in this program. The seminars and the Education Retreat are very helpful. Special thanks go to my NASA counterparts Dr. Sandor L. Lehoczky, Mr. Dale Watring and Dr. Frank Szofran for their suggestions and guidance and technical consultations on the use of the FIDAP program. I would also like to extend my sincere appreciation to Dr. Ching-Hua Su for his valuable discussions. The hospitality and friendships of all the members in the Electronic & Photonic Materials Branch has made this summer very enjoyable for me.

REFERENCES

1. Han J. C.,S. Motakef and P. Becla, "Residual Convection During Directional Solidification of II-VI Pseudo-Binary Semiconductors." in 30th Aerospace Sciences Meeting & Exhibit, Jan. 6-9, 1992, Reno, NV.
2. KIm D. H. and R. A. Brown, "Models for convection and Segregation in the Growth of HgCdTe by the Vertical Bridgman Method," J. Crystal Growth, 96 (1989) 609-627
3. Lehoczky, S. L. and F. R. Szofran, "Directional Solidification and Characterization of $Hg_{1-x}Cd_xTe$ Alloys", in Materials Research Society Symposium Proceeding--Material Processing in the Reduced Gravity Environment of Space, ed., Guy E. Rindone (Elsevier, New York), 409 (1983).
4. Lehoczky, S. L. and F. R. Szofran, "Advanced Methods for preparation and Characterization of Infrared Detector Materials", NASA report, NAS8-33107 (September 1981).
5. Lehoczky, S. L., F. R. Szofran, and B. G. Martin, "Advanced Methods for preparation and Characterization of Infrared Detector Materials", NASA report, NAS8-33107.(July 1980).
6. Hart, J.E., "On sideways diffusive instability",J. Fluid Mech. 49 (1971), pp 279-298.
7. Thorpe, S.A.,P.K. Hutt and R.Soulsby, J.Fluid Mech.38 (1969),375-400.
8. Szofran F. R. , D Chandra, J. C. Wang, E. K. Cothran and S. L. Lehoczky, "Effect of Growth Parameters on Compositional Variations in Directional Solidified HgCdTe Alloys", J. Crystal Growth 70 (1984) pp343-348.

1993

NASA/ASEE SUMMER FACULTY FELLOWSHIP PROGRAM

MARSHALL SPACE FLIGHT CENTER
THE UNIVERSITY OF ALABAMA IN HUNTSVILLE

USING NEURAL NETWORKS TO ASSIST IN OPAD DATA ANALYSIS

Prepared By: Kevin W. Whitaker, Ph.D.

Academic Rank: Assistant Professor

Institution and Department: The University of Alabama
                                       Department of Aerospace Engineering

MSFC Colleagues: W. T. Powers
                                     Anita E. Cooper

NASA/MSFC:

        Laboratory: Astrionics
           Division: Instrumentation and Control
             Branch: Instrumentation

INTRODUCTION

Plume emission spectroscopy can be applied to rocket engine testing by treating the engine plume as a precisely-controlled laboratory flame for chemical analysis. Test stand or remotely-mounted telescopes can collect engine plume emissions and direct the light, via a grating spectrometer system, onto a linear array of silicon photodetectors. In a quantitative manner, light from many wavelengths of interest can be compared to identify elements, ratioed to recognize alloys, or monitored as a function of time to establish trends and the onset of significant material erosion.

The space shuttle main engine (SSME) became the subject of plume emission spectroscopy in 1986 when researchers from NASA-Marshall Space Flight Center (MSFC), Arnold Engineering Development Center (AEDC), and Rocketdyne went to the SSME test stands at the NASA-Stennis Space Center and at Rocketdyne's Santa Susana Field Laboratory to optically observe the plume. Since then, plume spectral acquisitions have recorded many nominal tests and the qualitative spectral features of the SSME plume are now well established. Significant discoveries made with both wide-band and narrow-band plume emission spectroscopy systems led MSFC to promote the Optical Plume Anomaly Detection (OPAD) program with a goal of instrumenting all SSME test stands with customized spectrometer systems.

A prototype OPAD system is now installed on the SSME Technology Test Bed (TTB) at MSFC. The OPAD system instrumentation consists of a broad-band, optical multiple-channel analyzer (OMA) and a narrow-band device called a polychrometer. The OMA is a high-resolution (1.5-2.0 Angstroms) "super-spectrometer" covering the near-ultraviolet to near-infrared waveband (2800-7400 Angstroms), providing two scans per second. The polychrometer consists of sixteen narrow-band radiometers: fourteen monitoring discrete wavelengths of health and condition monitoring elements and two dedicated to monitoring background emissions. All sixteen channels are capable of providing 500 samples per second. To date, the prototype OPAD system has been used during 43 SSME firings on the TTB, collecting well over 250 megabytes of plume spectral data.

One goal of OPAD data analysis is to determine how much of an element is present in the SSME plume. Currently these element concentrations are determined iteratively with the help of a computer code, SPECTRA4, developed at AEDC. Experience has shown that iteration with SPECTRA4 is an incredibly labor intensive task and not one to be performed by hand. What is really needed is the "inverse" of SPECTRA4 but the mathematical model for this inverse mapping is tenuous at best. However, the robustness of SPECTRA4 run in the "forward" direction means that accurate input/output mappings can be obtained. If the mappings were inverted (*i.e.*, *input* becomes *output* and *output* becomes *input*) then an "inverse" of SPECTRA4 would be at hand but the "model" would be specific to the data utilized and would in no way be general. Building a generalized model based upon known input/output mappings while ignoring the details of the governing physical model is possible through the use of a neural network.

The research investigation described in this report involves the development of a neural network to provide a generalized "inverse" of SPECTRA4. The objectives of the research were to design an appropriate neural network architecture, train the network, and then evaluate its performance.

NEURAL NETWORK MODEL OF SPECTRA4

The computer code SPECTRA4 generates spectra (intensity versus wavelength plots) based on concentrations of fourteen elements in the SSME plume. The goal of the current research project was to quickly and accurately predict these concentrations from a given spectrum using a neural network. To that end, an optimally connected neural network architecture was selected for study because of its fast training and subsequent execution speed. In contrast, a traditional neural network is usually fully-connected, requiring more training and slightly longer execution times. Also, by locating and removing all redundant connections, the resulting optimally connected network will be more robust and efficient.

SPECTRA4 generates spectra for wavelengths ranging from 3092 Å to 7000 Å for a given set of element concentrations. These concentrations are values ranging anywhere from 0.01 ppm to 100 ppm. Past experience with OPAD data analysis has revealed that the region of primary interest in any spectrum lies in the wavelength band of 3300 Å to 4330 Å. In order to discretize a spectrum, this region was broken into 42 subintervals of 25 Å each. The maximum intensity in each of these subintervals was then used as a neural network input, resulting in a network with 42 input neurons. The corresponding element concentrations which produced the spectrum in question were used as desired outputs, dictating a network with 14 output neurons. With the number of input and output neurons specified, the network was then trained for varying numbers of hidden neurons.

The design and training of an optimally connected neural network consists of two distinct phases. In the first phase, all connections between neurons in the network are fully established. Random numbers are assigned as interconnection weights. Then a genetic algorithm[1] optimizes the connections, de-linking all those found to be unnecessary. In the second phase, backpropagation of error is used to adjust the remaining weights. Backpropagation is a supervised mode of learning wherein the partial derivatives of the error with respect to the weights are used to adjust the weights until a minimum error is reached.[2] Once training is completed, the neural network with optimized connections and weights can be used to predict element concentrations given intensity versus wavelength information.

RESULTS

Once a neural network was trained, it was tested against randomly generated spectra. Typical results for a network with 60 hidden neurons and a training sample consisting of 50 data sets can be seen in Figure 1. The prediction error for some elements is very small while for others it is quite large. This suggests that the error criteria or the discretization of the spectra during training were not correct. However, it does appear that an optimally connected network is capable of modeling the "inverse" of SPECTRA4.

A study was also carried out to determine how the number of hidden neurons in a network affects the prediction error. Three networks with 30, 60 and 90 hidden neurons were considered. The total prediction error dependence upon the number of hidden neurons is presented in Figure 2. What is readily apparent is that blindly increasing the number of hidden neurons in a network does not guarantee increased prediction accuracy. This suggests that after a point the network is memorizing patterns rather that learning the relationships between them. An optimum number of neurons exists and must be determined.

SPECTRA4 SENSITIVITY STUDY

Another aspect of the current investigation was the sensitivity of the SPECTRA4 code. Since the concentrations of all the fourteen elements could vary between 0.01 ppm and 100 ppm, network training became extremely time-consuming. Also, the mapping space was found to be very large and noisy. In order to address these concerns, a sensitivity study of SPECTRA4 was initiated. To obtain a robust neural network, training data must be chosen from those regions of the mapping space for which the concentrations of elements are most sensitive.

Some preliminary results from the sensitivity study currently underway are available. They show that perturbing the concentrations of elements such as copper, sodium, lithium or magnesium do not cause any change in the values of the intensity peaks of all the subintervals in a discretized spectrum. Other elements, such as calcium, manganese, silver or aluminum cause a change in only a few subintervals. Elements such as iron, molybdenum, cobalt and nickel were found to be extremely sensitive as they cause a change in the intensity peaks of almost all intervals. These preliminary results are very interesting but more study is required to substantiate them.

CLOSING REMARKS

Optimally connected neural networks have been developed to grossly model the "inverse" of SPECTRA4. They will certainly aid in the analysis of OPAD data by eliminating some of the time-consuming iteration currently utilized. However, in order for the networks developed to be useful, the prediction error must be reduced for all elements and the robustness of the network demonstrated. These aspects are currently under study.

REFERENCES

1. Goldberg, D. E., *Genetic Algorithms in Search, Optimization, and Machine Learning,* Addison-Wesley Publishing Co., Inc., 1989.

2. Werbos, P., "Beyond Regression: New Tools for Prediction and Analysis in the Behavioral Sciences," Ph.D. Dissertation, Committee on Applied Mathematics, Harvard University, Nov. 1974.
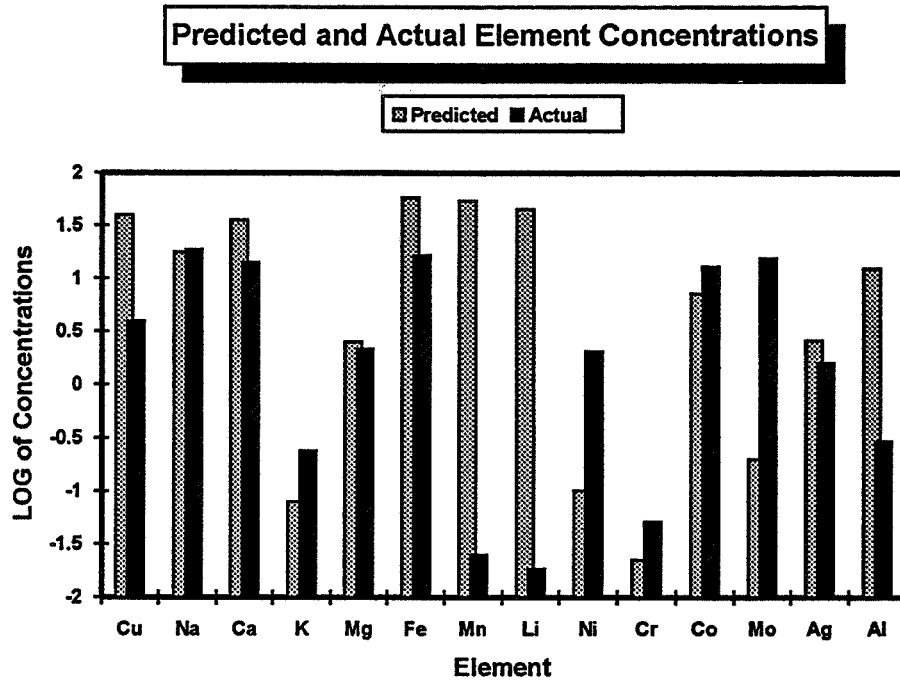
Figure 1. A comparison of predicted and actual element concentrations for a network with 60 hidden neurons
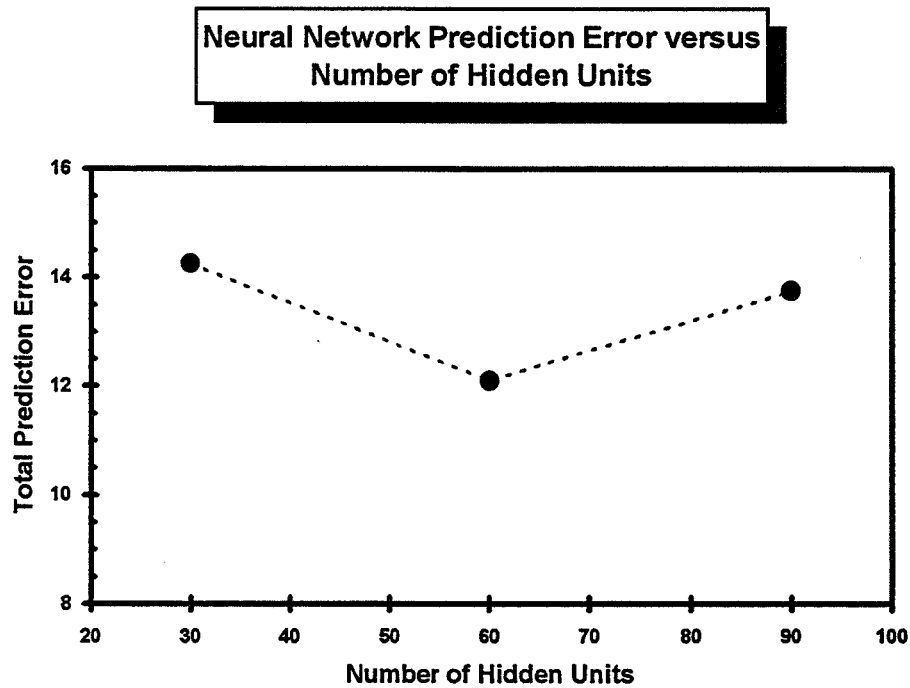
Figure 2.   Relationship between prediction error and number of hidden neurons

1993

NASA/ASEE SUMMER FACULTY FELLOWSHIP PROGRAM

THE FAR ULTRAVIOLET (FUV) AURORAL IMAGER FOR THE INNER MAGNETOSPHERIC IMAGER (IMI) MISSION: OPTIONS

Prepared By: Gordon R. Wilson, Ph.D.

Academic Rank: Assistant Research Professor

Institution and   The University of Alabama in Huntsville
  Department: Department of Physics, and
                             Center for Space Plasma and Aeronomic Research

MSFC Colleagues: Les Johnson
                             Dennis Gallagher, Ph.D.

NASA/MSFC:

  Office: Program Development
  Division: Payload & Orbital Systems
  Branch: SP Science and Applications

Introduction

The change from an intermediate class mission (cost ceiling of $300 million) to a solar-terrestrial probe class mission (cost ceiling of $150 million) will require some major changes in the configuration of the IMI mission. One option being considered is to move to a small spin-stabilized spacecraft (with no despun platform) which could be launched with a smaller Taurus or Conestoga class booster. Such a change in spacecraft type would not present any fundamental problems (other than restrictions on mass and power) for the He$^+$ 304 Å plasmasphere imager, the high and low energy neutral atom imagers, and the geocoronal imager, but would present a challenge for the FUV auroral imager since the original plan called for this instrument to operate from a despun platform. Since the FUV instrument is part of the core payload it cannot be dropped from the instrument complement without jeopardizing the science goals of the mission. A way must be found to keep this instrument and to allow it to accomplish most, if not all, of its science objectives. One of the subjects discussed here are options for building an FUV instrument for a spinning spacecraft. Since a number of spinning spacecraft have carried auroral imagers, a range of techniques exists. In addition, the option of flying the FUV imager on a separate micro-satellite launched with the main IMI spacecraft or with a separate pegasus launch, has been considered and will be discussed here.

Instrument Requirements

In order to accomplish its mission, and be at least current with the state of the art in auroral imaging, the FUV auroral imager will need to have the following characteristics (as identified by the science working group for the original baseline design):

1. A large field-of-view of 30° × 30°.
2. A small angular resolution of 0.03° × 0.03°.
3. Ability to obtain separate images of the auroral oval at 1304 Å, 1356 Å and in the LBH band (1200–1800 Å).
4. High time resolution; image repetition rate of one minute or less.

Despinning the Image

If the FUV imager is carried on a spinning spacecraft then one task it must perform is the despinning of the image. Several auroral imaging instruments have flown on spinning spacecraft in the past which have performed the despinning task in three different ways. These include (1) the Scanning Auroral Imager (SAI) which flew on the DE 1 spacecraft[3]. This instrument used the spacecraft's rotation to scan a small instantaneous field-of-view (0.32°) across the sky in one dimension. Scanning in the perpendicular direction was accomplished by a movable mirror. This technique gave long image construction times (12 min) and short image exposure times (4 ms). (2) The second technique was used on the V5 instrument flown on the Swedish Viking satellite. This instrument had a large instantaneous field-of-view (20° × 25°) through which the image would sweep each spacecraft rotation[1]. To compensate for rotation the accumulated charge in the CCD rows were stepped across the detector at the same rate the image swept across the field-of-view[6]. With this system an image was obtained each spacecraft rotation (20 s) with an exposure time of 1.2 s. (3) The third technique was used by the ATV instrument flown on the Japanese satellite EXOS-D (Akebono). This instrument used a despun mirror, which spun opposite to the direction the spacecraft was spinning, to compensate for image motion[7].

Telescopes

One way to get the large total field-of-view that the FUV instrument will need is to build it up from successive scans as was done by the SAI instrument which flew on DE 1. The alternative is to use an optical system with a large instantaneous field-of-view. There exists a number of space flown (or soon to be flown) telescope designs which have large instantaneous fields-of-views. These include: (1) the VIKING V5 Instrument[1] which is an inverse Cassegrain, Burch-type with a field-of-view of 20° × 25°, a focal length of 22.4 mm (f/1) and an angular resolution of 0.077° × 0.077°; (2) the NUVIEWS Astronomical Instrument[2,10] which is a three mirror anastigmat (TMA) off axis imager with a 20° × 40° field-of-view, a focal length of 90 mm (f/3) and an angular resolution of 0.058°; and (3) the POLAR VIS Earth Camera[1] which is also a three mirror anastigmat (TMA) off-axis system with a 20° × 20° field-of-view with an angular resolution of 0.08°.

Among this list the NUVIEWS telescope comes closest to meeting the requirements for the FUV instrument. As originally designed the NUVIEWS instrument had a 40° × 40° field-of-view. Down sizing to a telescope with a 30° × 30° field-of-view would not present a problem. It would have the added benefit of increasing the angular resolution (to less than 0.058°) and reducing various aberrations (spherical, coma, astigmatism) which affect image quality and resolution.

Filtering The Image

All instruments designed to image the aurora in the VUV have had to filter the incoming light so as to remove scattered sunlight in the visible and near ultraviolet. The SAI instrument on DE 1, the V5 instrument on VIKING, the ATV instrument on EXOS-D, and the VIS Earth Camera on POLAR all use fairly broadband (150–500 Å FWHM) filters which would be inadequate for the FUV instrument on IMI. The filtering system to be used on the POLAR UVI instrument was designed for spectral resolution close to the IMI requirements. It is based on the use of specifically designed multilayer reflection and transmission filters[9]. Each of the five filters is a small optical system with three flat mirrors and a transmission filter. The band widths of the five filters are: 1304 – 30 Å, 1356 – 50 Å, LBHs – 80 Å, LBHl – 90 Å, and Solar Spectrum – 100 Å [8]. The FUVIM instrument proposed for the IMAP small explorer[5] would use a diffraction grating, in place of transmission filters, to spectrally separate the incoming light. Since FUVIM will be a line scanning instrument it will be an imaging diffractometer. The position of the diffraction grating (moved by a stepper motor) will determine which part of the spectrum, from the imaged slit, falls on the detector. With the characteristics of the diffraction grating (3600 lines/mm, blaze angle of 13.5°), the internal geometry of the instrument, and the size of the detector, FUVIM will have a FWHM passband of 34 Å at any desired wavelength.

Detectors

Imagers which do single pixel or line imaging (such as the SAI instrument on DE 1) can use simple detectors that do not require special cooling. Imagers which do instantaneous two-dimensional imaging require more sophisticated detectors. There are two basic types which can be used. One involves an image intensifier coupled to a charge coupled device (CCD) and the other involves a microchannel plate (mcp) connected to a position sensitive anode. The CCD based detector is the detector of choice because the mcp/anode detector is a single event detector. That is it counts one photon at a time and while the anode electronics is reading out the results of one photon event it cannot see another which might arrive in the mean time. The total number of counts per second which such a detector can see before performance is degraded depends then on the speed of the anode readout electronics. Current performance for these detectors is low enough so that will be saturated by auroral VUV light intensities. CCD detectors do not have this problem since each pixel in the array can count photons independent of whether the other pixels are also currently counting photons.

Instrument Sensitivity

One of the most important criteria for measuring an imaging instrument's performance is its sensitivity S. S can be expressed thus: $S = (F/4\pi)Ar^n F_r \Omega_p T_g Q_c C_m T_e$ where F is the flux of photons (photons/cm^2/s), 4π is the number of steradians in a full sphere, A is the aperture area of the imager, r is the reflectivity of the mirrors in the optical system, n is the number of such mirrors, F_r is the filter response, Ω_p is the solid angle of the pixel, T_g is the transmission of the detector's glass window, Q_c is the quantum efficiency of the photocathode material, C_m is the collection efficiency of the microchannel plate, and T_e is the exposure time. The units of S are counts/kR/pixel/Ip where kR is kiloRayleighs and Ip is the integration period. S will depend on the wavelength of the photons since r, F_r, T_g, and Q_c are all wavelength dependent. As an example of the use of this equation the SAI derived instrument planned for the MARIE mission had the following values for each factor (at 1304 Å): $A = 20.3$ cm^2, $r = 0.95$, $n = 4$, $F_r = 0.3$, $\Omega_p = 1.9 \times 10^{-5}$ st, $T_g = 0.95$, $Q_c = 0.13$ electrons/photon, $C_m = 0.85$, and $T_e = 0.004$ s. With a flux of 1 kiloRayleigh ($F = 10^9$ photons/cm^2/s) $S = 3.2$ counts/kR/pixel/Ip. This sensitivity is small enough that some of the weaker, but important, signals would not be seen by this instrument. The main thing that can be done to increase S is to increase the exposure time T_e but this value can't be larger than the desired time resolution. Another thing that can be done is to increase Ω_p but this action degrades the angular resolution of the instrument which is undesirable. Achieving high sensitivity is always a trade-off with achieving small angular and temporal resolution.

Possible Configurations for an FUV Auroral Imager

Option 1. The first option for the IMI FUV auroral imager would be to use the Far UltraViolet Imaging Monochromator (FUVIM) as proposed for the IMAP small explorer, as it is. Advantages of using the FUVIM instrument are: (1) it is small, has a low mass, small power need, and low data rate; (2) the design has over twenty years of flight heritage; (3) the FUVIM uses detectors which do not require special cooling; (4) FUVIM can also perform the task of geocoronal imaging; and (5) it does not place extreme requirements on the spin axis stability of the spacecraft. Disadvantages of this option include: (1) the angular resolution is not very small being $0.25° \times 0.25°$; and (2) it may lack the sensitivity to produce images with statistically significant count levels for the 1356 Å and LBH images.

Option 2. For the second option one could use four or five VIKING V5 cameras where each camera is optimized for a desired wavelength. The transmission filter at the front entrance and the reflection filter coatings applied to the two mirrors in each camera would be designed after the Zukic method[9]. During one minute of elapsed time images of the aurora at each of four or five passbands (1216 Å, 1304 Å, 1356 Å, 1400-1600 Å, and 1600-1800 Å) could be obtained with an exposure time of 4 s (assuming an instrument field-of-view of $25° \times 25°$). For the weaker features longer exposure times could be used without sacrificing one minute, or shorter, time resolution for the stronger features. Estimates of the sensitivity of each camera using a CsI photocathode and the angular resolution of the V5 instrument give values of 150 (1304 Å), 274 (1356 Å), 223 (1500 Å), and 100 (1700 Å) counts/kR/pixel/Ip. There also appears to sufficient out of band rejection to separate these four features from hydrogen Lyman-α although the 1356 Å feature will be partially contaminated by 1304 Å radiation.

Advantages of this approach include: (1) small total instrument mass ≤ 20 kg; (2) the basic camera design has about 4–5 years of flight heritage; (3) the instrument could perform the task of geocoronal imaging; (4) This instrument could obtain all of the separate auroral images, at different wavelengths, simultaneously; and (5) image motion is compensated for by electronic scanning, eliminating the need for moving mirrors. Disadvantages of this option include: (1) the angular resolution ($0.076° \times 0.076°$) is larger then the IMI requirements; (2) the original V5 camera design had problems with stray light which may persist; (3) using the full temporal and spectral resolution which this instrument concept could provide would require a fairly large data rate; (4) additional cooling for the detectors would be needed; and (5) the spacecraft spin axis would be required to remain stable to about $0.08°$/min.

Option 3. For this option one could use a single imaging head with an optical system based on the NUVIEWS telescope modified to have a $30° \times 30°$ field-of-view, with an angular resolution of $0.03° \times 0.03°$ (or as close to that as possible). The instrument would stair out the side of the IMI spacecraft (perpendicular to the spacecraft's spin axis) and use electronic sweeping of the CCD array to provide longer integration times of about 5 s in a one minute period. The filter system would be that designed for the POLAR UVI instrument with the possible inclusion of a filter designed for hydrogen Lyman-α at 1216 Å. In operation this camera could sum images gained in successive revolutions until the one minute period was reached or sufficient counts had been obtained. The detector would be an image intensifier/CCD combination using a large format CCD array (1000×1000 pixels). Estimates of the sensitivity of such an instrument, based on the POLAR UVI sensitivities scaled for the shorter integration time, are: 27 (1304 Å), 46 (1356 Å), 76 (1500 Å), and 24 (1700 Å) counts/kR/pixel/Ip.

Advantages of this approach include: (1) small total instrument mass ~ 22 kg; (2) this instrument could perform the task of geocoronal imaging; and (3) image motion is compensated for by electronic scanning, eliminating the need for moving mirrors. Disadvantages of this option include: (1) the angular resolution may not reach the IMI goal (it would at least be $0.05° \times 0.05°$); (2) the design may not have sufficient sensitivity; (3) the CCD detectors would need to be cooled to at least $-55°$ C; and (4) a stable spacecraft spin axis is required ($0.05°$/min).

Option 4. In this design one could use the imager described in option 3 above, but instead of seating the instrument so that it looked out the side of the spacecraft perpendicular to the spin axis, it is positioned so that it looks out one end of the spacecraft parallel to the spin axis and into a despun mirror tilted at 45° to stair continuously at the earth. This would allow much longer integration times, and increase the instrument sensitivity. Estimates of such sensitivities, based on the POLAR UVI values with a 30 s integration time are: 163 (1304 Å), 277 (1356 Å), 456 (1500 Å), and 144

(1700 Å) counts/kR/pixel/Ip. (These sensitivities assume a 0.03° × 0.03° angular resolution, an aperture size, mirror reflectivity, filter response and detector response of the POLAR UVI instrument.) These sensitivities would allow the possibility of achieving the IMI goals of angular resolution and temporal resolution for the FUV instrument.

Disadvantages of this option include: (1) the angular resolution may not reach the IMI goal (it would at least be 0.05° × 0.05°); (2) the despun mirror would add complexity and cost to the instrument design, (3) the design would not allow the possibility of geocoronal imaging; (4) the CCD detectors would need to be cooled to at least −55° C; and (5) a stable spacecraft spin axis would be required (0.08°/min).

Option 5. This last option would take the instrument from option 3 and place it on a nadir viewing three-axis stabilized micro-satellite. This approach would provide the high sensitivities of option 4 without the need for the complexity of a despun mirror. There would also be no need for electronic scanning of the image for motion compensation. It may also eliminate some of the pressure on the resources of the spinning satellite portion of IMI. The added complexity of a second spacecraft would have to be evaluated carefully to see if it was worth these potential gains.

Advantages of this approach include: (1) much higher sensitivities would be possible, comparable to those in option 4; and (2) the instrument would be simpler, since it would not need a despun mirror. Disadvantages of this option include: (1) the angular resolution may not reach the IMI goal (it would at least be 0.05° × 0.05°); (2) the micro-sat might not be able to provide the pointing stability, accuracy or knowledge without excessive cost; (3) adding a second spacecraft would add to the overall management and operations cost of the mission; and (4) the CCD detectors would need to be cooled to at least −55° C.

From this list of options one can conclude that an FUV like instrument can be carried on a small spinning spacecraft. Options 4 and 5 illustrate ways that such an instrument could meet, or come close to meeting the IMI requirements. If option 4 or 5 is ruled out because of cost or some other factor then fall back positions exist which are still fairly attractive. They would however, require the sacrifice of some of the original goals for the IMI FUV instrument.

References

1. Anger, C. D., et al., An ultraviolet imager for the Viking spacecraft, *Geophys. Res. Lett.*, 14 (1987) 387–391.
2. Fleischman, J. R., C. Martin, and P. G. Friedman, Rocket survey instrument to map diffuse C IV, H_2 fluorescence, and far UV continuum in the galaxy, *Bull. Am. Astron. Soc.*, 24, (1992) 1281.
3. Frank, L. A., Craven, J. D., Ackerson, K. L., English, M. R., Eather, R. H., and Carovillano, R. L., Global auroral imaging instrumentation for the dynamics explorer mission, *Space Sci. Instr.*, 5, (1981) 369–393.
4. Frank, L. A., J. B. Sigwarth, R. L. Brechwald, S. M. Cash, T. L. Clausen, J. D. Craven, J. P. Cravens, J. S. Dolan, M. R. Dvorsky, J. D. Harvey, P. K. Hardebeck, D. W. Muller, H. R. Peltz, and P. S. Reilly, The visible imaging instrument for the POLAR spacecraft, *GGS PI Instrument Manuel*, (1992).
5. Frank, L. A., D. J. Williams, and E. C. Roelof, Imagers for the magnetosphere, aurora and plasmasphere (IMAP), *SPIE*, 2008, (1993) 11–34.
6. Murphree, J. S., and L. L. Cogger, The application of CCD detectors to UV imaging from a spinning spacecraft, *SPIE*, 932, (1988) 42–49.
7. Oguti, T., E. Kaneda, M. Ejiri, S. Sasaki, A. K. Kadokura, T. Yamamoto, K. Hayashi, R. Fujii, and K. Makita, Studies of aurora dynamics by aurora-TV on the Akebono (EXOS-D) satellite, *J. Geomag. Geoelectr.*, 42, (1990) 555–564.
8. Torr, M. R., D. G. Torr, M. Zukic, J. Spann, and R. B. Johnson, An ultraviolet imager for the international solar-terrestrial physics mission, submitted, (1993).
9. Zukic, M., D. G. Torr, J. Kim, J. F. Spann, and M. R. Torr, Far ultraviolet filters for the ISTP UV imager, *SPIE*, 1745, (1992) 99–107.
10. Zukic, M., D. G. Torr, J. Kim, J. R. Fleischman, and C. Martin, Wide field of view 83.4 nm self-filtering camera, *SPIE*, in press, (1993).

1993

NASA/ASEE SUMMER FACULTY FELLOWSHIP PROGRAM

MARSHALL SPACE FLIGHT CENTER
THE UNIVERSITY OF ALABAMA IN HUNTSVILLE

EVALUATION OF ADVANCED MATERIALS THROUGH EXPERIMENTAL MECHANICS AND MODELLING

Prepared By: Yii-Ching Yang, Ph.D.

Academic Rank: Assistant Professor

Institution and
Department: Tuskegee University
                        Aerospace Science Engineering

MSFC Colleague: Samuel Russell, Ph.D.

NASA/MSFC:

    Laboratory: Material Processes
    Division: Engineering Physics
    Branch: Non-Destructive Evaluation

INTRODUCTION

Composite materials has been frequently used in aerospace vehicles. Very often it is inherited defects during the manufacture or damages during the construction and services. It becomes critical to understand the mechanical behavior of such composite structure before it can be further used. One good example of these composite structure is the cylindrical bottle of solid rocket motor case with accidental impact damages. Since the replacement of this cylindrical bottle is expensive, it is valuable to know how the damages affects the material, and how it can be repaired. To reach this goal, the damage must be characterized and the stress/strain field must be carefully analyzed.

First the damage area, due to impact, is surveyed and identified with a shearography technique which uses the principle of speckle shearing interferometry to measure displacement gradient(1). Within the damage area of a composite laminate, such as the bottle of solid rocket motor case, all layers are considered to be degraded. Once a lamina being degraded the stiffness as well as strength will be drastically decreased. It becomes a critical area of failure to the whole bottle. And hence the stress/strain field within and around a damage should be accurately evaluated for failure prediction.

To investigate the stress/strain field around damages a Hybrid-Numerical method which combines experimental measurement and finite element analysis is used. It is known the stress or strain at the singular point can not be accurately measured by an experimental technique. Nevertheless, if the location is far away from singular spot, the displacement can be found accurately. Since it reflects the true displacement field locally regardless the boundary conditions, it is an excellent input data for a finite element analysis to replace the usually assumed boundary conditions. Therefore, the Hybrid-Numerical method is chosen to avoid the difficulty and to take advantage of both experimental technique and finite element analysis.

Experimentally, the digital image correlation technique(2-4) is employed to measure the displacement field. It is done by comparing two digitized images, before and after loading. Numerically, the finite element program, ABAQUS (version 5.2)(5), is used to analyze the stress and strain field. It takes advantage of the high speed and huge memory size of modern supercomputer, CRAY Y-MP, at NASA Marshall Space Flight Center.

DIGITAL IMAGE CORRELATION

Digital image correlation is based on the comparison between two digital images. The system uses a standard CCD video camera attached to video digitizer card to acquire digital images. The digitizer transforms an image to a 512 x 512 set of numbers representing the image. Each number represents the

intensity of light impinging on a small area of camera sensor, which is called a pixel. The value of each pixel ranges from 0 to 255 with the lowest value representing black, highest value representing white, and values in between representing different shades of gray. An image processing software in a personal computer is then used to compare subsets of numbers between the two digital images. To measure how well the subsets match, a correlation function is used. By minimizing the correlation factor, the values of displacement and strain at any location of image can then be determined.

FINITE ELEMENT ANALYSIS

Finite element analysis for stress/strain of a structure is based on the following equations of equilibrium:

$$[K]\ \{q\} = \{F\} \quad \dots\dots\dots\dots\dots\dots\dots\dots\dots\dots\dots\dots [1]$$

It is resulted by minimizing the potential energy of the whole structure. Where {q}, {F}, and [K] represent nodal deformation, nodal loads, and structural stiffness matrices, respectively. Each member in {q} matrix is a degree of freedom. It is corresponding to a nodal force or moment in the same direction. For the static linear elastic problem, a degree of freedom is either unknown or known by fact or assumption. In the later case, the corresponding nodal force is unknown and to be solved as a reaction. In the Hybrid-Numerical approach, some parts of {q} matrix will be filled with the displacements measured by the digital image correlation besides the regular assumed boundary conditions. Providing the stiffness matrix of structures, [K], the unknowns in both {q} and {F} can be solved with a high speed computer.

The stiffness matrix of a structure, [K], is assembled from the stiffness matrices of element. Each member of [K] matrix relates a degree freedom to an associated nodal force or moment. The value of each member is determined by the geometry and the material properties of associated elements. Since composite laminates is used as examples, the stiffness matrix of each layer, [Q], must be first formed in the structural coordinates system, or loading directions. And the load-displacement relations is then constructed as the following form(6):

$$\begin{pmatrix} [A] & [B] \\ [B] & [D] \end{pmatrix} \cdot \begin{pmatrix} [\epsilon^o] \\ [k] \end{pmatrix} = \begin{pmatrix} [N] \\ [M] \end{pmatrix} \quad \dots\dots\dots\dots\dots\dots\dots\dots\dots\dots (2)$$

Where [A], [B], and [D] are determined by integrating the stiffness of all layers. Using above equations as the constitute equations of thin shell elements, the stiffness matrix of elements made of composite laminate can be formed.

This stiffness matrix of elements can be different depending on the material properties of individual element. In this study, a degraded material has been assumed to the damage areas. The elastic constants related to the transversal direction of a degraded lamina is assumed to be decreased by a degradation factor. By Using these constants the load-displacement relations of damaged lamina can be found, and hence the stiffness matrix of damaged elements.

FAILURE ANALYSIS

As it has been described, the above combination of experimental technique and finite element analysis will provide a more accurate results of stress and strain in the singular zone. Assuming the composite materials responds linearly under a set of given load, the output stress from finite element analysis can be used to predict the loading level of lamina and laminate failure. The Tsai-Wu Tensor Theory(7) is chosen to determine the stress level of failure since it is mostly adopted for a polymer composite lamina. According to this theory a lamina will have initial crack in polymer matrix, and hence degraded if its stress state fail to satisfy the following inequality:

$$F_{ij} \sigma_i \sigma_j + F_i \sigma_j < 1 \qquad \dots\dots\dots\dots\dots \text{[3]}$$

Furthermore, since the linear elasticity has been assumed, the ratio of the stress state at failure to that under the given load, R, can be calculated with the following equation:

$$(F_{ij} \sigma_i \sigma_j) R^2 + (F_i \sigma_i) R = 1 \qquad \dots\dots\dots\dots\dots \text{[4]}$$

This ratio can be interpreted as how many times of given load would cause a lamina to degrade. Once a lamina is degraded the stresses in every layer will be redistributed so that the next lamina may be degraded at a higher loading level. The loading level of that all laminae being degraded is referred as the Last Ply Failure of laminates. At this stage an intensive acoustic events of fiber breaking may be heard experimentally.

EXAMPLES AND CALCULATION

In this study the cylindrical rocket motor cases are investigated. They are cylindrical pressure vessels made of IM7/Epoxy with the winding layout of $[78.5/-78.5/0/0]_2$ from inside out. In which the 0 degree is referred to the circumferential direction. It is about 5.75 inches in diameter and 4 inches long (does not count both semispherical dome at ends). Every bottle has been subjected to a low speed impact test. They are three different impact energy levels, 3, 5, and 7 foot-pound applied at the middle of bottle and perpendicular to the composite laminate skin. The size of damage areas has

been measured with shearography technique. It has been seen the smallest damage is scattered within 1"x1" area; and the highest is 3"x3". Based on the identified patten of damage, the associated elements in the finite element analysis are assigned to the degraded material group.

During the burst test of each pressure vessel, two images has been taken, one at free load and the other at 1000 psi pressure level. The calculation of digital image correlation runs over about 300 by 300 pixels. It covers an area of composite laminate about 1.90" by 1.61". The resulting displacements are then input as boundary in the finite element analysis. A mesh diagram with 20 by 20 rectangular thin shell elements is constructed. Using a computer code, ABAQUS, the stresses and strains of shell elements are calculated. And the stresses is then checked with Tsai-Wu Tensor Theory to predict the pressure level at the Last Ply Failure of cylindrical bottle skin. The preliminary results show it agrees with that of the acoustic observation.

REMARK AND FUTURE WORK

Due to the complexity of test and shortage of facility and manpower, only few pressure vessels have been bursted. Although the preliminary result shows promising, more vessels should be tested; and more analyses must be done before a firm conclusion can be reached. By then it may be better understood how an impact affects the rocket motor cases and how to repair it if necessary.

REFERENCES

1. Toh, S.L., Shang, H.M., Chaw, F.S., and Tay, C.J., "Flaw Detection in Composites Using Time-Average Shearography," Optics & Laser Technology, 23 (1991)
2. Peters, W.H. and Ranson, W.F., "Digital Imaging Techniques in Experimental Stress Analysis," Opt. Eng., 21 (1982) 427-431
3. Sutton, M.A., Cheng, M., Peters, W.H., Chao, Y.J., and McNeill, S.R., "Application of an Optimized Digital Correlation Method to Planar Deformation Analysis," Image and Vision Computing 4 (1986) 143-150
4. Bruck, H.A., McNeill, S.R., Sutton, M.A. and Peters, W.H., "Digital Image Correlation Using Newton-Raphson Method of Partial Differential Correction," Experimental Mechanics, 29 (1989) 261-267
5. ABAQUS version 5.2, Bibbitt, Karlsson & Sorensen, Inc. (1993)
6. Jones, R.M., Mechanics of Composite Materials, Mcgraw-Hill Book Company (1975)
7. Tsai, S.W., and Wu, E.M., "A General Theory of Strength for Anisotropic Materials," Journal of Composite Materials, January (1971) 58-80

1993

NASA/ASEE SUMMER FACULTY FELLOWSHIP PROGRAM

MARSHALL SPACE FLIGHT CENTER

THE UNIVERSITY OF ALABAMA IN HUNTSVILLE

USING CONTOUR MAPS TO SEARCH FOR

RED-SHIFTED 511 keV FEATURES

IN BATSE GRB SPECTRA

Prepared By: Peter G. Varmette

Academic Rank: Graduate Student

Institution and
  Department: Mississippi State University
                                       Department of Physics
                                       and Astronomy

MSFC Colleague: Gerald Fishman, Ph.D.

NASA/MSFC:
    Laboratory: Space Science
    Division: Astrophysics
    Branch: Gamma-Ray Astronomy

L

Since their discovery twenty years ago, the origin of gamma-ray bursts (GRB's) has remained an intriguing mystery. The quest to understand these objects has given rise to a plethora of competing theories. Several theories suggest that GRB's are galactic in origin while others suggest that GRB's are cosmological (Harding 1993).

One piece of evidence that might provide scientists with a key to understanding the origin of GRB's may be whether or not spectral emission and absorption features exist in burst spectra. If the features exist and can be attributed to either cyclotron lines or to red-shifted 511 keV annihilation lines then credence would be given to those theories that support a galactic origin, i.e. near neutron stars (Barat 1984, Mazets 1980, Mitrofanov 1984, Nolan 1984).

A method of searching for spectral features in burst spectra (BATSE HER data) will be outlined in this paper. The method was used to investigate the energy range between approximately 350 keV to 600 keV. This energy range was chosen because previous experiments have reported emission features in gamma-ray bursts around 400 keV to 500 keV. These features have been interpreted as gravitationally red-shifted 511 keV annihilation radiation produced near a neutron star (Barat 1984, Mazets 1980, Mitrofanov 1984, Nolan 1984).

The first step was to calculate a background model representing the ambient background radiation. The model was used to separate the burst spectrum from that of the background. Next, we construct the incident "photon" spectrum from the recorded "count" spectrum. To do this involves convolution with matrices that contain information on the detector's efficiency as a function of energy, as a function of angle of incidence of radiation, and also the detector's sensitivity to that fraction of the incident radiation caused by scattering off the Earth's atmosphere. The combination of all of these is called the detector response matrix (DRM) shown in Figure 1.

The BATSE HER data for a single burst can be binned into different time intervals and each interval forms a spectrum. Burst 1B 911221 was binned into 8 spectra each lasting approximately 9 secs. A fit of the spectrum that ranged in time from 9.7 secs

to 18.2 secs produced the best fit results. Figure 2 shows the fit that was made to this spectrum using a Broken Power Law, the form of which can be seen in Equation 1.
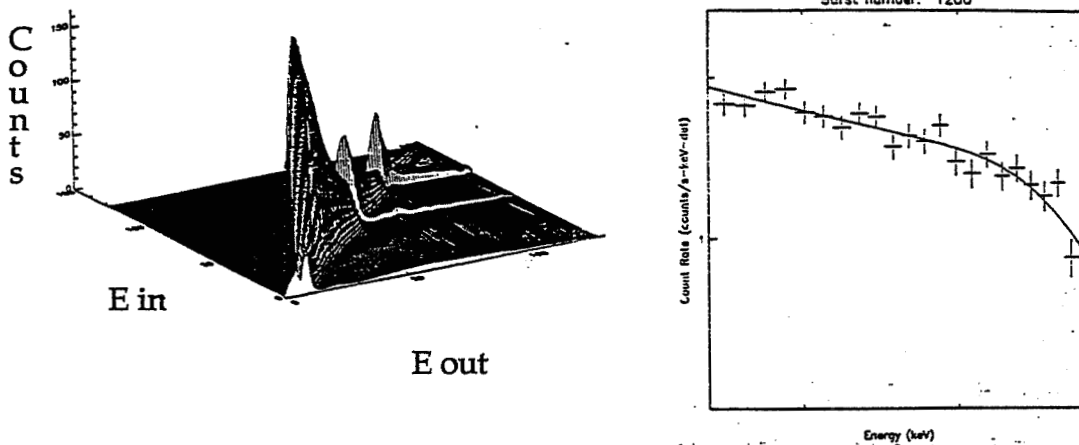

Figure 1 A detector response matrix.

Figure 2 A fit using a Broken Power Law.

$$A(\frac{E}{Epivot})^{\lambda_1} \ \text{if E} \leq \text{Ebreak}$$

$$\text{or} \qquad\qquad\qquad\qquad [1]$$

$$A(\frac{Ebreak}{Epivot})^{\lambda_1^-} (\frac{E}{Ebreak})^{\lambda_2} \ \text{if E} \geq \text{Ebreak}$$

The fit shown in Figure 2 produced a χ^2 of 23.4 with 22 degrees of freedom. After the initial fit was made to this spectrum, a batch fit was made to the other 7 spectra by adjusting the parameters of the first fit to find the best fit for each of the others.

The batch fits form the basis of a continuum model which was then subtracted from the data. These residuals were then divided by the standard deviation, σ, that was associated with each energy value. Contour maps of the residuals plotted against energy and time were then generated. Figure 3 shows the contour map that was generated for burst 1B 911221.

The contour lines are displayed for values of 2 σ, 3 σ, 4 σ, and 5 σ. When examining the structure in contour plots the resolution of the detector at the particular energy must be considered in order to determine whether the structure is real or not. Equation 2 gives the resolution of the detector as a function energy.
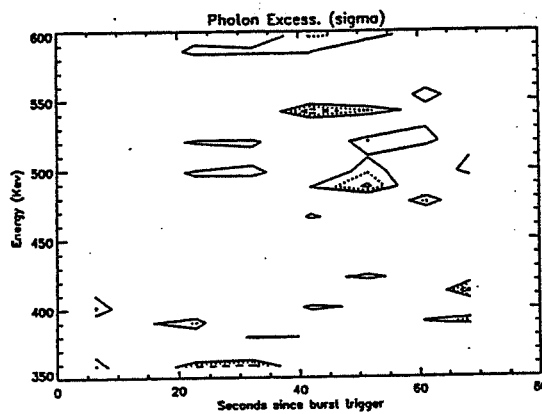
Figure 3 Contour map generated for burst 1B 911221.

$$Res = 0.079E \left(\frac{E}{511}\right)^{-0.42} \qquad [2]$$

At 545 keV the resolution is 42 keV. Therefore, the structure seen at 545 keV between 36 secs and 57 secs is probably a detector anomaly. The detector resolution at 490 keV is 39 keV. The observed structure ranges from 480 keV to 510 keV, so the feature is probably not real but further investigation is warranted. Figure 4 shows a plot over a larger energy range chosen to show the features at 490 keV in the context of a larger continuum. The figure shows that, in the energy range of 480 keV to 510 keV, there are no significant features.

The feature searching method described above provides a means of searching through a vast amount of data, looking for regions which warrant further and more thorough searches.

The new searching method also allows us to evaluate our background subtracting and fitting routines. For instance, if there were a lot of structure around 511 keV it might indicate that the background subtraction routines were not working properly.

Future work will be done to improve and enhance this searching method while analyzing GRB's for spectral emission features.
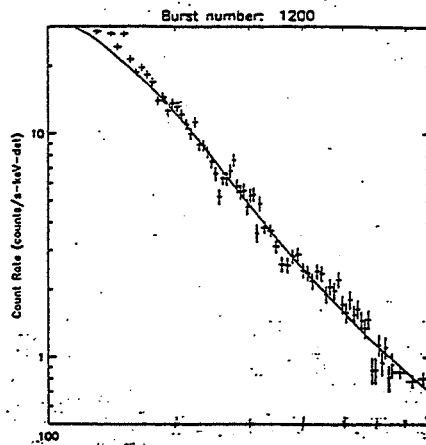
Figure 4 Fit of a broken power law over the energy range 170 keV to 900 keV.

Acknowledgment:

I would like to thank the members of the BATSE group for unselfishly aiding me with my research especially G. J. Fishman, C. A. Meegan, M. S. Briggs, G. N. Pendleton, W. S. Paciesas, R. D. Preece, and M. N. Brock.

1. Barat, C.et al, Possible Short Annihilation Flashes in the 1978 November 4 Gamma-ray burst, The Astrophysical Journal, 286:L11-L13, November 1, 1984.

2. Hardin, A. K., Gamma-ray burst theory: back to the drawing board, ApJ, Supplement, January 11-15, 1993.

3. Mazets, E. P. et al, Lines in the Energy Spectra of Gamma-ray Bursts, Pis'ma Astron. Zh. 6,706-711, November 1980.

4. Mitrofanov, I. G. et al, Rapid Spectral Variability of Cosmic Gamma-ray Bursts, Astron. Zh. 61, 939-943, September-October, 1984.

5. Nolan, P. L. et al, Spectral Feature of 31 December 1981 γ-ray Burst not Confirmed, Nature 311, September 27, 1984.